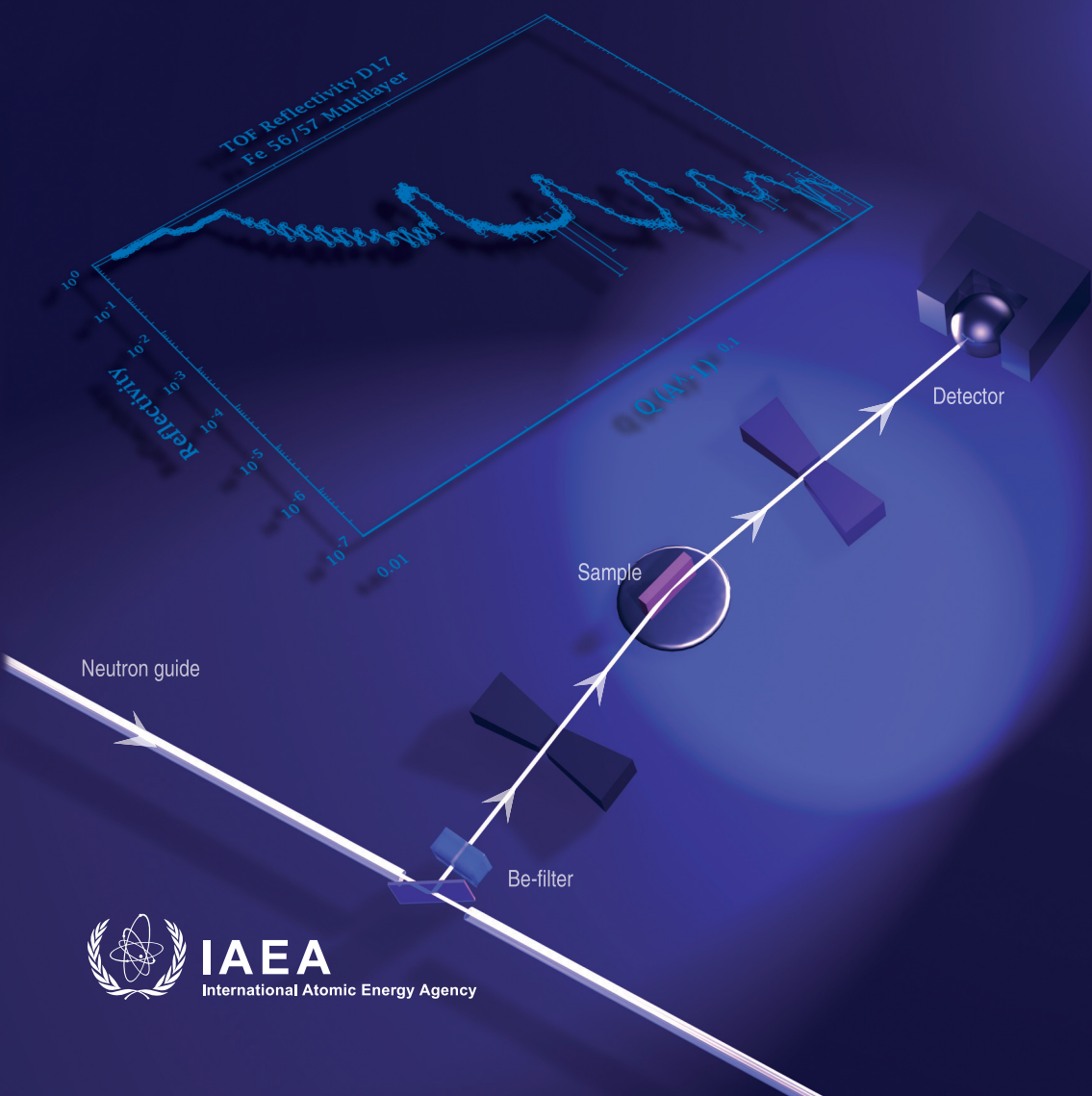


# Neutron Reflectometry A Probe for Materials Surfaces

Proceedings of a Technical Meeting  
Vienna, 16–20 August 2004



**IAEA**  
International Atomic Energy Agency

NEUTRON REFLECTOMETRY:  
A PROBE FOR MATERIALS  
SURFACES

The following States are Members of the International Atomic Energy Agency:

AFGHANISTAN	GHANA	PAKISTAN
ALBANIA	GREECE	PANAMA
ALGERIA	GUATEMALA	PARAGUAY
ANGOLA	HAITI	PERU
ARGENTINA	HOLY SEE	PHILIPPINES
ARMENIA	HONDURAS	POLAND
AUSTRALIA	HUNGARY	PORTUGAL
AUSTRIA	ICELAND	QATAR
AZERBAIJAN	INDIA	REPUBLIC OF MOLDOVA
BANGLADESH	INDONESIA	ROMANIA
BELARUS	IRAN, ISLAMIC REPUBLIC OF	RUSSIAN FEDERATION
BELGIUM	IRAQ	SAUDI ARABIA
BELIZE	IRELAND	SENEGAL
BENIN	ISRAEL	SERBIA
BOLIVIA	ITALY	SEYCHELLES
BOSNIA AND HERZEGOVINA	JAMAICA	SIERRA LEONE
BOTSWANA	JAPAN	SINGAPORE
BRAZIL	JORDAN	SLOVAKIA
BULGARIA	KAZAKHSTAN	SLOVENIA
BURKINA FASO	KENYA	SOUTH AFRICA
CAMEROON	KOREA, REPUBLIC OF	SPAIN
CANADA	KUWAIT	SRI LANKA
CENTRAL AFRICAN REPUBLIC	KYRGYZSTAN	SUDAN
CHAD	LATVIA	SWEDEN
CHILE	LEBANON	SWITZERLAND
CHINA	LIBERIA	SYRIAN ARAB REPUBLIC
COLOMBIA	LIBYAN ARAB JAMAHIRIYA	TAJIKISTAN
COSTA RICA	LIECHTENSTEIN	THAILAND
CÔTE D'IVOIRE	LITHUANIA	THE FORMER YUGOSLAV REPUBLIC OF MACEDONIA
CROATIA	LUXEMBOURG	TUNISIA
CUBA	MADAGASCAR	TURKEY
CYPRUS	MALAYSIA	UGANDA
CZECH REPUBLIC	MALI	UKRAINE
DEMOCRATIC REPUBLIC OF THE CONGO	MALTA	UNITED ARAB EMIRATES
DENMARK	MARSHALL ISLANDS	UNITED KINGDOM OF GREAT BRITAIN AND NORTHERN IRELAND
DOMINICAN REPUBLIC	MAURITANIA	UNITED REPUBLIC OF TANZANIA
ECUADOR	MAURITIUS	UNITED STATES OF AMERICA
EGYPT	MEXICO	URUGUAY
EL SALVADOR	MONACO	UZBEKISTAN
ERITREA	MONGOLIA	VENEZUELA
ESTONIA	MOROCCO	VIETNAM
ETHIOPIA	MYANMAR	YEMEN
FINLAND	NAMIBIA	ZAMBIA
FRANCE	NETHERLANDS	ZIMBABWE
GABON	NEW ZEALAND	
GEORGIA	NICARAGUA	
GERMANY	NIGER	
	NIGERIA	
	NORWAY	

The Agency's Statute was approved on 23 October 1956 by the Conference on the Statute of the IAEA held at United Nations Headquarters, New York; it entered into force on 29 July 1957. The Headquarters of the Agency are situated in Vienna. Its principal objective is "to accelerate and enlarge the contribution of atomic energy to peace, health and prosperity throughout the world".

PROCEEDINGS SERIES

NEUTRON REFLECTOMETRY:  
A PROBE FOR MATERIALS  
SURFACES

PROCEEDINGS OF A TECHNICAL MEETING  
ORGANIZED BY THE  
INTERNATIONAL ATOMIC ENERGY AGENCY  
AND HELD IN VIENNA, 16-20 AUGUST 2004

INTERNATIONAL ATOMIC ENERGY AGENCY  
VIENNA, 2006

## COPYRIGHT NOTICE

All IAEA scientific and technical publications are protected by the terms of the Universal Copyright Convention as adopted in 1952 (Berne) and as revised in 1972 (Paris). The copyright has since been extended by the World Intellectual Property Organization (Geneva) to include electronic and virtual intellectual property. Permission to use whole or parts of texts contained in IAEA publications in printed or electronic form must be obtained and is usually subject to royalty agreements. Proposals for non-commercial reproductions and translations are welcomed and will be considered on a case by case basis. Enquiries should be addressed by email to the Publishing Section, IAEA, at [sales.publications@iaea.org](mailto:sales.publications@iaea.org) or by post to:

Sales and Promotion Unit, Publishing Section  
International Atomic Energy Agency  
Wagramer Strasse 5  
P.O. Box 100  
A-1400 Vienna  
Austria  
fax: +43 1 2600 29302  
tel.: +43 1 2600 22417  
<http://www.iaea.org/books>

© IAEA, 2006

Printed by the IAEA in Austria  
August 2006  
STI/PUB/1246

### **IAEA Library Cataloguing in Publication Data**

Neutron reflectometry : a probe for materials surfaces : proceedings of a technical meeting / organized by the International Atomic Energy Agency and held in Vienna, 16-20 August 2004. — Vienna : The Agency, 2006.

p. ; 24 cm. — (Proceedings series, ISSN 0074-1884)

STI/PUB/1246

ISBN 92-0-103906-9

Includes bibliographical references.

1. Reflectometer — Congresses.
  2. Neutrons — Congress.
- I. International Atomic Energy Agency. II. Series: Proceedings series (International Atomic Energy Agency).

IAEAL

05-00447

## FOREWORD

Research reactors play an important role in delivering the benefits of nuclear science and technology. The IAEA, through its project on the effective utilization of research reactors, has been providing technical support to Member States and promotes activities related to specific applications. Neutron beam research is one of the main components in materials science studies.

Neutron reflectometry is extremely useful for characterizing thin films and layered structures, polymers, oxide coatings on metals and biological membranes. The neutron has been a major probe for investigating magnetic materials. Development of magnetic multilayers is important for diverse applications in sensors, memory devices, etc. The special nature of the interaction of the neutron with matter makes it an important tool to locate low  $z$  elements in the presence of high  $z$  elements, which is useful in biology and polymer science.

The role of neutron reflectometry in research and development in materials science and technology was discussed in a consultants meeting held in 2003. Following this, a technical meeting was organized from 16 to 20 August 2004 in Vienna to discuss the current status of neutron reflectometry, including the instrumentation, data acquisition, data analysis and applications. Experts in the field of neutron reflectometry presented their contributions, after which there was a brainstorming session on various aspects of the technique and its applications. This publication is the outcome of deliberations during the meeting and the presentations by the participants.

This publication will be of use to scientists planning to develop a neutron reflectometer at research reactors. It will also help disseminate knowledge and information to material scientists, biologists and chemists working towards characterizing and developing new materials. The IAEA thanks all the experts for their active participation in the meeting, for the manuscripts of their presentations and for their contribution in preparing the summary. Thanks are also due to A.R.Wildes from the Institut Laue-Langevin, Grenoble, France, for his paper on polarized neutron reflectometry.

The IAEA officer responsible for this publication was S.K. Paranjpe of the Division of Physical and Chemical Sciences.

## *EDITORIAL NOTE*

*These Proceedings have been edited by the editorial staff of the IAEA to the extent considered necessary for the reader's assistance. The views expressed remain, however, the responsibility of the named authors or participants. In addition, the views are not necessarily those of the IAEA, the governments of the nominating Member States or the nominating organizations.*

*The report does not address questions of responsibility, legal or otherwise, for acts or omissions on the part of any person.*

*The use of particular designations of countries or territories does not imply any judgement by the publisher, the IAEA, as to the legal status of such countries or territories, of their authorities and institutions or of the delimitation of their boundaries.*

*The mention of names of specific companies or products (whether or not indicated as registered) does not imply any intention to infringe proprietary rights, nor should it be construed as an endorsement or recommendation on the part of the IAEA.*

*The authors are responsible for having obtained the necessary permission for the IAEA to reproduce, translate or use material from sources already protected by copyrights.*

## CONTENTS

SUMMARY.....	1
Principles of reflectometry with reactors and pulsed sources .....	29
<i>J. Penfold</i>	
Specular neutron reflectivity: Applications to soft matter .....	45
<i>J. Penfold</i>	
Design of a neutron reflectometry at a research reactor .....	59
<i>Z. Tun</i>	
Polarized neutron reflectivity on D17 at the Institut Laue-Langevin.....	69
<i>R. Cubitt</i>	
Oxide films and corrosion.....	79
<i>J.J. Noël</i>	
Neutron reflection studies of solid–liquid interfaces.....	85
<i>A.R. Rennie</i>	
Neutron reflectometry in Australia: Present and future.....	95
<i>A. Nelson, M. James, J.C. Schulz, A. Brule</i>	
Development of a TOF reflectometer at the Greek Research Reactor... ..	103
<i>K. Mergia, G. Apostolopoulos</i>	
Neutron reflectometer at the Budapest research reactor with polarization option.....	117
<i>L. Cser</i>	
Neutron reflectometry at Dhruva reactor: Specular and off-specular neutron reflectivity studies .....	129
<i>S. Basu, S. Singh</i>	
Application of polarized neutron reflectometry .....	145
<i>A.R. Wildes</i>	

<i>n</i> /X materials science reflectometer at FRM-II in Garching . . . . .	161
<i>A. Rühm, U. Wildgruber, J. Franke, J. Major, H. Dosch</i>	
Neutron specular reflectometry: Some aspects of theory . . . . .	177
<i>H. Leeb</i>	
List of Participants . . . . .	197

# SUMMARY

## 1. REVIEW OF NEUTRON REFLECTOMETRY

### 1.1. Introduction

Neutron reflectometry (NREF) is a relatively new technique that has widespread applications as a powerful analytical tool to analyse interfacial structure and composition. The recent upsurge in phenomena occurring over the nanometre scale and the unusual properties of low dimensional materials, compared with their bulk counterparts, are expected to yield a range of new products for electronics, photonics, etc. NREF is poised to help address the questions that will arise in the development of advanced thin film devices and functional interfaces of active materials with large surface areas.

In its simplest form this technique measures the intensity of a specularly (angle of incidence = angle of reflection) reflected neutron beam as a function of wavelength and/or angle. If the thin film surface constitutes the  $(x, y)$  plane and the  $z$  axis is normal to the surface, then for specular reflectivity, momentum transfer  $Q_x$  and  $Q_y$  are zero and  $Q_z$  is given by:

$$Q_z = (4\pi/\lambda)\sin(\theta) \quad (1)$$

where  $\lambda$  is the wavelength of the incident neutron beam and  $\theta$  the angle of incidence (or reflection). A neutron beam of very low divergence ( $\sim 1\text{--}5$  arc/min) is made to impinge on a thin film surface at a grazing incidence. For most of the materials the refractive index ' $n$ ' for neutrons is given by:  $n = 1 - \delta$ , where  $\delta \sim 10^{-6}$ . Up to a critical angle of incidence the neutron beam undergoes total external reflection and beyond that the beam penetrates the stratification and gets reflected at the interfaces. The reflected neutron beam bears the signature of the thickness of the layers, their densities, interface roughness, etc., of the thin film sample. Specular reflectivity is usually measured as a function of  $Q_z$ , which can easily be obtained with knowledge of the wavelength and the sample reflection angle from the above relation.

If one measures reflectivity outside the specular condition, i.e. angle of reflection  $\neq$  angle of incidence, then the reflected beam will also have non-zero  $Q_x$  and  $Q_y$  components. Such measurements constitute the class of experiments under diffuse neutron scattering and provide information on the in-plane height–height correlation function at various interfaces in the thin film.

Although various techniques are available (Table 1) for studying surface properties, the special features of neutron interaction with matter make NREF

## SUMMARY

TABLE 1. SURVEY OF TECHNIQUES AVAILABLE FOR SURFACE STUDIES

Technique	Acronym	Comment
X ray reflection		Complementary to NREF. Excellent for chemical density profile, but cannot distinguish between neighbouring elements or isotopes of the same element.
Ellipsometry and optical reflectivity		
X ray photoelectron spectroscopy	XPS	Only about 50 Å depth from surface can be probed. Provides local chemical environment.
Secondary ion mass spectrometry	SIMS	Depth sensitive, but poorer resolution compared to NREF. Also destructive.
Scanning probe microscopy	AFM, STM, etc.	Can study only the top surface, but provides direct view of the sample surface.
Optical spectroscopy, Raman, infrared	IRRAS: Infrared reflection absorption spectroscopy; SFG: second frequency generation spectroscopy	
Auger electron spectroscopy	AES	
Electrochemical impedance spectroscopy	EIS	

an important tool. The advantage of the method is that isotopic labelling can be exploited to enhance signal from a particular component of the sample. Neutrons are sensitive to magnetic moments arising from spin and orbital angular momentum, and can be used to probe magnetic structures. The penetration of neutron beams allows buried surfaces and the interfaces between bulk components (solids and liquids or between two liquid phases) to be observed. The basic use of specular neutron reflection has been to determine the average structure normal to an interface but is now being extended by the use of surface scattering in off-specular directions to look at lateral structures.

## SUMMARY

NREF can be used to solve problems in science and technology ranging from materials science, polymers and soft matter, thin film magnetism, chemistry and biology. It is currently used to address issues in important areas involving energy, nanotechnology, environment and medicine. A list of NREF facilities is given in Appendix I.

## 2. ROLE OF NEUTRON REFLECTOMETRY IN SCIENCE AND TECHNOLOGY

### 2.1. Materials science

NREF works very well in situ with electrochemical experiments and has been used to study aqueous corrosion, the influence of interfacial electrical fields on the adsorption/desorption of surfactants and thin organic films, and electric charge storage devices, such as nickel hydroxide electrodes and lithium ion intercalation systems. Reaction kinetics studies have become possible with improvements in the flux and the data acquisition systems.

Templated growth of thin films can give rise to useful nanostructured and microstructured materials. These synthetic routes to materials for catalyst supports and photonic devices involve surfactants with mesophase structures in the bulk or at interfaces. The mechanisms of these reactions are subject of a number of NREF studies and off-specular scattering is also becoming important in this area [1, 2]. NREF can also contribute to the understanding of abrasion resistant surface films and the interface between the coating and underlying material, e.g. hard carbon (diamond) coatings and metal nitride films.

Important aspects of heterogeneous catalysts may be probed with NREF to complement information gained from other analyses. Significant questions that can be addressed include active surface structure, void content, and compositional segregation and changes in these properties during catalyst activation and deterioration.

The strong interactions of neutrons with hydrogen give NREF a unique ability to investigate, non-destructively, the concentrations, locations and movements of hydrogen in solids, which is useful in the development of hydrogen storage alloys and fuel cells, and in studies of hydrogen embrittlement of structural metals.

NREF is an important tool for the materials scientist in that it can provide important information on the nature of corrosion, metal fatigue and hydrogen absorption. Corrosion scientists have begun using reflectometry to probe metal

## SUMMARY

and alloy dissolution rates and the growth of passive films, both in and ex situ, at solid–liquid and solid–gas interfaces.

This technique can contribute to nuclear technology in a number of ways. In fission reactors, fuel element cladding, reactor vessels and cooling circuits would benefit from an understanding of corrosion behaviour aided by NREF to help enhance operational efficiency, plant life, and costs. NREF studies of corrosion and hydrogen absorption on candidate materials for nuclear fuel waste containers have already begun. Understanding surface properties of materials and the interaction with hydrogen is crucial for development of fusion reactor technology.

### **2.2. Magnetic thin films**

Today, a myriad of fabrication techniques exists to control magnetic interactions on the nanoscale. Confinement in one, two or all dimensions via the creation of multilayers, wires or dots can lead to novel magnetic behaviour with a variety of technical applications in areas such as magnetic sensing, magnetic recording and magneto-electronics. NREF is intrinsically suitable for the study of monolayer thick layers [3, 4] and arrays of micrometre size dots [5].

For superconductors, the magnetic depth profiling on a thin film surface can provide the value of London penetration depth [6, 7] and information about the vortex structure [8]. Measurements of the magnetic depth profile at a surface and at the interfaces of magnetic and non-magnetic layers have provided valuable information on surface magnetization and the transfer of magnetic moment across a boundary [4].

### **2.3. Devices for neutron optics**

Multilayers are an inherent part of many neutron scattering instruments like neutron guides, beam deflectors, frame overlap devices, wide band monochromators, etc. A majority of instruments using polarized neutron beams employ polarizing supermirrors as polarizing devices. The efficiency of neutron transportation along neutron guides/the monochromatization of a periodical layer systems and the polarization efficiency of supermirrors depends on the quality of the multilayers.

NREF is the most appropriate tool for collecting information about main properties of multilayers, e.g. thickness, density, roughness, amorphicity, formation of nanocrystals, etc., that can be used as feedback in the manufacture of the multilayer devices to improve their quality.

## 2.4. Polymer thin film systems

The study of polymer thin films has been one of the mainstays of NREF research over the past two decades. One of the advantages is the ease in contrast variation between different polymer layers by deuteration. The high sensitivity of NREF to the shape and width of interfaces between the polymer layers [9] makes it an excellent tool to probe inter-diffusion and self-diffusion of polymers. Block copolymers are commonly used in industry as compatibilizers between two immiscible polymers because of their tendency to migrate to the interface between two dissimilar polymers. This property is also exploited in enhancing adhesion between different polymer films. Understanding of interfacial structure of block polymer films both with and without the presence of homopolymers is of fundamental interest.

Chemi- or physi-sorbed polymer layers, called polymer brushes, form another area of interest, from both the experimental and theoretical point of view. Detailed studies of segment density profiles of polymer brushes under various solvent and temperature conditions have been done [10]. Langmuir monolayers of polymer brushes at the air-liquid interface have been also widely explored [11]. More recently, studies of polymer films under high pressure in supercritical CO<sub>2</sub> have revealed very interesting properties [12].

## 2.5. Soft condensed matter

Adsorption of surfactants, surfactant mixtures, polymers and polymer-surfactant mixtures are important in a wide range of industrial, technological and domestic applications, like detergents, personal care products, pharmaceuticals, lubrication, sensors, etc. They impinge upon all aspects of everyday life.

Understanding, manipulating and improving their functionality in these diverse areas requires a detailed knowledge of adsorbed amounts, and of the structure of the adsorbed layer (at the interface or surface). The unique features of the NREF technique make it ideally suited to obtain such information, and this is an area where the technique has already made a significant impact. It has provided information that is not accessible using other techniques, and has enabled the data from other techniques (such as surface tension measurement) to be interpreted. However the drive towards the use of more complex multi-component systems and the demand for more sophisticated and specific surface or interfacial functionality in many of the areas of application guarantees the likelihood of a continuing strong and growing demand for the technique. The increasing complexity of multi-component mixtures will require high throughput and sensitivity to be able to probe the parameter space and to probe minority components in order to understand

## SUMMARY

such systems. In many applications the surface/interface will be in equilibrium with some bulk structure or meso-phase, and in situ determination of the surface and near surface structures are vital in order to remove the uncertainties introduced by perturbation of the system. Many of the studies to date have been on 'model' systems but further developments of the technique will allow access to a wider range of solid solution and liquid-liquid interfaces, which are closer to 'real' environments.

### 2.6. Biology and food technology

The adsorption of proteins at interfaces is an important issue in applications such as use of medical implants and also because proteins are surface active agents in many natural products (e.g. food). Depending on the stability of the quaternary or tertiary structure the protein may or may not retain this structure at an interface. The stronger globular proteins, e.g. lysozyme, are found to retain their structure at the air-water interface and furthermore their position in the interface can be identified [13]. Unexpectedly the molecule protrudes from the water surface to a significant extent. Such a result, which has implications for the interaction of proteins with other species at interfaces, could only be obtained by NREF. The biological role of phospholipids is entirely interfacial and NREF is potentially a powerful tool for probing the interactions of other species with phospholipid bilayers. There have been several groups working on preparation of a range of model membranes [14, 15]. For example, NREF has been able to give otherwise inaccessible information about the binding of the structural proteins spectrin and actin to a phospholipid monolayer (an important combination in eukaryotic cells) [16].

The production and stability of many 'new' food products is predominantly a colloid science problem, related to emulsion stability. The adsorption of proteins to oil-water, air-water and air-oil interfaces and the stability of those interfaces is an important parameter in food stability.

### 3. REAL TIME NREF

In many applications, like kinetics of inter-diffusion in polymer films, in film drainage, and foam stability, where non-equilibrium processes are dominant, access to kinetic information over a wide range of timescales is essential. With continuous improvements in NREF instruments and more powerful neutron sources, it is now possible to do real time studies. Some of these experiments have already been carried out at several neutron sources.

## SUMMARY

With the start-up of spallation neutron source (SNS) in the USA it would be possible to do these measurements with time bins of 1 s or less.

### 4. DESIGN OF A REFLECTOMETER

#### 4.1. General reflectometer

All reflectometers have some basic common requirements. Figure 1 shows a schematic layout of a general instrument.

Reflectivity is the ratio of reflected to incoming intensity on a mirror-like sample. A well collimated beam is directed to a sample surface at a glancing angle and a detector is used to capture the reflected intensity. The incoming intensity is measured using a beam monitor or directly on the detector with sample removed. The collimation not only defines the resolution but the size of the beam relative to the sample. Samples are typically  $\sim 1\text{--}10\text{ cm}^2$  and reflection angles are small ( $0.1^\circ\text{--}10^\circ$ ). The cross-section of the sample seen by the incoming beam within the scattering plane is also small leading to collimation slits that typically need to range from 0.1–5 mm with a precision and reproducibility better than 10  $\mu\text{m}$ . The sample translation table, which enables the sample to be placed at the centre of the beam (the incoming beam should always pass through the sample rotation axis), requires a similar precision. Sample and detector rotations typically require a precision and reproducibility better than  $0.01^\circ$ . It is possible to avoid motorized collimation slits by having a fixed beam width set greater than the largest footprint expected but the beam ‘flypast’ can be a cause of unwanted background.

The purpose of the monochromator and chopper (via time of flight) is to define the wavelength of the neutron. Reflectivity is usually measured as a function of  $Q$ , which can easily be obtained with knowledge of the wavelength and the sample reflection angle via the following relation:

$$Q = (4\pi/\lambda)\sin(\theta) \quad (2)$$

where  $\lambda$  is the wavelength of the neutron and  $\theta$  is the sample reflection angle. In a monochromatic instrument a single wavelength is produced, with a certain spread, and  $\theta$  is varied. In a time of flight (TOF) instrument a chopper is used to pulse a white beam with  $\theta$  fixed. In this case  $\lambda$  (and therefore  $Q$ ) is deduced from the time of flight from the chopper to the detector. In either case there is a certain precision in the ability to define the wavelength, which, along with the beam collimation contributes to the resolution in  $Q$ ,  $\delta Q$ , defined as a full width

## SUMMARY

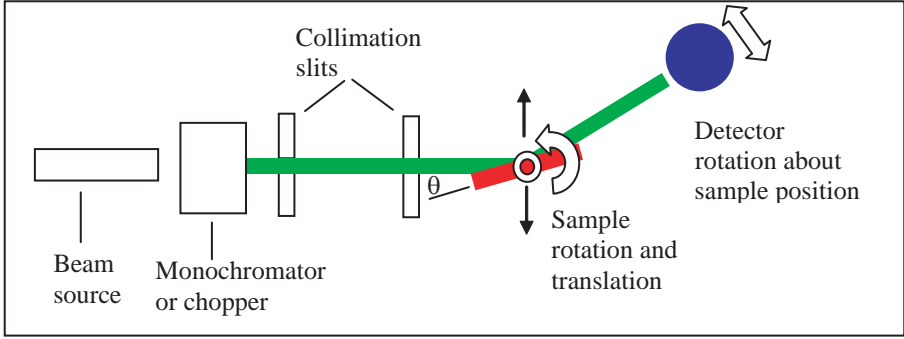


FIG. 1. Layout of a general reflectometer. The view could be either from the top for a horizontal reflection plane instrument or from the side for a vertical plane. Generally, a monochromator will Bragg-reflect the beam so this type of instrument would require a second rotation axis about the monochromator. The beam is highly collimated in the reflection plane and can be quite divergent in the other plane (out of the page).

at half maximum (FWHM) spread. These two principal contributions to the resolution contribute to  $\delta Q$  by the following relation:

$$\left(\frac{\delta Q}{Q}\right)^2 = \left(\frac{\delta\lambda}{\lambda}\right)^2 + \left(\frac{\delta\theta}{\theta}\right)^2 \quad (3)$$

In the case of a monochromator,  $\delta\lambda/\lambda$  is determined by the mosaic spread of the crystal/multilayer and in the case of the chopper it is equal to  $\delta t/t$  where  $\delta t$  is the pulse width in time and  $t$  is the TOF for the neutron. Figure 2 shows a reflectivity profile from a  $^{56}\text{Fe}/^{57}\text{Fe}$  multilayer measured with a  $Q$  resolution of 1–4%. The peaks are due to the layer separation and the fine oscillations from the total thickness of the multilayer, which would not be resolvable if  $\delta Q$  was too wide.

It can be seen from Fig. 2 that the maximum  $Q$  measured ( $\sim 0.4 \text{ \AA}^{-1}$ ) was in fact determined from the point where the reflectivity merged into the background. The background is very often the factor, which determines the minimum reflectivity and hence the maximum  $Q$ . Reflective minimum is same for both high and low flux instrument except the measurement time. Background can come from many places such as, air scattering from the incoming beam, thermalization of fast neutrons near the instrument, gamma rays from slits and shielding and electronic detector noise. Evacuated flight tubes, avoiding fast neutron sources such as a direct view of the reactor core,

## SUMMARY

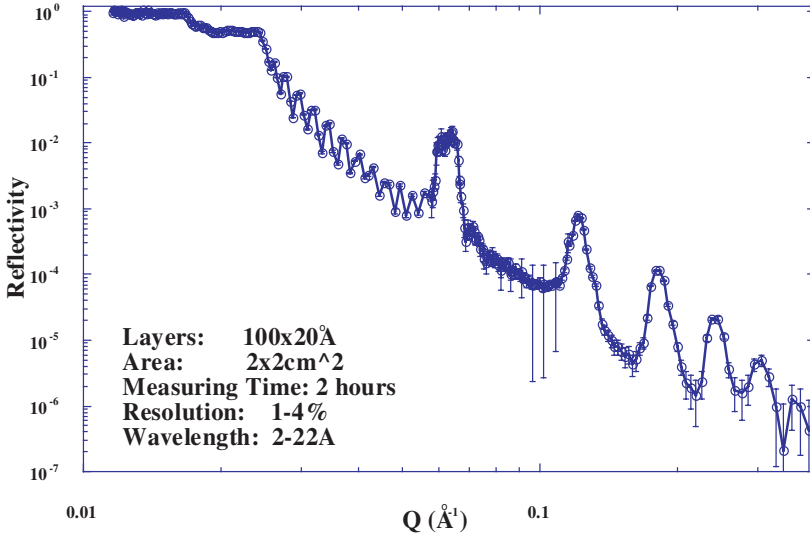


FIG. 2. Reflectivity curve measured on D17, ILL showing the need for good resolution.

gamma rejection in the detector electronics and careful detector shielding can help in reducing the background.

### 4.2. Taking into account the neutron source available

The type of reflectometer best suited to a particular site depends on many factors including the neutron spectrum available, the position at which the reflectometer is to be situated (reactor face or guide hall) and the beam geometry available.

Reflectometry is a low  $Q$  technique and longer wavelengths usually are advantageous. Given a choice one should always choose a cold source over a thermal or hot source of neutrons. A guide hall position is preferred mainly due to lower background and available space. The available space could determine the choice between a vertical and horizontal reflection plane. If only a limited space on either side of the beam axis is available then a horizontal reflection plane may not be practical, as the detector needs to turn about a vertical axis. Figure 3 [17] shows two examples of the two types of machine.

Areas with high vibrations either airborne or through the floor are not suitable for an instrument intended to study free liquid surfaces, unless effective isolation can be employed. Reflectometers require a low neutron and gamma background environment thus neighbouring instruments such as those creating high fast neutron fluxes should be avoided. Reflectometers require

SUMMARY

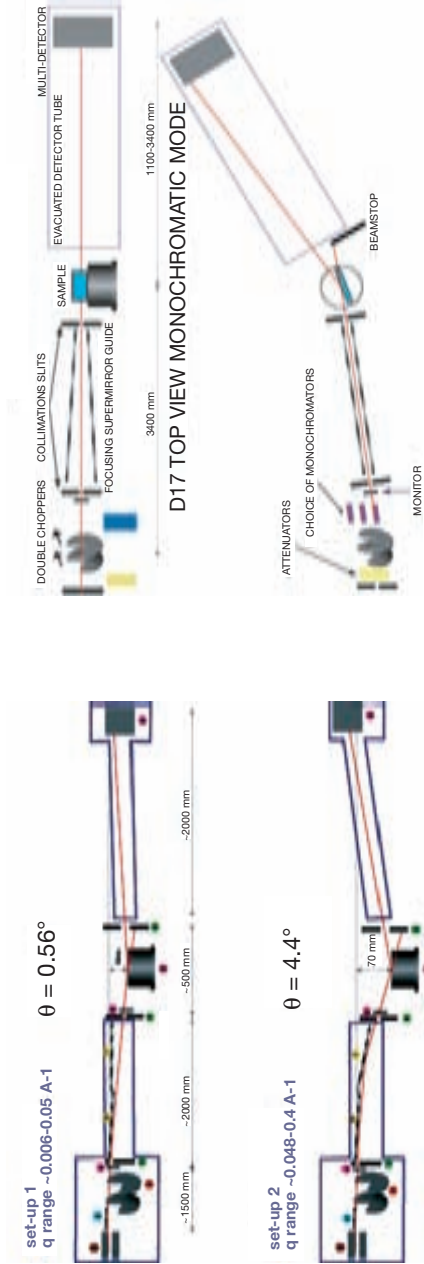


FIG. 3. Left: The proposed vertical reflection plane reflectometer principally designed for free liquid surfaces known as HORIZON at the ILL. Right: A picture of D17 with a horizontal reflection plane. A vertically focused guide (D-17 top right) gives a gain in flux [17].

## SUMMARY

good collimation (angular resolution) only in one direction leading to a beam profile with a high aspect ratio, the good resolution being in the direction of the thin beam defined by the collimation slits. Often the height of a neutron guide is much more than the width so that the number of instruments viewing a given source can be maximized. If such situation exists then a vertical beam, horizontal reflection plane machine is the most efficient, but not the only method of using the guide. At the reactor face there is a distinct advantage of being able to choose the shape of the beam channel to match the required aspect ratio. However, a price is always to be paid by having to deal with increased background.

### 4.3. Local resources

Another important factor to be considered in developing a reflectometer is the existing/anticipated user base, and the type of experiments that they wish to perform.

If there is no demand for free-liquid surfaces then there will be less reason to justify building a vertical scattering plane reflectometer. This argument also applies when deciding to include a polarization option. However, it is also important to consider future demand, as one may not be able to modify the instrument at a later stage.

Local expertise will have an effect in the design considerations. Local knowledge is often essential for regular maintenance. If this maintenance is not performed within an organization then help from outside experts will be required, which will add to operating costs.

There may be a situation in which higher performance (but more expensive) options may be of benefit to the intended users in the long run. A risk-benefit analysis (performance, expense, reliability, local knowledge) will identify if this situation applies to a particular facility. On the other hand if local knowledge is available, then there may be scope to develop equipment in house (e.g. detector electronics), which will save money over an externally bought solution.

When developing an instrument one should consider whether an intended option (for example, polarization capability) will degrade the performance for a different type of experiment (for example flux loss for unpolarized measurements if devices cannot be removed).

### 4.4. Costing

The approximate construction/running costs will vary on the exact aspects included in each instrument. The amount will also vary considerably depending

## SUMMARY

on whether equipment is bought, or is developed in-house. Contacting established reactor sources might identify unused equipment that may be acquired at reasonable cost. Costs will also vary from country to country.

As a rough guide, a minimum starting budget with a lot of local expertise infrastructure and development is approximately US \$70 000. A more fully advanced and state of art reflectometer with the very best components can cost from \$300 000 up to \$2 000 000.

## 5. TYPES OF REFLECTOMETER

### 5.1. Constant wavelength reflectometer

In a constant wavelength reflectometer the wavelength near the peak of the neutron Maxwellian spectrum is utilized. A monochromator with a large mosaicity ( $0.5^\circ$  corresponding to  $\delta\lambda/\lambda \sim 1\%$ ) and high reflectivity should be chosen. Pyrolytic graphite seems to be the best choice for either 2.4 or 4.5 Å, corresponding to beam deflections of  $41^\circ$  and  $90^\circ$ . These two particular wavelengths are well suited for higher harmonics filtering. Employment of a focusing device within the plane of the sample surface would be of an advantage since it increases the intensity without deterioration of resolution in  $Q$ . If a graphite monochromator is used a filter is required to suppress contamination from higher order reflections ( $\lambda/2$ ,  $\lambda/3$ ). Accurate monochromator positioning devices are not needed if the variation of wavelength is not important. For specular reflectivity measurements the sample and the detector are moved in  $\theta$ - $2\theta$  mode to cover the desired  $Q$  range. The sample ( $\theta$ ) scan can be accomplished by a goniometer or rotation table whereas the  $2\theta$  detector scan may be accomplished by a translation table or a rotation arm. Unlike the rotation stage for the monochromator, these rotation stages need to be far more accurate, at least to  $0.01^\circ$  and preferably to  $0.001^\circ$ . A constant wavelength instrument is the simplest and probably the cheapest type of reflectometer.

### 5.2. TOF reflectometer

In a TOF reflectometer, a broad wavelength range is used by the employment of a suitable chopper, which pulses the white neutron beam from the reactor and the time of flight of neutrons from the chopper to the detector determines the neutron wavelength (5 Å neutrons have a speed of  $\sim 800$  m/s).

One of the advantages of a TOF instrument is that with a  $1\theta$  and  $2\theta$  setting a large  $Q$  range can be covered, which is defined by the range of wavelengths. The useful wavelength range is determined by the useful intensity

## SUMMARY

(flux spectrum) available and the  $Q$  range required for a given sample angle. A mirror is placed in the beam to remove wavelengths greater than the longest wavelength we wish to use. The period of the chopper is then set just above the time of flight of the longest wavelength to avoid frame overlap (fast neutrons catching up with the slowest neutrons from the previous pulse). The sector opening and the angular velocity of a single chopper determine  $\delta t$  (see Eq. (2)). The chopper blades should cut the small dimension of the beam for better resolution in time. This means for a vertical reflection plane instrument the neutron window is at 3 or 9 o'clock position, and at 6 or 12 o'clock position for the horizontal scattering machine. A second chopper with a large opening can be used if one wishes to have  $\delta t/t$  constant with wavelength.

Measuring the TOF of neutrons requires more expensive detector electronics than for a constant wavelength reflectometer and the choppers often require high maintenance. However, the convenience of simultaneously measurement over a range of  $Q$  and the flexibility of resolution can balance these disadvantages.

### 5.3. Polarized neutron reflectometer

Detailed information about magnetic thin film systems can be obtained by polarized neutron reflectometry (PNREF) [18–20], which analyses the modification of the neutron spin by the magnetization in the sample. In particular, specular PNREF is sensitive to the depth dependence of the *vector* magnetization, while off-specular PNREF provides a spatially averaged characterization of the magnetic roughness and of magnetic domains both at the film surface and within buried layers.

Several major application areas of PNREF are: (a) determination of magnetic moment density as a function of depth in a magnetic thin film; (b) determination of magnetic field penetration in thin films of superconductors; (c) determination of in-plane magnetic structure; and (d) determination of the coupling between magnetic layers across non-magnetic layers in multilayer stratifications.

Application of PNREF for determination of collinear magnetic depth profile requires measurement of reflectivity profiles for neutrons polarized parallel ( $R^+$ ) and anti-parallel ( $R^-$ ) with respect to the sample's quantization axis. Depending on the polarization of the neutron beam the neutron sees a step potential, given by:

$$\bar{V}(r) = \frac{2\pi\hbar^2}{m} N b \pm \mu_n \cdot \bar{B} = \frac{2\pi\hbar^2}{m} N [b(r) \pm p(r)] \quad (4)$$

## SUMMARY

where  $N$  is the number density of the medium,  $b(r)$  the coherent nuclear scattering length and  $p(r)$  the magnetic moment per scattering unit. The  $\pm$  sign corresponds to the up and down polarization of the neutron with respect to the sample polarization.

If one needs to determine the in-plane magnetic structure and the nature of magnetic coupling in more complex magnetic multilayers, additionally one needs to analyse the polarization state of the reflected neutron beam. In this case one obtains four reflectivity profiles, ( $R^{++}$ ,  $R^{--}$ ,  $R^{+-}$ ,  $R^{-+}$ ). In the first approximation the non-spin flip (NSF) components determine the component of the magnetic moment parallel to the quantization axis and the spin flip (SF) components determine the perpendicular component. PNREF in polarization analysis mode has provided valuable information on the nature of magnetic coupling in GMR multilayers and helped in understanding the nature of spin dependent electron transport in these materials [21, 22].

Another class of studies to obtain the in-plane structure of surfaces and interfaces requires measurement of the intensity of off-specularly scattered neutrons (angle of incidence  $\neq$  angle of reflection) in either polarized and/or non-polarized mode. While the polarization-independent scattering determines the in-plane chemical structure, the polarization-dependent scattering determines, e.g. the magnetic roughness at the interface. It has been known widely that the quality of the thin film devices depend strongly on the in-plane structure at surfaces and interfaces and off-specular measurements can provide valuable insight in such issues (Fig. 4).

Polarizing the neutrons reduces the neutron intensity at least by a factor of two (or a factor of four, if polarization analysis is also performed).

For a polarized reflectometer the following additional components are needed:

- (a) A polarizing supermirror placed before the sample position. Reflection geometry of the polarizing supermirror is less convenient due to the deflection of the beam but in principle preferable since there is a smaller contamination by the unwanted neutron spin state. Alternatively, a polarizing monochromating multilayer or a polarizing monochromator crystal such as a Heusler crystal can be used.
- (b) A spin flipper (either DC or RF): An RF flipper is preferable since there are no components in the beam and even a white beam can be flipped. However, a DC Mezei flipper takes up much less space along the beam (10 mm as opposed to  $\sim 300$  mm for an RF flipper)
- (c) A guide field of the order of 1–2 mT is required to maintain the polarization along the instrument beam path.

## SUMMARY

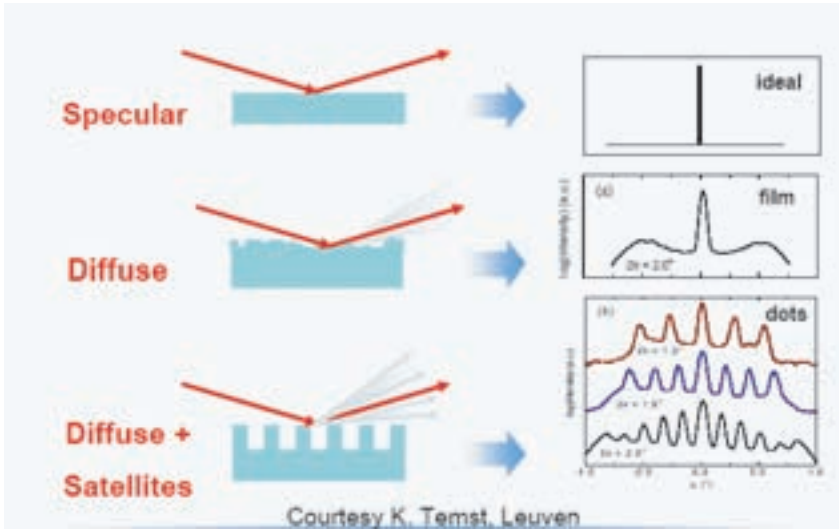


FIG. 4. Off-specular scattering from non-ideal surfaces.

Polarization analysis can be performed either by another polarizing supermirror placed after the sample or by a  $^3\text{He}$  spin filter, in combination with a second spin flipper.  $^3\text{He}$  spin flippers are convenient because a large angular range (important only for off-specular measurements) can be covered. They can be used over a limited wavelength range for TOF instruments also. To achieve good polarization efficiency, however, a considerable price in intensity has to be paid.

## 6. CHOICE OF DETECTOR

If the sample is perfectly flat and smooth, then the reflected beam will be entirely specular, i.e.  $\theta_{\text{in}} = \theta_{\text{out}}$  as shown in Fig. 5.

Information about the in-plane structural variation is found as a function of  $2\theta$  at constant  $\theta_{\text{in}}$  or outside of the reflection plane. The  $2\theta$  spectrum can be most efficiently recorded with a one or two dimensional, position sensitive detector (1D-PSD). If one has a single detector, then a scan of the detector angle without moving the sample would measure the off-specular scattering. Unfortunately, these scans take a long time to complete and so this arrangement may not be suitable, especially if the sample/instrument is not stable in time. Background should also be measured in an off-specular position, which could be confused with real off-specular signal from the sample if the full

## SUMMARY

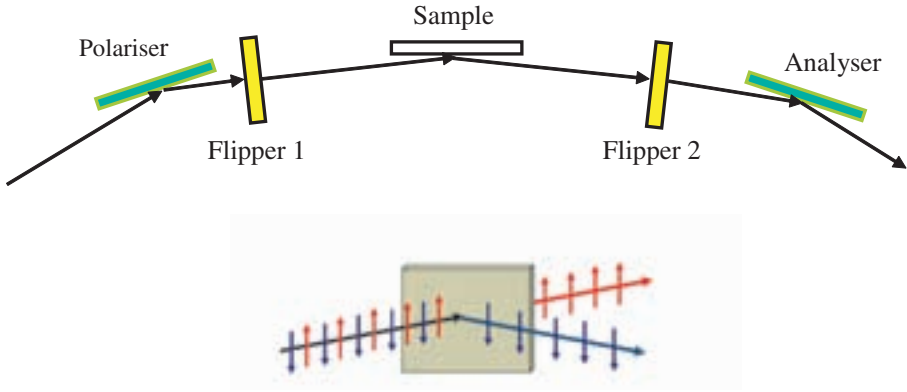


FIG. 5. General layout of a polarized neutron reflectometer measuring four combinations of incoming and outgoing polarization. Below is a schematic showing the transmitted and reflected polarization from a supermirror polarizer.

picture is not seen with a multidetector. An area multidetector is needed if the beam is large (often due to focusing) and a simultaneous measurement of an off-specular signal is required. This type of detector can often be prohibitively expensive but the advantage of capturing the specular and the off-specular signal simultaneously corresponds to a high effective gain in reducing measurement time. When off-specular scattering is to be studied extensively it can be advantageous in terms of neutron flux to implement one of the emerging neutron spin echo techniques [23].

## 7. SAMPLE ENVIRONMENT

The range of user experiments will dictate the sample environments required for the instrument. Often there is a need to vary temperature and the magnetic field but more specific requirements depend on the type of sample, as shown in Table 2.

## 8. DATA ANALYSIS AND SOFTWARE

### 8.1. Data sets

A unique analysis of specular reflection data require full knowledge (modulus and phase) of the complex reflection coefficient  $R(Q)$ . However,

## SUMMARY

TABLE 2. TYPICAL TYPES OF SAMPLE ENVIRONMENT USED IN NREF EXPERIMENTS

Experiment	Sample environment
Solid/liquid interfaces: polymers, surfactants	Silicon single crystal block with Teflon water bath. Variable temperature water bath: 10–80 deg. sample changer.
Biological samples	Controlled humidity cell.
Electrochemistry	Conducting substrate (doped Si or metal coated Si) combined with solid/liquid cell Potentiostat
Magnetic thin films and multilayers	Cryomagnet (9T 1.5K) cryostat (1.5–300K) Electromagnet (1T) Permanent magnets (0.5T) Dilution insert (40 mK)
Solid interfaces	Furnace (2000K)
Multiple samples	Sample changer
Air liquid	Langmuir trough

standard reflectometers provide only the reflectivity  $r(Q) = |R(Q)|^2$ . The increased use of polarized neutron reflectometry for the study of magnetic properties will result in additional polarization measurements of the reflected beam. Nevertheless, even in the case of complete polarization measurements, there remains one phase undetermined [24]. There are essentially two possibilities to overcome this so-called phase problem of specular reflection:

- (i) Determination of the phase of  $R(Q)$ ;
- (ii) Modelling and fitting the variable parameters.

Although several methods for the phase determination were proposed [24–29], none of them has reached the level of actual application. At present analyses of reflectivity data are exclusively performed via the ansatz of a realistic parameterized model and subsequent optimization of the adjustable parameters.

Modern reflectometers are increasingly capable to measure also in off-specular mode which provides information on the lateral structure as well as on the surface roughness. Theoretical description of off-specular reflection is much more involved and essentially on the level of the Distorted Wave Born Approximation (DWBA). However, this approach suffices because the off-specular signal is several orders of magnitude smaller than the specular

reflection. Rigorous results on uniqueness or the phase determination have not been tackled so far.

## 8.2. Retrieval of the scattering length density profile

As mentioned above, the knowledge of the reflection coefficient  $R(Q)$  allows the retrieval of the scattering length density profile uniquely via inverse scattering techniques [28] or modelling. The former yields model independent results, but is not applicable for standard reflectometer data sets because of the missing phase information. In general modelling is applied, which provides the most flexible way to analyse the reflectivity data. This flexibility concerns the ansatz of the model (with variable parameters) as well as the additional data, which are taken into account simultaneously in the optimization procedure, e.g. X ray reflectivity data from the same sample. In addition, specular and off-specular data can be considered together. The price to be paid for this flexibility is the loss of control on the uniqueness of the procedure. In addition, due to the model assumptions one introduces a bias in an uncontrolled way, which might hamper to find new interesting structures.

The quality of the data analysis relies not only on the use of a realistic model, but also on the optimisation criterion and the procedures applied. There are essentially two methods for optimization: (a) the least square technique; and (b) the method of maximum entropy. Both the methods operate via multiple solutions of the direct reflection problem. Since most of the samples consist of well defined layers, the transfer matrix [31–34] or the super matrix formalism [35] is applied. Today there exists a comprehensive collection of software tools, often specialized for certain instruments, for the analysis and visualization of reflectometry data. Many of these program packages are available on the Internet (see Appendix II) or can be requested from the author(s).

In most cases the optimization of the open parameters of the model is performed via a  $\chi^2$  fit to the measured data. The criterion to judge the quality of reproduction at given parameter set  $\mathbf{a}$  is usually given by

$$\chi^2 = \sum_{j=1}^{N_j} w_j \sum_{i,l}^{N_i} (O_j^{\text{exp}}(i) - O_j^{\text{mod}}(i, \mathbf{a})) (M^{-1})_{il} (O_j^{\text{exp}}(l) - O_j^{\text{mod}}(l, \mathbf{a}))$$

where  $O_j^{\text{exp}}(i)$  and  $O_j^{\text{mod}}(i, \mathbf{a})$  are the experimental and the model value of the  $j$ th observable at the argument value  $i$ . Here  $M$  is the experimental covariance matrix

## SUMMARY

$$M_{ii} = \langle \Delta r(Q_i) \Delta r(Q_i) \rangle$$

which provides the experimental uncertainties. However in most analyses only the variance  $\sigma_j^{\text{exp}}(i) = \Delta^2 O_j^{\text{ex}}(i)$  stemming from the statistical uncertainties is used in the least square fit. Although this procedure is well defined the relative weight between different ( $j$ ) measured quantities is a question of subjective judgement.

### 8.3. Error analyses and covariance matrix

An essential step in the analysis of reflectivity data is the determination of the uncertainties in the reflectivities. A good error analysis implies a precise determination of the background as well as other systematic errors. The total error of the reflectivity measurement is given by

$$\Delta^2 r(Q) = \Delta^2 r_{\text{stat}} + \Delta^2 r_{\text{syst}} \quad (\text{Ref. [36]})$$

Complete information about uncertainties is given by the covariance matrix,

$$M_{ij} = \langle \Delta r(q_i) \Delta r(q_j) \rangle$$

which is not determined in most experiments.

At the beginning of the analyses one has usually only coarse knowledge of the sample and therefore the parameters of the model are not well known. In the optimization process the code is looking for the route of deepest descent (of  $\chi^2$ ) to find the optimal parameter set. Although these modified Newton algorithms are very effective, there is no guarantee that the method converges to the physical solution because there are in general many local minima in the hypersurface defined by  $\chi^2$ . Statistical significance is reached if the optimal parameter set leads to  $f = \chi^2_{\text{min}} / (N - M) \lambda I$ , where  $N$  is the number of data points and  $M$  is the number of variable parameters.

Following standard statistics [37], the least squares fit leads to the covariance matrix of the parameter uncertainties

$$\langle \Delta a_i \Delta a_j \rangle = \alpha_{ij}^{-1} f$$

where

$$\alpha_{ij} = \frac{1}{2} \frac{\partial^2 \chi^2}{\partial a_i \partial a_j}$$

## SUMMARY

Via error propagation one obtains the errors in the profile. In principle one may decrease the best  $\chi^2$ -value by increasing the number of parameters, thus increasing the flexibility of the model. In general, such an increase in flexibility results in correlations between the parameters. Thus, some eigenvalues vanish and lead to a significant increase of the error bars. In order to obtain reasonable uncertainties one must apply a reasonable regularization procedure. Two possibilities are: (i) the parametric regularization (reduction of the number of parameters); and (ii) the statistical regularization [38], which includes a priori knowledge in a statistical way.

At the end it should be mentioned that the uncertainties in the profile give an idea about the relative reliability of the reflectivity profile. But it is difficult to associate a probability content with the variances because of the highly non-local relationship between the model parameters and the profile.

## 9. CONCLUSIONS AND RECOMMENDATIONS

- NREF has been identified as an important tool for many areas of science that are currently studied as well as having potential for new applications. The use of NREF should therefore be supported and the availability of this technique at more neutron sources should be encouraged.
- The activity will be enhanced by measures to support transfer of knowledge and training. Fellowships to enhance mobility between existing centres of expertise and new facilities would be useful.
- Exchange of information on the performance and the availability of components such as monochromators, polarizers, sample environments, choppers and data analysis would be useful.
- Collaborations among the developing countries are recommended for promoting NREF. There is active development of both hardware and experimental methodology that will be enhanced by cooperative exchange of information and collaboration between facilities.
- Instrumentation at smaller neutron sources provides innovative test beds for development of NREF techniques.
- Neutron reflectometers are simple instruments and important training tools for neutron science. They are therefore to be considered as a high priority for neutron sources.

## SUMMARY

## REFERENCES

- [1] BROWN, A. S., HOLT, S. A., REYNOLDS, P. A., PENFOLD, J., WHITE, J. W., Growth of highly ordered thin silicate films at the air-water interface, *Langmuir* **14** (1998) 5532.
- [2] BRENNAN, T., HUGHES, A.V., ROSER, S. J., MANN, S., EDLER, K.J., Concentration dependent formation mechanism in mesophase silica surfactant films, *Langmuir* **18** (2002) 9838.
- [3] SATO, M., ABE, K., Interface magnetization of Fe-SiO multilayer film studied by neutron Bragg reflection, *Solid State Commun.* **26** (1978) 95.
- [4] CHENG, L., et al., Pd Polarization and interfacial moments in Pd-Fe multilayers, *Phys. Rev. B* **69** (2004) 1444031.
- [5] FRITZSCHE, H., TEMST, K., VAN BAEL, M.J., Recent Res. Devel. Appl. Phys. **6** (2003) 105.
- [6] FELCHER, G.P., KAMPWIRTH, R.T., GRAY, K.E., FELICI, R., Polarized neutron reflections: A new technique used to measure the magnetic field penetration depth in superconducting niobium, *Phys. Rev. Lett.* **52** (1984) 1539.
- [7] MONSOUR, A., et al., Magnetic field penetration into the high temperature superconductor  $\text{YBa}_2\text{Cu}_3\text{O}_{7-x}$ , *Physica B* **156** and **157** (1989) 867.
- [8] HAN, S.W., et al., Distribution of vortices in Nb/Al multilayers studied by spin-polarised neutron reflectivity and magnetization, *Physica B* **336** (2003) 162.
- [9] AKPALU, Y.A., SATIJA, S.K., BALSARA, N.P., Suppression of lateral phase separation in polyolefin thin blend films, *Macromolecules* **34** (2001) 1720.
- [10] WESLEY, R.D., et al., Hydrodynamic layer thickness of a polybase brush in the presence of Salt, *Langmuir* **16** (2000) 4467.
- [11] KENT, M.S., MAJEWSKI, J., SMITH, G.S., LEE, L.T., SATIJA, S.K., Tethered chains in poor solvent conditions: An experimental study involving Langmuir diblock copolymer monolayers, *J. Chem. Phys.* **110** (1999) 3553.
- [12] KOGA, T., et al., Density induced swelling of polymer thin films in carbon-dioxide, *Phys. Rev. Lett.* **89** (2002) 125506.
- [13] LU THOMAS, in *Physical Chemistry of Biological Interfaces* (BASKIN, A., NORDE, W., Eds), Dekker, New York (2000).
- [14] FRAGNETO, G., Neutron reflectivity at the solid/liquid interface: example of applications in biophysics, *J. Phys. Condens. Matter* **13** (2001) 4973.
- [15] KRUEGER, S., et al., Investigation of hybride bilayer membranes with neutron reflectometry: probing the interactions of melittin, *Langmuir* **17** (2001) 511.
- [16] JOHNSON, S.J., et al., Coupling of spectrin and polylysine to phospholipid monolayers studied by specular reflection of neutrons, *Biophys. J* **60** (1991) 1017.
- [17] CUBITT, R., FRAGNETO, G, D-17: The new reflectometer at the ILL, *Appl. Phys. A* **74** (2002) S329.
- [18] CSER, L., FÜZI, J., RIECSANSZKY, L., Gy. TÖRÖK, Polarized neutron reflectometer at the Budapest research reactor, *Appl. Phys. A* **74** (Suppl) (2002) 8213.

## SUMMARY

- [19] NUNEZ, V., et al., Improvements to the polarized-neutron reflectometer CRISP, *Physica B* **241** (1998) 148.
- [20] JAMES, M., et al., A new neutron reflectometer at Australia's HIFAR research reactor, *Nucl. Instrum. Methods Phys. Res.* **A536** (2005) 165.
- [21] SCHREYER, A., et al., Direct observation of non-collinear spin structures in Fe Cr (100) superlattices using spin-polarised neutron reflectivity, *Physica B* **198** (1994) 173.
- [22] SCHREYER, A., et al., Oscillatory exchange coupling in Co-Cu (111) superlattices, *Phys. Rev. B* **47** (1993) 15334.
- [23] MAJOR, J., et al., Combining of neutron spin echo and reflectivity: A new technique for probing surface and interface order, *Physica B* **336** (2003) 8.
- [24] KASPER, J., LEEB, H., LIPPERHEIDE, R., Phase determination in spin-polarized specular reflection, *Phys. Rev. Lett.* **80** (1998) 2614.
- [25] LEEB, H., KASPER, J., LIPPERHEIDE, R., Determination of the phase in neutron reflectometry by polarization measurements, *Phys. Lett. A* **239** (1998) 147.
- [26] MAJKRZAK, C.F., BERK, N.F., Exact determination of the phase in neutron reflectometry, *Phys. Rev. B* **52** (1995) 10827.
- [27] DE HAAN, V.O., VAN WELL, A.A., ADENWALLA, S., FELCHER, G.P., Retrieval of phase information in neutron reflectometry, *Phys. Rev. B* **52** (1998) 10831.
- [28] AKTOSUN, T., SACKS, P., Inversion of reflectivity data for nondecaying potentials, *SIAM J. Appl. Math.* **60**, 1340 (2000); Phase recovery with nondecaying potentials, *Inverse Problems* **16** (2000) 821.
- [29] LEEB, H., GRÖTZ, H., KASPER, J., LIPPERHEIDE, R., Complete determination of the reflection coefficient in neutron specular reflection by absorptive nonmagnetic media, *Phys. Rev. B* **63** (2000) 45414.
- [30] LIPPERHEIDE, R., REISS, G., LEEB, H., FIEDELDEY, H., SOFIANOS, S.A., Solution of the inverse scattering problem in specular reflection, *Phys. Rev. B* **51** (1995) 11032.
- [31] MENDIRATTA, S.K., BLUME, M., Dynamical theory of thermal neutron scattering. I. Diffraction from magnetic crystals, *Phys. Rev. B* **14** (1976) 144.
- [32] FELCHER, G.P., et al., Polarized neutron reflectometer: A new instrument to measure magnetic depth profiles, *Rev. Sci. Instrum.* **58** (1987) 609.
- [33] BLUNDELL, S.J., BLAND, J.A.C., Polarized neutron reflection as a probe of magnetic films and multilayers, *Phys. Rev. B* **46** (1992) 3391.
- [34] MAJKRZAK, C. F., Polarized neutron scattering methods and studies involving artificial superlattices, *Physica B* **156** and **157** (1989) 619.
- [35] RÜHM, A., TOPERVERG, B.P., DOSCH, H., Supermatrix approach to polarized neutron reflectivity from arbitrary spin structures, *Phys. Rev. B* **60** (1990) 16073.
- [36] FRÖHNER, F.H., Assigning uncertainties to scientific data, *Nucl. Sci. Eng.* **126** (1997) 1.

## SUMMARY

- [37] BEVINGTON, P.R., Data Reduction and Error Analysis for Physical Sciences, McGraw-Hill, New York (1969).
- [38] TURCHIN, V.F., KOZLA, V.P., MALKEVICH, M.S., The use of mathematical-statistics methods in the solution of incorrectly posed problems, Physics-Uspokhi **13** (1971) 681 [Russian original, Usp. Fiz. Nauk. **102** (1970) 345].

## SUMMARY

## BIBLIOGRAPHY

BUCKNALL, D.G., HIGGINS, J.S., Neutron Reflection Studies of Polymer–Polymer Interfaces,

<http://users.ox.ac.uk/~dgmbuck/people/bucknall/research/NREF.htm>

DAILLANT, J., GIBAUD, A. (Eds), X-ray and Neutron Reflectivity: Principles and Applications, Springer, Berlin. (1999).

DOSCH, H., AI USTA, K., LIED, A., DREXEL, W., PEISL, J., Rev. Sci. Instrum. **63** (12) (1992) 5533.

DOSCH, H., Critical Phenomena at Surfaces and Interfaces: Evanescent X-Ray and Neutron Scattering, Springer, New York (1992).

HIGGINS, J.S., BENOIT, H., Polymers and Neutron Scattering Oxford University Press, Oxford (1996).

LEKNER, J., Theory of Reflection, Nijhoff, Dordrecht (1987).

Neutron Reflectivity Principles — Description of Basic Theory from LLB,

<http://www-llb.cea.fr/menl/ref/reflecto/reflecto1.html>

NORM BERK'S Surface Roughness Page,

<http://rrdjazz.nist.gov/staff/nfb/nxnsr.html>

PENFOLD, J., WEBSTER, J.R.P., BUCKNALL, D.G., Neutron Reflection from Hydrogen/Deuterium Containing Materials,

[http://www.isis.rl.ac.uk/largescale/crisp/documents/neut\\_refl\\_HD.htm](http://www.isis.rl.ac.uk/largescale/crisp/documents/neut_refl_HD.htm)

SEARS, V.F., Neutron Optics, Oxford University Press, Oxford (1989)

SQUIRES, G.L., Introduction to the Theory of Thermal Neutron Scattering, Cambridge University Press, Cambridge (1978).

STUDSVIK, A Brief General Introduction to the Reflection Technique,

<http://www.studsvik.uu.se/education/reflectintro1.htm>

THOMAS, R., A Simple Introduction to Neutron Reflectivity, Oxford University,

<http://physchem.ox.ac.uk/~rkt/techniques/NREFmain.html>.

## SUMMARY

### Annex I

#### NREF FACILITIES – CURRENT AND PLANNED

Facility	Country	Instrument	Sample orientation
ANSTO	Australia	HIFAR Reflectometer	Horizontal
ANSTO	Australia	Platypus Reflectometer (Project for OPAL reactor)	Horizontal
BENSC	Germany	V6 Reflectometer	Horizontal
BENSC	Germany	V14 Reflectometer	Vertical
BRR, KFKI	Hungary	REF	Vertical
Chalk River	Canada	C5	Vertical
Chalk River	Canada	D3 (under construction)	Vertical
Demokritos	Greece	TOF (under construction)	Horizontal
Dhruva	India	PNREF	Vertical
ETTR-2	Egypt	Reflectometer (NG1A) (Project)	Horizontal
FRM2 Munich	Germany	MatSci-R (Project)	Horizontal
FRM2 Munich	Germany	REFSANS (Project)	Horizontal
FZ Jülich	Germany	HADAS	Vertical
GKSS	Germany	TOREMA	Vertical
ILL	France	ADAM	Vertical
ILL	France	D16	Vertical
ILL	France	D17	Vertical
ILL	France	HORIZON (Project)	Horizontal
IPNS	USA	POSY I	Vertical
IPNS	USA	POSY II	Vertical
IRI Delft	Netherlands	ROG	Horizontal
ISIS	UK	CRISP	Horizontal
ISIS	UK	SURF	Horizontal
ISIS	UK	INTER	Horizontal
ISIS	UK	offSPEC	Horizontal
ISIS	UK	polREF	Horizontal
JAERI	Japan	MINE	Vertical
JINREF, Dubna	Russian Fed.	REFLEX-P	
JINREF, Dubna	Russian Fed.	REFLEX-N	
JINREF, Dubna	Russian Fed.	SPN	Vertical

## SUMMARY

Facility	Country	Instrument	Sample orientation
KEK, KENS	Japan	ARISA	Horizontal
KEK, KENS	Japan	Pore	Vertical
LANSCE	USA	SPEAR	Horizontal
LLB	France	DESIR	Horizontal
LLB	France	EROS	Horizontal
LLB	France	PRISM	Vertical
MIT Reactor	USA	4DH4 Reflectometer	
MURR	USA	Reflectometer	
NIST	USA	AND/R	Vertical
NIST	USA	NG1 Reflectometer	Horizontal
NIST	USA	NG7 Reflectometer	Horizontal
ORNL-HFIR	USA	HB3A/Mirror Reflectometer	Vertical
ORNL-SNS	USA	Liquids Reflectometer (project)	Horizontal
ORNL-SNS	USA	Magnetism Reflectometer (project)	Vertical
PIK, PNPI	Russian Fed.	REVERAN (project)	Horizontal
RINSC	USA	Reflectometer	Variable
Risø	Denmark	TAS8 Two-circle Reflectometer	Vertical
Risø	Denmark	TAS9 Liquids Reflectometer	Horizontal
SINQ, PSI	Switzerland	AMOR	Horizontal
SINQ, PSI	Switzerland	TOPSI	Vertical
Studsvik, NFL	Sweden	Reflectometer (project)	

\* Only the incident beam is polarized.

Geometry means the sample plane, i.e. vertical geometry is a horizontal reflection plane.

Catalogue of neutron reflection facilities on the Internet,

<http://www.studsvik.uu.se/research/NREF/reflect.htm>

## SUMMARY

### Annex II

#### COMPUTER PROGRAMS FOR DATA ANALYSIS

The following list provides information about computer programs used for the analysis of NREF data. In some cases copies of the software are made available to other users. The Internet pages may provide further details.

- Neutron Reflection Analysis DRYDOC and LPROF by Adrian Rennie  
<http://www.ch.kcl.ac.uk/kclchem/staff/arr/drydoc.htm>
- AFIT written by Paul Thirtle (3.1) is available from Oxford  
<http://physchem.ox.ac.uk/~rkt/links.html>
- Description of Norm Berk's programs and papers  
<http://rrdjazz.nist.gov/staff/nfb/NREF.html>
- Description by Jeff Penfold of programs at ISIS  
<http://www.isis.rl.ac.uk/largescale/crisp/documents/datareduction.htm>
- SURFace – A Package for Analysis of Reflectivity Data, J. R. P. Webster and S. Langridge, RAL  
<http://www.isis.rl.ac.uk/largescale/surf/technical/surface.htm>
- Neutron reflection analysis programs used at the ILL  
[http://www.ill.fr/lss/data\\_treatment/REF\\_analysis.html](http://www.ill.fr/lss/data_treatment/REF_analysis.html)
- Winfit and Superfit Software for X-Ray Reflectivity, Polarized Neutron Reflectivity and Off-specular Polarized Neutron Scattering, A. Rühm, J. Major, B. Toperverg, MPI f. Metallforschung, Stuttgart, Germany  
[http://www.mf.mpg.de/en/abteilungen/dosch/software/software\\_en.shtml](http://www.mf.mpg.de/en/abteilungen/dosch/software/software_en.shtml)
- Calculate neutron reflectivity on the Internet. Alan Munter has provided an Internet site at the NIST Center for Neutron Research  
<http://www.ncNREF.nist.gov/resources/reflcalc.html>
- NIST reflectivity analysis packages:  
[http://www.ncNR.nist.gov/programs/reflect/data\\_reduction/software/](http://www.ncNR.nist.gov/programs/reflect/data_reduction/software/)
- Reflec95 (for W95/NT) and ReflecMCA (Mathematica) programs for simulation of reflection from magnetic layers available at the LLB, Saclay, France  
<http://www-llb.cea.fr/prism/programs/programs.html>
- Description of Parrat32 for multilayer reflectivity calculation and fits. Available from BENSCH, Germany.
- Description of SERF Spreadsheet Software from the University of Delaware  
<http://www.che.udel.edu/SERF/>
- Homepage for GUIDE/WALL programs to calculate transport in neutron guides and reflectivity of interfaces. These are written by H.M.

## SUMMARY

Shimizu (RIKEN) and Y. Suda (Hokkaido University).

<http://stj.riken.go.jp/~shimizu/nfl/guide/>

– IMD – IDL package by D.L. Windt for optical reflectivity calculations

<http://cletus.phys.columbia.edu/~windt/idl/imd/>

– A program for analysing grazing incidence small angle X-ray scattering on nanostructures by R. Lazzi, F. Leroy, C. Revenant-Brizard and G. Renaud, Grenoble.

[http://www.esrf.fr/computing/scientific/joint\\_projects/IsGISAXS/isgisaxs.htm](http://www.esrf.fr/computing/scientific/joint_projects/IsGISAXS/isgisaxs.htm)

# PRINCIPLES OF REFLECTOMETRY WITH REACTORS AND PULSED SOURCES

J. PENFOLD

ISIS, Rutherford Appleton Laboratory,

Chilton, Didcot,

Oxfordshire, United Kingdom

## Abstract

The use of the specular reflectivity of neutrons for the study of surfaces and interfaces is briefly reviewed. The main features and advantages of the techniques are introduced and discussed. There is a strong emphasis on the experimental requirements and constraints imposed by the technique, and these are discussed in the context of both reactor and pulsed neutron sources.

## 1. INTRODUCTION

Specular reflectivity of neutrons is in essence a surface depth profiling technique which provides directly information about concentration and composition profiles in a direction perpendicular to the surface or interface. Its application to a wide range of problems in surface science has been extensively reviewed [1, 2]. It is in many ways analogous to optical interference or ellipsometry, and more directly equivalent to X ray reflectivity. Phenomenologically, it is equivalent to the situation for the reflection of electromagnetic radiation where the electric vector is perpendicular to the plane of incidence [3], and theoretically it can be treated either using classical thin film optics [4], or using scattering theory [5]. Neutron reflectometry has a number of features which makes it particularly attractive as a surface probe. It can probe length scales from a few angstroms to approximately 3000 Å. The ability to manipulate the refractive index, through D/H isotopic substitution, provides access to detailed structural information, and helps greatly with the uniqueness of interpretation. It is a penetrating probe, and so access to buried and complex interfaces is tractable. In addition to the nuclear interaction, there is a magnetic contribution to the refractive index and spin polarized reflectivity provides information about magnetic moment distributions in thin films. Measurements can be performed in situ, and the technique (unlike many other surface probes) is non-destructive. However, the technique does require optical quality

surfaces, and neutron fluxes (in comparison with X rays and light) are such that measurement times are longer and sample sizes need to be correspondingly larger. However, the clear advantages of the technique often outweigh those constraints and the technique has been applied in recent years to study a wide range of problems in soft matter, biological surfaces and interfaces, magnetic thin films and multilayers, and in electrochemistry: areas which all encompass the broad remit of surface science.

## 2. REFRACTIVE INDEX

The specular reflectivity of neutrons at a surface or interface can be described in the same way as electromagnetic radiation with the electric vector perpendicular to the plane of incidence [3], such that the refractive index can be expressed as:

$$n = \frac{k_1}{k_0} \tag{1}$$

that is, the ratio of the wave vectors ( $2\pi/\lambda$ ) in the two media at the interface (see Fig. 1(a)).

The refractive index can be expressed as:

$$n = 1 - \lambda^2 A - i\lambda B \tag{2}$$

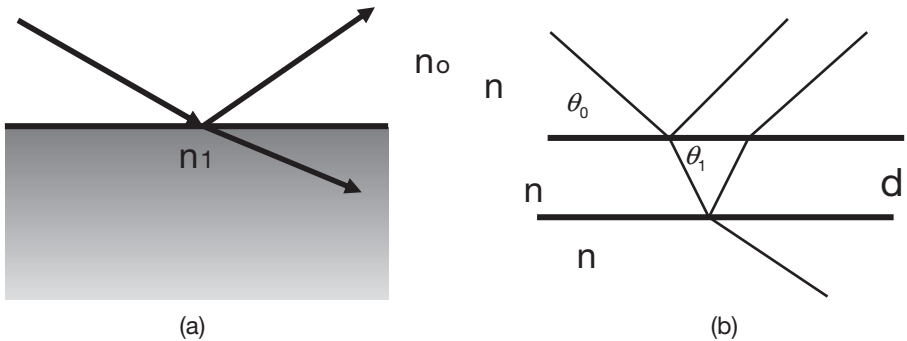


FIG. 1. Reflection geometry for (a) simple interface and (b) thin film.

## PRINCIPLES OF REFLECTOMETRY

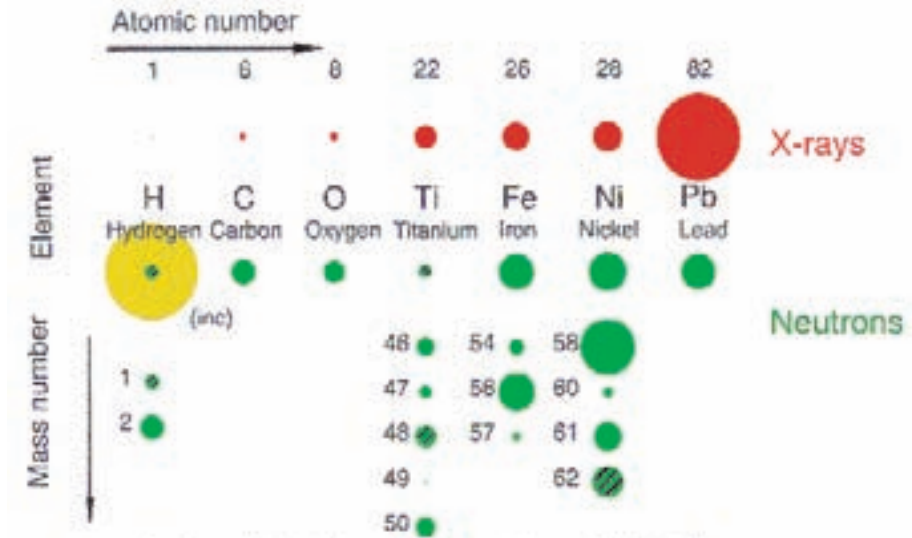
where for neutrons  $A = Nb/2\pi$  and  $B = N(\sigma_a + \sigma_i)/4\pi$ ,  $b$  is the neutron scattering length, and  $\sigma_a$ ,  $\sigma_i$  are the absorption and incoherent scattering cross-sections. For X rays  $A = N\lambda^2 z R_e/2\pi$  and  $B = \lambda\mu/4\pi$ , where  $z$  is the atomic number and  $\mu$  the linear absorption coefficient. Figure 2 shows schematically the variation in neutron scattering length with increasing atomic number for some selected elements, highlighting the difference between what neutrons and X rays measure.

For most materials,  $b$  is positive and so the refractive index is usually  $<1.0$ , that is, total external reflection is usually observed. From Snell's law we can write:

$$n_1 \sin\theta_1 = (n_1^2 - n_0^2 \cos^2\theta_0)^{1/2} \quad (3)$$

At total reflection  $\theta_0 = \theta_c$  and  $\theta_1 = 0.0$  ( $\cos\theta_1 = 1.0$ ) and so:

$$\cos\theta_c \sim 1 - Nb\lambda^2/2\pi \quad (4)$$



The diameters of the circles shown scale with the scattering amplitude  $f_x(\sin\theta = 0)$  for x-rays, and  $b_{\text{coh}} \cdot 10$  for neutrons. Hatching indicates negative scattering amplitudes.

FIG. 2. Schematic representation of neutron and X ray scattering length variation with element, for selected elements.

where  $\theta_c$  is the critical glancing angle. Table 1 lists some typical values of  $\theta_c$  and  $\sigma_a$  for some common elements.

### 2.1. Specular reflectivity

The specular reflectivity from a simple interface can be expressed in terms of scattering theory or from thin film optics (Fresnel's law) by the approximation:

$$R(q) = \frac{16\pi^2}{q^4} \Delta\rho^2 \tag{5}$$

where  $q$  is the wave-vector transfer in the perpendicular direction ( $z$ ), given by  $q=k_0-k_1=4\pi\sin\theta_0/\lambda$ , and  $\Delta\rho$  is the change in scattering length density across the interface. Within the Born approximation [5] the full expression is:

$$R(q) = \frac{16\pi^2}{q^2} \left| \int \rho(z) e^{-iqz} dz \right|^2 \tag{6}$$

where  $\rho(z)$  is the scattering length density profile in the direction perpendicular to the interface. From thin film optics [4] Fresnel's law can also be written exactly as:

$$R = \left| \frac{n_0 \sin\theta_0 - n_1 \sin\theta_1}{n_0 \sin\theta_0 + n_1 \sin\theta_1} \right|^2 \tag{7}$$

TABLE 1. SELECTED VALUES OF  $\theta_c$  AND  $\sigma_a$

Material	$\theta_c$ (deg/Å)	Material	$\sigma_a$ (barn)
Ni	0.1	Si	0.17
Si	0.047	Cu	3.78
Cu	0.083	Co	37.2
Al	0.047	Cd	2520
D <sub>2</sub> O	0.082	Gd	29400

Note that for most elements,  $s_a$  is small and so the imaginary component of the refractive index can usually be ignored.

A typical reflectivity profile, for a  $\lambda/10$  optical flat, is shown in Fig. 3(a).

For a single thin film at the interface (see Fig. 1(b)), an exact expression for the reflectivity can be expressed in terms of thin film optics as Ref. [4]:

$$R(q) = \left| \frac{r_{01} + r_{12}e^{-2i\beta}}{1 + r_{01}r_{12}e^{-2i\beta}} \right|^2 \quad (8)$$

where  $r_{ij} = \frac{(p_i - p_j)}{(p_i + p_j)}$ ,  $p_i = n_i \sin \theta_i$ , and  $\beta_i = \frac{2\pi}{\lambda} n_i d_i \sin \theta_i$

Figure 3(b) shows a typical reflectivity profile for a thin film of approximately 1000 Å in thickness. The period of the interference fringes obtained is inversely proportional to the film thickness, and the visibility of the fringes is affected by resolution, sample quality and the ‘contrast’ (the refractive index of the film relative to air and the substrate).

## 2.2. Surface roughness

The treatment of reflectivity so far assumes optically perfect surfaces. In practice, on some length scale, all surfaces have imperfections (see Fig. 4). If the curvature of the surface is  $\ll$  coherence length of the radiation then the surface appears to be wavy; and affects the data in a way similar to resolution. If, on the other hand, the curvature is  $\gg$  coherence length, then the surface appears to

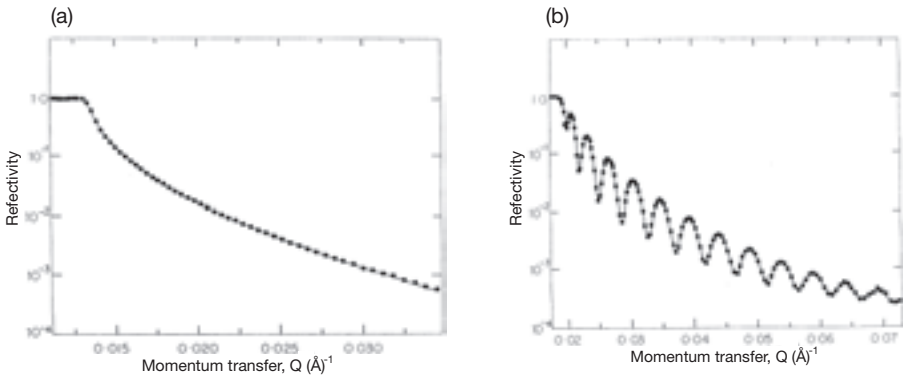


FIG. 3. (a) Reflectivity for a  $\lambda/10$  optical flat; (b) 1200 Å deuterated Langmuir–Blodgett film on silicon.

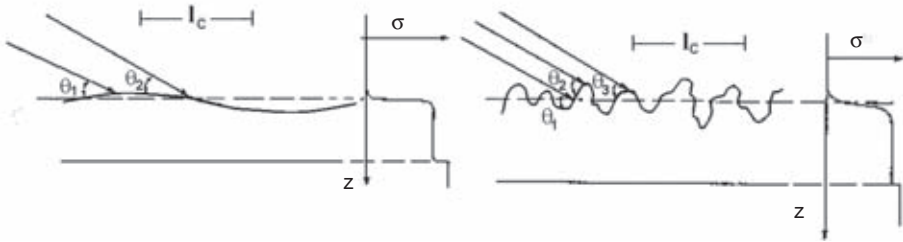


FIG. 4. Schematic representation of surface roughness with respect to curvature and coherence length.

be rough (or diffuse). Indeed in terms of the specular reflectivity, roughness and diffusiveness are equivalent and can be treated as affecting the reflection coefficients by a Debye–Waller type factor, as demonstrated by Nevot and Croce [6] such that:

$$r_{ij} = \frac{(p_i - p_j)}{(p_i + p_j)} \exp -0.5q_i q_j \sigma^2 \quad (9)$$

where  $\sigma$  is the rms roughness.

In very broad terms, the roughness causes the reflectivity to fall off faster with increasing  $q$  than the  $q^{-4}$  from Fresnel's law, and dampens interference fringes at high  $q$  values. The reflectivity data shown in Figs 3(a) and 3(b) for a simple interface and for a thin film have been modelled by incorporating roughness as described in Eq. (9). In practice, the effects can be more complex and depend upon the relative values of refractive index across the interfaces.

### 2.3. More complex structures, multilayers

Analysis of a more complex structure at an interface, whether it is a discreet multilayer structure, or some gradient of refractive index that can be conceptually treated as a series of layers, can be done straightforwardly by an extension of the methods developed for thin film optics, for example, see Born and Wolf [4]. However, a convenient method is that of Abeles [7] where in optical terms a characteristic matrix per layer is defined from the relationship between the electric vectors in successive layers such that:

$$C_{ij} = \begin{bmatrix} e^{i\beta_i} & r_j e^{i\beta_i} \\ r_j e^{-i\beta_i} & e^{-i\beta_i} \end{bmatrix} \quad (10)$$

The reflectivity then arises from the product of the matrices from each layer. This is an extremely convenient way to formulate this problem, as a roughness term (of the form in Eq. (9)) can be included at each interface. Figure 5 shows this applied to the reflectivity data from a 15 bilayer Ni/Ti multilayer sample.

#### 2.4. Thin layers and partial structure factors

The kinematic approximation [8] provides a convenient framework for the analysis of the structure and adsorption of the thin layers that are typical of adsorption of surface active species at interfaces (see Eq. (6)). Considering as an example the distribution of the components of a surfactant monolayer at the air-water interface (Fig. 6), we can write the scattering length density distribution in terms of the number density distributions,  $n(z)$ , of the individual components, such that:

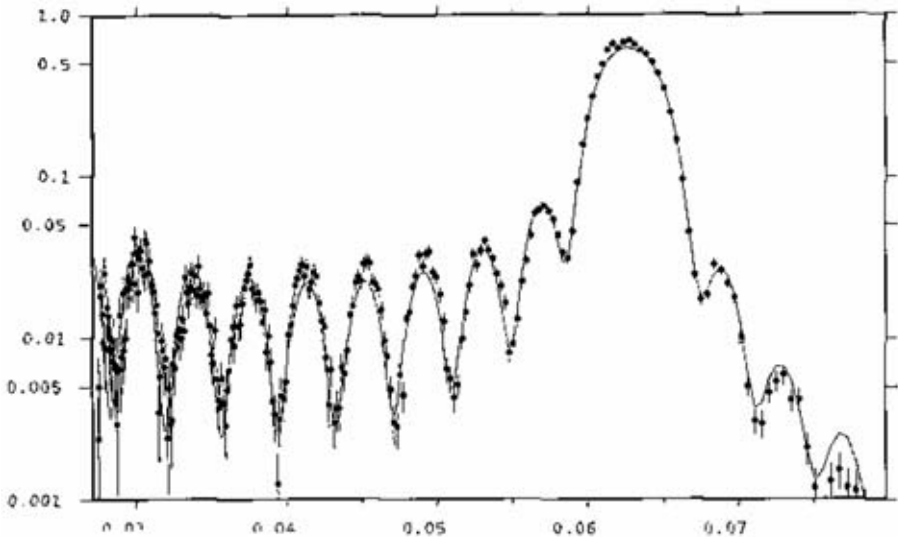


FIG. 5. Reflectivity for 15 bilayer Ni/Ti multilayer, in the region of a first order Bragg peak.

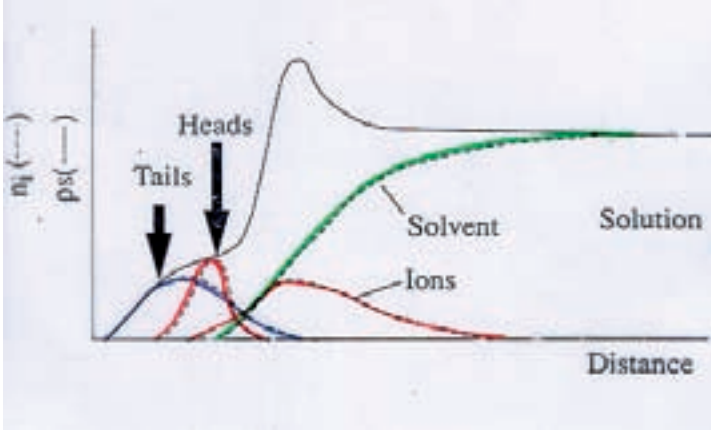


FIG. 6. Schematic representation of surfactant component distributions at the air–water interface.

$$\rho(z) = b_c n_c(z) + b_h n_h(z) + b_s n_s(z) \quad (11)$$

where c, h and s refer to the alkyl chain, head group and solvent, and  $b_i$  is the scattering length of that component. Substituting into Eq. (6) gives:

$$R = \frac{16\pi^2}{q^2} \times \left[ b_c^2 h_{cc} + b_h^2 h_{hh} + b_w^2 h_{ww} + 2b_c b_h h_{ch} + 2b_c b_w h_{cw} + 2b_h b_w h_{hw} \right] \quad (12)$$

The partial structure factors [8],  $h_{ij}$ , are one dimensional Fourier transforms of  $n_i(z)$ , where the self terms ( $h_{cc}$ ,  $h_{hh}$  and  $h_{ss}$  in Eq. (12)) describe the distributions of the individual components at the interface, and the cross-terms ( $h_{ch}$ ,  $h_{hs}$ ,  $h_{cs}$  in Eq. (12)) describe the relative positions of those distributions at the interface. In Eq. (12), six different reflectivity measurements with the different components deuterium labelled enables a solution for the  $h_{ij}$  and  $h_{ij}$  factors to be obtained and interpreted in terms of  $n_i(z)$ ; and this has been applied to a wide range of systems [9]. A particularly simple example of this is applied to determining the amount of surfactant adsorption at the air–water interface. Describing the surfactant distribution as a Gaussian yields:

$$h_{aa} = \frac{q^4}{16\pi^2} R(q) = \pi\sigma^2 \frac{\rho^2}{4} q^2 \exp(-q^2\sigma^2) \quad (13)$$

where  $\sigma$  is the Gaussian width and  $\rho$  is the density of the layer. Plotting  $\log h_{aa}$  against  $q^2$ , as shown in Fig. 7, is a straight line where the intercept at  $q(\kappa)$  is 0 is related to the adsorbed amount and the slope to the thickness of the layer.

### 3. POLARIZED NEUTRON REFLECTOMETRY

For magnetic materials magnetized in the plane, the refractive index is spin dependent (Refs [10, 11]):

$$n_{\pm}(z) = 1 - \frac{N\lambda^2}{2\pi} (b \pm C\mu) \quad (14)$$

where  $C$  is a constant, and  $\mu$  is the magnetic moment/atom. The  $\pm$  sign arises from the neutron spin being either parallel or anti-parallel to the magnetization. This gives rise to a spin dependent reflectivity [10, 11] which provides information about the distribution of magnetic moment at the surface or interface; it has been extensively used to study thin magnetic films and multilayers [12], and is discussed in more detail in related papers in these proceedings.

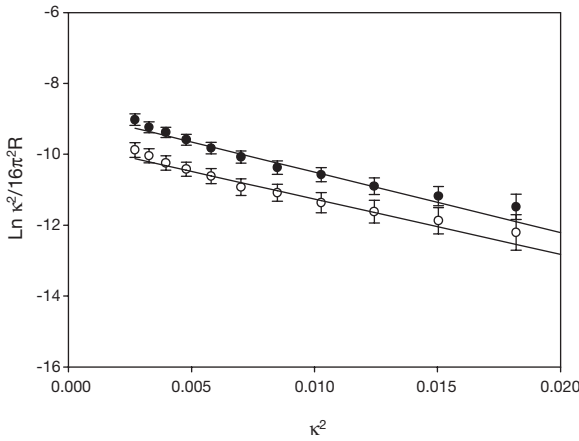


FIG. 7.  $\ln \kappa^2 / 16\pi^2 R$  versus  $\kappa^2$  for  $dC_{12}H_8$  in *n*rw and (•)  $9 \times 10^{-5} M$  and (o)  $9 \times 10^{-6} M$ , the solid lines are calculated curves assuming a Gaussian distribution.

4. OFF-SPECULAR SCATTERING

The focus of this review is specular reflectivity; however, for completeness, diffuse or off-specular scattering should be mentioned. Imperfections in the surface (such as surface roughness) and lateral inhomogeneities will result in scattering off the specular direction and provide information about these lateral inhomogeneities [13]. Figure 8 shows the definition of the scattering vectors associated with off-specular scattering, such that  $q_z = 2k\sin\theta$ ,  $q_x = k(\cos\theta_0 - \cos\theta_1\cos\psi)$  and  $q_y = k\cos\theta_0\sin\psi$ .

In the distorted wave Born approximation [13] the diffuse scattering can be written as:

$$\frac{d\sigma}{d\Omega} \approx |T_i(k_i)|^2 |T_f(k_f)|^2 S(q) \tag{15}$$

where  $S(q)$  is related to the Fourier transform of the in-plane inhomogeneity distribution.

5. INSTRUMENTATION

The essence of a neutron reflectivity measurement is to measure the variation of the reflectivity with the scattering vector,  $q_z$ , over a wide range of  $q$

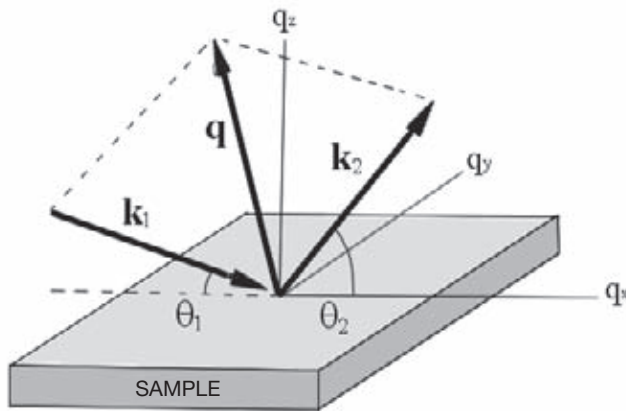


FIG. 8. Schematic representation of the geometry for specular and off-specular scattering.

## PRINCIPLES OF REFLECTOMETRY

values. This can be done at a fixed geometry using the white beam time-of-flight (TOF) method (that is, with a fixed angle of incidence and a range of neutron wavelengths) or using a monochromatic beam and a variable angle of incidence. The TOF method and the monochromatic beam method can both be used on reactor sources, but the TOF method is the natural choice for pulsed neutron sources. The SURF and CRISP reflectometers [14, 15] at ISIS use the TOF method, whereas D17 at the ILL, France [16] has both TOF and monochromatic modes. In contrast, the reactor based reflectometers at NIST, USA [17] both used the monochromatic mode.

The small angles of grazing incidence (typically in the range  $0.25\text{--}5^\circ$ ) dictate the use of fine collimation slits in the  $z$  direction and the use of relatively small beams, even for relatively large footprints ( $> 10\text{ cm}^2$ ). Intensity is usually gained by using slit geometry and by relaxing the resolution in the  $q_y$  direction. This does not, to first order, impact upon the  $q_z$  resolution but does mean that there is only usable off-specular resolution in the  $q_x$  direction. This also results in a mismatch of the out of plane and in-plane length scale that are accessible (see the earlier definition of  $q_z$ ,  $q_x$ ), with an out of plane dimension range of approximately  $10\text{--}4000\text{ \AA}$  and an in-plane length scale of approximately  $1\text{--}50\text{ }\mu\text{m}$ .

Other papers in these proceedings (i.e. Cubitt and Rühm) describe in detail the specification and design features of some reactor based instruments, but the focus here is on the pulse source instrumentation at ISIS [18]. The schematic layouts of CRISP [14] and SURF [15] reflectometers at ISIS are shown in Figs 9(a) and 9(b), and both instruments have horizontal geometry for convenient access to liquid surfaces.

The principal features on both instruments are broadly similar, except that CRISP has the added complexity of a polarized neutron mode [19]. The typical wavelength range usable on SURF is  $0.7\text{--}6.7\text{ \AA}$ , covering a  $q_z$  range of approximately  $2 \times 10^{-3}$  to  $0.5\text{ \AA}^{-1}$ ;  $q_{\text{min}}$  will be limited to 0.05 if only the intrinsic angle of incidence ( $1.5^\circ$ ) is used. The angle of incidence can be varied for both liquid and solid surfaces, and typically for studies of the liquid–solid interface three different angles,  $0.35$ ,  $0.8$  and  $1.8^\circ$  are used (see Fig. 10).

The value of  $q_{\text{max}}$  ( $d_{\text{min}}$ ) is determined predominantly by the sample background, and is, typically, approximately  $1.5 \times 10^{-6}$  for  $\text{D}_2\text{O}$ , approximately  $4 \times 10^{-5}$  M for  $\text{H}_2\text{O}$ , and  $\ll 10^{-6}$  for silicon. The higher backgrounds for the aqueous samples arise from incoherent scattering. For the solid–liquid interface reducing the liquid layer thickness to  $<10\text{ }\mu\text{m}$  is practical, and this will reduce the background by approximately  $\times 10$ . Beyond that the background is limited predominantly by air scattering after the sample and ultimately by the detector quiet counts.

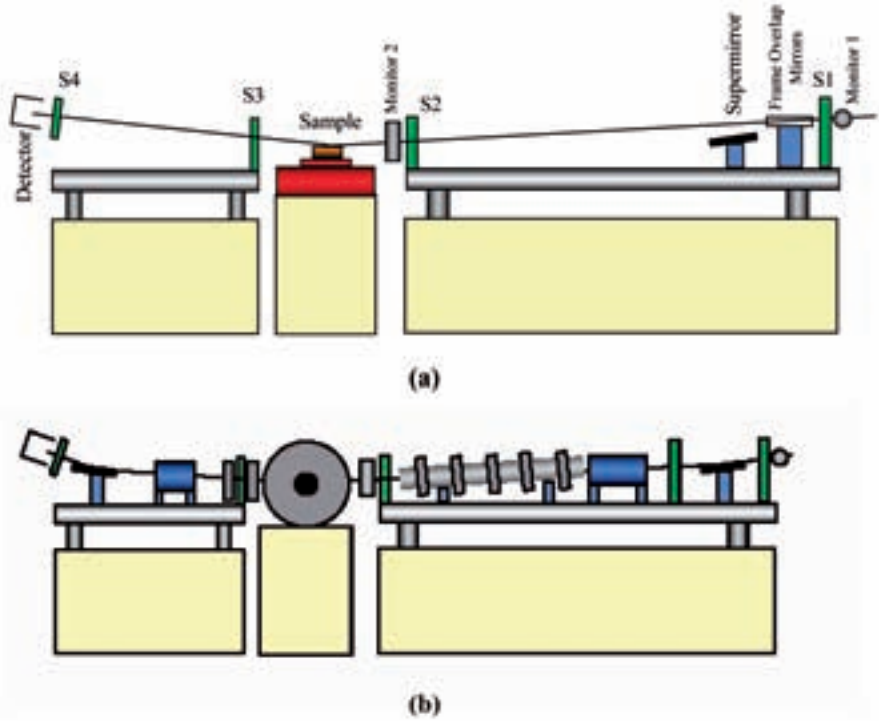


FIG. 9. Schematic layout of (a) SURF and (b) CRISP reflectometers at ISIS.

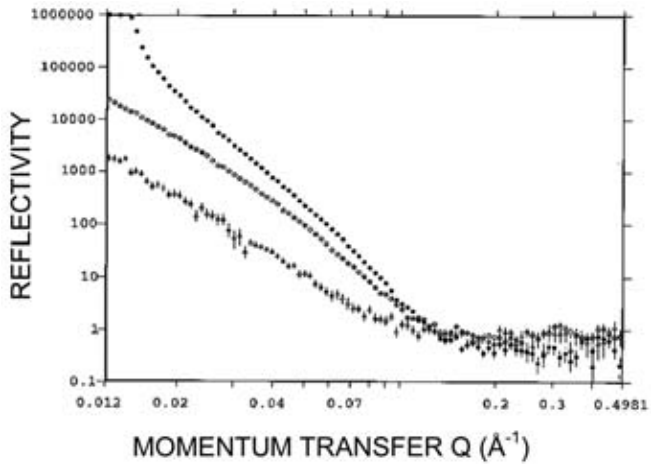


FIG. 10. Reflectivity for silicon-water interface for angles of 0.35, 0.8 and 1.8°, and different solvent contrasts, from top to bottom  $\text{Si}/\text{D}_2\text{O}$ ,  $\text{Si}/\text{H}_2\text{O}$ ,  $\text{Si}/\text{cmSi}$ .

## PRINCIPLES OF REFLECTOMETRY

The value of  $d_{\max}$  is determined by the resolution in  $q$ ,  $\Delta q/q$ .  $\Delta q/q$  has two contributions, such that:

$$\frac{\Delta q^2}{q^2} = \frac{\Delta t^2}{t^2} + \frac{\Delta \theta^2}{\theta^2} \quad (16)$$

where  $\Delta t/t$  is the ratio of the neutron pulse width to the TOF (essentially the  $\Delta\lambda/\lambda$  contribution), and  $\Delta\theta/\theta$  is the angular divergence from the collimation. For the current pulsed source instruments, the  $\Delta\theta/\theta$  term dominates and  $\Delta t/t$  is intrinsically small. Resolution has to be carefully chosen as a compromise between intensity and information content, as an increased  $\Delta q/q$  will for thicker films smear the region adjacent to the critical edge and dampen interference fringes (see Fig. 11).

The measured intensity has to be corrected for detector efficiency, incident beam spectral distribution and background, and set on an absolute scale, such that:

$$R(q(\lambda, \theta)) = f \frac{[I_d(\lambda) - b_d(\lambda)] \varepsilon_m(\lambda)}{[I_m(\lambda) - b_m(\lambda)] \varepsilon_d(\lambda)} \quad (17)$$

where  $d$ ,  $m$  refer to the detector and beam monitor,  $b$  is the measured background, and  $f$  is a scale factor. The effect of these factors is shown as a function of wavelength in Fig. 12.

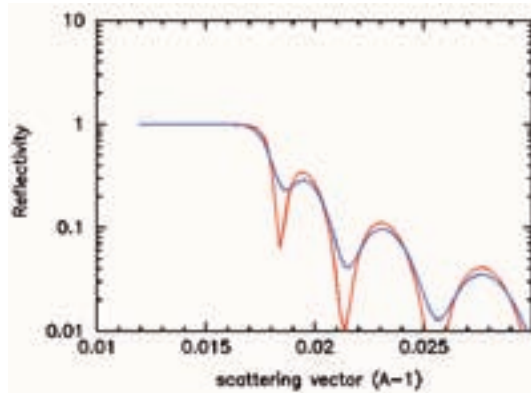


FIG. 11. Calculated reflectivity curves for 1000 Å film on silicon with  $\Delta\theta/\theta$  of (red) 2% and (blue) 6%.

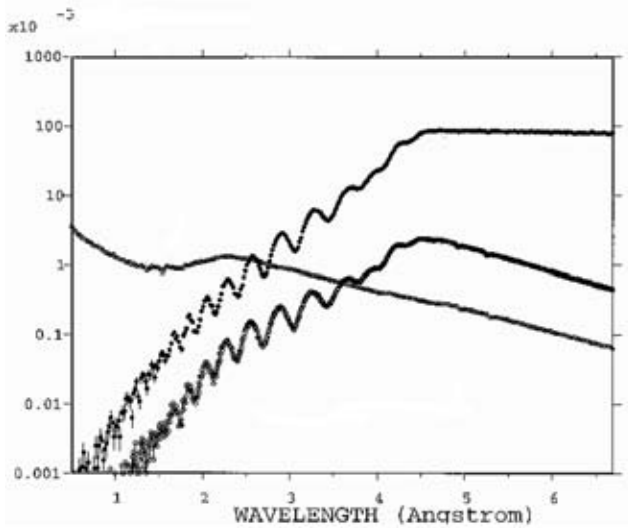


FIG. 12. Wavelength dependence of the raw data, monitor spectrum and corrected reflectivity.

The incident beam spectral shape is measured using a low efficiency detector (monitor) placed immediately after the final collimation slit, and before the sample. The scale factor is determined by reference to a known surface (usually  $D_2O$ ) or by reference to the 'direct' beam. The background is ideally measured by offsetting the detector to an off-specular angle, or by integration on an area detector. To exploit some of the analysis methods (for example, the partial structure factor approach), accurate absolute data with minimal systematic errors ( $< 1\%$ ) is required.

To fully exploit the technique and instrumentation, sophisticated sample environment equipment is required as routine, and at ISIS a wide range of equipment which includes liquid troughs, Langmuir troughs, sample changers for liquid and solid samples, liquid–solid cells, furnaces, electrochemical cells and cells with controlled environments (for liquid–liquid studies and other measurements), are available.

## 6. CONCLUSIONS AND FUTURE PROSPECTS

From our experience at ISIS some of the key areas of future scientific application include the study of kinetics and non-equilibrium effects, multi-component mixtures, surface and near-surface structures and their relationship

## PRINCIPLES OF REFLECTOMETRY

to the bulk structure, access to surface ordering effects and lateral structure, and the study of more complex or difficult interfaces and environments. This inevitably imposes constraints and demands upon the current and future instrumentation; requiring more intensity and access to a broader simultaneously measured  $q$  range, an improved signal/noise ratio, and access to shorter length scale in-plane.

At ISIS, the Second Target Station (TS-2) [20], with a design optimized for cold neutron production and a broad range of accessible wavelengths (10 Hz frequency), will provide flux gains over the existing target station (due to optimized coupled moderators, and the use of more efficient moderator materials available only on lower power targets). This will provide an ideal location for the next generation of reflectometers at ISIS. Three reflectometers will form part of the 'day one' instrument suite, due to be fully operational in mid-2008. These will include INTER for the study of chemical surfaces and interfaces, polREF (a polarized neutron reflectometer optimized for the study of magnetic thin films) and offSPEC optimized for off-specular studies. The instruments will all use a broad wavelength range to provide a simultaneously broad  $q$  range with improved intensity ( $>\times 10$ ) due to both source and instrument factors. offSPEC is a unique instrument providing access to a wide  $q_z$ ,  $q_x$  range and with the incorporation of neutron spin echo [21–23] to provide  $q_y$  access in the same  $q$  range as  $q_z$ . This will in particular open up many new areas of interesting science.

The combination of spin echo techniques with reflectivity (using the neutron spin precession to encode path length, as pioneered by Rekveldt and others [23]), provides the opportunity to distinguish between specular and off-specular, measure the specular reflectivity with a highly divergent beam, and most importantly to measure the off-specular in the  $q_y$  plane over length scales comparable to the  $q_z$  direction. This promises to be one of the major developments of the technique.

## REFERENCES

- [1] PENFOLD, J., THOMAS, R.K., The application of the specular reflection of neutrons to the study of surfaces and interfaces, *J. Phys. Condens. Matter* **2** (1990) 1369.
- [2] RUSSELL, T.P., X-ray and neutron reflectivity for the investigation of polymers, *Mater. Sci. Rep.* **5** (1990) 171.
- [3] GOLDBERGER, M.L., SEITZ, F., Theory of the refraction and the diffraction of neutrons by crystals, *Phys. Rev.* **71** (1947) 294.
- [4] BORN, M., WOLF, E., *Principles of Optics*, Pergamon Press, Oxford (1970).

- [5] CROWLEY, T.L., et al., The use of contrast variation in the specular reflection of neutrons from interfaces, *Colloids Surf.* **52** (1991) 85.
- [6] NEVOT, L., CROCE, P., Utilisation of specular x-ray reflection, diffuse x-ray reflection or planar x-ray reflection to study thin films or surfaces, *Rev. Phys. Appl.* **15** (1980) 761.
- [7] HEAVENS, O.S., *Optical Properties of Thin Films*, Dover, Mineola, NY (1955).
- [8] LU, J.R., et al., Detailed surface structure of the hydrocarbon chain at the air/water interface: Neutron reflection from hexadecyltrimethyl ammonium bromide, *J. Phys. Chem.* **99** (1995) 8233.
- [9] LU, J.R., THOMAS, R.K., Surfactant layers at the air/water interface: Structure and composition, *Adv. Colloid Interface Sci.* **84** (2000) 142.
- [10] BLAND, J.A.C., et al., Polarised neutron reflection as a probe of magnetic thin films and multilayers, *Phys. Rev. B* **46** (1992) 3391.
- [11] FELCHER, G.P., et al., Polarised neutron reflectometer: A new instrument to measure magnetic depth profiles, *Rev. Sci. Instrum.* **58** (1992) 609.
- [12] ZABEL, et al., Polarised neutron reflectivity and scattering studies of magnetic heterostructures, *J. Phys. Condens. Matter* **15** (2003) 5505.
- [13] SINHA, S.K., et al., X-ray and neutron scattering from rough surfaces, *Phys. Rev. B* **38** (1988) 2297.
- [14] PENFOLD, J., et al., A time of flight reflectometer for surface and interfacial studies, *J. Phys. E* **29** (1987) 1411.
- [15] PENFOLD, J., et al., Recent advances in the study of chemical surfaces and interfaces by specular neutron reflection, *J. Chem. Soc., Faraday Trans.* **93** (1997) 3899.
- [16] CUBITT, R., et al., The new reflectometer at the ILL, *Appl. Phys. A* **74** (2000) 5329,  
<http://www.ill.fr/yellowbook/D17/D17web/>
- [17] <http://www.ncnr.nist.gov/instruments/ng7refl/>; [ng1refl/](http://www.ncnr.nist.gov/instruments/ng1refl/)
- [18] <http://www.isis.rl.ac.uk/>
- [19] FELICI, R., et al., A polarised neutron reflectometer for studying surface magnetism, *Appl. Phys. A* **45** (1988) 169.
- [20] A second target station at ISIS: New opportunities for inter-disciplinary research using neutrons, CCLRC Int Rep, RAL-TR-2000-032 (2000),  
<http://www.isis.rl.ac.uk/targetstation2/>
- [21] PYNN, R., et al., Does beam divergence matter in neutron reflectometry, *Physica B* **336** (2003) 1.
- [22] MAJOR, R., et al., Combining neutron spin echo and reflectivity: A new technique for probing surface and interface order, *Physica B* **336** (2003) 8.
- [23] REKVELDT, T., et al., Novel SANS instrument using neutron spin echo, *Nucl. Instrum. Methods Phys. Res. Sect. B* **114** (1996) 366.

# **SPECULAR NEUTRON REFLECTIVITY**

## ***Applications to soft matter***

J. PENFOLD  
ISIS, Rutherford Appleton Laboratory,  
Chilton, Didcot,  
Oxfordshire, United Kingdom

### **Abstract**

The applications of neutron reflectivity for the study of surfaces and interfacial problems in soft matter are discussed. Recent studies of the adsorption of surfactants, surfactant mixtures and polymer-surfactant mixtures are discussed, and examples of studies in thin polymer films and interfaces are presented. The examples cited illustrate the current trends in the study of complex mixtures, complex interfaces and in kinetics. The potential for future studies in the nature of surfaces in equilibrium with a bulk structure, surface ordering (the effects of confinement and flow), a wider range of liquid–solid and liquid–liquid interfaces, lateral surface structure and non-equilibrium effects (kinetics).

### 1. INTRODUCTION

In recent years, neutron reflectivity has emerged as a major technique for the study of surfaces and interfaces, with a wide range of applications in soft matter [1, 2]. These applications include adsorption of surfactants [3] and polymers at a variety of interfaces, the nature of polymer thin films and interfaces [4, 5], bio-surfaces and membranes [6]. The ability to explore such an extensive range of applications in soft matter arises from some key advantages of the technique compared with other surface analysis techniques. The ability to manipulate ‘contrast’ or refractive index by isotopic substitution (primarily H/D), the ability to access buried interfaces, and the non-evasive nature of the technique are all important features. A further and important aspect of these areas of application is the applied nature of the studies, with particular relevance to detergency, personal care products, cosmetics, adhesives, lubrication, sensors and devices, and coatings.

2. SURFACTANT ADSORPTION AT INTERFACES

The use of neutron reflectivity to study surfactant adsorption at the air-solution interface has been extensively reviewed [1, 2]; where the technique provides not only information about the adsorbed amount, but also detailed structural information about the adsorbed layer. For a deuterium labelled surfactant in null reflecting water, nrw, (a 0.088 mole fraction  $D_2O/H_2O$  mixture with a scattering length density of 0, a refractive index for neutrons of unity) the specular reflectivity arises only from the adsorbed layer. This is shown in Fig. 1(a) for  $C_{12}E_8$  ( $dC_{12}hE_8$ ) at surfactant concentrations of  $9 \times 10^{-6}$  and  $9 \times 10^{-5}$  M. To good approximation [7] the adsorbed layer can be described as a thin layer of uniform density, such that the thickness,  $\tau$ , and scattering length density,  $\rho$ , provide an estimate of the adsorbed amount,  $\Gamma$ ,

$$\Gamma = \frac{\rho\tau}{Na\sum b} \tag{1}$$

where  $Na$  is Avogadro's number and  $\sum b$  is the sum of scattering lengths of the surfactant molecule. Alternatively, as shown in the paper on the technique in these proceedings, it can be modelled as a Gaussian, and this is shown in Fig. 1(a). It is then straightforward to map out the adsorption isotherm, as shown in Fig. 1(b) for  $C_{12}E_8$ .

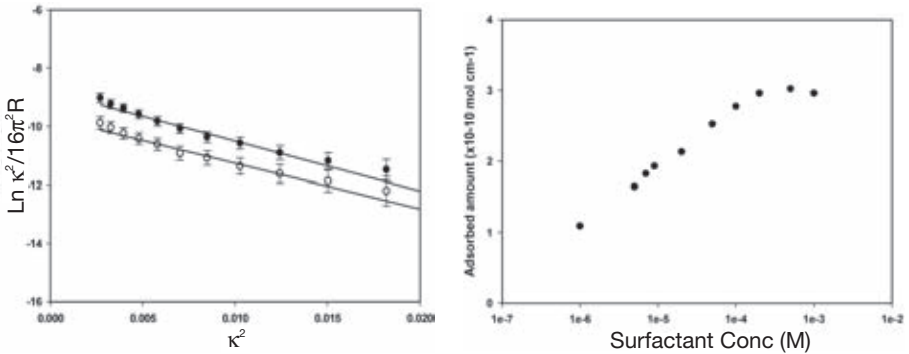


FIG. 1. (a)  $\text{Ln} \kappa^2/16\pi^2R$  versus  $\kappa^2$  for  $dC_{12}hE_8$  in nrw and (●)  $9 \times 10^{-5}$  M and (○)  $9 \times 10^{-6}$  M, the solid lines are calculated curves using a Gaussian description; (b) adsorption isotherm for  $C_{12}E_8$ , adsorbed amount,  $\Gamma$ , ( $\times 10^{-10}$  mol  $cm^{-2}$ ) as a function of surfactant concentration (M).

## SPECULAR NEUTRON REFLECTIVITY

The particularly powerful aspects of this approach are the ability to make measurements over a wide concentration range, from dilute solutions to concentration well in excess of the critical micellar concentration (cmc) [3], and to study multi-component mixtures [8]. Even in the dilute regime where techniques, such as surface tension are routine, neutron reflectivity has made some important contributions. It has demonstrated the role of divalent counterion impurities on ionic surfactant adsorption [9, 10], established the correct pre-factor for the application of the Gibbs equation for Gemini surfactants [11], and highlighted the role of wetting and de-wetting in the measurement and interpretation of surface tension data [7]. However, for surfactant mixtures, the combination of selectivity through H/D isotopic substitution and the ability to measure over a wide concentration range, has provided unique information about the mixing behaviour at the air–water interface [3]. This is illustrated in Fig. 2(a), which shows the neutron reflectivity for a binary non-ionic surfactant mixture of an equimolar solution of  $C_{12}E_3 / C_{12}E_8$ .

The three isotopically labelled combinations in nrw,  $dC_{12}hE_3 / dC_{12}hE_8$ ,  $hC_{12}hE_3 / dC_{12}hE_8$ ,  $dC_{12}hE_3 / hC_{12}hE_8$ , using an extension of Eq. (1),

$$\tau\rho = \frac{\sum b_1}{A_1} + \frac{\sum b_2}{A_2} \quad (2)$$

where for a binary mixture  $\sum b_i$ ,  $A_i$  refers to the scattering length and area/molecule of components 1 and 2, and provides a measure of the total

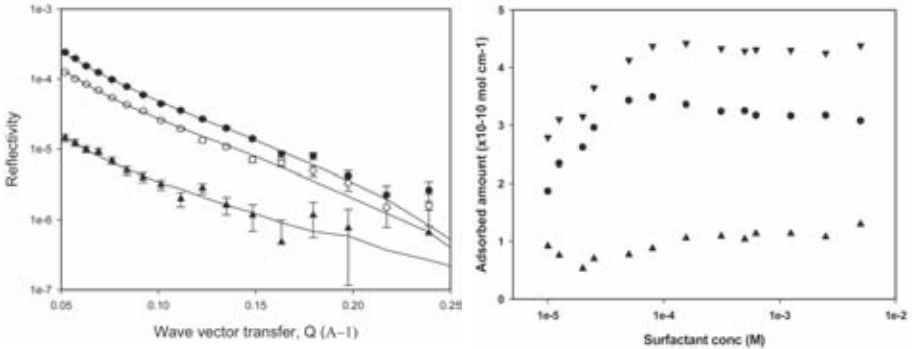


FIG. 2. (a) Specular reflectivity for  $5 \times 10^{-4} M$  50/50 mole %  $C_{12}E_3 / C_{12}E_8$  in nrw, (●)  $dd$ ,  $\tau = 19.7 \text{ \AA}$ ,  $\rho = 3.54 \times 10^{-6} \text{ \AA}^{-2}$ , (○)  $dh$ ,  $\tau = 18.7 \text{ \AA}$ ,  $\rho = 2.74 \times 10^{-6} \text{ \AA}^{-2}$ , (Δ)  $hd$ ,  $\tau = 14.1 \text{ \AA}$ ,  $\rho = 1.19 \times 10^{-6} \text{ \AA}^{-2}$ ; (b) adsorption isotherm for equimolar mixture of  $C_{12}E_3 / C_{12}E_8$  (▼) total adsorption, (●)  $C_{12}E_3$ , and (▲)  $C_{12}E_8$ .

adsorption, and the adsorption of the two components,  $C_{12}E_3$  and  $C_{12}E_8$ , respectively. The isotherm in Fig. 2(b) shows the evolution of the surface composition from below to some two orders of magnitude above the cmc. This was the first experimental verification of the abrupt change in surface composition due to the formation of mixed micelles in solution and the associated change in the monomer composition and concentration on micellization [8]. Furthermore, it illustrates the strong preference of the more surface active component,  $C_{12}E_3$ , for the interface.

A more recent example, which highlights one of the trends described earlier is the recent work of Penfold et al. [12] on the surface adsorption behaviour of the di-akyl chain cationic/non-ionic surfactant mixture of DHDAB/ $C_{12}E_6$ . This is an extreme example of surfactant mixing behaviour, in which the surface is in equilibrium with a changing bulk microstructure; and here it is imperative to understand both the surface and solution properties. Figure 3 shows the variation in surface composition with solution composition for DHDAB/ $C_{12}E_6$  in the absence and presence of electrolyte.

An extreme departure from ideal mixing and what is expected from the standard treatments of non-ideality, such as Regular Solution Theory, is observed. In the absence of electrolyte, below a solution composition of 50 mole %  $C_{12}E_6$  the surface is totally dominated by the DHDAB. The

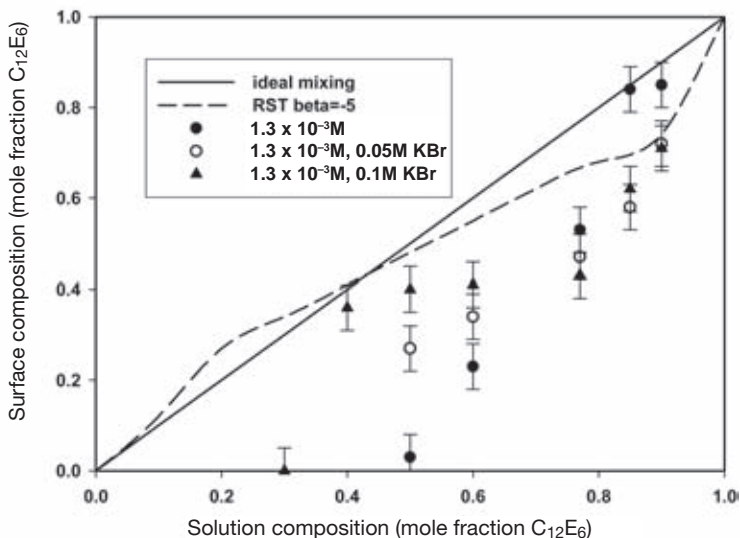


FIG. 3. Surface composition (mole %  $C_{12}E_6$ ) for  $1.3 \times 10^{-3}$  M DHDAB /  $C_{12}E_6$ , in  $D_2O$ , 0.05 M KBr, and 0.1 M KBr (symbols as indicated in the text insert in the figure).

## SPECULAR NEUTRON REFLECTIVITY

transition in surface composition at that solution composition coincides with a change in the solution microstructure, from globular (elliptical) micelles for solutions rich in the non-ionic to a lamellar phase for the cationic rich solutions. In electrolyte (0.1M KBr) the surface behaviour is somewhat different, and at intermediate solution compositions the surface composition has a plateau region. This region of constant composition at the surface coincides with a bi-phasic region in the bulk solution, with the coexistence of lamellae and micelles. The surface behaviour is hence reflecting the role of the bulk solution phase to mediate changes in the monomer concentration and composition.

For surfactant adsorption, the information available from neutron reflectivity measurements extends beyond the determination of adsorbed amounts to provide detailed structural information about the adsorbed layer. Using H/D isotopic labelling, the distributions and relative positions of the labelled fragments can be determined [13]. In the simplest case this means the head group, alkyl chain and solvent, and a range of cationic, anionic and non-ionic surfactants have been studied [2], and compared with computer simulation [14, 15]. The same approach has also been applied to binary surfactant mixtures [16]. Using more detailed labelling schemes (deuterium labelling different fragments of an alkyl or ethylene oxide chain), information about the mean conformation of the molecule at the interface can be obtained at a resolution determined by the labelling [13]. A recently published example is the study of the role of isomeric form on the adsorption of aromatic counter ions in a cationic  $C_{16}$ TAB monolayer at the air–water interface [17]. Labelling parts of the  $C_{16}$  alkyl chain and the counter ion (hydroxybenzoate in this case) enables the stoichiometry and the location of the counter ion at the interface to be determined (see Fig. 4). The volume fraction distributions in Fig. 4 show that

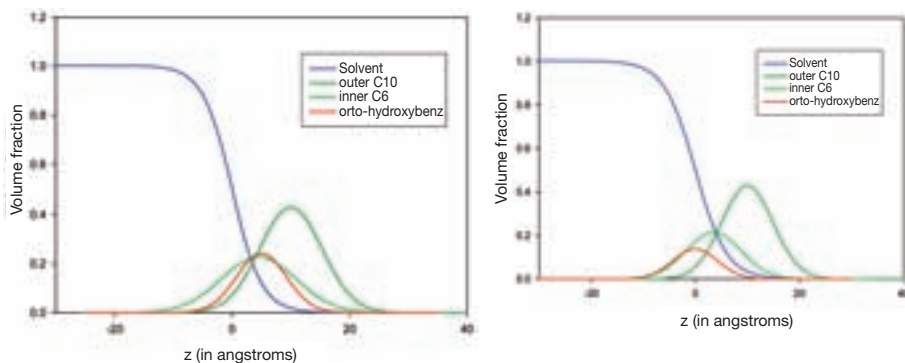


FIG. 4. Volume fraction distributions for  $C_{16}$ TAB/hydroxybenzoate at the air–water interface (see figures for annotation): (a) *ortho*-hydroxybenzoate; (b) *para*-hydroxybenzoate.

the ortho-hydroxybenzoate counter ion is located in the hydrophobic alkyl chain region, and that the number of counter ions/anion is approximately 0.85. In contrast, the para-hydroxybenzoate counter ion is located in the head group region, and there is approximately 0.5 counter ions/anion. From the simple micellar packing arguments [18] the difference in counter ion location rationalizes the different micellar behaviour, that is, the ortho isomer induces massive micellar growth, whereas the para isomer does not.

At higher surfactant concentrations, surface and near surface ordering has been observed at the air–water interface and solid–solution interfaces; consisting of micellar layers [19] and lamellar ordering [20]. This is an area that is relatively underexploited, and with the advent of new instrumentation is a potentially rich area for investigation.

At the solid–liquid interface the pattern of adsorption is fundamentally different from that observed at the air–water interface, and cooperative adsorption occurs [21]. That is, at a hydrophilic silica–solution interface the adsorption occurs at the cmc in the form of a ‘fragmented bilayer’, or a ‘flattened’ micellar structure. Neutron reflectometry can currently probe the solid–liquid interface by transmission through an upper crystalline solid phase (such as silicon, quartz or sapphire) where, in this case, the reflectivity against a predominantly  $D_2O$  solvent often provides the greatest sensitivity. This has been applied to a range of non-ionic [23] and ionic [24] surfactants, where the same deuterium labelling schemes can be used to probe more detailed structural information or to probe mixtures. Figure 3 shows an example of this approach to the study of anionic/non-ionic mixed surfactant adsorption at the hydrophilic silica–solution interface [25]. Figure 5 shows the variation in the adsorbed amount and surface composition as a function of the solution composition for the SDS/ $C_{12}E_6$  mixture. In the absence of the non-ionic surfactant, there would be no measurable adsorption of the SDS to the anionic silica surface. For solutions rich in the non-ionic surfactant  $C_{12}E_6$  the adsorption of the SDS at the interface is due to its co-adsorption with the  $C_{12}E_6$ , and by the time the solution composition is equimolar there is little or no adsorption.

This is another area that is relatively underexploited, and the systematic studies required are only just starting.

### 3. POLYMER/SURFACTANT MIXTURES AT INTERFACES

The behaviour of polymer-surfactant mixtures at the air–water interface is a good example of how neutron reflectivity has provided unique information

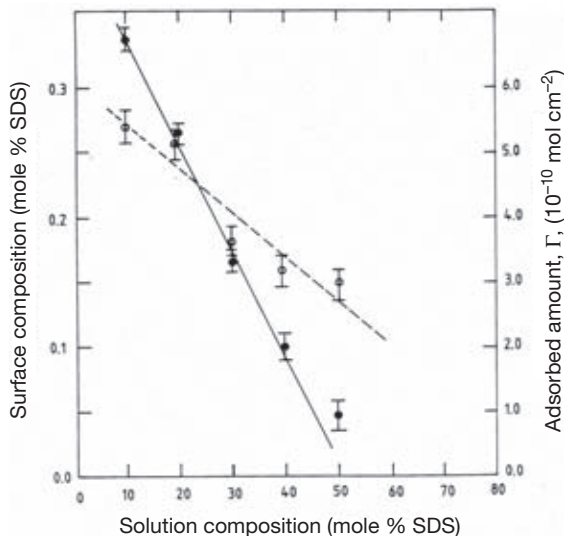


FIG. 5. Adsorbed amount and surface composition (mole fraction SDS) for  $10^{-3}$  M 20/80 SDS/ $C_{12}E_6$  at the hydrophilic silica–solution interface (o) composition (●) adsorbed amount.

about adsorbed amounts and surface structure that was not obtainable from other techniques. The solution behaviour of non-ionic polymer–ionic surfactant mixtures is relatively well understood [26]. However, the quantitative interpretation of the surface adsorption behaviour was provided by neutron reflectivity for a number of different systems, including SDS/PEO [27] and SDS/PVP [28], and was relatively straightforward. However, the strong in bulk and at the interface, resulting in surface complex formation, between the polyelectrolytes and surfactants of opposite charge result in a ‘rich’ pattern of surface tension behaviour [29–32]. These cannot be interpreted by the simple theories [26] that explain non-ionic polymer/ionic surfactant behaviour, and require neutron reflectivity measurements to unravel the complexity of behaviour. A range of different surface tension behaviour has been observed and can be rationalized in terms of the relative competition to form bulk and surface polymer-surfactant complexes [29–31]. A number of different systems have now been studied by surface tension and neutron reflectivity and include NaPSS/ $C_n$ TAB [29–32] and poly-dmdaac/SDS [32]. These two particular examples represent the extremes of behaviour studied, where in the first case surface complexes are more energetically favoured, and in the latter case both surface and bulk complexes have similar free energies. This predominance of surface complex formation in the NaPSS/ $C_n$ TAB mixtures is manifested in the formation of a

layered structure at the air–water interface in the region of concentration that corresponds to a plateau in the surface tension behaviour. This is illustrated in Figs 6(a) and (b).

#### 4. THIN POLYMER FILMS AND INTERFACES

The nature of thin polymer films and polymer–polymer interfaces is of much current interest [4, 5]. Although a wide range of techniques has been used [4, 5], neutron reflectivity, because of its selectivity through D/H isotopic substitution and the length scale of the probe, is an important tool [4, 5]. A wide range of systems and different circumstances have been studied and include the effects of confinement, the nature of the interface between miscible, immiscible and partially miscible polymers and the role of copolymers at such interfaces [4, 5]. In a fundamental study of the nature of polymer–polymer interfaces, Sferrazza et al. [33] identified and quantified the capillary wave contribution to the polymer–polymer interfacial width with some preliminary measurements on PS-PMMA bilayers as a function of polymer film thickness. The measured thickness,  $\Delta$ , is related to the intrinsic thickness and the capillary wave contribution:

$$\Delta^2 = \Delta_0^2 + \langle \Delta \zeta^2 \rangle \quad (3)$$

where  $\Delta_0$  is the intrinsic width of the interface and  $\langle \Delta \zeta^2 \rangle$  the capillary wave contribution. The short wave-vector cut-off of the capillary wave spectrum is due to the dispersion forces acting across the film, such that:

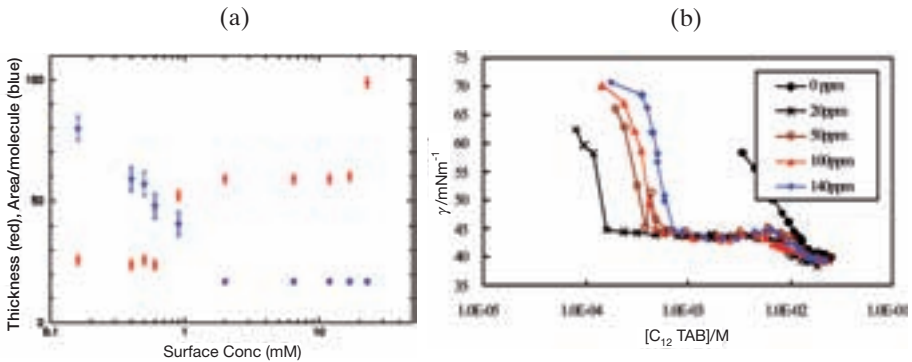


FIG. 6. (a) Variation in film thickness (red) and effective area/molecule (blue) for  $C_{14}TAB/140$  ppm NaPSS with surfactant concentration; (b) surface tension as a function of surfactant concentration for different polymer concentrations.

$$\langle \Delta \zeta^2 \rangle \frac{k_B T}{4\pi\sigma_0} \ln \frac{\left(2\pi/\Delta_0\right)^2}{\left(2\pi/\lambda_{coh}\right)^2 + \left(2\pi/a_{disp}\right)^2} \quad (4)$$

where  $\lambda_{coh}$  is the in-plane coherence length and  $a_{disp}$  the dispersion capillary length. A plot of  $\Delta$  versus Log film thickness,  $d$ , (related to  $a_{disp}$ ) shows a linear dependence which levels off when  $a_{disp} \sim \lambda_{coh}$  (see Fig. 7), confirming the theoretical approach and rationalizing the experimental data with mean field predictions.

More recently, Bucknall et al. [34], Higgins et al. [35] and Gupta et al. [36] have used the same experimental approach to probe the kinetics of interdiffusion for plasticizer ingress (280, polymer–oligomer interdiffusion [35]) and the effects of super critical  $\text{CO}_2$  on polymer interdiffusion [4, 5]. By careful choice of film thickness and the  $q$  range of the measurement, measurement times as short as 20 s have been achieved. Figure 8(a) shows the variation of the reflectivity with time for a d-PMMA (200k MW) thin film against a low molecular weight plasticizer, dioctyl phthalate. In Fig. 8(b) the variation of the PMMA film thickness with time is shown for two different plasticizers, resulting in an increase in the film thickness,  $\Delta d$ , due to the swelling of the polymer by the plasticizer ingress.

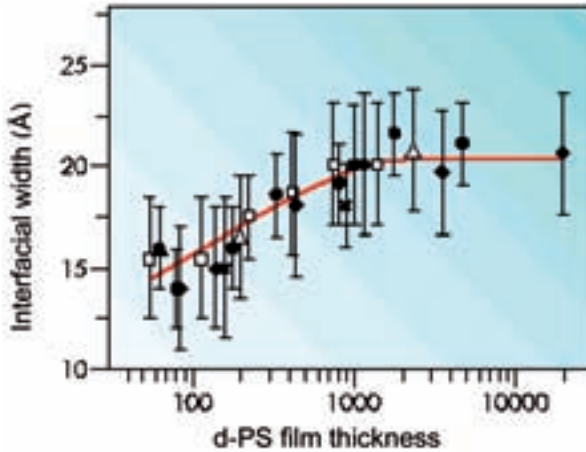


FIG. 7. Plot of  $\Delta$  versus Log film thickness,  $d$ , for d-PS/PMMA bilayers with varying PS film thickness from 50 to 10 000 Å.

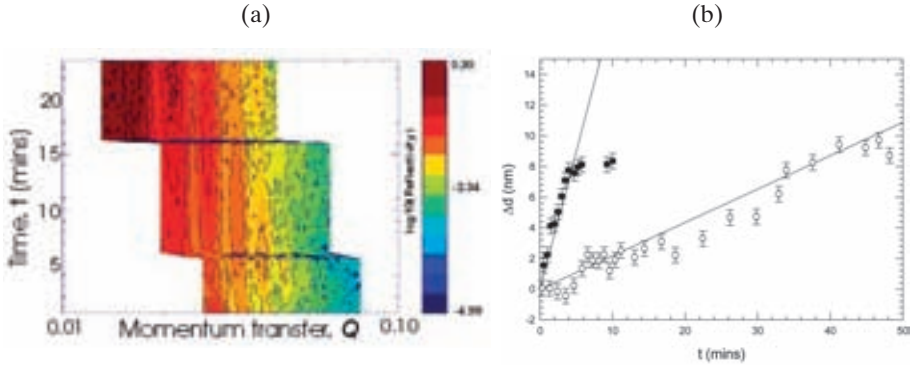


FIG. 8. (a) Reflectivity from *d*-PMMA (200k MW) thin film against the plasticizer dioctyl phthalate; (b) variation in film thickness,  $\Delta d$ , for (o) diisononyl phthalate, and (●) dioctyl phthalate.

## 5. CONCLUSIONS AND FUTURE PROSPECTS

The paper illustrates some of the trends in the study of soft matter at interfaces and surfaces by neutron reflectivity, with some recent examples of surfactant adsorption, polymer-surfactant adsorption and of the structure of thin polymer films and interfaces. In the future neutron source developments, such as the Second Target Station at ISIS [37], the SNS in the USA [38] and JPARC in Japan [39], and the development of new instrumentation, will provide new and exciting opportunities in the study of soft matter. Some of the key areas are:

- Study of interfaces in equilibrium with a complex bulk structure (simultaneous reflectivity and SANS);
- Surface and near surface ordering, due to confinement, interface and flow;
- Access to a wider range of liquid–liquid and liquid–solid interfaces;
- Investigation of lateral (in-plane) structure, arising from in-plane inhomogeneities, surface micellization, segregation and de-wetting;
- Study of non-equilibrium effects, kinetics of adsorption, surface rearrangements, dynamic surface tension;
- High throughput, to be able to cover parameter space required for multi-component mixtures in finite measurement times.

## REFERENCES

- [1] PENFOLD, J., Neutron reflectivity and soft matter, *Curr. Opin. Colloid Interface Sci.* **7** (2002) 139.
- [2] PENFOLD, J., THOMAS, R.K., Neutron and x-ray reflectivity of interfacial systems in colloid and polymer chemistry, *Curr. Opin. Colloid Interface Sci.* **1** (1995) 23.
- [3] LU, J.R., THOMAS, R.K., PENFOLD, J., Surfactant layers at the air/water interface: Structure and composition, *Adv. Colloid Interface Sci.* **84** (2000) 143.
- [4] JONES, R.A.L., RICHARDS, R.W., *Polymers at Interfaces*, Cambridge University Press, Cambridge (1999).
- [5] BUCKNALL, D.G., et al., Neutron reflectivity of polymer interfaces, *J. Phys. Chem. Solids* **60** (1999) 1273.
- [6] FRAGNETO, G., et al., Phospholipid bilayer formation at a bare Si surface: A time resolved neutron reflectivity study, *J. Phys. Condens. Matter* **16** (2004) S2469.
- [7] SIMISTER, E.A., et al., Comparison of neutron reflection and surface tension measurements of the surface excess of tetradecyltrimethyl ammonium bromide layers at the air/water interface, *J. Phys. Chem.* **96** (1992) 1383.
- [8] STAPLES, E.J., THOMPSON, L., TUCKER, I., PENFOLD, J., Effect of dodecanol on mixed non-ionic and non-ionic/anionic surfactant adsorption at the air/water interface, *Langmuir* **10** (1994) 4236.
- [9] AN, S.W., et al., Apparent anomalies in surface excesses determined from neutron reflectivity and the Gibbs equation in ionic surfactants, with particular reference to perfluorooctanoates at the air/water interface, *Langmuir* **12** (1996) 446.
- [10] LU, J.R., et al., Adsorption of dodecyl sulphate surfactants with monovalent metal counterions at the air/water interface studied by neutron reflection and surface tension, *J. Colloid Interface Sci.* **158** (1993) 303.
- [11] LI, Z.X., et al., Neutron reflectivity studies of the surface excess of Gemini surfactants at the air–water interface, *Langmuir* **15** (1999) 4392.
- [12] PENFOLD, J., et al., Surface and solution behaviour of the mixed di-alkyl chain cationic and non-ionic surfactants, *Langmuir* **20** (2004) 1269.
- [13] LU, J.R., et al., Detailed structure of the hydrocarbon chain in a surfactant monolayer at the air–water interface: Neutron reflection from hexadecyltrimethyl ammonium bromide, *J. Phys. Chem.* **99** (1995) 8233.
- [14] BOCKER, J., et al., Molecular dynamics simulation of a n-hexadecyl trimethyl ammonium chloride monolayer, *J. Phys. Chem.* **96** (1992) 9915.
- [15] TAREK, M., et al., Molecular dynamics simulation of tetradecyl trimethyl ammonium bromide monolayers at the air–water interface, *J. Phys. Chem.* **99** (1995) 1393.
- [16] PENFOLD, J., et al., The structure of the mixed nonionic surfactant monolayer of C12E3 and C12E8 at the air–water interface, *J. Colloid Interface Sci.* **2001** (1998) 223.

- [17] PENFOLD, J., et al., Adsorption of aromatic counterions at the surfactant/water interface: A neutron reflection study of hydroxybenzoate and chlorobenzoate counterions at the hexadecyl trimethyl ammonium bromide surfactant water interface, *Langmuir* **20** (2004) 8054.
- [18] ISREALACHIVILLI, J.N., et al., Theory of self assembly of hydrocarbon amphiphiles into micelles and bilayers, *J. Chem. Soc. Faraday Trans.* **72** (1976) 1525.
- [19] LU, J.R., et al., Structure of the surface of a surfactant solution above the cmc, *J. Phys. Chem.* **97** (1993) 13907.
- [20] LI, Z.X., et al., Adsorption of the lamellar phase of AOT at the solid-liquid and air-liquid interfaces, *J. Phys. Chem.* **103** (1999) 10800.
- [21] BRINK, J., TIBERG, F., Adsorption behaviour of two binary nonionic surfactant systems at the silica-water interface, *Langmuir* **12** (1996) 5042.
- [22] LEE, E.M., et al., Determination of the structure of a surfactant layer adsorbed at the silica-water interface by neutron reflectivity, *Chem. Phys. Lett.* **162** (1989) 196.
- [23] McDERMOTT, D.C., et al., Study of adsorption from aqueous solution of C12E6 on silica substrates using the technique of neutron reflectivity, *Langmuir* **8** (1992) 1204.
- [24] FRAGNETO, G., et al., Neutron reflectivity from C16TAB adsorbed on rough and smooth surfaces, *Langmuir* **12** (1996) 6036.
- [25] PENFOLD, J., et al., Adsorption of mixed anionic and nonionic surfactants at the hydrophilic silicon surface, *Langmuir* **18** (2002) 5755.
- [26] GODDARD, E.D., Polymer/surfactant interactions: Interfacial aspects, *J. Colloid Interface Sci.* **256** (2002) 228.
- [27] COOKE, D.J., et al., Interaction between PEO and monovalent dodecyl sulfates studied by neutron reflectivity, *Langmuir* **14** (1998) 1990.
- [28] PURCELL, I.P., et al., Adsorption of SWDS at surface of aqueous solution of PVP studied by neutron reflectivity, *Langmuir* **14** 1 (1998) 1637.
- [29] TAYLOR, D.J.F., et al., Adsorption of oppositely charged polyelectrolyte/surfactant mixtures: Neutron reflection from alkyl trimethyl ammonium bromides and PSS at the air-water interface: The effect of the alkyl chain length, *Langmuir* **19** (2003) 3172.
- [30] TAYLOR, D.J.F., THOMAS, R.K., PENFOLD, J., Adsorption of oppositely charged polyelectrolyte/surfactant mixtures: Neutron reflectivity from C12TAB/PSS at the air/water interface, *Langmuir* **18** (2002) 4748.
- [31] TAYLOR, D.J.F., THOMAS, R.K., HINES, J.D., HUMPHREYS, K., PENFOLD, J., Adsorption of oppositely charged polyelectrolyte/surfactant mixtures at the air/water interface: Neutron reflectivity from C12TAB/PSS and SDS/PVP, *Langmuir* **18** (2002) 9783.
- [32] PENFOLD, J., et al., Organisation of polyelectrolyte/surfactant mixtures at the air-water interface: Poly-dmdaac, SDS, C12E6, *Langmuir* **18** (2002) 5139.
- [33] SFERRAZZA, M., et al., Evidence for capillary waves at immiscible polymer/polymer interfaces, *Phys. Rev. Lett.* **78** (1997) 3693.

## SPECULAR NEUTRON REFLECTIVITY

- [34] BUCKNALL, D.G., HIGGINS, J.S., BUTLER, S.A., Early stages of oligomer-polymer diffusion, *Chem. Eng. Sci.* **56** (2001) 5473.
- [35] HIGGINS, J.S., BUTLER, S.A., BUCKNALL, D.G., Neutron reflectivity of polymer-plasticiser diffusion, *Macromolecules Symp.* **190** (2002) 1.
- [36] GUPTA, R.R. et al., Self-diffusion of polystyrene in a CO<sub>2</sub>-swollen polystyrene matrix: A real time study using neutron reflectivity, *Macromolecules* **36** (2003) 346.
- [37] A second target station at ISIS: New opportunities for inter-disciplinary research using neutrons, CCLRC Int Rep, RAL-TR-2000-032 (2000),  
<http://www.isis.rl.ac.uk/tatrgtstation2/>
- [38] <http://www.sns.gov/>
- [39] <http://j-parc.jp/>



# DESIGN OF A NEUTRON REFLECTOMETER AT A RESEARCH REACTOR

Z. TUN

National Research Council of Canada,  
Chalk River Laboratories,  
Chalk River, Ontario, Canada

## Abstract

A neutron reflectometer is a custom-built instrument optimized for measuring reflectivity of a sample consisting of one or more flat interfaces. Its components include stepper motor drives for angles and/or slits, neutron detectors for beam monitoring and signal counting, several neutron optics elements for beam tailoring, a dedicated computer for control, and a massive radiation shielding made of neutron absorbers, steel and lead. One possible interface that a user wishes to study with reflectometry could be the surface of a liquid, and hence the most general purpose reflectometer is for horizontal sample geometry. The machine then of course operates in a vertical scattering plane. Due to mechanical complexity, however, such an instrument is more challenging to build than a machine with a horizontal scattering plane. The maximum  $Q$  one could reach in the horizontal sample geometry is often quite limited. The choice between horizontal and vertical sample geometry is just an example of many issues involved in the design of a reflectometer. As for all other neutron instruments, designing a reflectometer is a balancing act between competing issues: general functionality of the machine versus complexity and cost; high neutron flux versus as-low-as-possible background; resolution versus the extent of the dynamic  $Q$  range, etc. No universal solution exists as all research reactors are different and each presents a unique situation.

## 1. INTRODUCTION

The data acquisition system needed to perform neutron reflectometry (NREF) is a custom designed instrument specifically for a reactor or a spallation neutron source. Two fundamentally different kinds of reflectometers are in common use. The first kind operates with a monochromatic neutron beam (constant  $\lambda$ ) while the second is a time-of-flight instrument that performs scans by sweeping  $\lambda$  contained in polychromatic neutron pulses. For a pulsed neutron source the sweeping- $\lambda$  type is intrinsically suitable. For a continuous source, both types could be built, either by using a monochromating device (e.g. a crystal monochromator) or with a system of beam choppers. We note here

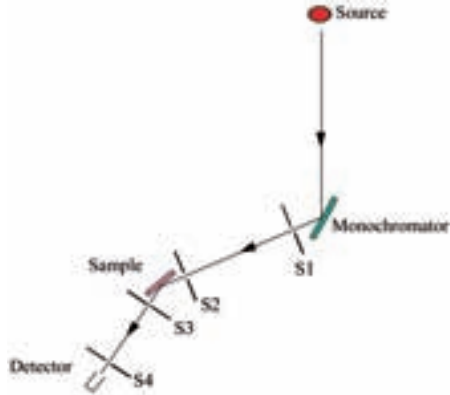


FIG. 1. Essential components of a fixed- $\lambda$  NREF.

that most spallation neutron sources are pulsed sources, whereas most research reactors operate in continuous mode.

A reflectometer is basically a diffractometer optimized for measuring reflectivity of a flat sample containing one or more interfaces. Figures 1 and 2 schematically show the main components of the two types of reflectometers described above. The components include either a monochromator or choppers, stepper motor drives for angles and/or slits, neutron detectors for beam monitoring and signal counting, several neutron optics elements for beam tailoring, a dedicated computer for control, and a massive radiation shield made of neutron absorbers, steel and lead mostly at the front end of the instrument but also for the detector. The computer is usually loaded with a special program so that the user could specify scans in terms of scattering vector  $Q$ . The program also performs housekeeping tasks, such as sample environment control and data storage.

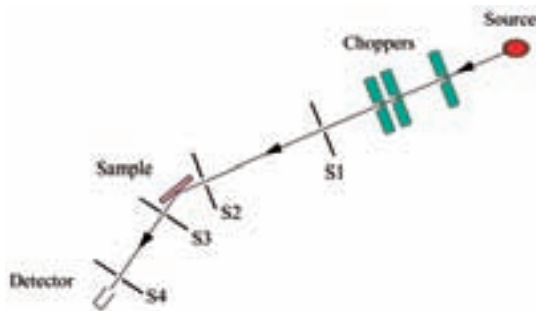


FIG. 2. Essential components of a sweeping- $\lambda$  NREF.

## DESIGN OF A NEUTRON REFLECTOMETER

As for all other neutron instruments, designing a reflectometer requires making choices based on competing issues, for example, general functionality of the machine versus complexity and cost; high neutron flux versus as-low-as-possible background; resolution versus the extent of the dynamic Q range, etc. No universal solution exists as all reactors are different. Even at a given reactor, each beam location presents a unique situation. Here, these issues are identified and pros and cons associated with the choices are presented.

Before continuing with the discussion, it is useful to review the relationship that defines the magnitude of scattering vector Q in an elastic scattering event (i.e. no change of neutron energy due to creation or annihilation of excitations in the sample). The details at the sample position, along with the definition of the  $\theta$  and  $2\theta$  angles are shown in Fig. 3. The magnitude of Q is given by:

$$Q = (4\pi/\lambda) \times \sin(\theta) \quad (1)$$

Obviously, to perform a scan one could vary either the incident angle  $\theta$ , or the wavelength  $\lambda$  (or both). The Q range of interest is typically from  $Q_{\min} = 0.005$  to  $Q_{\max} = 0.2$ , albeit some users wish to explore beyond this range. Note that the ratio between  $Q_{\min}$  and  $Q_{\max}$  is approximately 40. A typical sample we wish to study with reflectometry is of the size  $1 \times 1$  to  $5 \times 5$  cm<sup>2</sup>. Even in case of a bigger sample, we will assume that the user wishes to collect data only from the central  $5 \times 5$  cm<sup>2</sup> in order to avoid seeing edge-effects and/or in-plane inhomogeneity.

### 2. FIXED- $\lambda$ OR SWEEPING- $\lambda$ MACHINE?

The major advantage of a sweeping- $\lambda$  reflectometer is that it can collect data over a range of Q using polychromatic neutrons contained in each pulse and the measured counts could later be summed to produce data with enough statistics. If the dynamic range of  $\lambda$  were wide enough one would be able to get the entire reflectivity curve (i.e. with the ratio  $Q_{\min}:Q_{\max} \sim 1:40$ ) without moving



FIG. 3. Details at the sample position.

the sample or the detector. Unfortunately, this requirement is not met, as explained in the following example.

Consider a near room-temperature moderator whose Maxwell-Boltzmann distribution of flux is depicted in Fig. 4. We need high flux of short wavelength neutrons in order to measure much reduced reflectivity at high-Q end. The flux requirement is not as crucial at low-Q end where the reflectivity is almost 1. As suggested by the horizontal dashed lines in the figure, the source, at most, provides practical neutron flux spanning from  $\sim 0.8$  to  $4.8 \text{ \AA}$ . The ratio  $Q_{\min}:Q_{\max}$  with one  $\theta$  angle setting then is only 1:6. A similar limitation exists for neutrons extracted from a fully thermalized cold moderator.

For this reason, a sweeping- $\lambda$  machine cannot be totally free of moving parts, i.e. it still requires provision of collecting data at several incident angles  $\theta$  and the corresponding  $2\theta$  angles. In addition, it requires timing electronics for the detector and precise synchronization of the choppers. The construction cost of a sweeping- $\lambda$  machine is therefore higher than for a fixed- $\lambda$  reflectometer. Operation cost is also higher since maintenance of the chopper system is relatively expensive.

The choice between the two types of reflectometer is mostly based on cost and the kind of experiments one wishes to perform. The sweeping- $\lambda$  machine is more expensive, but it does allow measuring entire reflectivity with

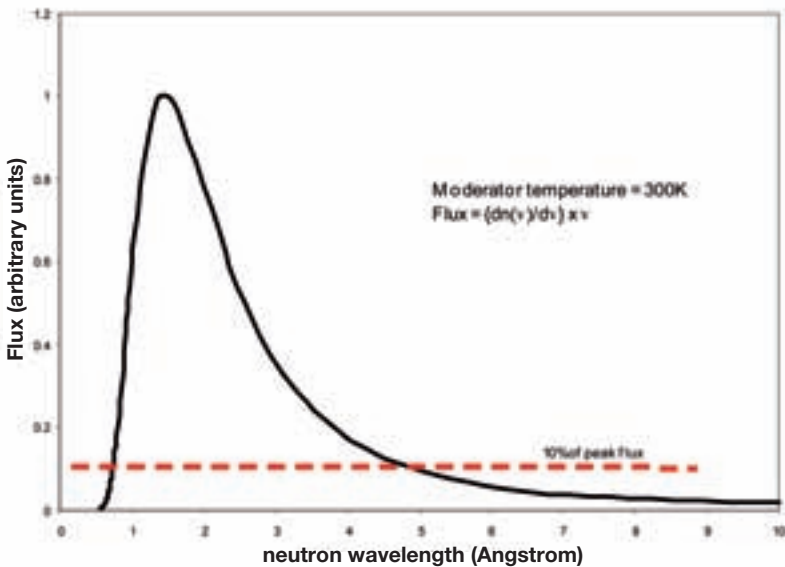


FIG. 4. Thermal flux distribution.

only two or three angle settings, making it more suitable for time-resolved studies. Experience at the laboratories where both types of reflectometer are in operation suggests that the time-integrated performance of the two types is very similar for samples that are not evolving with time.<sup>1</sup>

### 2.1. Orientation of the scattering plane

Most diffractometers (including those for X ray and light scattering) operate in a horizontal scattering plane. In this geometry the source, the sample and the detector are all at the same elevation. This has the advantage of the detector swinging in the horizontal plane, and the drive mechanism easier to design than for any other plane. The sample whose reflectivity is to be measured then has to be mounted vertically on the  $\theta$  rotation drive.

Neutron reflectometry has proved itself to be a very powerful technique in the study of liquid–air interfaces. Since the surface of a liquid can only be horizontal, it is desirable to design a reflectometer with vertical scattering plane. It would then be a general purpose machine as solid–air or solid–liquid samples could also be studied on the same machine. Unfortunately, the design is more complicated, the maximum  $Q$  reachable tends to be limited, and there is a price to be paid in the flux on the sample. On the positive side, a vertical scattering machine tends to require less floor space.

Extra complexity of vertical scattering geometry arises since the elevation of the source, i.e. the reactor, cannot be changed. Most beam tubes radiate out from the reactor horizontally. This is the case also for neutron guides emanating from a cold source. Consequently, the beam needs to be tilted down (or up) using a mirror to arrive at the horizontal surface of the sample at a small grazing angle. To increase  $Q$  during a scan, for instance, the beam is tilted down, the sample table translated downward and the detector, mounted on a vertical arm, swings up. In order not to disturb the liquid surface, the sample table motion must be very smooth. Moreover, a good vibration isolation is required so that the liquid surface is not disturbed by the vibrations caused by the nearby instruments and pedestrian traffic. Active vibration cancellation may also be required if the machine is in a high airborne vibration area.

The requirement to lower the sample table in the vertical scattering geometry leads to a rather restrictive  $Q_{\max}$  as the travel of the table is limited by the floor. It is possible and desirable to design so that the sample table could be lifted up instead as an option, but then the need to lower the detector arm leads

---

<sup>1</sup> CUBITT, R., personal communication, September 2004.

to a similar restriction. In case of the horizontal scattering plane, provided there is enough room to swing the detector,  $Q_{\max}$  is essentially unlimited.

As explained in the next section, reflectometry measurements benefit greatly if the incident beam is focused onto the sample in a plane orthogonal to the scattering plane. This means vertical focusing for horizontal scattering geometry, and horizontal focusing for vertical scattering geometry. Given that the beam is originally horizontal, vertical focusing is achieved more efficiently. Horizontal focusing is less efficient leading to lower flux on the sample.

Thus, we see that the only real reason for choosing vertical scattering geometry is to allow study of liquid–air interfaces. Ideally a facility needs two reflectometers, one in the horizontal scattering plane and the other in the vertical scattering plane. If only one reflectometer is to be built, the choice comes down to choosing between maximum performance in studying solid–air or solid–liquid interfaces and the ability to study liquid–air interfaces.

## 2.2. Choice of neutron wavelength

Both simulations and practical experience have shown that a neutron reflectometer performs better on a cold neutron source than on a thermal source. This is the case for both fixed- $\lambda$  and sweeping- $\lambda$  instruments. The advantage of a cold source includes higher data throughput, ease of instrument and sample alignment and lower background, especially if the instrument is to be located at the end of a long neutron guide. The selected wavelength on a cold source is usually just beyond the cut-off wavelength of a beryllium filter, approximately 4.5 Å.

If a fixed- $\lambda$  instrument is to be constructed at a facility where only thermal neutron source is available, the choice of wavelength is either 2.37 Å, the popular graphite filter wavelength, or 4 Å, the beryllium cut-off. If a 4 Å monochromatic beam is to be produced by Bragg reflection off a regular crystal (e.g. pyrolytic graphite, or PG) it would have a  $\Delta\lambda/\lambda$  too tight for reflectometry, i.e. unnecessarily paying a high price in intensity. In principle, one could avoid this by using a multilayer mirror as a monochromator. The  $\Delta\lambda/\lambda$  problem thus solved, one will have to weigh the advantage of using longer wavelength neutrons (larger grazing angle on the sample and the ease of mechanical alignment) versus the loss of neutron flux as a result of being in the tail region of the thermal spectrum. Figure 4 shows that the price paid in flux by selecting 4 Å instead of 2.37 Å is a factor or  $\sim 3$ . The grazing angle of the sample will be only  $\sim 2$  times higher, not enough to compensate the price in flux. Therefore, the wavelength 2.37 Å is generally preferable.

### 2.3. Choice of location: Reactor hall versus guide hall

Reflectivity measurements at small  $Q$  require very thin beams in the direction parallel to scattering plane as the sample is almost parallel to the incident beam and its cross-section seen by the beam is small. This gives the impression that high neutron flux is needed for these experiments. However, experience at various neutron laboratories is that, although high flux allows faster data collection, the performance of the machine ultimately depends on the background level. At low  $Q$  the reflectivity of the sample is almost 1 and data collection time is not excruciatingly long even with a relatively low flux. As  $Q$  increases, the reflectivity drops rapidly and the signal ultimately becomes indistinguishable with the background. Therefore, for samples that are not changing with time, low background is of primary importance in order to achieve data over a large dynamic range.

Consequently, locating a reflectometer as far away as possible from the reactor in a guide hall is always desirable. At a facility without a guide hall, the machine should be located away from instruments known to 'spray' neutrons to the surrounding area. A generous amount of shielding should be provided not only for the monochromator/chopper assembly but also for the detector.

### 2.4. Beam focusing

Although both  $\theta$  and  $2\theta$  angles are varied during a scan, reflectivity can be thought of as a function of  $\theta$  only. The purpose of the  $2\theta$  arm is to position the detector at the appropriate angle, either exactly at  $2\theta$  to measure specular reflectivity or at a slightly offset angle to measure off-specular reflectivity. With a 1D position sensitive detector or an area detector, no physical movement of the detector is needed, but different parts of the detector need to be appropriately identified as specular or off-specular signals.

One can take advantage of this dependence on the  $\theta$  angle only to boost neutron intensity on the sample. By focusing the incident beam in the direction perpendicular to the scattering plane, the number of neutrons incident on the sample at approximately the same grazing angle  $\theta$  is increased. Within the 'fan' of converging neutrons there is indeed a small variation of effective  $\theta$ , leading to a small increase in the resolution  $\Delta Q$  of the scattering vector. However, the increase is minimal at small grazing angles. The design of a 'tall' focused PG monochromator, along with a tower of PG filter for suppression of  $\lambda/2$  neutrons, is shown in Fig. 5.

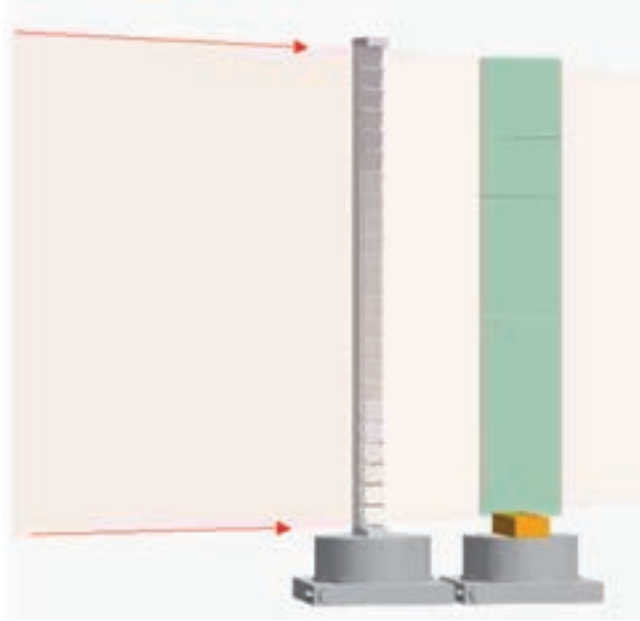


FIG. 5. A vertically focused monochromator (~30 cm tall) specifically designed for neutron reflectometry, and the associated graphite filter tower for rejecting  $\lambda/2$  and  $\lambda/3$  neutrons at the chosen wavelength of  $\lambda = 2.37 \text{ \AA}$ .

### 3. NEUTRON POLARIZATION

The study of magnetic thin films and multilayers is a very active field of research where neutron reflectometry is recognized as a uniquely powerful technique. As such, polarized neutron capability should be incorporated into a reflectometer.

All types of polarizers available for neutron scattering are applicable to neutron reflectometry. The available polarizers are:

- (1) Crystal monochromators;
- (2) Transmission or reflection supermirrors;
- (3) Spin-state dependent filters (e.g. polarized  $^3\text{He}$ ).

Since the incident beam is relatively small in one dimension (width for vertical sample geometry and height for horizontal sample geometry), transmission polarizers are often most suitable. However, one should keep in mind

## DESIGN OF A NEUTRON REFLECTOMETER

that polarizer technology is rapidly changing and the incident side and the detector side shielding should allow future modifications (e.g. separate shielding blocks that could be removed and replaced and room to accommodate larger devices).

On the detector side, one could use a transmission polarizer to split the reflected beam into two beams (reflected and transmitted). Such an arrangement, though challenging to set up, provides the advantage of measuring two spin channels simultaneously using a multidetector.

### 4. CHOICE OF DETECTOR

With the need to measure off-specular reflectivity growing, newer reflectometers are likely to be equipped at least with a 1D position-sensitive detector or preferably a 2D detector. There is a concern about whether the larger beam channel leading to the detector might cause increased background. Experience with existing reflectometers suggest that this is not the case if the channel is properly designed so that each part of the detector ‘sees’ only the sample region. The only advantage of a single detector thus seems to be its lower cost and simpler electronics.

### 5. CONCLUSION

In this paper, we have identified the issues that must be addressed in the early stage of the design of a reflectometer. The discussion is intended not only to assist the designer to make the appropriate choices but also to highlight the importance of building a good quality instrument tailored to the specific needs of the local user community. The international community has seen time and again that a properly designed and optimized reflectometer, even at a medium flux reactor, could be a workhorse instrument for high quality research in many diverse disciplines. Such an instrument in a developing nation will undoubtedly provide a strong impetus to the national R&D.



# **POLARIZED NEUTRON REFLECTIVITY ON D17 AT THE INSTITUT LAUE-LANGEVIN**

R. CUBITT  
Institut Laue-Langevin,  
Grenoble, France

## **Abstract**

A general outline of the polarized neutron reflectivity (PNR) technique is presented. The neutron as a microscopic magnetic probe allows us to deduce information that cannot be gleaned from macroscopic techniques, such as magnetometry. This means we can see anti-ferromagnetic structures and with polarization analysis, deduce the tilt of any moments that are not parallel to an applied field. The paper will cover scientific problems applicable to the PNR, experimental technique, instrumentation and data analysis.

## 1. INTRODUCTION

Polarized neutron reflectivity (PNR) is a powerful tool for investigating layered magnetic structures. Without polarization analysis, it is possible to quantify magnetization components parallel and anti-parallel to the applied field for each layer. This can be applied to anti-ferromagnetically aligned layers where no signal is found using a macroscopic technique, such as a SQUID magnetometer. With polarization analysis all in-plane components of the magnetization can be deduced. With the use of a multidetector or by scanning a single detector, further information can be deduced about structures within a surface layer, such as domains or helical magnetization. This paper describes the decisions that have to be made when designing a polarized neutron reflectometer based on the experience of the D17 reflectometer at the Institut Laue-Langevin (ILL) in Grenoble, France [1, 2].

## 2. HORIZONTAL OR VERTICAL SURFACES?

The principal reason for designing a machine for horizontal surfaces (vertical reflection plane) is the ability to measure a liquid surface (air-liquid liquid-liquid interfaces). A vertical surface machine (horizontal reflection

plane) can still measure liquid samples if they are interfaced with a solid substrate. A reflectometer in either geometry can easily have a polarized neutron option but some considerations have to be taken into account. Unless a vertical reflection plane reflectometer is placed near to a large source, a deflection mirror is required to reflect the beam down onto the sample. This could be a supermirror such as Ni/Ti which is magnetic. To avoid problems depolarizing the beam, the Ni has to be made non-magnetic by the addition of vanadium during the manufacture. Obviously the same applies to any focusing system which may exist with either geometry machine. D17 is a horizontal reflection plane machine. Liquid surfaces will be studied on a new machine presently known as HORIZON and due to be constructed in 2005–2007.

### 3. TIME-OF-FLIGHT OR MONOCHROMATIC?

From the outset, the philosophy for D17 was to make it as flexible a machine as possible but not to have any modes of operation which could diminish the optimal operation of any other. There are two basic methods for coding the wavelength with a reflectometer. The first, which is always used at pulsed sources such as ISIS, is to measure the time for the neutrons to arrive at the detector having reflected from a fixed sample angle. On a reactor source the beam is pulsed by a rotating chopper. The advantage of doing this on a reactor source is that with clever design of the chopper system, one may have complete control over the wavelength resolution, which is always related to the intensity. Often at high  $q$  a reflectivity curve has little structure so a low resolution measurement with high flux is the optimum configuration. In addition, if the sample structure is time dependent, then time-of-flight (TOF) has the advantage of being able to capture a range of  $q$  over the same time (on D17 this is an order of magnitude in  $q$  using 2–20 Å). Finally, the simple convenience of having a large simultaneous  $q$ -range without scanning any motors makes it easy to align and make quick judgements on the nature of a sample.

With a monochromator, a single wavelength with a certain spread defining the resolution is used and the reflection angle is scanned to cover the desired  $q$  range. To make best use of the available intensity from the source, the wavelength chosen is at the peak intensity of the spectrum. In theory, with the same resolution as a TOF measurement, one should be able to cover a given  $q$ -range much faster for the same statistics, as the TOF method would be limited by the low flux at the long wavelength end of the spectrum. In practice, this does not seem to be the case, as shown in Fig. 1 for a largely structureless curve measured with silicon.

## POLARIZED NEUTRON REFLECTIVITY ON D17

It is much simpler to polarize a monochromatic beam than a range of wavelengths as is required with the TOF method, as the efficiency is constant over the whole measure reflectivity profile. The most common method is to use a polarizing supermirror which has many orders of magnitude higher reflectivity for one polarization state than the other over a certain range of  $q$ . Figure 2 shows a reflectivity curve for polarization with and against the applied field on the mirror. The limited wavelength range over which the beam can be efficiently polarized means that a curve which could normally be measured with TOF in two angles (see Fig. 1) would require four or five, limiting one of the main advantages of the TOF method. For a monochromatic beam the supermirror would simply be oriented at an angle such that the desired wavelength was just under the  $m = 3$  critical edge.

In a PNR experiment, we wish to measure the reflectivity at polarizations with and against the sample applied field direction. For this a flipper is required. The simple Mezei flipper can be used for a monochromatic beam which has the advantage of taking up very little space along the beam axis ( $\sim 10$  mm). For a range of wavelengths, a radio frequency (RF) flipper is needed which may not efficiently flip the polarization over the required wavelength range and occupies far more space ( $\sim 300$  mm along the beam).

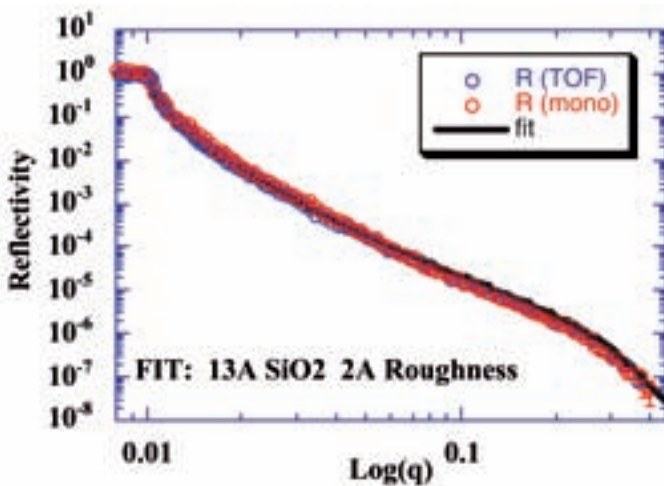


FIG. 1. Comparison of a TOF and monochromatic measurement measured on the same Si sample for the same measurement time of eight hours on D17. The TOF measurement was made over two angles. The TOF data do not suffer from the low flux at the long wavelength end of the spectrum due to re-binning and overlap of the two sets of data.

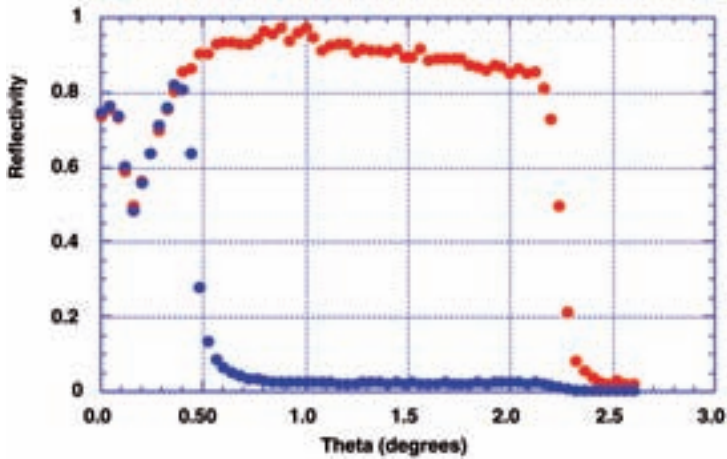


FIG. 2. Reflectivities  $R^+$  and  $R^-$  for an  $m=3$  Fe/Si supermirror measured in monochromatic mode at  $4.5 \text{ \AA}$ . The data show that there is a significant difference between the two curves for only a factor of 4 in theta ( $q$ ). This means that for D17 where we wish to use  $2\text{--}20 \text{ \AA}$  in TOF we would in fact be restricted to  $5\text{--}20 \text{ \AA}$ .

Space was very limited in the blockhouse for D17 and, given the fact we could switch from TOF to monochromatic without any disadvantages for each method, the machine was designed to do both with PNR in the monochromatic mode. For space reasons we could not have a standard graphite monochromator/supermirror combination.

#### 4. POLARIZING AND MONOCHROMATING THE BEAM

D17 was designed to be as flexible as possible without any options compromising others. For convenience of data taking, the flexibility of resolution and the ability to measure kinetic processes, a TOF option was considered essential. Although it is possible to polarize a white beam, it was considered simpler when dealing with polarizing and flipping to have the polarized option in a monochromatic mode. Given space constraints, it was not possible to have a monochromator with a take-off angle greater than  $25^\circ$ . The present system for monochromating and polarizing the beam for  $5.5 \text{ \AA}$  is a Fe/Si multilayer stack on silicon substrates. The advantage of achieving two processes in a single device is unfortunately annulled by the need for a filter and soller collimator essential for removing contamination of wavelengths

## POLARIZED NEUTRON REFLECTIVITY ON D17

above 6 Å. A model of the reflectivity from the device is shown in Fig. 3 which demonstrates the need for the filter.

The filter consists of a stack of 1000 Å Ni on silicon in three sections to avoid double reflections. The device is arranged such that the first section's angle to the beam places the critical edge of nickel relative to silicon to totally reflect wavelengths above 6 Å. In order for this device to work efficiently a soller collimator with an output angular range  $\pm 0.4^\circ$  is required. The transmission of the soller collimator plus the absorption through the silicon in the filter accounts for a loss of a factor of 4 in the intensity of 5.5 Å neutrons. This must be compared with the alternative option of using a graphite monochromator followed by a polarizing mirror plus a wavelength filter, such as beryllium, to remove half wavelength contamination. The transmission of these devices is estimated to be approximately 50% but one needs to take into account resolution effects. The natural resolution of our multilayer device is 5%. That is  $d\lambda/\lambda$ , where  $d\lambda$  is the FWHM spread of wavelengths. Often the natural  $d\lambda/\lambda$  from a graphite monochromator is too good and flux is lost needlessly. Figure 4 shows a close-up of a few layers of the system, indicating how it avoids double reflections of long wavelength neutrons contaminating the beam along with the layout of the optical devices required to produce a clean, polarized monochromatic beam.

The resultant spectrum is shown in Fig. 5 which should be compared with the right hand panel in Fig. 3.

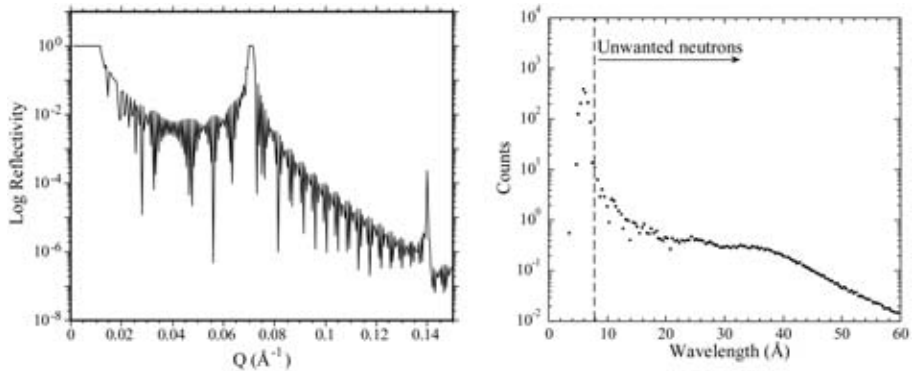
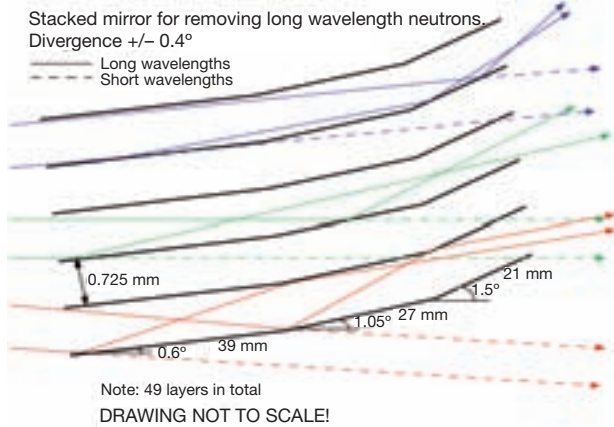


FIG. 3. Reflectivity profile for one polarization (left panel). The right panel shows the resultant reflectivity from the mirror showing the need to remove long wavelengths reflected above the dashed line.

(a)



(b)

Scale drawing of the finalized devices for the monochromator option of D17B.

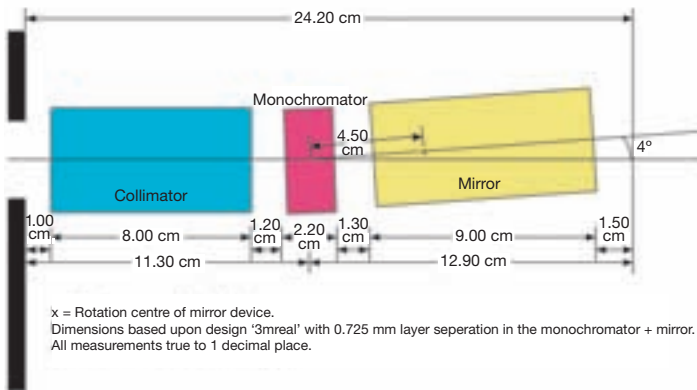


FIG. 4. (a) Layout of a selection of layers of the Ni long wavelength filter showing how double reflections are moved away from the transmitted beam; (b) shows the dimensions and layout of the collimator, polarizing monochromator and filter.

An important aspect when dealing with polarized neutrons is not just the ability to polarize efficiently but to maintain that polarization from the polarizer to the sample or analyser if it is present. A guide field is required to ensure that the polarized beam does not pass through any regions of zero fields where the polarization can be lost. Typically, a guide field of the order of 1 mT is sufficient in the direction of the applied field on the polarizer.

## POLARIZED NEUTRON REFLECTIVITY ON D17

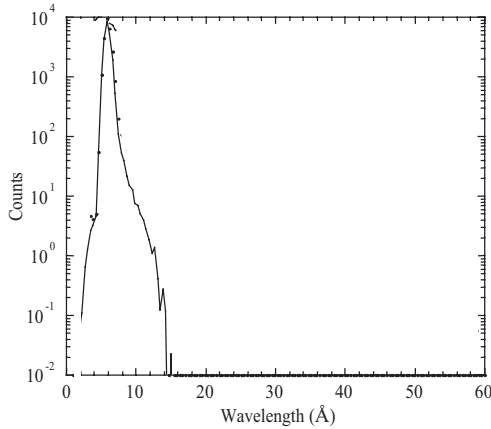


FIG. 5. Wavelength distribution at the sample position after all the optical devices.

### 4.1. Flipping the polarization of the beam

Two devices for flipping the beam were mentioned in the discussion about TOF or monochromatic methods. On D17 we use both methods. For a monochromatic beam the only disadvantage of a Mezei type flipper is the presence of material in the beam. This is not a problem before the collimation, as it corresponds to a simple attenuation and not a spread of the beam width which could affect the angular resolution. So, in the blockhouse we use a Mezei type flipper. It simply consists of two coils of wire wound perpendicularly to each other, one of which creates a field that opposes the guide field and the other provides a field perpendicular to the polarization which is adjusted such that the neutrons spin precesses exactly  $180^\circ$  while traversing the device. A schematic representation of such a device showing the principle is shown in Fig. 6. Typically, for 1 mm diameter wire (preferably anodized aluminium), currents of the order of 1–7 A are required depending on the wavelength and guide field strength.

The optimization of such a device involves using the analyser mirror or replacing the sample with an analyser (polarizing supermirror) which reflects the polarization in the same direction as the polarizer. All that is required is for both currents to be iteratively scanned until a minimum intensity is seen through the polarized/flipper/analyser system. The ratio of intensity with the flipper off to on is known as the flipping ratio and is a useful measure of the combined efficiency of the three devices. Typically, flipping ratios of 20–30 are expected for mirror polarizers and a Mezei flipper.

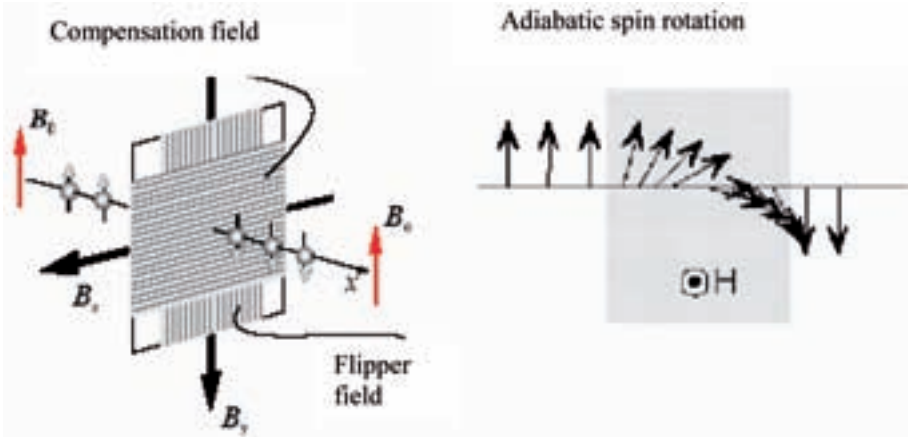


FIG. 6. Diagram showing the design and principle of a Mezei flipper.

On D17, we have a focusing guide above and below the beam reducing the beam height from 200 to 70 mm. The gain in intensity is paid for with increased vertical divergence leading to a beam approximately 200 mm high at the detector 3 m from the sample. To capture this intensity and have the ability to measure off-specular scattering led to the installation of an area

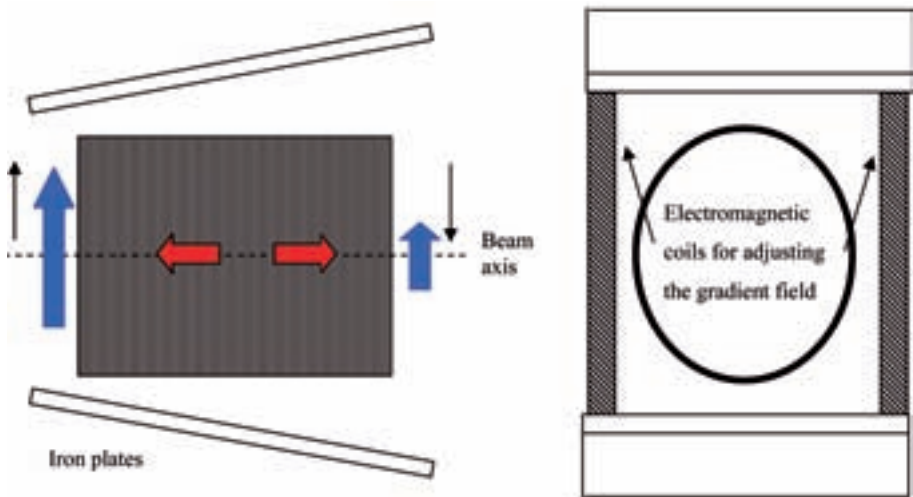


FIG. 7. Layout of an RF flipper. The blue arrows represent the strength and direction of the gradient field and the red arrows show the direction of the RF field along the cylinder axis.

multidetector. Analysing and flipping all beams in the solid angle defined by the sample to the area detector is challenging. Extra scattering in the flight path from a Mezei flipper was avoided by using an RF flipper, which works on the principle of NMR. This type of flipper consists of a hollow cylinder with a coil wound around the outside, about the cylinder axis. Through this coil a RF signal is passed at approximately 100 kHz in a field gradient varying from 1–2 mT for 5.5 Å neutrons. Along the length of the cylinder, the guide field is modified so as to have a strong gradient in field. This is accomplished by the use of diverging iron plates separated by iron core electromagnets to adjust the gradient field. To optimize the device, the RF amplitude and the field gradient need to be scanned to minimize the intensity in the same way as described for a Mezei flipper. On D17, this device is placed in the detector vacuum tank just after the sample. Care must be taken to shield stray fields from the sample area to this device. A steel shield around the sample cryomagnet 1 m away from the flipper allows operation up to 1.4 T before the efficiency is affected.

## 5. ANALYSING THE REFLECTED POLARIZATION

If there is no off-specular reflectivity (the sample has no in-plane structure) and the instrumental background is not important, then a simple polarizing supermirror can be used to analyse the reflected beam polarization. Mirrors are the most efficient method of polarization and have the highest intensity of the desired polarization state. As even with a supermirror the reflection angles are still of the order of 1–2°, an unfeasibly long mirror is required to cover off-specular angles. On D17, we have a supermirror analyser and a He<sup>3</sup> cell especially for off-specular studies and can easily switch between the two. He<sup>3</sup> gas is polarized such that the transmission is a strong function of the polarization. At present, the gas can only be polarized to ~60% so there is significant absorption of the desired polarization state of ~70%. The polarization for our 5.5 Å neutrons is 90% but this falls with a characteristic time of 100 hours. In practice, this means we start with a fresh cell having a flipping ratio of ~10 which drops to ~7 after 24 hours. The cell must be filled on a daily basis and, to avoid having to break the detector vacuum, a system of remote filling via a capillary has been developed. He<sup>3</sup> is very sensitive to stray field gradients so the gas cell is placed in a mu metal shield and if a cryomagnet is used, the stray field from this must also be shielded. Figure 8 shows the need for the cell to be able to cover the 4° of the detector in the horizontal plane.

## CUBITT

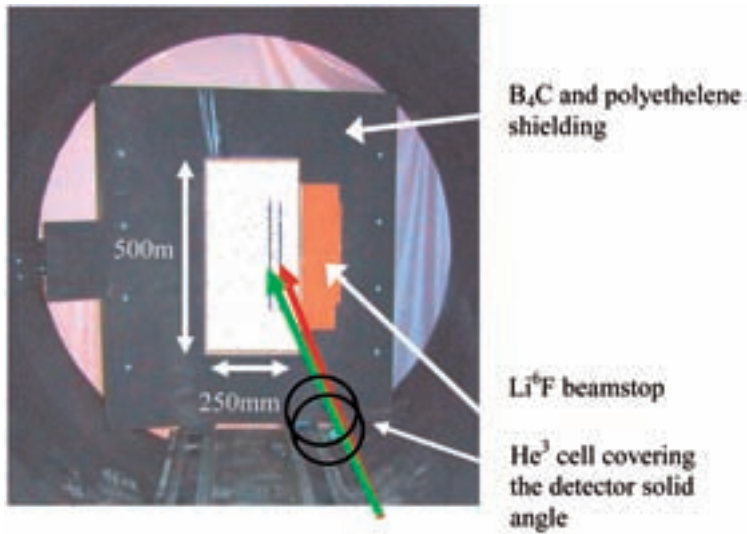


FIG. 8. The picture of the multidetector shows a main beam plus a reflection transmitted through a He<sup>3</sup> cell.

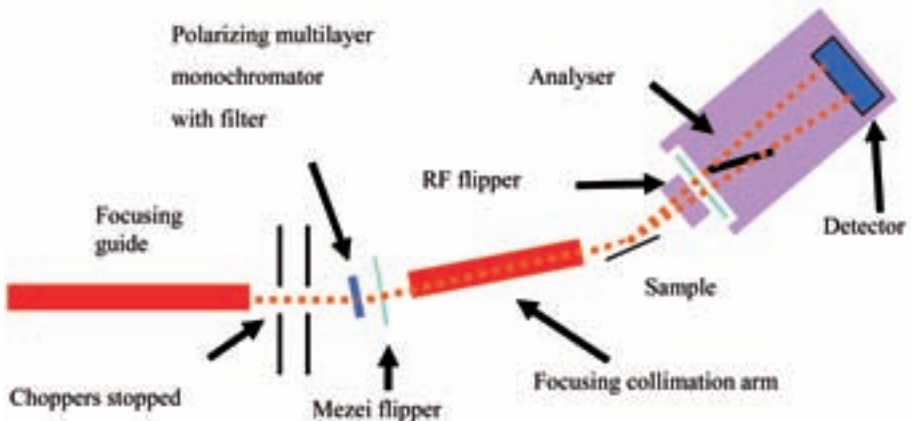


FIG. 9. A D17 layout in polarization mode showing all the components.

## REFERENCES

- [1] <http://www.ill.fr/YellowBook/D17/>
- [2] CUBITT, R., FRAGNETO, G., D-17: The new reflectometer at the ILL, Appl. Phys. A **74** (2002) S329–S331.

# OXIDE FILMS AND CORROSION

J.J. NOËL

Department of Chemistry,  
University of Western Ontario,  
London, Ontario, Canada

## Abstract

Neutron reflectometry has been successfully applied in a small number of corrosion and passivity experiments. It has many important advantages and unique features that make it a valuable tool to corrosion scientists. As a new method it offers many opportunities for interesting applications and technique development, as well as several challenges.

## 1. INTRODUCTION

Corrosion of structural metals and alloys is an extensive and expensive industrial problem that is estimated to consume about 3% of the GDP of industrialized nations, annually. According to a report commissioned by the United States Federal Highway Administration Office of Infrastructure Research and Development [1], corrosion cost the economy of the United States of America  $\$2.757 \times 10^{11}$  in 1998 alone. Clearly, there remain many unsolved problems, both fundamental and applied, in the corrosion field.

Corrosion can be described very broadly as the oxidative degradation of materials. For the purposes of this paper, we focus specifically on metals and alloys and their compounds. Metal/alloy corrosion involves the dissolution of the material and/or the formation of corrosion product film or deposit on its surface. Corrosion may be general (uniform) or localized in form.

The most important structural metals (e.g. Fe, Ni, Ti, Mg, Cu, Cr, etc.) are thermodynamically unstable in air and water. Their longevity and suitability for long term industrial applications is therefore determined by kinetic considerations. Frequently, their ability to withstand their environment depends very strongly on the protection afforded by a thin passivating film, which is often an oxide layer, but may consist of a sulphide, phosphate or other highly stable metal-containing compound. The passive film is often a layer only a few nanometres thick, and is usually formed by reaction of the outermost atomic layers of the metal surface with the surrounding environment. This thin film

then acts as a barrier between metal and environment that slows further oxidation of the underlying metal, sometimes to an exceedingly low rate.

A wide variety of analytical techniques is employed by corrosion scientists to quantify the rate and extent of corrosion damage and to investigate the corrosion mechanism, including such straightforward methods as weight change measurements and optical microscopy, and progressing through more sophisticated techniques, such as optical and electron spectroscopies, a plethora of electrochemical methods, scanning probe microscopies, ellipsometry, and X ray and neutron scattering procedures, both in and ex situ. The purpose of this paper is to outline the contribution to corrosion and passivation studies already made by neutron reflectometry (NREF), its unique advantages and limitations, challenges to be overcome, and future directions for NREF applied to corrosion science and oxide films.

## 2. NEUTRON REFLECTOMETRY IN CORROSION SCIENCE

Information of interest to corrosion scientists includes atomic and/or molecular-level information on composition, speciation, crystal phases layer structure, inhomogeneities, reaction rates, reaction orders and mechanisms, defect densities and transport, and stress effects. In gathering data of an underlying or fundamental nature, eventual applicability to commercial metals and alloys and real environments should be kept in mind. To the corrosion scientist, some of the outstanding features of NREF are that it can be performed in situ in a wide range of applicable environments, under relevant conditions (pH, temperature, pressure, etc.); is non-destructive; can be performed simultaneously with other analytical techniques, such as electrochemical methods; probes buried interfaces, as well as the outermost one; has nanometre-scale resolution; easily observes hydrogen; and can readily distinguish between isotopes of the same element in many cases. These characteristics are difficult to find (and some are unique) among other techniques available to the corrosion scientist, making NREF a very valuable tool in some corrosion studies, especially for determining information on structural variation with depth, extent of hydration or interfacial roughness.

The first NREF work in the corrosion and passivity area was reported in 1992 [2]. In the 12 years since, NREF has been used in only a handful of corrosion studies, but these have covered both aqueous corrosion [2–9] and gas phase oxidation [10, 11]. Investigations of oxide films for other purposes, such as electrochemical charge storage [12, 13] and materials for neutron supermirrors [14], have also yielded relevant information. Although this paper is limited to the corrosion of metals and metal oxides, it should be noted that a

body of work has been published that focuses on oxidation of non-metallic materials, especially silicon (for example, see Refs [15, 16]).

NREF scans have been performed both on magnetic materials, such as Fe and Co, and on non-magnetic materials, such as Ti and Zr, using spin-polarized neutrons in the former cases and non-polarized neutrons in the latter. Some efforts have also been made to couple reflectometry with other analytical methods in situ, including electrochemical polarization measurements and electrochemical impedance spectroscopy. Using these approaches, researchers have demonstrated that it is possible to follow the growth of an oxide film on a metal, in situ, under conditions of anodic polarization, to measure its Pilling Bedworth and anodization ratios, specific resistivity, and dielectric constant. They have quantified the rate of oxide film dissolution and metal corrosion in chemically aggressive solutions and have observed hydrogen progressing through the passive film and into the underlying metal.

Neutron reflectometry is especially well suited to look at electrochemical situations in situ. A generic arrangement for electrochemistry that could be oriented in any direction for use on NREF instruments operating with either vertical or horizontal geometries is shown in Fig. 1.

### **2.1. Opportunities**

Since very little work has been done so far using NREF to study corrosion and passive films, many opportunities remain, such as exploring other metals and alloy systems and expanding on the range of chemical environments, treatments and physical conditions to which the material of interest is exposed. Isotopic labelling and contrast matching experiments also offer a wide range of possibilities, not only for aiding in the interpretation of reflectivity scans, but also for tracking atomic movements in mechanistic investigations. In addition, there remains plenty of scope for coupling NREF with other analytical tools to enhance the quality and quantity of information obtainable by both methods and to compensate for some of their shortcomings with complementary features.

### **2.2. Challenges**

Some formidable challenges also remain to be overcome in NREF in order to aid and enhance its applicability to corrosion science and passive film studies, among other things. For example, sample preparation is an important concern. In this case, the large neutron beam footprint necessitates relatively large sample sizes — too large to be prepared in some instances — and the

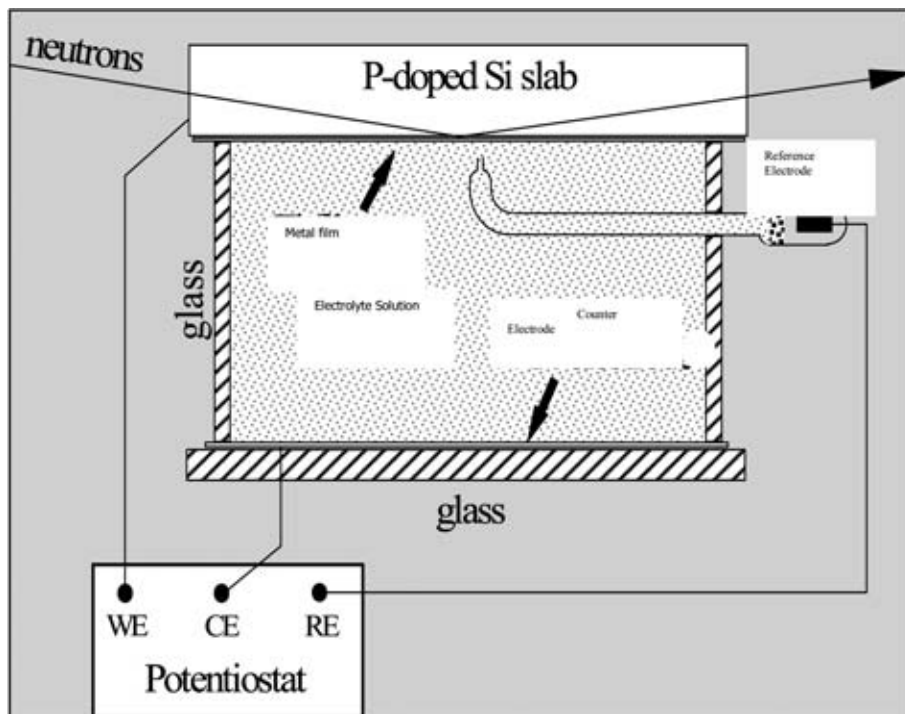


FIG. 1. Neutron reflectometry on a metal film in an electrochemical cell.

requirement for extreme flatness, which has commonly been dealt with by depositing thin films on polished substrates, has so far precluded the use of ‘real’ bulk industrial alloy specimens. Being able to use smaller and more representative samples would be significant improvements. Faster measurements (at good signal-to-noise ratios) and modulation techniques would enable better kinetic studies to be undertaken. Interpreting the results of NREF scans is another topic for future refinement, both in terms of finding reliable and practical ways to determine, unambiguously, the correct scattering length density profile from Q space scans, and also in gaining some ‘in-plane’ spatial resolution, perhaps by deciphering off-specular scattering data. In the published literature so far, there are several reports of significant NREF efforts resulting in uninterrupted results [2–4, 11], which can be considered a negative or discouraging sign to those considering the application of NREF in their research.

Neutron scientists have taken up some of these challenges and are making significant progress in a number of areas, such as sample size, scan

acquisition rates and interpretation of specular scattering data. Progress seems to be somewhat more elusive yet in some areas, such as analysis of off-specular scattering data.

### 3. CONCLUSIONS

In summary, the application of NREF to corrosion and oxide film studies has been successfully demonstrated in a small number of cases. Many important advantages and unique features make it a valuable tool for corrosion scientists. Being new, it offers many opportunities for innovative applications and technique development, as well as a number of challenges to surmount.

### REFERENCES

- [1] US DEPARTMENT OF TRANSPORTATION, FEDERAL HIGHWAY ADMINISTRATION, Corrosion Costs and Preventive Strategies in the United States, Rep. FHWA-RD-01-156, CC Technologies Laboratories, Inc., Office of Infrastructure Research and Development, McLean, VA (2001).
- [2] KREBS, L.A., et al., Neutron reflectivity studies of the passive film on iron, Proc. Electrochem. Soc. **92-22** (1992) 580.
- [3] KREBS, L.A., et al., "Passive film studies using neutron reflectivity", Proc. 12th Int. Cong. on Corrosion, NACE, Houston, **5B** (1993) 863.
- [4] KRUGER, J., et al., Passivity of metals and alloys and its breakdown: New results from new non-electrochemical techniques, Mater. Sci. Forum **185-188** (1995) 367.
- [5] WIESLER, D.G., MAJKRZAK, C.F., Neutron reflectometry studies of surface oxidation, Physica B **198** (1994) 181.
- [6] WIESLER, D.G., MAJKRZAK, C.F., Growth and dissolution of protective oxide films on titanium: An in-situ neutron reflectivity study, Mater. Res. Soc. Symp. Proc. **376** (1995) 247.
- [7] TUN, Z., NOËL, J.J., SHOESMITH, D.W., Electrochemical modifications on the surface of a Ti film, Physica B **241-243** (1998) 1107.
- [8] TUN, Z., NOËL, J.J., SHOESMITH, D.W., Electrochemical modification of the passive oxide layer on a Ti film observed by in-situ neutron reflectometry, J. Electrochem. Soc. **146** (1999) 988.
- [9] NOËL, J.J., JENSEN, H.L., TUN, Z., SHOESMITH, D.W., Electrochemical modification of the passive oxide layer on Zr-2.5Nb observed by in situ neutron reflectometry, Electrochem. Solid-State Lett. **3** (2000) 473.
- [10] RIEKER, T., HUBBARD, P., MAJEWSKI, J., SMITH, G., MOODY, N., Neutron reflectivity investigation of the effects of harsh environments on Ta<sub>2</sub>N thin films, Thin Solid Films **346** (1999) 116.

- [11] METELEV, S.V., et al., The study of oxidation of thin metal films by neutron reflectometry, *Physica B* **297** (2001) 122.
- [12] SAVILLE, P.M., GONSALVES, M., HILLMAN, A.R., CUBITT, R., Dynamic neutron reflectivity measurements during redox switching of nickel hydroxide films, *J. Phys. Chem. B* **101** 1 (1997) 1.
- [13] PENFOLD, J., et al., Recent advances in the study of chemical surfaces and interfaces by specular neutron reflection, *J. Chem. Soc. Faraday Trans.* **93** 22 (1997) 3899.
- [14] MUNTER, A.E., HEUSER, B.J., SKULINA, K.M., Neutron reflectivity measurements of titanium-beryllium multilayers, *Physica B* **221** (1996) 500.
- [15] ASHWORTH, S., MESSOLORAS, R.J., STEWART, PENFOLD, J., A neutron reflectivity study of hydrogenated silicon-silicon oxide thin films, *Semicond. Sci. Technol.* **4** (1989) 1.
- [16] DURA, J.A., RICHTER, C.A., MAJKRZAK, C.F., NGUYEN, N.V., Neutron reflectometry, X-ray reflectometry, and spectroscopic ellipsometry characterization of thin SiO<sub>2</sub> on Si, *Appl. Phys. Lett.* **73** 15 (1998) 2131.
- [17] MAJKRZAK, C.F., BERK, N.F., SILIN, V., MUSE, C.W., Experimental demonstration of phase determination in neutron reflectometry by variation of the surrounding media, *Physica B* **283** (2000) 248.
- [18] MAJKRAZAK, C.F., BERK, N.F., Phase sensitive reflectometry and the unambiguous determination of scattering length density profiles, *Physica B* **336** (2003) 27.

# NEUTRON REFLECTION STUDIES OF SOLID-LIQUID INTERFACES

A.R. RENNIE

Studsvik Neutron Research Laboratory,  
Uppsala University,  
Uppsala, Sweden

## Abstract

The paper presents some of the key areas in interface science that can be studied using neutron reflection. Buried interfaces between two bulk phases are good examples of systems that are easy to study using neutron beams but can be particularly difficult to investigate using other techniques. Neutron reflection can provide information about the structure and composition of interfaces. It has been used extensively to look at adsorption of surfactants from solution, grafted layers at solid interfaces as well as surface layers prepared by Langmuir-Blodgett and Langmuir-Schaeffer deposition. These interfaces can be taken as examples of substrates for a variety of industrial applications of surfactants, such as detergents, wetting agents and fabric conditioners. However, the interest is much wider as the properties of biological systems may often be dependent on interactions at surfaces. Pulmonary surfactants are important in respiratory function, a range of surfactants are used in pharmaceutical delivery systems and lipid bilayers are essential features of cell membranes along with a range of other components. The range of science mentioned benefits hugely from a technique that can unambiguously identify the composition of interfacial layers as well as providing structural information. Use of isotope substitution and isotopic labelling of particular molecules or parts of molecules is very valuable in this respect and often neutron reflection is the only technique that can be readily used to provide the necessary information. The paper outlines the practical issues concerning studies of solid-liquid interfaces. In addition, it provides specific examples of studies of surfactants and mixed surfactants at a range of interfaces.

## 1. INTRODUCTION

This paper is intended to provide an introduction and a rationale for the choice of neutron reflection as a tool to study solid-liquid interfaces. In this area, a particular emphasis is made on studies with surfactants as other topics are discussed extensively by other participants. Even within this area, it is not appropriate to attempt a full review as the literature is extensive and studies of

solid–liquid interfaces cover a wide range of topics from wetting behaviour, detergency and model biological membranes.

Interfaces and thin films are important in many areas of science and technology. Chemical reactions often occur at the interface between bulk phase of reagents or at the interface with a heterogeneous catalyst. In biology, transport across membranes controls many important functions such as respiration. Many of these interfaces are complex. There may be several components present and some may be selectively found at the boundary. Neutron reflection is particularly important as a tool because it determines the structure and isotopic labelling can be used to identify particular components or parts of molecules.

Several recent conferences and papers have provided reviews of particular aspects of neutron reflection, for example, in 2003 a collection of papers appeared in the journal *Langmuir*, following the REFILL meeting in Grenoble held during autumn 2002 that described recent work [1]. See Ref. [2] for information available on the Internet about facilities for these studies. There are also some general descriptions of the reflection technique [3] and its applications [4, 5].

## 2. PRACTICAL ASPECTS OF STUDIES OF SOLID–LIQUID INTERFACES

There have been major advances in recent years as regards the performance of neutron reflectometers although much of this work has been performed at spallation sources [5]. Even with the best facilities, the flux available remains limited and the time for measurement can be restrictive. Typical samples need to be of the order of 1 or several cm<sup>2</sup>. Measurement times usually vary from a few minutes to a few hours, depending on requirements of resolution and range of Q. In a few cases, kinetic experiments have permitted time resolution of less than a minute in observations of interdiffusion in thin polymer films [6].

There is a particular constraint as regards samples which need to be both flat and smooth, since the reflectivity will normally decrease as  $\exp(-Q^2\sigma^2)$  where  $\sigma$  is characteristic of the root mean square roughness normal to the interface [7]. We see that at a typical Q value of 0.15 Å<sup>-1</sup>, a roughness of 10 Å would reduce the reflectivity by almost a factor of 10! In practice, surfaces can be prepared routinely on solid samples with a roughness around 5 Å. The signal corresponding to one monolayer of substrate deposited here can be measured. For studies of solid–liquid interfaces, the solid substrates, which are relatively large, must be carefully prepared, polished and cleaned. Model calculation showing the effect of roughness on reflectivity is seen in Fig. 1.

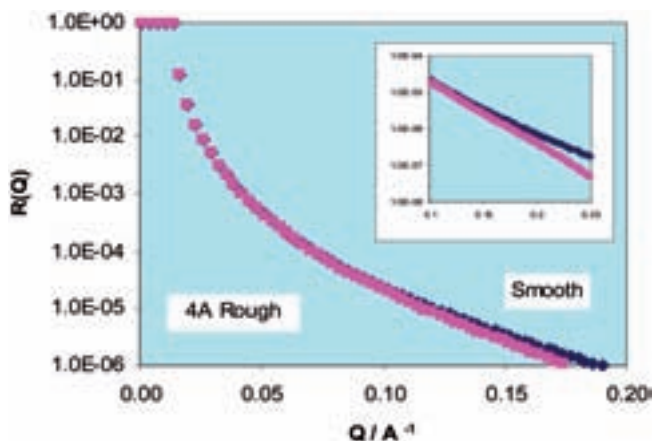


FIG. 1. The important effect of roughness is seen in the model calculation for neutron reflection from a silicon- $D_2O$  interface with a small roughness of  $4 \text{ \AA}$  (pink) compared with a completely smooth interface.

The design of reflectometers is not discussed explicitly in this article but some comments about the sample environment and features that are useful in the study of solid-liquid interfaces are appropriate. To study the interface between two bulk phases, at least one of the materials must be adequately transparent to the neutron beam. In the case of the solid-liquid interfaces, it has been common to use a single crystal as the solid substrate. Most experiments have been performed with silicon as large crystals are readily available and easily polished. However, other crystals such as sapphire and quartz can be used. On reactor instruments that use long wavelength neutrons, amorphous silica can be used. The range of interfaces that can be investigated is further extended by physical or chemical modification of the solid surface with grafted layers, spin coating of polymers, evaporation of metals or other techniques, such as Langmuir-Blodgett and Langmuir-Schaeffer deposition.

A schematic diagram of a cell for solid-liquid interfaces is shown in Fig. 2. Apart from the components shown, there will be filling ports that are possibly designed for flow through, flushing or mixing of solutions, as well as arrangements to thermostat the sample at a specific temperature. The design of these cells is important for optimum data collection. For example, they should inhibit formation or deposition of bubbles at the reflecting interface, as well as provide minimal surfaces parallel to the interface of interest that might be aligned, such as to give parasitic reflection [8].

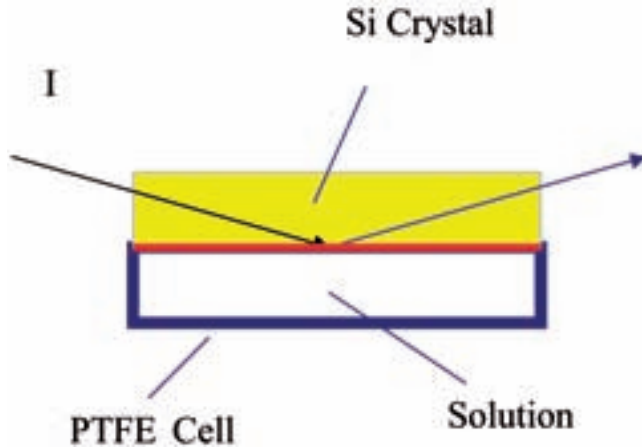


FIG. 2. Schematic diagram of a sample cell for the study of solid-liquid interfaces.

### 3. EXAMPLES OF INVESTIGATIONS WITH NEUTRON REFLECTION

The examples shown in this section are chosen to illustrate how careful choice of measurements with restricted data and the use of isotopic labelling with deuterium to either hide or identify particular components at an interface.

#### 3.1. Use of contrast to confirm structural models

Some early work [9] involved the study of cationic surfactants dissolved in water adsorbed at the interface with amorphous silica. The surface excess of hexadecyltrimethyl ammonium bromide ( $C_{16}TAB$ ) on amorphous silica (Fig. 3) was seen to vary with both concentration and pH of the solution.

This example is included for two reasons. Fifteen years ago when the experiment was performed, facilities were less sophisticated and neutron reflection data were more difficult to collect. However, even a few data points could provide important information. Further, the problem with ambiguity of interpretation (lack of uniqueness in a structure modelled to a reflectivity curve) is resolved by making measurements with a second contrast of water to effectively compensate for the lack of phase information in a single data set by making a controlled change of contrast and phase. At all coverages, a layer of about 35 Å was observed. Work in this area of surfactant adsorption has been

## NEUTRON REFLECTION STUDIES OF SOLID-LIQUID INTERFACES

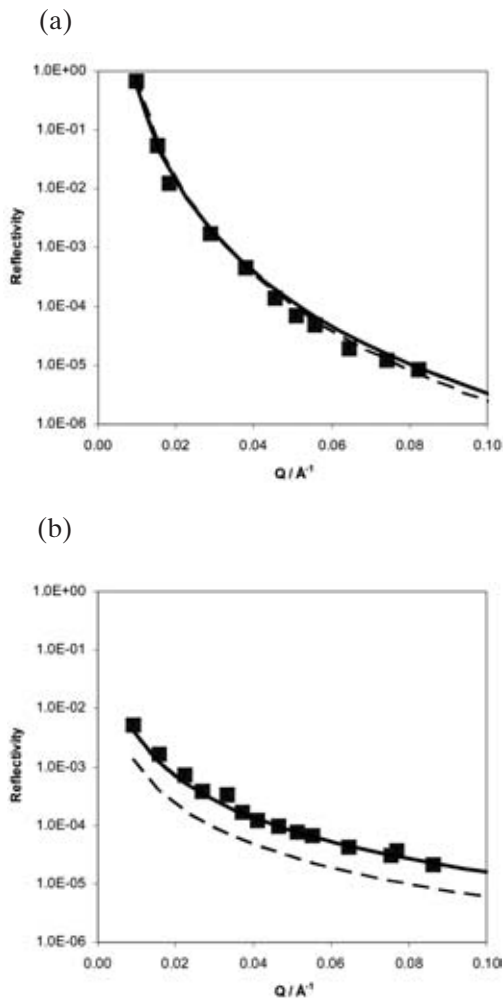


FIG. 3.  $C_{16}TAB$  in (a)  $D_2O$  and (b)  $CMSiO_2$  at  $6 \times 10^{-4} M$  at  $27^\circ C$ . The solid line is a model with a 'bilayer' and the dashed line corresponds to a 'monolayer' (from Ref. [9]).

extended to look at mixtures of surfactants at the solid-liquid interface (e.g. see Refs [10, 11]), which extends the more extensive work at air-liquid interfaces [12].

### 3.2. Modified substrates

The range of substrates that can be investigated poses some limitations but chemical or physical modification of an interface of a substrate allows a range of different surfaces to be studied. For example, layers can be deposited on single crystals by grafting [13] or spin-coating. In the first case, reactions of trichlorosilanes with silica and thiols with gold have proved useful routes to surfaces with a range of functionalities. Polymers can be deposited by spin-coating as well as grafting reactions and this system is illustrated by the data shown in Figs 4 and 5 [14].

The data in Fig. 4 show how a relatively complex interface of silicon with an oxide layer and a polymer film of polystyrene can be studied using multiple

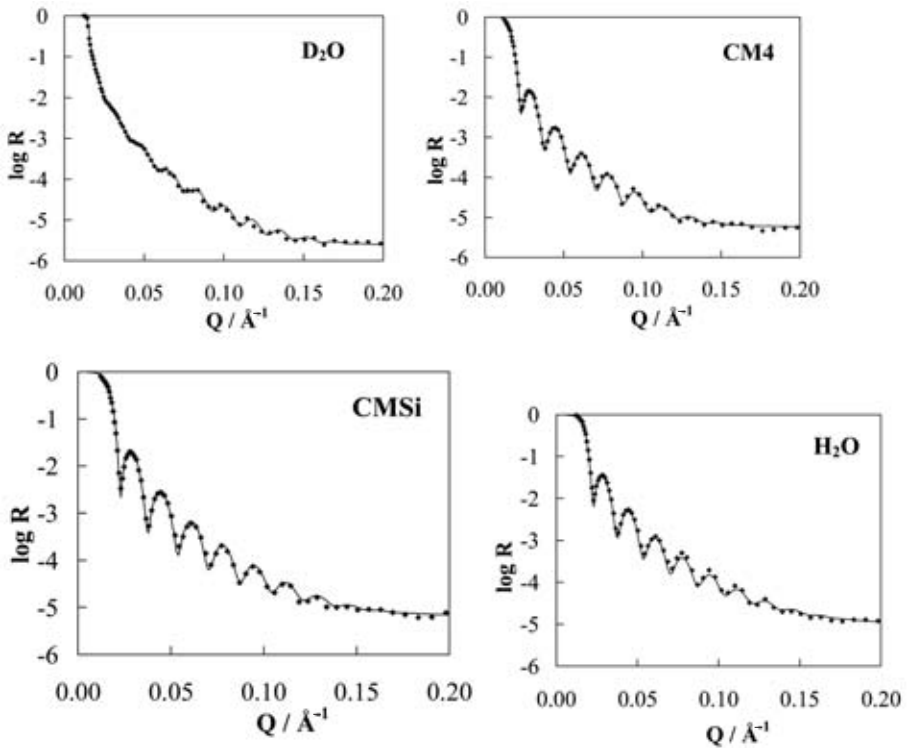


FIG. 4. Reflectivity profiles (blue diamonds) and fits (lines) for a silicon crystal coated with deuterated polystyrene in four different contrasts of water:  $D_2O$  and  $H_2O$  and mixtures of the two: CM4 contrast matched to scattering length density  $4.0 \times 10^{-6} \text{ \AA}^{-2}$  and CMSi contrast matched to silicon ( $2.07 \times 10^{-6} \text{ \AA}^{-2}$ ).

isotopic contrasts. The deuterated polystyrene film is almost matched in scattering length density (refractive index) by  $D_2O$ . In practice, the oxide layer is characterized prior to putting the polymer on the substrate. In this example, the oxide layer of about 20 Å and the polymer film of 275 Å can be determined accurately and then further experiments of adsorption from a solution to the polymer surface are conducted. An example is shown in Fig. 5.

Surfactant adsorption to polymer surfaces can thus be investigated even though a bulk phase of polymer would not be sufficiently transparent to a neutron beam. The data also illustrate that the substrate can be used for multiple adsorption experiments as the surfactant could be removed readily by rinsing.

### 3.3. Biological materials

The range of applications of neutron reflection to biological interfaces is now growing rapidly. Cleaning of food materials is an industrial activity but work in this area is important [15]. The removal of proteins and other materials with surfactant solutions has been investigated extensively. In more fundamental areas of biology, there are several approaches to the study of model membrane systems [16–19]. Many of these systems are looking at bilayers or multilayers of deposited phospholipids. Other work is looking at

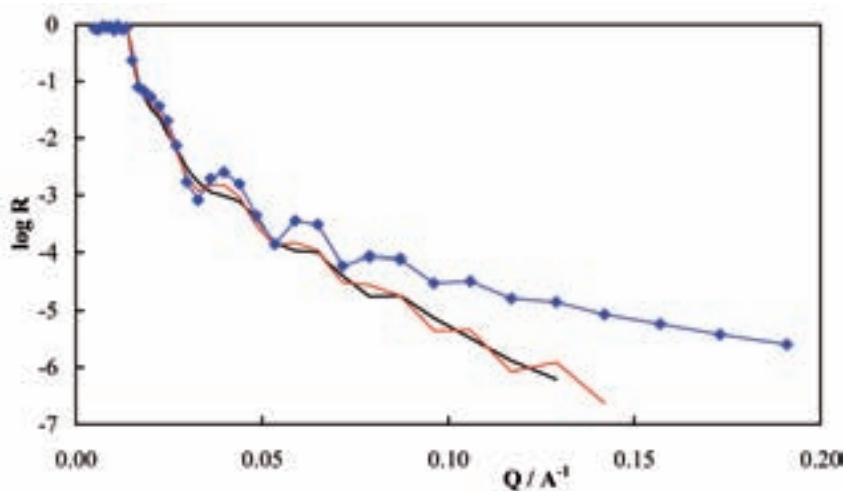


FIG. 5. Reflectivity profiles for a 275 Å *d*-polystyrene layer in  $D_2O$  before adsorption (black line), with an adsorbed layer of hydrogenous SDS at its CMC (blue diamonds) and after the adsorbed layer had been rinsed five times (red line).

lung surfactants, enzymes and surfactants and proteins in saliva. The complexity of these materials can only be understood if labelling techniques are applied to highlight or mask individual components.

#### 4. CONCLUSION

The examples presented in this short paper have been chosen to indicate that neutron reflection is a powerful and growing technique for the study of solid–liquid interfaces. The data can be very simply interpreted but care may be needed to avoid ambiguities from loss of phase information. Careful choice of contrasts can permit complicated, multicomponent interfaces to be studied. Even when isotopic labelling of some species is not possible, choice of substrate and solution contrasts may be sufficient to provide detailed information.

#### REFERENCES

- [1] CUBITT, R., FRAGNETO, G., GHOSH, R.E., RENNIÉ, A.R., Advances in the study of interfaces with neutron reflection, REFILL2002, Langmuir **19** (2003) 7685 and following papers.
- [2] Catalogue of neutron reflection facilities, <http://www.studsvik.uu.se/research/NR/reflect.htm>
- [3] DAILLANT, J., GIBAUD, A. (Eds), X-ray and Neutron Reflectivity: Principles and applications, Springer, Berlin (1999).
- [4] PENFOLD, J., et al., Recent advances in the study of chemical surfaces by specular neutron reflection, J. Chem. Soc. Faraday Trans. **93** (1997) 3899.
- [5] PENFOLD, J., THOMAS, R.K., The application of the specular reflection of neutrons to the study of surfaces and interfaces, J. Phys. Condens. Matter **2** (1990) 1369.
- [6] BUCKNALL, D.G., HIGGINS, J.S., BUTLER, S.A., Early stages of oligomer–polymer diffusion, Chem. Eng. Sci. **56** (2001) 5473.
- [7] NÉVOT, L., CROCE, P., Characterization of surfaces by grazing X-ray reflection: Application to study of polishing of some silicate-glasses, Phys. Appl. **15** (1980) 761.
- [8] TURNER, S.F., Adsorption of Ionic Surfactants and Gelatin at Aqueous Interfaces, PhD Thesis, Univ. of Cambridge (1999).
- [9] LEE, E.M., SIMISTER, E.A., THOMAS, R.K., RENNIÉ, A.R., Structure of a cationic surfactant at the silica–water interface, Langmuir **6** (1990) 1031.
- [10] MCDERMOTT, D.C., et al., Study of the adsorption from aqueous solution of mixtures of non-ionic and cationic surfactants on crystalline quartz using the technique of neutron reflection, Langmuir **9** (1993) 2404.

## NEUTRON REFLECTION STUDIES OF SOLID-LIQUID INTERFACES

- [11] HINES, J.D., et al., Neutron reflection from mixtures of sodium dodecyl sulfate and dodecyl betaine at the hydrophobic solid/aqueous interface, *J. Colloid Interface Sci.* **189** (1997) 259.
- [12] PENFOLD, J., STAPLES, E., TUCKER, I., The study of partitioning in mixed surfactant systems, by neutron scattering techniques, *Adv. Colloid Interface Sci.* **68** (1996) 31.
- [13] THIRTLE, P.N., et al., Structure of non-ionic surfactant layers adsorbed at the solid/liquid interface on self-assembled monolayers with different surface functionality: A neutron reflection study, *Langmuir* **13** (1997) 5451.
- [14] TURNER, S.F., CLARKE, S.M., RENNIE, A.R., THIRTLE, P.N., THOMAS, R.K., Adsorption of sodium dodecyl sulfate to a polystyrene/water interface studied by neutron reflection and attenuated total reflection infra-red spectroscopy, *Langmuir* **15** (1999) 1017.
- [15] GREEN, R.J., SU, T.J., LU, J.R., PENFOLD, J., The interaction between SDS and lysozyme at the hydrophilic solid-water interface, *J. Phys. Chem. B* **105** (2001) 1594.
- [16] FRAGNETO, G.J., Neutron reflectivity at the solid/liquid interface: Examples of applications in biophysics, *Phys. Condens. Matter* **13** (2001) 4973.
- [17] FRAGNETO, G., GRANER, F., CHARITAT, T., DUBOS, P., BELLET-AMALRIC, E., Interaction of the third helix of antennapedia homeodomain with a deposited phospholipid bilayer: A neutron reflectivity structural study, *Langmuir* **16** (2000) 4581.
- [18] MAJKRZAK, C.F., et al., First-principles determination of hybrid bilayer membrane structure by phase-sensitive neutron reflectometry, *Biophys. J.* **79** (2000) 3330.
- [19] KRUEGER, S., et al., Investigation of hybrid bilayer membranes with neutron reflectometry: Probing the interactions of melittin, *Langmuir* **17** (2001) 511.



# NEUTRON REFLECTOMETRY IN AUSTRALIA

## *Present and future*

A. NELSON, M. JAMES, J.C. SCHULZ, A. BRULE  
Australian Nuclear Science and Technology Organisation,  
Menai, New South Wales, Australia

### **Abstract**

The number of scientists using the neutron reflectometry technique has expanded rapidly in the past few years, both in Australia and worldwide. This demand has led to the construction of a (monochromatic) reflectometer at the existing HIFAR reactor at the Australian Nuclear Science and Technology Organisation (ANSTO), as well as the design and construction of a new (time-of-flight) instrument at the new 20 MW reactor that is currently being built. The paper gives a detailed description of both instruments. The description of the current high flux Australian reactor (HIFAR) reflectometer includes details on how data collection has been optimized to make full use of (lowish) flux and how the background has been reduced for a reactor face instrument. The description of the new reflectometer provides details about design and construction progress. This is to be split into four sections: chopper systems, sample area design, detector choice (and detector tank), as well as software control.

### 1. INTRODUCTION

Neutron reflectometry is a relatively new technique to Australian researchers. In the past this has been due to the absence of a neutron reflectometer at the high-flux Australian reactor (HIFAR) at the Australian Nuclear Science and Technology Organisation (ANSTO). Despite the absence of a domestic neutron reflectometer, a significant number of Australian researchers have been making regular visits to overseas facilities to conduct reflectometry measurements. Recently, a monochromatic neutron reflectometer has been developed at HIFAR to service the needs of the Australian user community. This instrument is a stepping stone to a world class time-of-flight (TOF) neutron reflectometer planned for Australia's new 20 MW replacement research reactor (RRR). While the HIFAR instrument does not have the capacity to make polarized reflectometry measurements, the future time-of-flight reflectometer will have this capability. These two instruments will usher in a new era of surface science research using neutrons in Australia.

## 2. INSTRUMENTATION AND CAPABILITIES

### 2.1. The neutron reflectometer at HIFAR

A neutron reflectometer (Fig. 1) has been commissioned at Australia's 10 MW HIFAR facility [1]. The reflectometer operates in a monochromatic, angle-dispersive mode collecting reflectivity data as a function of angle. The reflectometer operates with a vertical scattering plane, and is suitable for the study of air–solid and solid–liquid surfaces.

A dog-leg monochromator, comprised of a matched pair of highly oriented pyrolytic graphite (HOPG) (002)  $0.4^\circ$  mosaic crystals, is used to select the neutron wavelength (approximately  $2.43 \text{ \AA}$ ). Non-diffracted neutrons and gamma rays are transmitted through the upper monochromator crystal, before hitting a beamstop (made of boroflex, lead and borated paraffin wax), which is contained inside the monochromator shielding. The purpose of the dog-leg is to trap energetic fast neutrons and  $\gamma$  rays within the monochromator shielding, while allowing the selected neutron wavelength to exit to the secondary

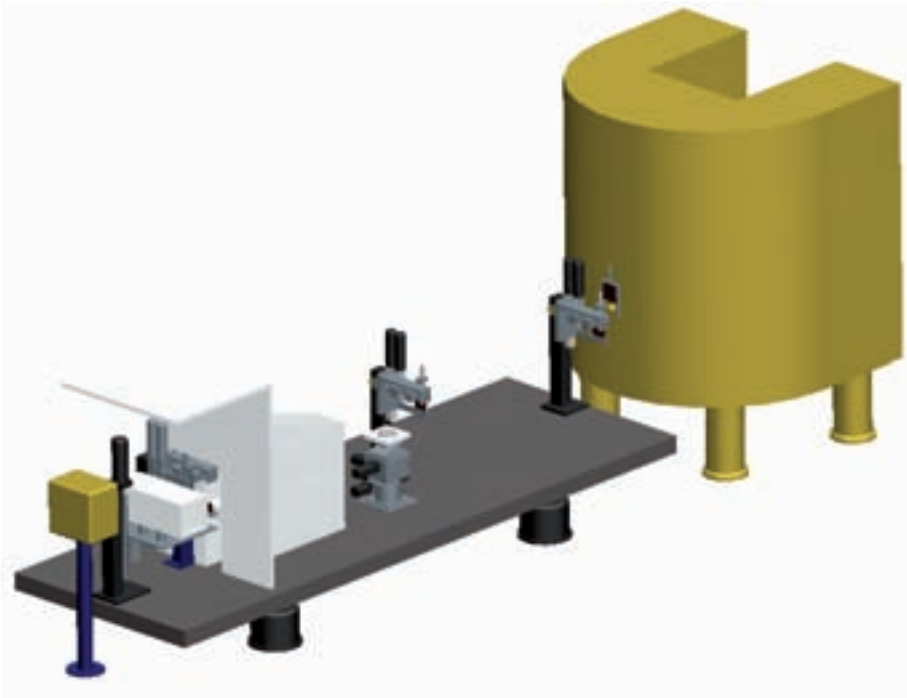


FIG. 1. The HIFAR neutron reflectometer.

spectrometer. The higher ( $\lambda/n = 2, 3, \dots$ ) harmonics produced by the monochromator crystals are removed from the beam that exits the monochromator using a filter of ( $3.5^\circ$  mosaic) HOPG (002) crystals with their crystallographic  $c$ -axis oriented along the beam direction. The filtered, monochromatic beam exits the monochromator shielding via a 150 mm long exit tube that contains a coarse horizontal collimator (20 mm high) made of lead and boroflex. The purpose of this collimator is to reduce highly vertically divergent neutrons from entering the secondary spectrometer, which would only increase the instrumental background.

The remaining components of the secondary spectrometer (excluding the neutron beamstop) are all mounted on an optical bench with pneumatic damping isolators in order to minimize vibrations from other equipment at the HIFAR facility.

The collimation system for the HIFAR reflectometer consists of two slit towers (S1 and S2), each tower supporting a slit package. Each slit package contains four blades of 3 mm thick hot-pressed  $B_4C$ . The horizontal blades used for defining the beam footprint on the sample are mounted on motorized precision linear stages, that can be repositioned within 3  $\mu\text{m}$  accuracy. The lower slit blade of each package is fixed to a motorized translation stage that is capable of substantial vertical movement. Also attached to this translation stage is a second motorized linear stage that moves the upper slit blade with respect to the lower blade. The resulting slit packages are thus capable of accurate independent motion over relatively large distances. These horizontal slit blades are offset so that they may pass each other. This enables the neutron beam to be completely closed at any slit position in the instrument. The vertical blades hang from the upper motorized linear stage. These slits are moved via a manually operated linear bearing. These slits allow the user to tailor the horizontal width of the incident neutron beam to that of the sample dimensions.

In order to reduce air scatter, a tube purged and filled with helium is placed between S1 and S2. The tube is lined with boroflex on the outside and possesses coarse cadmium slits at each end, through which the neutron beam enters and leaves the tube. The coarse slits have the effect of preventing neutrons 'spraying' from S1 (which would not hit the sample) proceeding any further down the instrument.

A single cylindrical  $^3\text{He}$  filled detector (10 atm) is used as a neutron beam monitor and is mounted between the horizontal and vertical slit blades of S2, viewing the edge of the neutron beam that passes through the slits to the sample. The monitor is used to monitor changes in neutron flux due to variation in the reactor power and also to record the increase in flux due to the

opening of the slits S1 and S2. A Huber motorized z-stage in combination with a Huber 2-circle goniometer forms the basis of a sample positioning system.

The instrument's detection system consists of a  $^3\text{He}$  detector mounted on a motorized z-stage that follows the reflected beam. This stage is capable of substantial travel (approximately 350 mm) with better than 10  $\mu\text{m}$  precision and is able to position the detector above and below the direct (horizontal) neutron beam. Also mounted to this platform is a slit tower (S3) of similar design to S1 and S2 that masks the entrance to the detector shielding. The purpose of S3 is to remove non-reflected neutrons that are scattered or transmitted by the sample. To the rear of the instrument is a re-entrant beam stop to contain any neutron or  $\gamma$  radiation that may pass through the detector shielding. The beam stop consists of sequential layers of boroflex, 5% borated polyethylene and lead in an aluminium casing.

The detector is filled with  $^3\text{He}$  to a pressure of 10 atm and is position sensitive along its length, operating using the charge division method. In order to reduce the background, the detector (apart from an entrance at the front) is surrounded by 100 mm of 5% borated polyethylene with a lining of boroflex. In addition, a further 60 mm of borated polyethylene + boroflex liner encloses the detector, its motorized Z-stage and the S3 slit tower. Since the area in which the instrument is situated has a high fast neutron background this shielding is essential in obtaining the lowest achievable reflectivity.

## 2.2. Some optimizations improving HIFAR collection rates (Fig. 2)

Early measurements on the instruments were made by using constant slit openings to collect several data points over a given Q range. The slits were then opened further for the next Q range, and so on. Unfortunately, this meant that the neutron flux onto the sample was not optimized, since the footprint onto the sample decreases as the angle the sample subtends to the beam and thus Q gets larger.

By changing the way that the control program is used, data acquisition is now taking place with a constant sample footprint and constant resolution ( $dQ/Q$ ). This ensures that the maximum number of neutrons hit the sample, boosting the data collection rate and hence, the statistics.

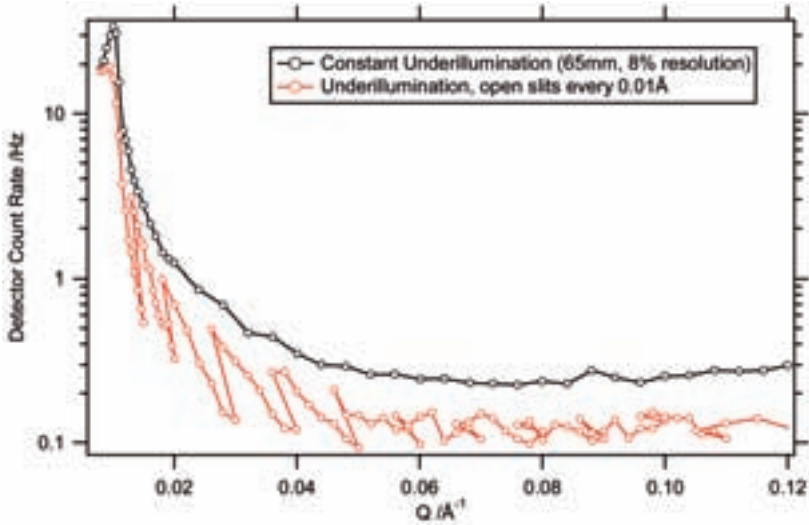


FIG. 2. Optimizing detector count rates for quartz- $D_2O$  interface.

### 3. THE PLATYPUS: TIME-OF-FLIGHT NEUTRON REFLECTOMETER AT AUSTRALIA'S NEW RESEARCH REACTOR

A TOF instrument to be built at the new 20 MW RRR in Sydney (Fig. 3) will serve the future requirements of neutron reflectometry in Australia. Unlike the existing HIFAR thermal beam facility, the new research reactor will operate with a liquid deuterium cold source that is expected to deliver a high neutron flux between 2 and 20 Å. The Platypus neutron reflectometer will be positioned at the end of a curved supermirror neutron guide that will provide optimal transmission of cold neutrons while removing fast neutrons and high energy  $\gamma$  rays. In contrast to the HIFAR instrument, the Platypus reflectometer will utilize a white neutron beam that will be pulsed using a series of disc choppers, and typically only three angle settings will be required to collect a complete reflectivity profile. The new instrument will also operate with a vertical scattering plane, making it suitable for both solid and 'free-liquid' surfaces.

The disc chopper system will feature four boron coated aluminium discs spaced over 800 mm, two of which will be used at any time. The spacing between the discs, as well as the disc phasing and speed will enable variable ( $\Delta\lambda/\lambda$ ) resolution and enable optimization of the neutron flux for each

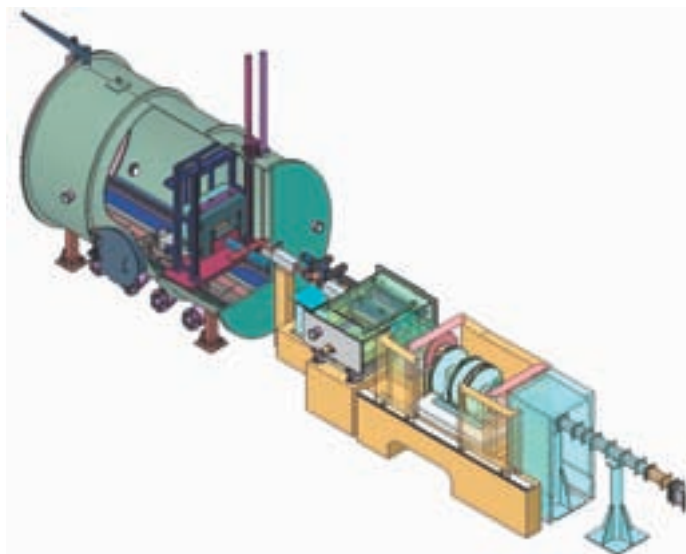


FIG. 3. The RRR neutron reflectometer.

experiment. The closest disc pair (100 mm apart) will be used to pulse the beam for high resolution experiments such as ‘thick’ films or magnetic multilayer systems. Low resolution experiments on ultra-thin films or surfactant monolayers spread at the air–liquid interface will utilize the two most widely spaced discs (800 mm apart) to maximize the flux delivered at the sample position.

A frame overlap mirror, attenuator, beam monitor and coarse slit will be positioned upstream of the first chopper. The purpose of the frame overlap mirror is the removal of wavelengths higher than 30 Å. The (variable) thickness attenuator will prevent the detector from being exposed to more neutrons than it can cope with at low Q values, since the beam is polychromatic with a high intensity. After the attenuator, a low efficiency beam monitor will be used to account for changes in incident flux due to the reactor and the attenuator. Finally, the coarse slit is present to reduce the large beam before it enters the disc chopper system.

The first high precision slit system (S1) will be situated after the chopper system, but before the collimation system. This slit system will contain four, 3 mm thick blades of hot-pressed B<sub>4</sub>C that will define the neutron beam in the vertical and horizontal directions. The blades will be slightly offset so that it is possible for them to move past each other to close the beam completely. Each of the blades will be able to be repositioned to better than 3 μm accuracy.

## NEUTRON REFLECTOMETRY IN AUSTRALIA

The focusing/deflection/polarization system will be mounted on a high precision translation stage that is housed in a vacuum chamber. The translation stage will be used to select one of five positions. The first position will comprise two  $m = 4$  supermirrors and will focus horizontally divergent neutrons, enabling improved measurement of small solid samples. The second position will contain a single ( $m = 4$ ) deflection supermirror for free-liquid samples. This mirror will rotate to deflect the horizontal neutron beam downwards onto the sample, at different angles. Position three will be a double-bounce deflection supermirror to enable higher Q measurements for free liquid samples. The fourth position will be empty. The last position will contain a polarizing supermirror, which will reflect spin-up neutrons out of the beam (to be absorbed by the guide), while transmitting the spin-down neutrons towards the sample. This will enable polarized reflectivity measurements.

Two slit towers containing precision slit packages (S2 and S3), that are identical to S1, will be situated either side of the sample stage, after the collimation system. These slit towers will be mounted on an optical rail and will be movable, which will allow sample environments of different sizes to be accommodated. The slit towers S1 and S2 will perform the fine collimation of the beam and will control the vertical height/divergence of the neutron beam. Situated just behind S2 will be a low efficiency monitor that will be used in the normalization of the detector counts to the incident beam. S3 following the sample will allow reflected neutrons through to the detector.

A high precision z stage in combination with a horizontal translation stage and a 2 circle goniometer forms the basis of a sample positioning system, which will also have vibration isolation. The horizontal translation stage will act as a sample changer, while the 2 circle goniometer will adjust the angle of incidence of (solid) samples with respect to the incident neutron beam. The sample area will be able to accommodate ( $500 \times 500 \text{ mm}^2$ ) large ancillaries (e.g. a Langmuir film balance for free-liquid samples).

Following the sample area, a large evacuated tank will house a 2D delay line area detector. The detector will be able to translate within this tank, in order to change the angle of reflection with respect to the sample. The detector will be 250 mm high by 500 mm wide, with 125 vertical pixels and 200 horizontal pixels. The area detector will allow off-specular measurements to be made. The detector can cope with a count rate of  $10^6$  Hz globally and  $10^4$  Hz locally. The time-of-flight detector signal will be processed by the DAE for storage in time histograms. A motorized beam shade will be located in front of the detector to shield it from the direct beam.

A polarization analyser (supermirror) and a spin flipper will be situated at the front of the detector tank and, allied with the polarization supermirror

and spin flipper in the collimation system, will allow all four magnetic reflectivities ( $R^{++}$ ,  $R^{--}$ ,  $R^{+-}$ ,  $R^{-+}$ ) to be measured.

Ancillary and instrument control will be via SICS (PSI) running on a network PC (operating system Redhat). The user will run the experiment from a remote computer using the Gumtree GUI, which is a Java based program developed at ANSTO. This control is standardized over all RRR instruments allowing the easy addition of new ancillary sample environments and uniform motion control systems.

#### 4. CONCLUSION

The constant wavelength neutron reflectometer operational at the HIFAR reactor at ANSTO and results of some of the studies are described. The details of the monochromator, shield to reduce the background and the detector system are described. Some of the salient features of the TOF reflectometer planned for the new research reactor (RRR) at ANSTO are presented. The instrument will be set up on a cold neutron source. Liquid and solid samples can be studied using this equipment.

#### REFERENCE

- [1] JAMES, M., et al., A new neutron reflectometer at Australia's HIFAR research reactor, Nucl. Instrum. Methods Phys. Res. Sect. A **536** (2005) 165.

# DEVELOPMENT OF A TOF REFLECTOMETER AT THE GREEK RESEARCH REACTOR

K. MERGIA, G. APOSTOLOPOULOS

National Centre for Scientific Research “Demokritos”,

Athens, Greece

## Abstract

The Greek research reactor GRR-1 is a continuous neutron source of 5 MW thermal power but without a cold source and without a neutron guide system. The principles of the new time-of-flight (TOF) reflectometer under installation are described. Different design parameters for the reflectometer are considered and optimized with the aim to obtain the best performance, satisfying different experimental needs and under the constraints of cost and local conditions. For measuring liquid samples the in-pile collimation system has been designed, such as the emerging from the reactor neutron beam is inclined by  $-0.8^\circ$  with respect to the horizontal axis. Thus beam inclination for the desirable  $\theta$  range is achieved by simply moving the apertures and the sample vertically of maximum value of  $-1.6^\circ$ . Different wavelength ranges are available and all of them have the same minimum wavelength of 0.15 nm utilizing, thus, the wavelengths with the maximum flux. The resolution is also a variable parameter in order to satisfy experimental needs for either high resolution or lower resolution but higher counting rate experiments. Pulse overlap is avoided by the employment of a supermirror. Since there are no guides and it is essential to reduce the background, a sapphire filter is used for the removal of the fast neutron component. For achieving an efficient removal of the fast neutrons without considerable reduction of the neutron flux in the wavelength range from 0.15 to 1.0 nm, the optimum sapphire thickness has been calculated by MCNP code. Further, towards a low background instrument, optimization of the shielding has been made by MCNP calculations.

## 1. INTRODUCTION

The paper describes the installation of a time-of-flight (TOF) reflectometer at the Greek research reactor GRR-1. GRR-1 is a continuous neutron source of 5 MW thermal power but without a cold source and a neutron guide system. Neutron reflectometry is a technique with a wide range of applications in surface science and nanotechnology, and it is strongly connected with research and development work carried out at the Greek universities and research centres. The TOF technique has the advantage that a large scattering

vector,  $q$ , range can be covered in one geometrical setting and a wide wavelength range can be utilized. In addition, the complexity and the time lost in a continuous change of  $\theta, 2\theta$  angles can be avoided and lower  $q$  values can be obtained. A TOF reflectometer is also a good choice for a low power reactor without cold source and it can be easily installed and maintained. What is essential for a low power reactor is to try to have the maximum possible counting rate and the maximum signal to noise ratio.

The requirements set for the installation of the TOF reflectometer at GRR-1 are the following:

- (a) The ability to measure both solid and liquid samples;
- (b) Utilization of the short neutron wavelength;
- (c) Availability of different wavelength ranges;
- (d) Ability to vary the resolution;
- (e) Easily maintainable detection system and electronics;
- (f) Reliable and easy alignment of samples;
- (g) Ability for the extension of the instrument for polarized neutrons.

## 2. CONSIDERATION OF A TOF REFLECTOMETER UNDER A STEADY STATE THERMAL NEUTRON SOURCE

For a TOF reflectometer at a steady state thermal source, two main ingredients have to be initially considered, i.e. the Maxwellian distribution of the neutron wavelengths and the functional form of the reflectivity curve. These two will give an indication of the useful wavelength ranges to be employed and also of the resolution effects on the reflected intensity.

Neutrons having a velocity  $v$  at equilibrium with a moderator at temperature  $T$  will have a Maxwellian velocity and the neutron flux, i.e. the neutrons passing through the unit surface per unit time and with wavelengths between  $\lambda$  and  $\lambda + d\lambda$  will be given by:

$$n(\lambda)d\lambda = 2 \frac{\lambda_T^4}{\lambda^5} \exp\left(-\frac{\lambda_T^2}{\lambda^2}\right) d\lambda, \quad \int_0^{\infty} n(\lambda)d\lambda = 1 \quad (1)$$

Equation (1) is maximized for  $\lambda_0 = \sqrt{2/5}\lambda_T$  and for  $T = 40^\circ\text{C}$  we have  $\lambda_0 = 1.1 \text{ \AA}$ . According to Eq. (1) the intensity for constant wavelength resolution  $\Delta\lambda$  can be written as:

## DEVELOPMENT OF A TOF REFLECTOMETER

$$dI(\lambda) = \int n(\lambda)d\lambda \cong \frac{25}{2} \frac{\lambda_0^4}{\lambda^5} \exp\left(-\frac{5\lambda_0^2}{2\lambda^2}\right) \Delta\lambda \quad (2)$$

For  $\Delta\lambda = c\lambda$  (i.e. constant  $\Delta\lambda/\lambda$  resolution) and for  $c \rightarrow 0$  the intensity is given by:

$$I(\lambda, c \rightarrow 0) = \int_{\lambda-\Delta\lambda/2}^{\lambda+\Delta\lambda/2} n(\lambda)d\lambda \cong n(\lambda)\Delta\lambda = c \frac{25}{2} \frac{\lambda_0^4}{\lambda^4} \exp\left(-\frac{5\lambda_0^2}{2\lambda^2}\right) = cI_0(\lambda) \quad (3)$$

It can easily be proven that Eq. (3) is a very good approximation for  $c \leq 0.2$ .

Thus, from Eqs (2) and (3), we may conclude that if we employ  $\Delta\lambda/\lambda = \text{const}$  the gain,  $G(\lambda)$ , in flux is:

$$G(\lambda) = \frac{c\lambda}{\Delta\lambda} \quad (4)$$

i.e. the gain varies linearly with the wavelength.

In order to calculate the reflected intensity, the reflectivity from a semi-infinite thickness layer will be considered. If it is assumed that the measurement starts from the critical edge and the glancing angle  $\theta_1$  is chosen such that:

$$\lambda_{\max} = \lambda_c(\theta_1) = \frac{4\pi}{Q_c} \sin\theta_1 \quad (5)$$

then the reflected intensity is given by:

$$N(\lambda_1) = \frac{25}{2} \int_{\lambda_1-\delta\lambda}^{\lambda_1+\delta\lambda} \frac{\lambda_0^4}{\lambda^5} \exp\left(-\frac{5\lambda_0^2}{2\lambda^2}\right) \left[ \frac{1 - \left(1 - \left(\frac{\lambda}{\lambda_c(\theta)}\right)^2\right)^{1/2}}{1 + \left(1 - \left(\frac{\lambda}{\lambda_c(\theta)}\right)^2\right)^{1/2}} \right]^2 d\lambda$$

$$= \int_{\lambda_1-\delta\lambda}^{\lambda_1+\delta\lambda} n\{\lambda_0, \lambda, \lambda_c(\theta)\} d\lambda \quad (6)$$

In Fig. 1, the logarithm of the function  $n\{\lambda_0, \lambda, \lambda_c(\theta)\}$  is presented versus the wavelength for different values of the maximum wavelength  $\lambda_{\max}$ . It is observed that the minimum wavelength that one may use is around  $1.7 \text{ \AA}$ , since below that the reflected intensity reduces abruptly. Figure 1 also points to another important fact. As the wavelength range extends to longer  $\lambda$  values, then the overall intensity decreases. This implies that different wavelength ranges should be available and preferably different wavelength resolutions. Another point to be noticed is that for  $\Delta\lambda = \text{const}$  the reflected intensity is almost invariant with the wavelength and is given by:

$$N_a(\lambda_1) = 2n(\lambda_1) \Delta\lambda \tag{7}$$

A reasonable choice for wavelength resolution could be  $\Delta\lambda = 0.1 \text{ \AA}$  which for  $\lambda_{\max} = 8 \text{ \AA}$  corresponds to a reflected intensity of the order of  $10^{-5}$  whereas for  $\lambda_{\max} = 12 \text{ \AA}$  to a reflected intensity of the order of  $10^{-6}$ .

For  $\Delta\lambda / \lambda = c$  the reflected intensity will be:

$$N_b(\lambda_1) = 2cn(\lambda_1) \lambda_1 \tag{8}$$

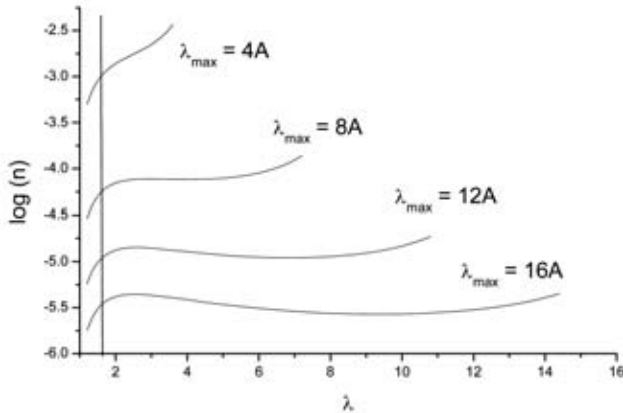


FIG. 1. The function of the reflected intensity (Eq. (6)) versus the wavelength for different values of the maximum wavelength.

## DEVELOPMENT OF A TOF REFLECTOMETER

That is, in the latter case the intensity will increase linearly with the wavelength, as it is expected since the resolution in wavelength is worsened. The variation of the reflected intensity versus wavelength is depicted in Fig. 2 for various wavelength ranges.

However, in an experiment of a given duration and if  $\Delta\lambda = c\lambda_{\min}$  the data for both cases at  $\lambda = \lambda_{\min}$  have the same statistics but the data at longer wavelengths in the second case have better statistics but worse resolution. The best choice has to be assessed in relation to the chopper and the desired overall performance of the instrument.

### 3. IN-PILE COLLIMATOR

Since one of the requirements for the TOF reflectometer is to be able to study liquid samples, horizontal geometry is required which corresponds to a vertical scattering plane. The inclination of the neutron beam is achieved by utilizing a special shape designed in-pile collimator as shown in Fig. 3. In this way,  $-0.8^\circ$  beam angle is achieved without the need to rotate the collimator. One can then calculate the intensity for a sample at a certain distance from the collimator as it is presented in Fig. 4 for a sample–collimator distance of 1800 mm. It is observed that the intensity remains constant at its maximum value up to an angle of  $-1.2^\circ$  and at an angle of  $-1.6^\circ$ , which is the maximum desirable angle, it is reduced by only 25%.

For liquid samples, the desirable  $\theta$  range is achieved by moving the sample and the apertures vertically as is shown in Fig. 5.

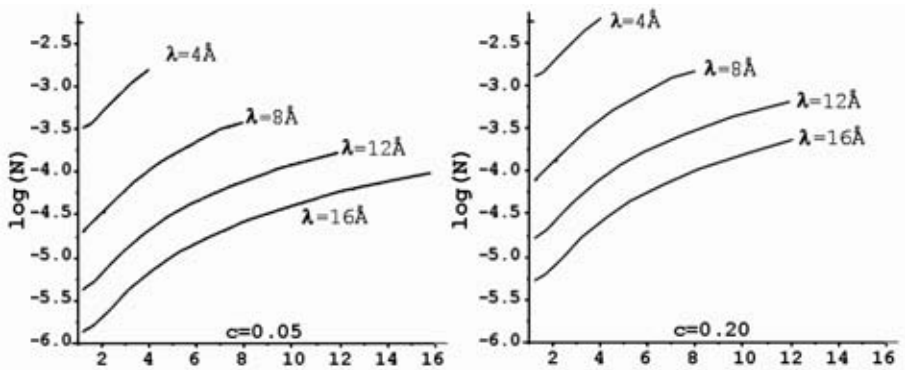


FIG. 2. The reflected intensity (Eq. (8)) versus the wavelength for different values of the maximum wavelength for (a)  $c = \Delta\lambda / \lambda = 0.05$ ; and (b)  $c = \Delta\lambda / \lambda = 0.2$ .

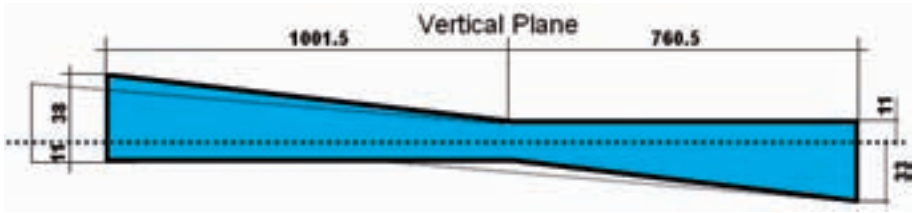


FIG. 3. Vertical plane of the in-pile collimator.

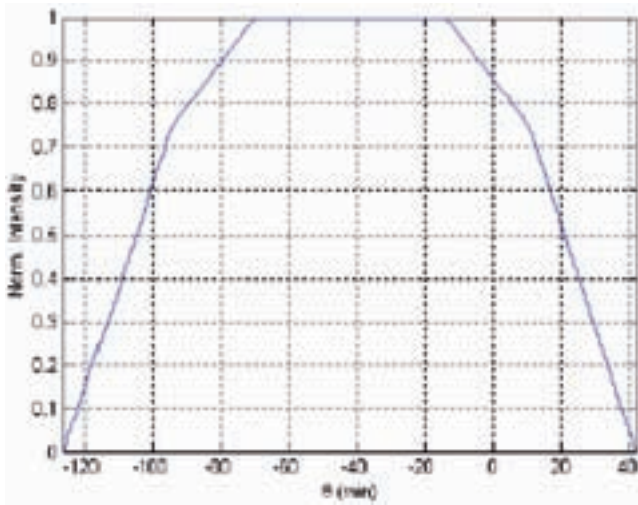


FIG. 4. Intensity per sample point versus  $\theta$ .

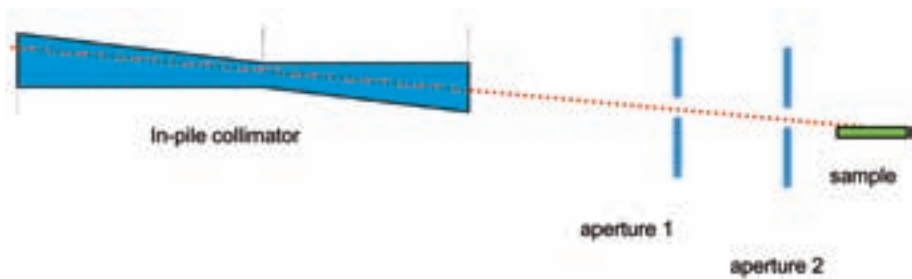


FIG. 5. Liquid samples can be measured by moving the apertures and the sample vertically.

4. CHOPPER CHARACTERISTICS

In a time–distance diagram describing a single chopper the following relation applies:

$$t(x) = c\lambda x + t(0), \quad c = 252.777 \frac{\mu\text{s}}{\text{\AA}\cdot\text{m}} \quad (9)$$

where  $x$  is the distance a neutron with wavelength  $\lambda$  makes in time  $t$ . Let us assume a single chopper with an opening  $\delta\varphi$ , which corresponds to an opening in time  $\delta\tau$ , that rotates with frequency  $f = 1/T$ . The mean wavelength and resolution are given as:

$$\begin{aligned} \langle\lambda\rangle &= \frac{t_0(\langle\lambda\rangle)}{cD} - \frac{\delta\tau}{2cD} \\ \delta\lambda &= \frac{\delta\tau}{2cD} = \frac{T}{2cD} \frac{\delta\varphi}{2\pi} \end{aligned} \quad (10)$$

where  $D$  is the detector–chopper distance.

We require the maximum intensity possible. We denote by  $n(\lambda)$  the neutrons spectrum in the beam, and by  $N_0$  the neutrons/cm<sup>2</sup>/s. The neutrons detected per second will be:

$$\frac{N_0 \int R(\lambda, \lambda_c) n(\lambda) d\lambda}{T} \delta\tau = F(\lambda) \frac{\delta\varphi}{2\pi} \quad (11)$$

where  $R(\lambda, \lambda_c)$  is the reflectivity of the sample. Since  $\delta\lambda$  is a parameter set by the requirements of the experiment in order to improve the intensity, we have to increase  $\delta\varphi$ .

In order not to have overlapping pulses the following equation must apply:

$$\lambda_{\max} \leq \frac{T}{cD} \quad \text{or} \quad \lambda_{\max} \frac{\delta\varphi}{2\pi} \leq 2\delta\lambda \quad (12)$$

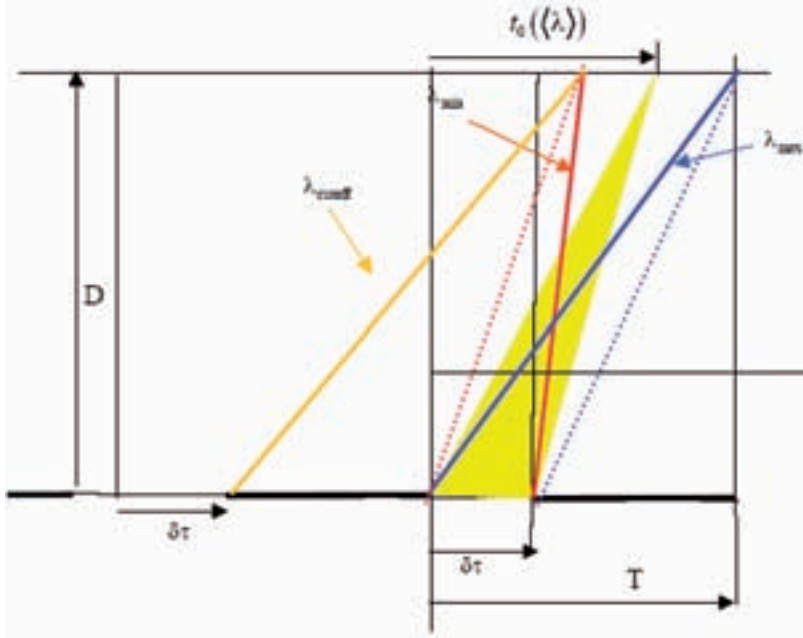


FIG. 6. The time–distance diagram of a single chopper.

Equation (12) shows that resolution and maximum wavelength are coupled and vary proportionally, which means that improvement of the resolution requires a decrease of  $\lambda_{\max}$ .

If we choose the best resolution we would like to use  $\delta\lambda (\text{min}) = 0.1 \text{ \AA}$  and as the maximum wavelength for this resolution as  $\lambda_{\max} (\text{min}) = 4 \text{ \AA}$ , we obtain from Eq. (12):

$$\delta\varphi_1 = 18^\circ \quad (13)$$

and for the detector–chopper distance  $D = 6 \text{ m}$  the maximum frequency is  $f_{\max} = 10\,000 \text{ rev./min}$ . By reducing the frequency from its maximum value we can increase the value of  $\delta\lambda$  as:

$$\frac{\delta\lambda}{\delta\lambda(\text{min})} = \frac{f_{\max}}{f} \quad (14)$$

## DEVELOPMENT OF A TOF REFLECTOMETER

A frame overlap mirror (FOM) is needed for the deflection neutrons with wavelength larger than a critical value,  $\lambda_c$ , in order not to overlap with the fast neutrons of the next chopper pulse. If we set the FOM such as:

$$\lambda_{\max} = 0.8\lambda_c(\theta) \rightarrow \lambda_{\text{cutoff}} = 1.25\lambda_{\max} \quad (15)$$

then the condition in order not to have overlap can be written as:

$$\lambda_{\min}(\text{min}) \geq 0.25\lambda_{\max}(\text{min}) \quad (16)$$

For  $\lambda_{\max}(\text{min}) = 4 \text{ \AA}$  we get  $\lambda_{\min}(\text{min}) = 1 \text{ \AA}$ , which is in accordance with the minimum wavelength of  $1.7 \text{ \AA}$  of the wavelength band that is meaningful to be used as it was argued in Section 2. In order to keep the same minimum wavelength for all frequencies, we have to satisfy the overlap condition:

$$\lambda_{\text{cutoff}}(f) - \lambda_{\min}(f) \leq \frac{T}{cD} = \frac{1}{fcD}$$

In Fig. 7, the variation is depicted of the wavelength versus the frequency for the detector–chopper distance  $D = 6 \text{ m}$  and for  $\Delta\phi=18^\circ$ .

The maximum frequency of the chopper can be lowered by half by having two openings in the chopper disk with the same total opening as in the case of one opening, without deterioration of the resolution and with the same wavelength range.

## 5. MINIMIZATION OF THE BACKGROUND

Another crucial parameter in the design of a reflectometer, especially in the case with a direct view of the reactor core, is the minimization of the background due to fast neutrons and gammas. There are two options for that problem: either (a) by using a thick chopper made of nimonic alloy; or (b) by using a thin chopper together with the use of a sapphire filter. The first option has the disadvantage of making the chopper system too heavy. Single crystals of  $\text{Al}_2\text{O}_3$  (sapphire) have proved an effective fast neutron filter. However, the use

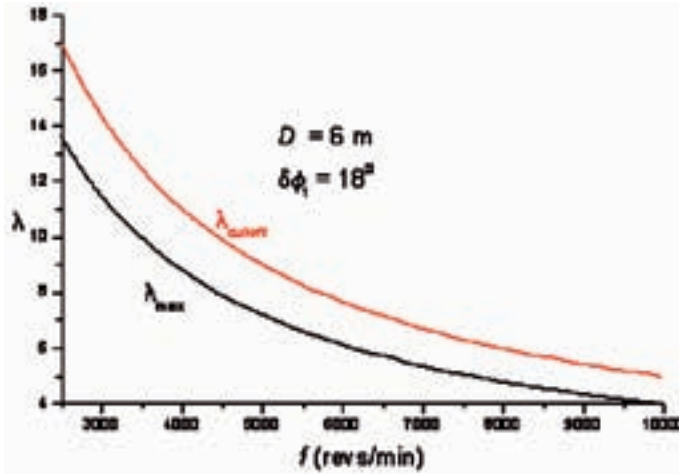


FIG. 7. Variation of neutron wavelength versus the frequency for the detector–chopper distance  $D = 6 \text{ m}$  and  $\Delta\phi = 18^\circ$ .

of such a filter needs to be accompanied by optimization of its parameters and its overall performance in reducing the neutron background of an instrument [1]. The sapphire filter has the additional advantage that it does not require cooling at liquid nitrogen temperature. Also, it acts as a filter for thermal neutrons with wavelengths less than 0.1 nm, due to a great density of high order reflections available to scatter the incident beam.

The parameters necessary for the description of the sapphire filter are its thermal and fast neutron transmission [2]. In the thermal region, the transmission has been measured. We have calculated the fast neutron properties of the sapphire by the MCNP code. Midner et al. [3] measured by transmission the macroscopic linear attenuation,  $\Sigma(\lambda)$ , for sapphire in the wavelength region 0.04–1.2 nm and found it to fit well a function given by Cassels [4]. Figure 8 presents the linear attenuation as a function of wavelength as given by Cassels' equation and the parameters determined by the least squares fit to the experimental data. Consequently, thermal neutron transmission of sapphire of different thickness versus the wavelength can be calculated (Fig. 9). It is observed that the transmission in the wavelength range of interest for a TOF reflectometer (0.17–0.8 nm) is almost constant and very close to unity depending on thickness. Its transmission in the fast neutron region was determined using the MCNP code. The results of the calculations are presented in Fig. 10. The calculated points can be fitted to the empirical equation:

## DEVELOPMENT OF A TOF REFLECTOMETER

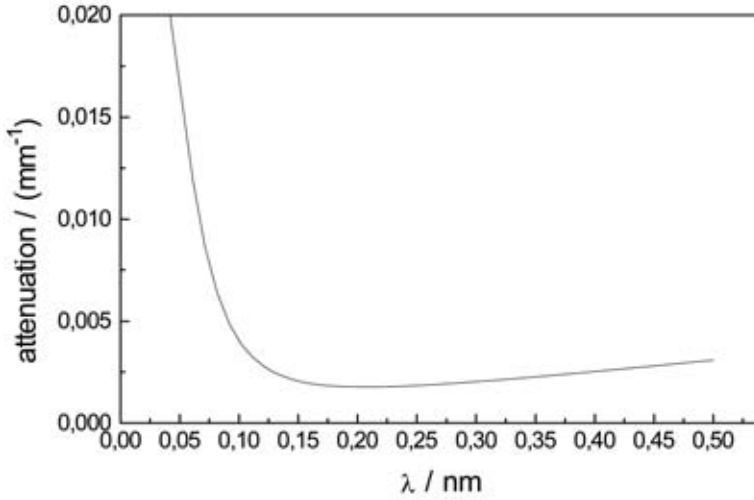


FIG. 8. Macroscopic linear attenuation factor for sapphire as a function of wavelength (line according to an equation given by Cassels [4]).

$$T = I / I_0 = \exp(-L / \langle L \rangle) \quad (17)$$

where  $L$  is the thickness of the crystal and  $\langle L / L_0 \rangle = 31.3 \text{ mm}$  obtained from a least squares fit to the MCNP calculated points.

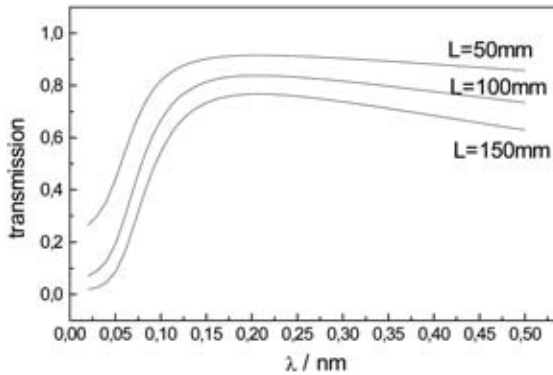


FIG. 9. Sapphire transmission as a function of wavelength for 50, 100 and 150 mm thick crystals (calculated using linear attenuation factor shown in Fig. 8).

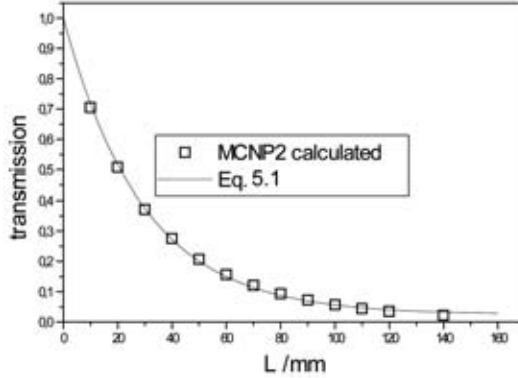


FIG. 10. Fast neutron transmission as a function of sapphire crystal thickness for fission neutrons.

The criteria of optimality of the sapphire filter are the thermal to fast neutron transmission ratio and also the effect of the filter on the neutron background at the vicinity of the instrument.

We define the quality factor of the filter as:

$$\begin{aligned}
 Q(\lambda, L) &= N_{thermal} c_1 T_{thermal} - N_{fast} c_2 T_{fast} \\
 &= A(T_{thermal}(\lambda, L) - \alpha T_{fast}(L))
 \end{aligned}
 \tag{18}$$

where  $N_{thermal}$ ,  $N_{fast}$  denote the flux and  $T_{thermal}$ ,  $T_{fast}$  the transmission of thermal and fast neutrons, respectively. The parameters  $c_1$  and  $c_2$  connect the neutrons emerging from the sapphire and those measured from the detectors in a neutron experiment. Parameter  $a$  should be minimized and in the worse case it would be around 1 assuming that the thermal and fast flux emerging from the reactor are almost equal. Figure 11 shows the filter quality factor  $Q$  as a function of thickness for  $a = 0.5$ . In the wavelength range 0.15–1.0 nm the optimum thickness of the sapphire crystal is around 40 mm.

The whole shielding around the instrument will be optimized with Monte-Carlo calculations using MCNP code.

## 6. GENERAL LAYOUT OF THE INSTRUMENT

The general layout of the TOF reflectometer to be installed at the GRR-1 is depicted in Fig. 12. The TOF reflectometer will have a direct view of the reactor core. Therefore, a sapphire crystal will be used to scatter the fast neutrons out of the main beam. The in-pile collimator will be of a specific

## DEVELOPMENT OF A TOF REFLECTOMETER

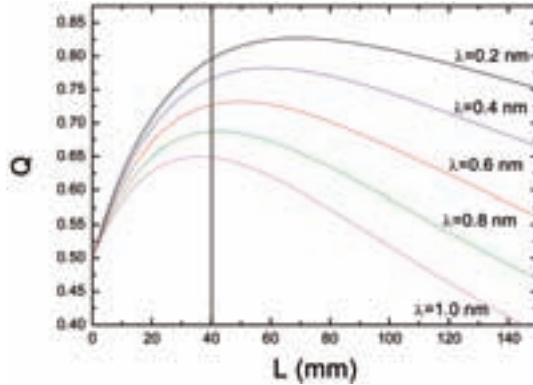


FIG. 11. Sapphire quality factor index  $Q$  as a function of crystal thickness for  $a = 0.5$ .

shape, inclined with respect to the horizon, giving the ability to measure liquid surfaces by moving the apertures together with the sample in the vertical direction.

A thin disk chopper with two window openings of  $9^\circ$  each and of a maximum frequency of 6000 rpm. will pulse the neutron beam. A frame overlap mirror, placed in between the apertures, will deflect the neutrons with wavelength larger than a critical value. Initially a single detector will be used for the detection of the reflected neutron beam. All the components will be able to move on rails.

## 7. CONCLUSION

A TOF neutron reflectometer is at the construction stage for installation at the 5 MW GRR-1 in Greece. Design details of the instrument are described. The in-pile collimator, neutron chopper and the shield are discussed.

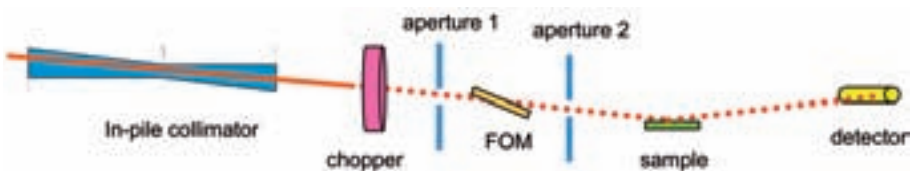


FIG. 12. General layout of the TOF reflectometer.

**ACKNOWLEDGEMENTS**

We acknowledge the financial support of the IAEA and the Greek Secretariat of Research and Technology for the installation of the TOF reflectometer.

**REFERENCES**

- [1] STAMATELATOS, I.E., MESSOLORAS, S., Sapphire filter thickness optimization in neutron scattering instruments, *Rev. Sci. Instrum.* **71** (2000) 70.
- [2] BORN, R., HOHLWEIN, D., SCHNEIDER, J.R., KAKURAI, K., Characterization of a sapphire single crystal for the use as filter in thermal neutron scattering, *Nucl. Instrum. Methods Phys. Res. Sect. A* **262** (1987) 359.
- [3] MIDNER, D.F.R., ARIF, M., STONE, C.A., The neutron transmission of single crystal sapphire filters, *J. Appl. Crystallogr.* **26** (1993) 438.
- [4] CASSELS, J.M., *Prog. Nucl. Phys.* **1** (1950) 185.

# **NEUTRON REFLECTOMETER AT THE BUDAPEST RESEARCH REACTOR WITH POLARIZATION OPTION**

L. CSER

Research Institute for Solid State Physics and Optics,  
Budapest, Hungary

## **Abstract**

A brief description of the history of the development of the reflectometer installed on the third neutron guide at the 10 MW research reactor in the Budapest Neutron Centre (BNC) is given. The performance of the reflectometer allows measurements to study both magnetic and non-magnetic surfaces and interfaces. The ability of the reflectometer is illustrated by some typical experimental results. These results prove that even at a moderate flux facility, useful experimental information can be collected on surface properties of condensed matter by the use of neutron reflectometry.

## **1. INTRODUCTION**

Neutron reflectometry is an effective tool for the study and quality control of thin layered structures of solid and liquid surfaces. The intensity distribution of the reflected neutrons is measured as a function of the scattering wave vector in a small angle specular and/or scattering configuration from an approximately smooth surface. The measured data are converted into structural information: the profile of the neutron scattering length density as a function of the depth perpendicular to the surface can be obtained from the specular scattering. The non-specular diffuse scattering is characteristic of the lateral distribution of surface inhomogeneities. In the present configuration of the reflectometer with vertical reflecting plane, mainly the specular scattering can be measured. The scattering wave vector is measured by scanning the reflection angle and leaving the wavelength spectrum unchanged.

## **2. DESCRIPTION OF THE INSTRUMENT**

The reflectometer with horizontal scattering plane is installed at the third neutron guide which supplies the instrument with cold neutrons from the liquid H<sub>2</sub> cold neutron source [1].

The schematic view of the reflectometer is shown in Fig. 1. The dimensions of the instrument are shown on the scheme of the non-polarizing arrangement (Fig. 2). The monochromatic beam is obtained using a pyrolytic graphite single crystal of mosaicity of 25 angular minutes. The wavelength used is 0.427 nm. The higher order Bragg reflections are filtered out using a Be filter cooled down to liquid nitrogen temperature. The beam is shaped by two slits, the width and position of which can be regulated with micrometer screws between the range of  $\pm 3$  mm and with an accuracy of 0.01 mm. The distance between the slits is 2 m.

The monochromatized beam is polarized by a  $2\theta_{\text{crit}}$  CoFe–Si supermirror 300 mm in length and 55 mm high which is inserted in an external magnetic field strong enough to saturate the mirror. For convenience, the transmitted component of the beam is used. A Mezei-type  $\pi$  flipper is used for reversing the spin orientation of the polarized neutrons. A magnetic guide field of several tens of Gauss is applied between the polarizer and the flipper to preserve the polarization of the beam. A horizontal coil compensates this guide field inside the flipper. A second sequence of guide field is applied between the flipper and the sample as well. The whole polarized beam track was carefully modelled using a 3D magnetostatic computation. The sample holder is mounted on a table rotating around the principal vertical axis of the reflectometer, which is also the axis of rotation of the detector unit with a  $\Theta$ – $2\Theta$  connection between the rotations of the sample and the detector. (Note that the detector can be moved individually also.) The rotating table is operated by a step motor and the

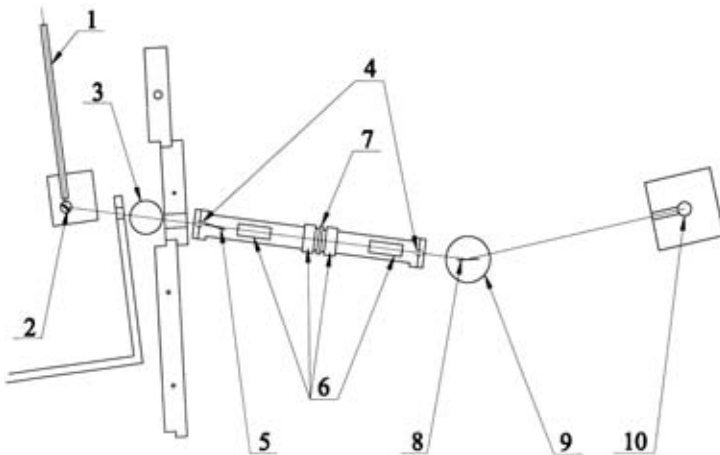


FIG. 1. The schematic view of the reflectometer layout: (1) neutron guide; (2) monochromator; (3) Be filter; (4) Cd slits; (5) polarizing supermirror; (6) guide field magnets; (7)  $\pi$  flipper; (8) sample; (9) sample-holder goniometer; (10) detector.

## NEUTRON REFLECTOMETER AT THE BUDAPEST RR

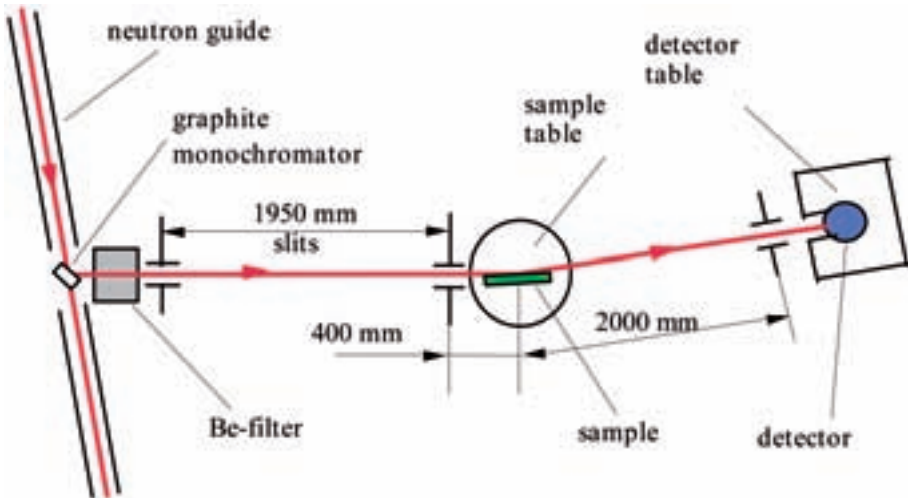


FIG. 2. Reflectometer layout with distances between various components.

precision value of the angles measured by an independent angular encoder, in the range of  $\pm 18^\circ$ , with an accuracy of  $\pm 18''$  (second of an arc) that is  $\pm 0.0055^\circ$ . The sample holder is capable of holding and positioning samples of sizes from  $1 \text{ cm}^2$  up to neutron-guide mirror samples deposited on glass substrates of a maximum size of  $800 \times 300 \text{ mm}^2$ . The mounted samples can be translated in a direction perpendicular to their plane in a range of  $\pm 30 \text{ mm}$ , and can be rotated around a horizontal axis perpendicularly to the principal axis of the reflectometer, in a range of  $\pm 3^\circ$ , with respect to the sample holder.

The reflected neutrons are counted by a  $^3\text{He}$  filled 0.5 inch diameter proportional counter. The efficiency of the detector is higher than 90% for the neutron wavelength 0.427 nm. This detector is shielded by a 12 cm thick boron-carbide column. The detector is moved by a second step motor and the position of it is controlled by double way. An angular encoder together with an independently operating MITUTOYO linear encoder fulfilled the above function. The angular accuracy of these devices is the same as that of the sample-holder one. The angular range covered by the detector extends up to  $13^\circ$ .

A program written in operating system C+ installed on a Pentium PC controls the operation of the whole system including the data collection and data acquisition.

When the reflectometer is used for study of non-magnetic materials, the polarizing supermirror and the flipper has to be removed for providing higher intensity.

The main characteristics of the reflectometer are given in Table 1.

As seen from the table, the quality and efficiency of the reflectometer was considerably increased due to the gains of both the supermirror guide and the cold neutron source.

### 3. RESULTS OF THE TEST MEASUREMENTS

#### 3.1. Estimation of the intensity gain

The number of neutrons reaching the sample position increased by a factor of 92 as compared with that before the installation of the cold source and

TABLE 1. CHARACTERISTICS OF THE REFLECTOMETER

Characteristics	Without cold source	With cold source
Neutron beam	Ni coated neutron guide	$2\theta_{\text{crit}}$ Ni-Ti supermirror multilayer coated neutron guide
Monochromator	Pyrolytic graphite single crystal	Pyrolytic graphite single crystal
Wavelength	0.412 nm	0.43 nm
Angular resolution	0.0055 grad	0.0055 grad
Flux of the non-polarized neutrons	$40 \text{ n}\cdot\text{cm}^{-2}\cdot\text{s}^{-1}$	$3.2 \times 10^3 \text{ n}\cdot\text{cm}^{-2}\cdot\text{s}^{-1}$
Polarizer	-	CoFe-Si supermirror
Flux of the polarized neutrons	-	$1.1 \times 10^3 \text{ n}\cdot\text{cm}^{-2}\cdot\text{s}^{-1}$
Background (for the whole detector)	0.02 (counts/s)	0.01 (counts/s)
Measured spin-flip ratio		> 10
Detector		$^3\text{He}$ filled proportional counter

the new neutron guide. The neutron guide alone increases the intensity by a factor of about five. So, the contribution of the cold source to the increase of

the intensity is equal to about 18. (This value characterizes only the intensity of the wavelength used for the reflectometer.)

### 3.2. The intensity/background improvement

The increase of the intensity together with the rather low background (see Table 1) allows us to carry out measurements with high precision.

The result shown in Fig. 3 demonstrates that the effects requiring the contrast of about 4 or 5 orders — such as scattering on the air filling the gap between the sample and the detector — are clearly detectable.

### 3.3. Typical experimental results

#### 3.3.1. Study of Ni–Ti multilayer systems

The test of the reflectivity of Ni–Ti supermirrors was a regular task carried out on the reflectometer. Some mirrors under investigation were found to be defective, i.e. their reflectivity was quite below the expectation (Fig. 4).

In order to clear up the origin of the imperfectness, an off-specular  $2\Theta$  scan was performed on this supermirror at two well-defined separate angles  $\Theta_1$

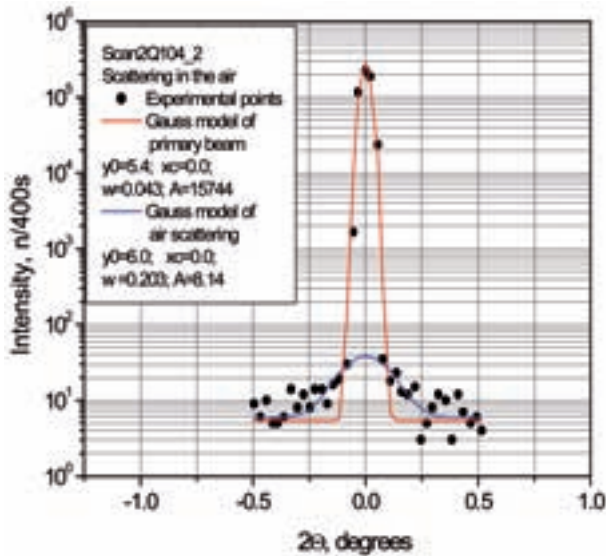


FIG. 3. Effect of air scattering on contrast.

and  $\Theta_2$ . The results are seen in Figs 5(a) and 5(b). At  $\Theta_1$  a broad shoulder in the scattered curve was observed. The appearance of this shoulder indicates the presence of inhomogeneities probably originating from the roughness of the substrate surface that causes a density variation in the directly contacting with the substrate part of the Ti layer. A similar feature was observed near the critical angle of the Ni-coated mirror too. This observation seems to support our hypothesis.

At  $\Theta_2$ , the shoulder displays a quasi-periodical structure (Fig. 5(b)). This oscillation may appear due to the quasi-periodical short range order of some nano-inhomogeneities in the multilayers. When the mirror production procedure was properly changed, these oscillations disappeared.

#### 4. OBSERVATION OF NEUTRON STANDING WAVES

Neutron standing waves (NSWs) generated above a flat layer system during total external reflection can be observed and used for measuring and characterizing the depth profile of the layer structure under investigation. Standing waves are formed by the interference between the incident and specular reflected plane waves above the reflecting surface. This non-destructive technique is particularly useful for measuring the thickness of buried layers. It was found that when the spatial period of NSW matches to the

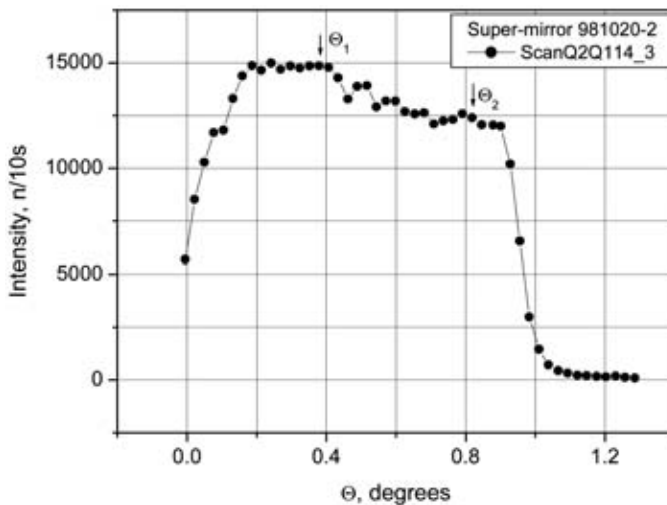


FIG. 4. Reflectivity curve of a 2-theta critical Ni-Ti supermirror.

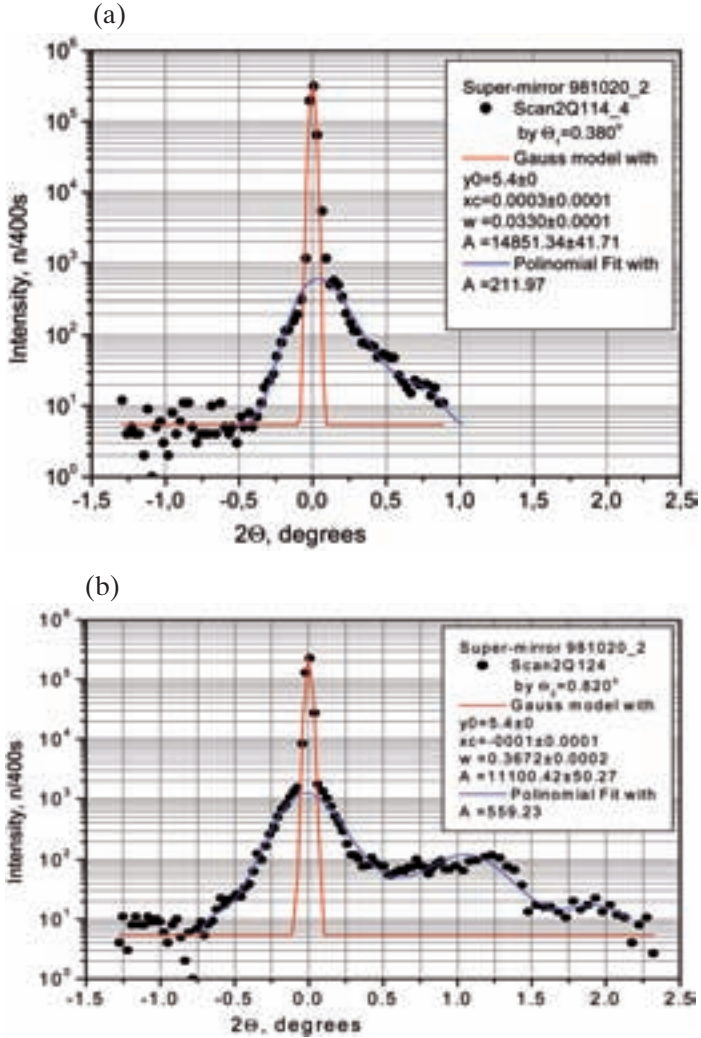


FIG. 5. (a) The scattering patterns at angle  $\theta_1$  and (b) the scattering patterns at angle  $\theta_2$ .

film thickness, their amplitude is amplified. This happens if a layer of higher scattering potential placed on the top of the film, then together with the reflecting mirror it forms a potential well, in which the so called resonance-enhancement takes place. If the top layer is made of neutron-absorbing material (emitting, for example prompt gamma rays following the neutron capture), then neutrons fulfilling the resonance conditions are partly absorbed. The absorption event can be registered in two ways, either by detecting of

enhanced gamma-yield, or by measuring the variation of the reflected neutrons. Due to the rather high gamma background, we were able to use the second way of the observation.

In our experiment we used the above mentioned phenomenon for the calibration of the rate of deposition of Ti by a magnetron sputtering machine. The layer system (estimated thickness of which is 1000 Å permalloy + 2000 Å Ti + 5 Å Gd + 10 Å Al) was deposited on a silicon wafer. The neutron scattering experiment was carried out at the constant wavelength ( $\lambda = 4.3 \pm 0.1$  Å) reflectometer. We used the best value of the angular resolution of the reflectometer, which is  $0.0055^\circ$ . Figure 6 shows the small angle part (below  $\theta = 0.025^\circ$ ) of the measured neutron reflectivity on linear scale. Despite the rather moderate resolution power, the minimums related to the several first modes of the NSW are clearly visible.

The data were evaluated by the use of a standard program PARRATT32. The real part of the 1D potential well is shown in Fig. 7. The calculated reflection pattern allowed to identify the modes and to evaluate the true thickness of the Ti layer and to estimate the thickness of the permalloy layer. Since there was no provision for applying resolution correction, full curve fitting could not be done. Nevertheless, the calculated patterns allow identification of the first five modes (see the insert in Fig. 6) and the quasi-periodical modulation of the reflection curve caused by the permalloy layer is also clearly seen in the large Q part of the scattering pattern. The position of the modes

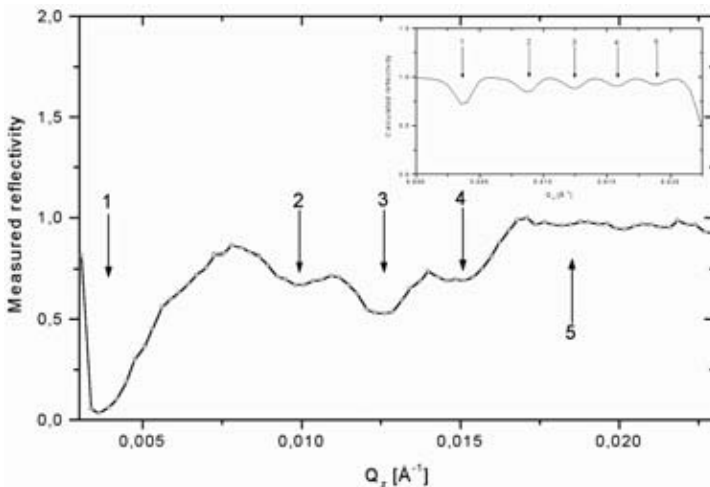


FIG. 6. The low angle part of the measured neutron reflectivity is shown; the insert shows the calculated reflectivity. The arrows with figures show the positions of the first five modes.

observed proves that the thickness of the Ti layer is equal to  $2100 \pm 5 \text{ \AA}$ . From the period of the oscillating behaviour, the thickness of this layer was also estimated. The obtained value is equal to  $980 \text{ \AA}$ , well in agreement with the expectation. Note that the oscillations at the high angle part of the reflection pattern are damped. This effect is evidently caused by the roughness of the layer surfaces and to some extent also by the interpenetration of the neighbouring Ti and permalloy layers.

## 5. ORDERING IN DEPOSITED THIN LAYER

C60 fullerene molecules were deposited from water suspension on a polished silicon wafer surface using the evaporation procedure. The amount of fullerene was chosen for resulting few monolayers of C60 molecules on the substrate.

Two measurements were done. In the first one, the reflectivity of the freshly deposited surface was studied. In the next step, the sample was given a heat treatment (24 hours at  $200^\circ\text{C}$ ) and the reflectivity curve measurement was repeated.

The results are shown in Fig. 8. From the model calculation (continuous line), one may see the influence of the heat treatment on the deposited layer.

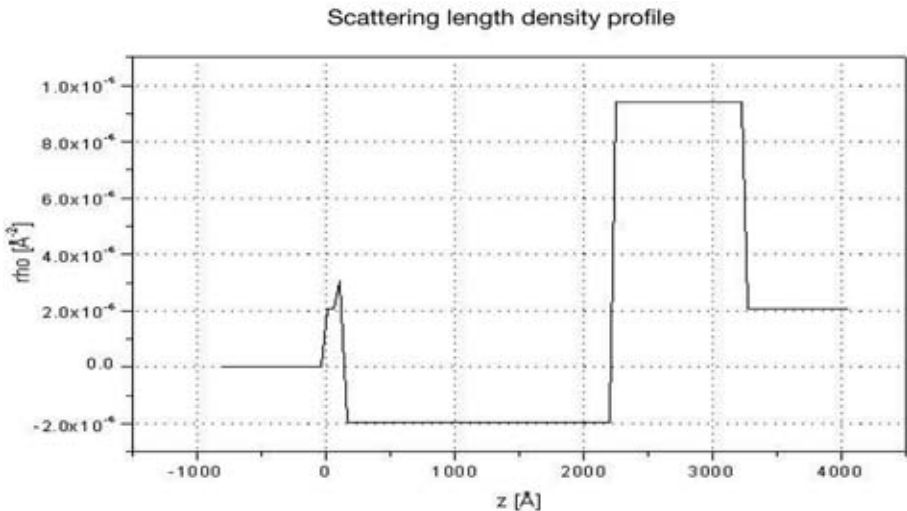


FIG. 7. The real part of the scattering potential well. The sequence of the layers from left to right: air – Al – Gd – Ti – permalloy – silicon. Here rho is the real part of the 1D scattering potential.

The density gets smaller and the thickness gets larger after the heat treatment. This result can be interpreted as a swelling of the layer accompanied with a disordering process due to the influence of the heating.

6. TEST OF THE POLARIZATION OPTION

The intensity gain due to the cold source and supermirror guides permits the implementation of polarization option. Note that during the course of the polarization, about two thirds of the neutrons are lost. Fifty per cent of the loss arises due to the fact that only one half of the neutrons have the proper spin

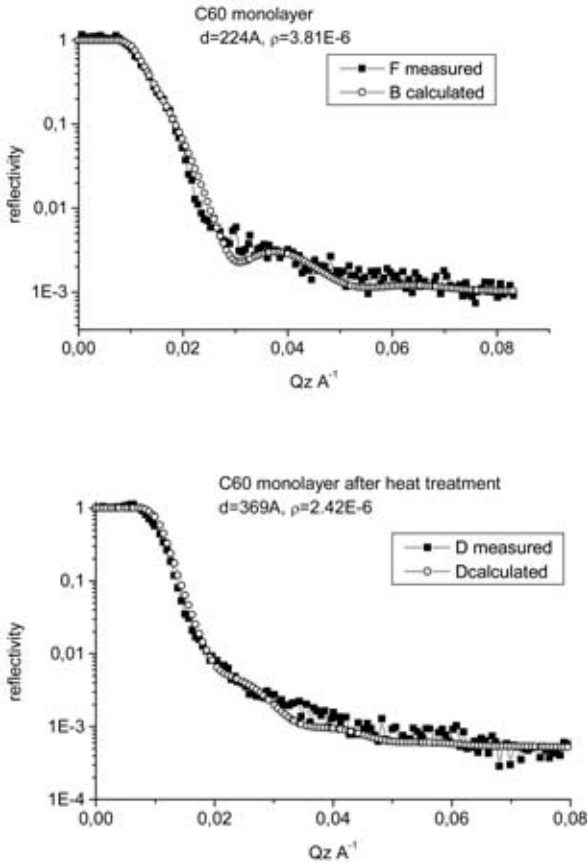


FIG. 8. The reflectivity curve of a C60 layer (a) before (upper curve) and (b) after (lower curve) heat treatment.

orientation and another 15% is due to the scattering of the beam from the silicon layer supporting the supermirror.

The first test measurement with polarized neutrons was carried out using a  $2\theta_{\text{crit}}$  Fe–Ag supermirror put on the place of the sample. The results of the measurement of the angular distribution for the flipper on and flipper off cases are shown in Fig. 9. The sawtooth shape of the scattered curves is caused by the imperfection of the Fe–Ag analyser multilayer. The estimated value of the flipper ratio on average is higher than 10.

## 7. CONCLUSIONS AND FUTURE PROSPECTS

From the above results, it can be seen that reflectometry can be done even at moderate flux research reactors. If the reactor is furnished with cold neutron source and neutrons are transported using neutron guides with supermirror coating, the luminosity of the reflectometer considerably increases.

By introducing focusing monochromator and 2D multidetector, the efficiency of the instrument will be further improved.

The polarization option with polarization analysis of the scattered beam allows us to apply the reflectometer for studying of thin magnetic layers and interfaces more extensively.

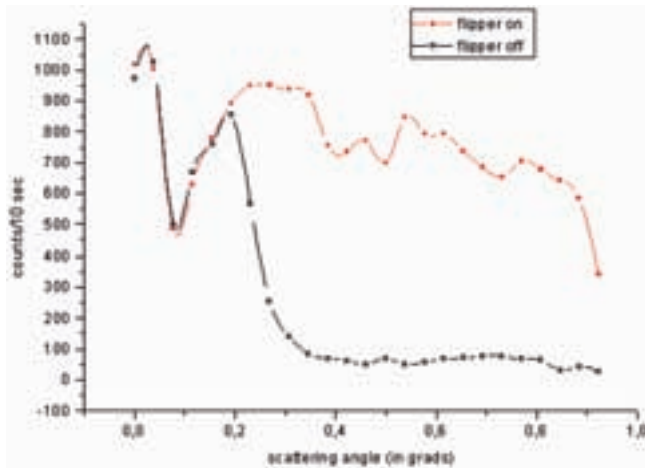


FIG. 9. The reflectometry pattern for the two states of the flipper (•: flipper on; ■: flipper off).

## ACKNOWLEDGEMENTS

The author is indebted to L. Rosta, Gy. Török and G. Vaspál for providing valuable illustrations for the paper.

## REFERENCE

- [1] CSER, L., FÜZI, J., RIECSANSZKY, L., TÖRÖK, Gy., Polarized neutron reflectometer at the Budapest Research Reactor, Appl. Phys. A **74** Suppl. (2002) 8213.

# NEUTRON REFLECTOMETRY AT DHRUVA REACTOR

## *Specular and off-specular neutron reflectivity studies*

S. BASU, S. SINGH

Solid State Physics Division,  
Bhabha Atomic Research Centre,  
Trombay, Mumbai, India

### **Abstract**

A polarized neutron reflectometer (PNR) has been installed at the Dhruva reactor, Trombay. This instrument has been designed for vertical sample geometry, where the reflectivity is measured in the horizontal plane of reflection. Polarized neutron reflectometry is an important non-destructive tool to determine the chemical as well as magnetic structure of thin film samples. Specular reflectivity data collected on a neutron monochromator and Fe/Ge multilayer sample is presented. Off-specular reflectivity data from Ni film has been used to obtain the morphology of the air–film interface and of a buried interface.

### 1. INTRODUCTION

Neutron reflectometry is a widely used tool at present for characterization of various types of surfaces, interfaces and thin films. The types of samples include solid–solid (magnetic–non-magnetic, semiconductor–magnetic) multilayer thin films, polymer–polymer interfaces, liquid–solid interfaces, molecular arrangements at liquid–air interfaces and biological interfaces. The usefulness of the technique has grown so much over the last two decades that most of the major neutron scattering centres have one or more neutron reflectometers installed. At present, there are nearly forty neutron reflectometers operating at various neutron sources. These numbers indicate the popularity of the technique for characterizing the surfaces and interfaces of thin films. The technique is simple and dates back to the initial days of neutron scattering, when Fermi and Zinn used it for obtaining coherent scattering length of materials. Neutron reflectometry is ideally suited for all types of neutron sources spanning a large range of neutron flux. Currently, there is intense interest to understand the physical properties of thin layers, interfaces and surfaces due to the possibility of these materials as devices. In this context, neutron reflectometer is an ideal tool among research reactor instruments.

We have installed a polarized neutron reflectometer (PNR) in the Guide Tube Laboratory at Dhruva, a 100 MW research reactor in the Bhabha Atomic Research Centre (BARC), Trombay, India. Dhruva is a thermal reactor with a peak flux  $1.7 \times 10^{14}$  n/cm<sup>2</sup>/s. The reflectometer is located in the Guide Tube Laboratory of Dhruva. This instrument has been designed for vertical sample geometry, where the reflectivity is measured in the horizontal plane of reflection. Specular neutron reflectometry is an important non-destructive tool to determine chemical as well as magnetic structure of thin film samples. Unpolarized and polarized neutron specular reflectivity data collected on a neutron monochromator and Fe/Ge multilayer sample, respectively, has been collected to obtain chemical density and magnetic moment density depth profiles in the respective multilayer samples. The instrument uses a  ${}^3\text{He}$  based position sensitive detector (PSD) to collect data. This allows one to collect off-specular or diffuse data around any specular peak. Off-specular neutron reflectivity data can be used to obtain in-plane height–height correlation function in thin film samples. Since one needs to measure the intensity of the scattered beam beyond the specular reflectivity condition, collecting diffuse neutron scattering data is difficult and is limited by background at the detector. In our spectrometer, the PSD allows us to collect diffuse scattering data around any specular peak at our medium flux reactor. Off-specular reflectivity data from an Ni film has been used to obtain the morphology of air–film interface and of a buried interface. These data will also be presented.

## 2. THEORY

### 2.1. Specular reflectivity

The Schrödinger equation for a neutron in a potential field  $V(r)$  is given by [1]:

$$\left[ \frac{\hbar^2}{2m} \nabla^2 + V(\vec{r}) \right] \Psi(\vec{r}) = E\Psi(\vec{r}) \quad (1)$$

where  $h$  is Planck's constant,  $m$  is the neutron mass. For a thin film,  $V(r)$  is the potential of the medium experienced by a neutron,  $E$  is the total energy of the neutron and  $\psi(r)$  is the neutron wave function. The potential for an isotropic medium is defined as

$$V(r) = \frac{2\pi\hbar^2}{m} Nb(r) \quad (2a)$$

For polarized neutrons:

$$\bar{V}(r) = \frac{2\pi\hbar^2}{m} Nb \pm \bar{\mu}_n \cdot \bar{B} = \frac{2\pi\hbar^2}{m} N[b(r) \pm p(r)] \quad (2b)$$

where  $\mu_n$ ,  $b$ ,  $B$ ,  $p$  and  $N$  are the neutron magnetic moment, coherent nuclear scattering length, magnetic field in the sample, average magnetic scattering length and the nuclear density, respectively. The  $\pm$  sign in the potential refers to the spin-up and spin-down states of the incident neutrons with respect to the sample polarization.

The above equation can be solved, for a stratification of  $N$  layers, using the transfer matrix method [2] by matching the wave function and its gradient at every interface. The solution is given in matrix form

$$\begin{pmatrix} 1 \\ r \end{pmatrix} = \begin{pmatrix} M_{11} & M_{12} \\ M_{21} & M_{22} \end{pmatrix} \begin{pmatrix} t \\ 0 \end{pmatrix} = M \begin{pmatrix} t \\ 0 \end{pmatrix} \quad (3)$$

where  $r$  is the reflectivity amplitude at the film–air interface. The matrix  $M$  is given by

$$M = D^{-1}(q_1) \left( \prod_{j=2}^{N-1} [D(q_j)P(q_j, d_j)D^{-1}(q_j)] \right) D(q_N) \quad (4)$$

where  $D(q_j)$  are the transmission matrices and  $P(q_j, d_j)$  are propagation matrices for the  $j$ th layer and these are given by

$$D(q_j) = \begin{pmatrix} 1 & 1 \\ q_j - q_j \end{pmatrix}, \quad P(q_j, d_j) = \begin{pmatrix} e^{-q_j d_j} & 0 \\ 0 & e^{q_j d_j} \end{pmatrix} \quad (5)$$

where  $q_j = \left( \frac{2m}{\hbar^2} (E - V_j) \right)^{1/2}$

The specular reflectivity and transmission coefficients,  $r$  and  $t$ , are then given by  $t = 1/M_{11}$  and  $r = M_{21}/M_{11}$ . The reflected intensity is defined as  $R = |r|^2$ . If there is an interfacial roughness the reflectivity amplitude at each interface will get modified and it is included like a Debye Waller factor [3] as given below:

$$r_j = r_j \exp(-q_j^2 \sigma_j^2 / 2) \quad (6)$$

where  $\sigma_j$  is the root mean square roughness at the  $j$ th interface and  $r_j$  is the reflectivity amplitude of that interface. We have used this matrix method to generate the specular reflectivity pattern for a given set of physical parameters of stratification.

Usually, specular reflectivity is measured as a function of ‘ $q$ ’, the wave vector change of the neutron due to reflection, normal to the plane of the thin film, given by:

$$q = \frac{4\pi}{\lambda} \sin \frac{\theta}{2} \quad (7)$$

where  $\theta$  is the angle of scattering and  $\lambda$  is wavelength of the incident neutron.

## 2.2. Off-specular reflectivity

Off-specular (diffuse scattering) reflectivity (DNS) measurement yields the lateral structure of rough interfaces (morphology of interfaces, i.e. the height–height correlation function and the corresponding cross-correlation functions) of thin films and multilayers. In the case of off-specular reflectivity, there is an in-plane component of the wave vector transfer ‘ $q$ ’. If the interfaces are rough, the specular component of the scattered beam is suppressed. Sinha et al. [4] formulated a distorted-wave Born approximation (DWBA) formalism for a single rough surface to analyse off-specular X ray reflectivity data. The DWBA formalism was further extended to layered structures by Holý et al. [5] and others [6, 7]. We determined the detailed morphology of the interfaces of Ni thin film on glass substrate from DNS measurements, using the formalism of Holý et al. Specular NR has been used to determine the thickness of the individual layers in the sample, density of the layers and interface roughness. The cross-section for diffuse scattering from a multilayer with  $N$  interfaces can be expressed in the DWBA as [5]:

## NEUTRON REFLECTOMETRY AT DHRUVA

$$\left(\frac{d\sigma}{d\Omega}\right)_{diff} = \frac{k_0^4}{16\pi^2} \sum_{i,j=1}^N (n_i^2 - n_{i+1}^2)(n_j^2 - n_{j+1}^2)^* I_{jk}(q_r) \sum_{m,n=1}^3 \tilde{G}_j^m \tilde{G}_k^{n*} \times \exp\left\{-\frac{1}{2}\left[(q_{z,j}^m \sigma_j)^2 + (q_{z,k}^{n*} \sigma_k)^2\right]\right\} \quad (8)$$

where  $I_{jk}(q_r)$  is given by:

$$I_{jk}(q_r) = \frac{1}{q_{z,j}^m q_{z,k}^{n*}} \int d^2r \left[ \exp\{q_{z,j}^m q_{z,k}^{n*} C_{j,k}(\bar{r})\} - 1 \right] \exp(iq_r \cdot \bar{r}) \quad (9)$$

$C_{j,k}(\bar{r})$  is the height–height correlation function,  $k_0$  is the magnitude of the incident wave vector and  $n$  is the refractive index of the reflecting medium. Subscripts ‘ $i$ ’ and ‘ $j$ ’ are the layer indices. The lateral roughness structure of the interfaces is taken into account in Eq. (8) by the correlation function, which can be expressed as

$$C_{j,k}(\bar{r}) = \langle h_j(\bar{r}) h_k(0) \rangle$$

$$\mathbf{q}_j^m = (q_r, q_{z,j}^m)^T$$

is the momentum transfer vector within each layer.  $q_{z,j}^m$  is the component of wave vector transfer normal to the plane and  $q_r$  is the in-plane component. The factor  $\tilde{G}_j^m$  is defined by

$$\tilde{G}_j^m = G_j^m \exp(-iq_{z,j}^m z_j)$$

The expressions for  $G_j^m$  and  $\mathbf{q}_j^m$  for each layer are denoted by [6, 7]

$$G_j^0 = T_{i,j} T_{f,j}, G_j^1 = T_{i,j} R_{f,j}, G_j^2 = R_{i,j} T_{f,j}, G_j^3 = R_{i,j} R_{f,j}$$

$$\mathbf{q}_j^0 = \mathbf{k}_{i,j} + \mathbf{k}_{f,j} \quad \mathbf{q}_j^1 = \mathbf{k}_{i,j} - \mathbf{k}_{f,j} \quad \mathbf{q}_j^2 = -\mathbf{q}_j^1 \quad \mathbf{q}_j^3 = -\mathbf{q}_j^0 \quad (10)$$

where the amplitudes  $T_{i,j}$  and  $R_{i,j}$  of transmitted and reflected waves in a multilayer with ideally smooth interfaces are defined for an incident wave vector  $k_i$  and for a scattered wave vector  $k_f$ , respectively.  $\sigma_j$  represents the total interfacial roughness for the  $i$ th interface, containing both its interface roughness amplitude and intermixing width [8].

The morphology of the  $j$ th interface is defined by the auto correlation function  $C_j(\mathbf{X}) = \langle h_j(x) h_j(x + \mathbf{X}) \rangle_x$ .  $h_j$  denotes the height of interface  $j$  at the

lateral position  $x$  with respect to the average interface height  $\bar{h}$ . All the interfaces are assumed to have self-affine morphologies [9], limited by a finite lateral cut-off [10]. Such a model gives a surface height–height correlation function

$$C_j(X) = \langle h(x)h(x+X) \rangle = \sigma_j^2 \exp\left\{-\left(X/\xi_j\right)^{2H_j}\right\} \quad (11)$$

where  $\sigma_j$  is the root mean square surface or interface roughness,  $\xi_j$  the correlation (cut-off) length, a measure of the lateral length scale of roughness and  $H_j$ , the Hurst parameter, describes the texture of roughness, of the respective interface. The Hurst parameter  $H_j$  can take a value  $0 < H_j < 1$  and gives fractal box dimension  $D_j = 3 - H_j$  of the interface [9]. Another function related to  $C_j(X)$ , the height difference correlation function  $g_j(X)$  is defined as:

$$\begin{aligned} g_j(X) &= \langle [h_j(x) - h_j(x+X)]^2 \rangle \\ &= 2\sigma_j^2 [1 - \exp\{-\left(X/\xi_j\right)^{2H_j}\}] = 2\sigma_j^2 - 2C_j(X) \end{aligned} \quad (12)$$

### 3. INSTRUMENT

#### 3.1. Description

The PNR is located on a neutron guide tube with a radius of curvature of 3.3 Km with a critical wavelength of 2.2 Å [11]. The schematic of the spectrometer is shown in Fig. 1. The [113] reflection of a cylindrical Si

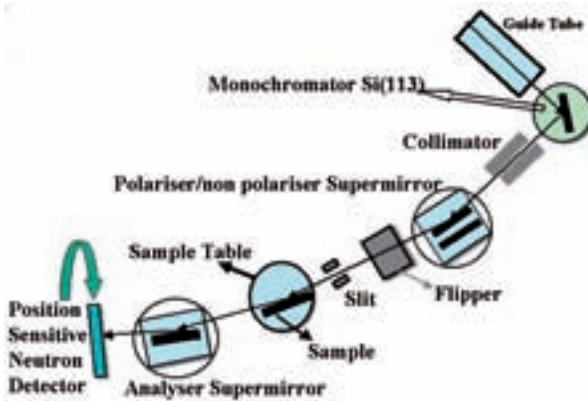


FIG. 1. Schematic diagram of the PNR at Dhruva Guide Tube Laboratory.

## NEUTRON REFLECTOMETRY AT DHRUVA

monochromator gives a monochromatic neutron beam of  $2.5 \text{ \AA}$ , reflected out at approximately 90 degree angle with respect to the guide tube axis. As the monochromatic neutron beam emerges from the monochromator shielding it passes through a collimator consisting of two vertical cadmium slits of 40 mm height located at a distance of 800 mm from each other. Different combinations of such slits can be used to get a vertical neutron beam of varying horizontal divergence in the range of 1 to 6 arc-minutes. Following the collimator, we have installed two vertical polarizer and non-polarizer neutron supermirrors parallel to each other on a translation/rotation stage combination. This allows us to easily switch from polarized to non-polarized mode by translating the required supermirror in the reflecting position for the collimated neutron beam. After the supermirror assembly, the beam passes through a third cadmium slit, similar to those in the collimator. The third slit is close to the sample and restricts *footprint effect* at the sample position. There is a D.C. flipper in the beam after the third slit, for flipping polarization direction, followed by the sample stage. The sample is placed on a high precision rotation stage between the poles of a permanent magnet. The smallest step size of the rotation stage is 0.001 degree with accuracy of  $\sim 15$  arc-seconds. There is option for an analyser supermirror after the sample for collecting data in polarization analysis mode as shown in Fig. 1. The reflected neutrons are counted using a  ${}^3\text{He}$  gas based linear position sensitive detector (PSD). A photograph of the instrument is shown in Fig. 2.

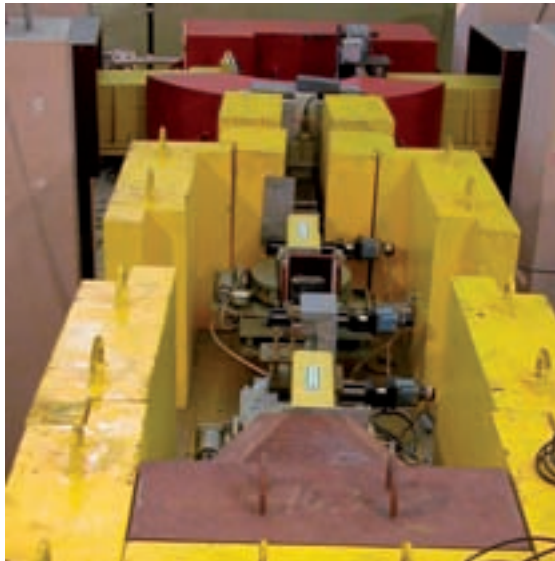


FIG. 2. The PNR at Dhruva.

The direct or reflected neutron beam produces a Gaussian peak at the detector, the width of which dictates the instrumental resolution. The peak width at the detector is a convolution of the angular divergence of the neutron beam and the position resolution of the PSD. The PNR works in step-scan mode. As we change the incident angle on the sample by rotating the sample table, the reflected beam travels on the PSD, which is indicated by the shift in the peak position of the Gaussian. Each point in the reflectivity curve is the background corrected integrated intensity under the Gaussian peak. From the shift in the peak position on the PSD one can calculate angle of reflection from simple geometrical considerations. Figure 3 shows the reflected peak at several angles and the integrated areas under the peaks have given the reflectivity profile in the inset of Fig. 3.

### 3.2. Control and data acquisition system

We have used a stepper motor-based control system for the reflectometer, with high precision translation and rotation stages. The monochromator is mounted on a tilt and rotation stage assembly. We have maximized the intensity of neutrons at the sample position by tilting the monochromator about a horizontal axis. The entire spectrometer from the collimator to the detector is mounted on a table along with shielding blocks, anchored to the monochromator stand. This table can rotate around the monochromator to facilitate  $\theta$ - $2\theta$  coupling between the monochromator and the table. The collimator is mounted on a high precision linear stage, which can move the collimator in steps of  $10\ \mu\text{m}$  across the beam. We

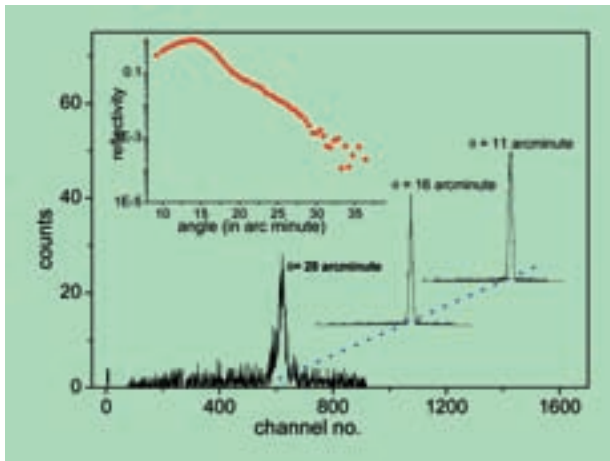


FIG. 3. The reflected intensity versus channel number for three different angles of reflection. The inset shows the integrated reflectivity versus angle of reflection.

also have a similar linear stage to move the second slit in the collimator across the first slit. These two stages were used initially to align the neutron beam on the sample table centre. The sample and the magnet are also mounted on a linear stage with one micron step size on top of the rotation stage. Initially the sample surface is brought to the centre of the rotation stage with the help of this linear stage. For the high precision rotation stage we have an optical encoder with 360 000 pulses per rotation located at the bottom of the rotation table. This optical encoder allows us to read true rotation of the table. The control system for all the stepper motors is an integral unit with the drivers and the power supplies located in it. It is operated from a PC through a serial port communication.

The Electronics Division, BARC, has developed the data acquisition system for the PSD based reflectometer [12]. We have the option for collecting data either for a fixed number of monitor counts or for a fixed time. The data acquisition software allows us to select the number of steps in the reflectivity scan and the angular step size. Once we set a run, the system collects data for fixed monitor counts (or time), saves the data channel wise in a file, moves to the new reflection angle and restarts the run. The software also displays the real time data in several modes that one is allowed to choose interactively.

### 3.3. Resolution

The resolution of the instrument for small angle of scattering, as in case of reflectometry, is given by:

$$\frac{\Delta q}{q} = \sqrt{\left(\frac{\Delta\lambda}{\lambda}\right)^2 + \left(\frac{\Delta\theta}{\theta}\right)^2} \quad (11)$$

where  $\Delta\lambda$  is the spread in the wavelength of the neutron and  $\Delta\theta$  is the angular divergence of beam. In the present case we are using a Si single crystal (113) monochromator for 2.5 Å neutrons. There is no second order contamination for the chosen reflecting plane. The monochromator crystal has a mosaic spread of about 10 arc-minutes. This gives  $\Delta\lambda/\lambda \sim 10^{-3}$  (0.1%). The major contribution towards  $q$  resolution comes from the angular divergence term,  $\Delta\theta/\theta$ , which is typically in the range of 0.03–0.2 in the present reflectometer.

## 4. RESULTS AND DISCUSSION

The PNR is routinely used to obtain chemical and magnetic density profile of single and multilayer thin film samples. In-plane morphologies of

several samples have also been determined from off-specular reflectivity measurements. We present some results of unpolarized and polarized neutron reflectivity measurements from which we have obtained chemical and magnetic depth profile of multilayer samples. We will also present results of off-specular neutron reflectivity from a Ni film, which gave the in-plane roughness morphology of the film.

#### 4.1. Specular neutron reflectometry

##### 4.1.1. Chemical density profile of multilayer neutron monochromator by unpolarized neutron reflectometry

We are using a sputter-deposited multilayer neutron mirror, made from ten periodic bi-layers of Ni–Mo alloy and Ti on float glass substrate, as the non-polarizing supermirror in our instrument. This supermirror was procured from PNPI, GATCHINA [13]. Since the design thickness of the layers, composition and the reflectivity profile of the mirror were known; we used this as a standard sample to calibrate our reflectometer. We had chosen an angular resolution of 0.85 arc-minute for a high resolution unpolarized run. The experimentally observed specular non-polarized reflectivity profile along with the fitted curve is shown in Fig. 4. We have developed a genetic algorithm [14] based  $\chi^2$

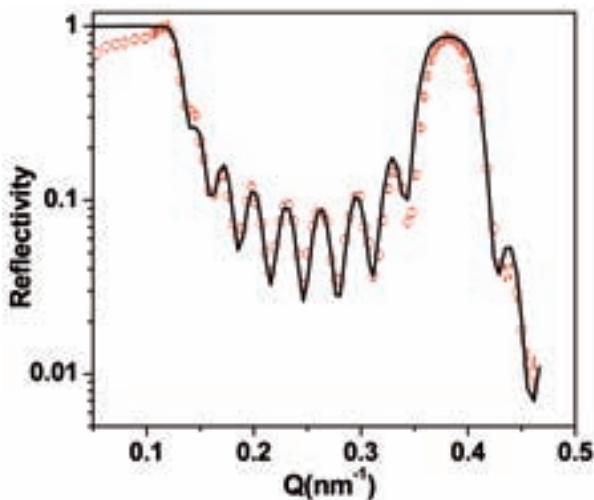


FIG. 4. Reflectivity of a Ni–Mo/Ti based neutron monochromator. Solid circles are the experimental points and the continuous line is the fitted reflectivity profile. Intensity at the Bragg peak at  $0.039 \text{ \AA}^{-1}$  is 70% of the reflectivity plateau.

TABLE 1. PHYSICAL PARAMETER OBTAINED FROM THE BEST FIT OF THE REFLECTIVITY PLOT (FIG. 4) OF [(NI-MO ALLOY)/TI]<sub>10</sub> SAMPLE

Layer material	Design thickness	Thickness from fit	Bulk scattering-length density	Scattering-length density from fit	Average interface roughness from fit
Ni-Mo alloy	86.0 Å	88.6 Å	$7.92 \times 10^{-6} \text{ \AA}^{-2}$	$7.00 \times 10^{-6} \text{ \AA}^{-2}$	10 Å
Ti	76.0 Å	78.7 Å	$-1.90 \times 10^{-6} \text{ \AA}^{-2}$	$-1.65 \times 10^{-6} \text{ \AA}^{-2}$	10 Å

minimization program [15] to obtain various physical parameters from the experimental reflectivity profile. The Kiessig oscillations due to total thickness of the film and the Bragg peak due to the periodic bi-layer are clearly resolved in the experimental pattern. The thickness values obtained from the fit and the design values match closely. The designed thicknesses and bulk densities along with the fitted thicknesses and densities are given in Table 1.

4.1.2. *Magnetic density profile of semiconductor-ferromagnet multilayer by polarized neutron reflectometry*

Electron transport across interfaces in layered structure of semiconductor-ferromagnetic materials [16, 17] and magnetic coupling between the ferromagnetic layers across the semiconductor [18] have shown novel features, which make these systems potential candidates for application as spin injection devices. We have characterized a sample of five bi layers of Fe and Ge, each 20 Å thick, deposited on a buffer layer of Ge (100 Å) on Si (100) substrate. The multilayer is covered on top by 30 Å of Au to prevent oxidation. The complete structure of the sample is: Si[100] substrate/Ge<sub>100Å</sub> [[Fe<sub>20Å</sub> | Ge<sub>20Å</sub>]<sub>5</sub>/Au<sub>30Å</sub>. The sample was deposited by a high precision RF sputtering unit. We obtained the chemical depth profile from unpolarized neutron reflectometry (not shown here) and magnetic density depth profile from polarized neutron reflectometry for this sample [19]. The PNR patterns at room temperature for up ( $R^+$ ) and down ( $R^-$ ) polarized neutrons are shown in Fig. 5. The solid circles in Fig. 5 represent  $R^+$  and the open circles represent the  $R^-$ , respectively. The continuous lines are the best fits for the observed reflectivity profiles. For analysis of the data in polarized mode we froze the structural parameters obtained from the reflectivity pattern in unpolarized mode and varied only the magnetic moment of the iron layer in a GA based  $\chi^2$  minimization process as mentioned earlier.

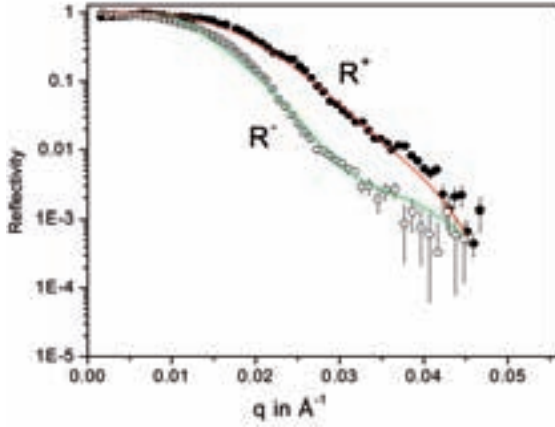


FIG. 5. Polarized neutron reflectivity profile for the Fe/Ge multilayer with up ( $R^+$ ) and down ( $R^-$ ) neutron with respect to the sample magnetization. Solid points are experimental data and continuous lines are the fitted profiles.

The average value of magnetic moment for iron, obtained from the fits to the spin-up ( $R^+$ ) and spin-down ( $R^-$ ) data was  $1.43\mu_B$ . This is considerably lower compared to the bulk magnetic moment value of  $2.2\mu_B$  for Fe.

#### 4.2. Interface morphology by off-specular (diffuse) neutron scattering from Ni film

Since the specular data are collected on a PSD, they also allow us to collect the off-specular data around any specular peak. This is equivalent to detector scan mode in a conventional  $\theta$ - $2\theta$  set-up [6]. We collected DNS data from a piece of Ni coated float glass guide element in Dhruva. We obtained the height-height correlation function at the interfaces of the Ni film from the data. Figure 6 shows the results of off-specular reflectivity measurements around specular peaks at  $Q_z$  values of  $0.022 \text{ \AA}^{-1}$  and  $0.03 \text{ \AA}^{-1}$  from this sample. The instrument integrates the data in the vertical direction (Y direction) and the plots correspond to scan in horizontal momentum transfer  $Q_x$  in the plane of the sample. The open circles and the solid lines represent the experimental data and the best fits, respectively. We have developed a  $\chi^2$  minimization program, which uses the formalism given in Eqs (7)–(10) to analyse the off-specular neutron reflectivity data.

The fits to the DNS data give the parameters  $\sigma_j$ ,  $\xi_j$  and  $H_j$  for the interfaces in the sample. For the present sample we found out from specular neutron reflectivity (not shown) that there is a  $1200 \text{ \AA}$  thick Ni layer of

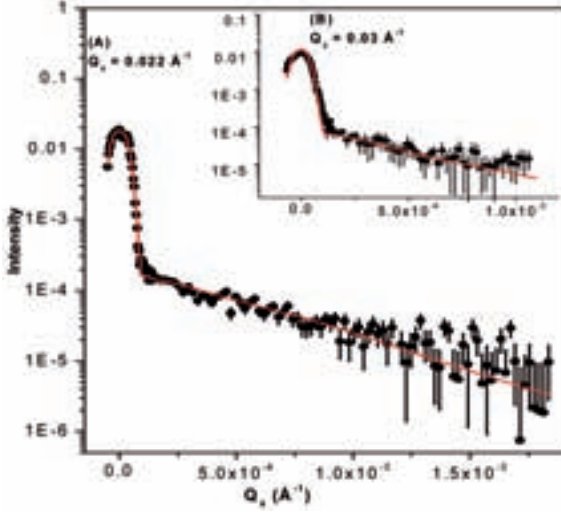


FIG. 6. Diffuse reflectivity patterns of the Ni film at  $Q_z$  values of  $0.022 \text{ \AA}^{-1}$  (A) and  $0.03 \text{ \AA}^{-1}$  (B). The solid points are the background corrected data and the continuous lines are the fitted reflectivity pattern calculated using the formalism of Holý et al. (see text).

near-bulk density on top of the float glass substrate and another low density layer (about 50% of bulk) of  $250 \text{ \AA}$  thickness above the high density layer. There are three interfaces in the film: air/low density layer, low density/high density layer and high density layer/substrate. In this case the DNS data contains information of all the interfaces because of deep penetrability of neutrons. For comparison, we also obtained the height difference correlation function  $g(R)$  at the air–film interface from atom force microscopy (AFM) in the contact mode using Si etched tips, on the same film. The function  $g(R)$  for the air–film interface obtained from AFM data and the DNS data are shown in Fig. 7 along with the experimental  $g(R)$ . The results obtained from the best fit of off-specular neutron data along with AFM results are given in Table 2. The physical parameter obtained from specular reflectivity e.g. thickness and scattering length density of each layer, is used to measure the transmission and reflection amplitudes  $T$  and  $R$ , respectively at each interface in Eq. (10). The results of AFM and DNS agree well for the top surface. Moreover, DNS also reveals the morphology of the underlying interface of low density and high density Ni layers. The two morphologies are quite different. The top surface has a Hurst parameter  $H$  equal to 0.52. This means that in short range the dimensionality (3-H) of the surface is close to 2.5. The lower interface has a local fractal dimension of  $\sim 2$ .

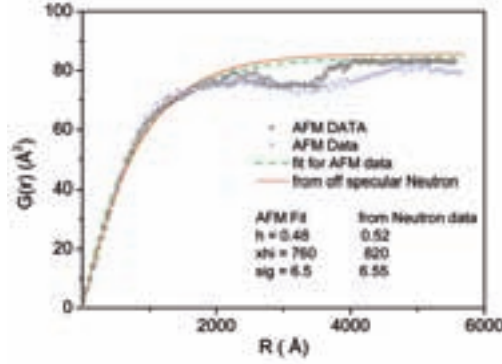


FIG. 7. Experimental height difference correlation function  $g(R)$  at the air–film interface as obtained from AFM for two different scan lengths (blue and black open circles). The discontinuous line is the fitted  $g(R)$  (Eq. (12)) to AFM data and the continuous line is  $g(R)$  from the best fit to diffuse neutron scattering data.

5. CONCLUSIONS

The PNR in Dhruva, Trombay, is successfully being used for characterizing thin films and multilayers. The instrument can be used for specular reflectivity in unpolarized and polarized modes. While it is used in the unpolarized mode, chemical density profile of films as a function of depth can be obtained. We have demonstrated this from the reflectivity profile of an Ni–Mo/Ti supermirror in this work. Specular reflectivity in polarized mode gives the magnetic moment density profile in magnetic films. We have presented the results of polarized neutron reflectivity results of an Fe/Ge multilayer. The

TABLE 2. RESULTS EXTRACTED FROM THE BEST FIT OF OFF-SPECULAR NEUTRON REFLECTIVITY MEASUREMENTS COMPARED WITH AFM RESULTS

Interface	Probe	$\sigma$ (Å)	$\xi$ (Å)	H
Air–film	AFM	6.50	760.0	0.48
	DNS	6.55	820.0	0.52
Low density–high density	DNS	9.60	385.0	0.87
Substrate–high density	DNS	10.00	1845.0	0.48

reflectometer uses a PSD for collecting reflectivity data. This allows us to collect off-specular (or diffuse) neutron reflectivity data. We have obtained in-plane morphology of an Ni film from DNS data collected on this reflectometer. The results presented in this paper clearly demonstrate the wide usability of neutron reflectometry as a non-destructive tool for characterizing thin films and multilayers.

### ACKNOWLEDGEMENTS

The high precision rotation stage was designed and fabricated at CDM, BARC. The Electronics Division, BARC, has developed the control and data acquisition system for the reflectometer. The authors would like to thank V. Holý for providing the FORTRAN program for generating diffuse scattering cross-section for X rays in the case of multilayer films. This program has been suitably modified to fit the diffuse neutron scattering data in the present studies.

### REFERENCES

- [1] LEKNER, J., in *Theory of Reflection of Electromagnetic and Particle Waves*, Nijhoff, Dordrecht (1987); ZABEL, H., *Festkörperprobleme* **30** (1990) 197.
- [2] BLUNDELL, S.J., BLAND, J.A.C., Polarized neutron reflection as a probe of magnetic films and multilayers, *Phys. Rev. B* **46** (1992) 3391.
- [3] NÉVOT, L., CROCE, P., Caractérisation des surfaces par réflexion rasante de rayons X. Application à l'étude du polissage de quelques verres silicates, *Rev. Phys. Appl.* **15** (1980) 761.
- [4] SINHA, S.K., et al., X-ray and neutron scattering from rough surfaces, *Phys. Rev. B* **38** (1988) 2297.
- [5] HOLÝ, V., BAUMBACH, T., Nonspecular x-ray reflection from rough multilayers, *Phys. Rev. B* **49** (1994) 10668.
- [6] SCHLOMKA, J.P., et al., X-ray diffraction from Si/Ge layers: Diffuse scattering in the region of total external reflection, *Phys. Rev. B* **51** (1995) 2311.
- [7] STETTNER, J., et al., Interface structure of MBE-grown  $\text{CoSi}_2/\text{Si}/\text{CoSi}_2$  layers on Si(111): Partially correlated roughness and diffuse x-ray scattering, *Phys. Rev. B* **53** (1996) 1398.
- [8] WORMINGTON, M., et al., Evidence for grading at polished surfaces from grazing-incidence X-ray scattering, *Philos. Mag. Lett.* **74** (1996) 211.
- [9] MANDELBROT, M., *The Fractal Geometry of Nature*, Freeman, New York, (1982); BARNESLEY, M.F., et al., *The Science of Fractal Images*, Springer, Berlin (1988).

- [10] PALASANTZAS, G., KRIM, J., Effect of the form of the height-height correlation function on diffuse x-ray scattering from a self-affine surface, *Phys. Rev. B* **48** (1993) 2873.
- [11] BASU, S., MADHAV RAO, L., Computer simulation study of neutron guide performance at the Dhruva reactor, *Physica B* **174** (1991) 409.
- [12] BEHERE, A., et al., Modernisation of electronics instrumentation for neutron diffractometers, *Solid State Phys. (India)* **45** (2002) 123; Pande, S.S., et al., Data acquisition and processing software for linear PSD based neutron diffractometers, *Solid State Phys. (India)* **45** (2002) 125.
- [13] <http://nrd.pnpi.spb.ru/nod/index.html>
- [14] GOLDBERG, D.E., in *Generic Algorithm in Search, Optimization and Machine Learning*, Addison-Wesley, Reading, MA (1989).
- [15] SURENDRA, S., BASU, S., Analysis of neutron reflectometry data using genetic algorithms, *Solid State Phys. (India)* **44** (2001) 257.
- [16] FIEDERLING, R., et al., Injection and detection of a spin-polarized current in a light-emitting diode, *Nature* **402** (1999) 787.
- [17] KNEEDLER, E.M., et al., Influence of substrate surface reconstruction on the growth and magnetic properties of Fe on GaAs (001), *Phys. Rev. B* **56** (1997) 8163.
- [18] XU, Y.B., et al., Evolution of the ferromagnetic phase of ultrathin Fe films grown on GaAs(100)-4 × 6, *Phys. Rev B* **58** (1998) 890.
- [19] SURENDRA, S., Ultrathin multilayer of Fe and Ge: Structure and magnetic properties, *Appl. Surf. Sci.* **240** (2004) 251.

# APPLICATION OF POLARIZED NEUTRON REFLECTOMETRY

A.R. WILDES  
Institut Laue-Langevin,  
Grenoble, France

## Abstract

A summary of the reflectometry techniques using polarized neutrons is presented. The cases for using these techniques and the information that can be gathered in the measurements are discussed. Examples taken from recent literature are included to illustrate the various points.

## 1. INTRODUCTION

Reflectometry is an experimental technique whereby an incident wave is reflected at an interface and the intensity and angle of the reflected wave is measured as a function of the incident angle and/or wavelength. The technique applies to any form of wave, however, it has become particularly popular for electromagnetic radiation due to its ability to penetrate a substance and measure the properties of buried interfaces. More recently, neutron reflectometry has emerged as a powerful and complementary technique to X ray reflectometry. Indeed, the popularity of the technique has evolved to a point where one of the first instruments to be considered essential and constructed at any new neutron source is a reflectometer.

Two features give neutron reflectometry a powerful and sometimes unique perspective on a scientific problem: the interaction of the neutron with the nucleus, meaning that the neutron has sensitivity to light elements and isotopes; and the interaction of the neutron with the magnetization of the sample. The second feature results from the fact that a neutron has a magnetic dipole moment that interacts with the magnetization in the sample. If all the neutrons in the beam have the same moment direction, this interaction can be measured and highly detailed and precise information on the magnetic structure can be obtained. Such a neutron beam is called polarized, thus the technique is called polarized neutron reflectometry (PNR).

As a general rule, polarized neutron scattering techniques are used for:

- The separation of nuclear from magnetic scattering;
- The determination of the magnitude and the orientation of the local magnetization of the sample;
- The measurement of the coupling between magnetic and nuclear structures.

Polarized neutron techniques are also sometimes used when the scattering from the sample has a significant incoherent contribution, as some incoherent scattering causes a rotation of the neutron spin. This technique is not generally used in PNR, and so will not be discussed here.

When used in reflectometry, polarized neutrons become powerful tools for measuring the magnetic properties of thin films and multilayers. These properties are of paramount importance for many applications in the popular field of nanotechnology, and many recent reviews have been written listing the systems that have been examined using PNR [1–4]. The current paper aims to give an overview of the types of problems that may be solved with the aid of polarized neutron reflectometry. A few select examples are given to illustrate the appearance of the data that is collected and the conclusions that may be drawn.

## 2. THEORY OF POLARIZED NEUTRON REFLECTIVITY

It is beyond the scope of this paper to provide detailed theory for polarized neutron scattering and PNR, which is described in a number of references (see Refs [5–11]), however, it is essential to provide some definitions and simple equations to better understand the examples. Neutron scattering theory requires solving the Schrödinger equation with the interaction operator,  $\hat{V}(\mathbf{r})$ , being written:

$$\hat{V}(\mathbf{r}) = V_n(\mathbf{r}) + V_m(\mathbf{r}) \quad (1)$$

$V_n(\mathbf{r})$  gives the interaction of the neutron with the nucleus and may be written:

$$V_n(\mathbf{r}) = \frac{2\pi\hbar^2}{m_n} (b + B\hat{\mathbf{I}} \cdot \hat{\mathbf{G}}) \delta(\mathbf{r}) \quad (2)$$

where  $m_n$  is the neutron mass,  $b$  is defined as a nuclear scattering length,  $B\hat{\mathbf{I}}$  is the nuclear spin and  $\hat{\boldsymbol{\sigma}}$  is the Pauli spin operator defining the direction of the neutron spin.  $V_m(\mathbf{r})$  is the operator describing the interaction of the neutron with the magnetic induction,  $\mathbf{B}(\mathbf{r})$ , and may be written:

$$V_m(\mathbf{r}) = -\gamma\mu_N\hat{\boldsymbol{\sigma}} \cdot \mathbf{B}(\mathbf{r}) \quad (3)$$

where  $\gamma = -1.91$  is the gyromagnetic ratio for the neutron and  $\mu_N$  is the nuclear magneton.

Equation (1) depends upon the direction of the nuclear spin, which is normally random and, therefore, results in incoherent scattering. This contribution is usually ignored in reflectometry. More importantly for magnetic experiments, Eq. (1) also depends on the direction of the neutron spin relative to the magnetic induction, determined by the local magnetization of the sample. If the neutron beam is polarized, Eq. (3) shows that  $V_m(\mathbf{r})$  may change depending on the dot product of the neutron spin, given by  $\hat{\boldsymbol{\sigma}}$ , with the local magnetization. The neutron polarization may, therefore, be used to determine the direction and magnitude of  $\mathbf{B}(\mathbf{r})$ .

A full treatment of polarized neutron scattering is well established within the kinematic first Born approximation and has been described in a density matrix formalism [8, 9] and by wave mechanics [7]. Polarized neutron reflectivity, however, requires a dynamic theory, which is still in development [6, 10, 11]. Perhaps the most tractable treatment to date is the *supermatrix method* [11, 12] which combines a density matrix formalism with the distorted-wave Born approximation [13]. In this treatment, the Fresnel reflectance, derived from the potentials in Eqs (1–3), is described by a  $(2 \times 2)$  matrix with eigenvalues  $R_+$  and  $R_-$ , and a complex unit vector  $\mathbf{b}_r$  analogous to the structure operator in crystallography. The resulting reflectivity,  $\mathfrak{R}$ , is described as a function of arbitrary incident and final neutron polarization. All the polarized neutron reflectometry experiments published to date, however, have constrained the neutron polarization to one axis, so that the neutron spin state may be said to be parallel (+) or antiparallel (–) to a guide field which is applied in the experiment. On scattering, the neutron polarization may change from (+) to (–), known as spin flip (SF), or may stay the same, being non-spin flip (NSF). For specular reflection, where the angle of incidence is equal to the angle of reflection, the reflectivity may be written:

$$\begin{aligned}\Re^{NSF} &= \left| (R_+ + R_-) + (R_+ - R_-) \cos \phi \right|^2 \\ \Re^{SF} &= \frac{1}{4} |R_+ - R_-|^2 \times \left[ |\mathbf{b}_r|^2 - |\cos \phi|^2 + \text{Im}(\mathbf{b}_r \times \mathbf{b}_r^*)_{\parallel} \right]\end{aligned}\quad (4)$$

where  $\parallel$  refers to a projection on to the axis of the initial polarization,  $\mathbf{P}_0$ , and  $\mathbf{b}_r \cdot \mathbf{P}_0 = \cos \phi$ . Equation (4) depends upon the choice of the direction of the incident polarization, thus giving flexibility to the design of the experiment and access to extra information for a more complete description of the scattering potential,  $\hat{V}$ . In the calculation of the reflectance matrix it must be noted that, due to the requirement that  $\nabla \cdot \mathbf{B} = 0$ , only those components of  $\mathbf{B}(\mathbf{r})$  that are perpendicular to the scattering vector  $\mathbf{Q}$  are observable.

### 3. EXAMPLES OF POLARIZED NEUTRON REFLECTOMETRY EXPERIMENTS

#### 3.1. Specular reflection

The majority of reflectometry experiments measure the specular reflectivity. These measurements are relatively straightforward to perform and the data may be analysed using a well established theory [5, 11]. The scattering potentials in Eqs (1–3) become one dimensional, with  $b \cdot \delta(\mathbf{r})$  and  $B_\alpha(\mathbf{r})$  being replaced by the mean scattering length density and magnetization density at a depth ( $r_\perp$ ) in the sample,  $\rho(r_\perp) \bar{b}(r_\perp)$  and  $B_\alpha(r_\perp)$ .

##### 3.1.1. A polarized incident beam with no analysis

The simplest type of PNR experiment uses a polarized incident beam, but does not determine the polarization of the reflected beam. This configuration is frequently used for samples that have a mean magnetization that is non-zero, e.g. collinear ferromagnets and ferrimagnets, for which  $\mathbf{b}_r$  is real, and it is assumed that the ferromagnetic axis and the incident polarization are collinear, i.e.  $\cos \phi = 0$ . The reflectivities of the (+) neutrons ( $\Re^+$ ) and the (–) neutrons ( $\Re^-$ ) are measured. When constrained to specular reflectivity, a dimensionless quantity called the spin asymmetry,  $S(q_\perp)$ , where:

$$S(q_\perp) = \frac{\Re^+(q_\perp) - \Re^-(q_\perp)}{\Re^+(q_\perp) + \Re^-(q_\perp)} \quad (5)$$

## APPLICATION OF POLARIZED NEUTRON REFLECTOMETRY

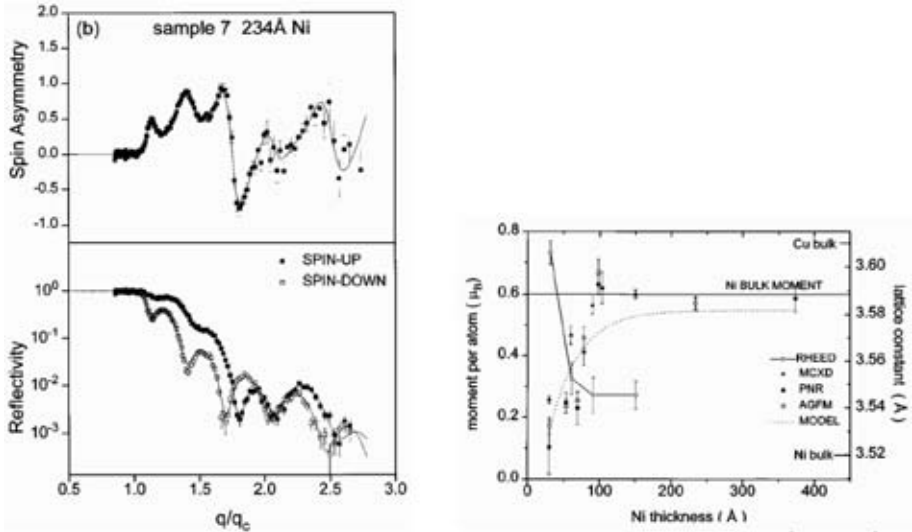


FIG. 1. (a) (left) An example of the polarization dependent specular reflectivity from a sample of Cu 50 Å/Ni 234 Å/Cu 600 Å/Si (001) sample, with the calculated spin asymmetry (given by Eq. (5)). Also shown are the fits, which derived a value for the magnetic moment on the nickel. The results from similar fits to a range of films are shown in (b) (right). (Figures reprinted with permission from Ref. [14]. Copyright 1997 by the American Physical Society.)

is frequently calculated. Fits to the spin asymmetry will give a precise and sensitive estimate of the magnetization as a function of depth to be determined to sub-nanometre precision [5].

An example of spin asymmetry data is shown in Fig. 1(a), which shows the results of measurements that were made on Cu/Ni/Cu thin film sandwiches [14]. Figure 1(a) shows an example of the measured polarization-dependent specular reflectivities and the spin asymmetry. The magnitude of the magnetic moment of the nickel, embedded in the non-magnetic copper, could be determined from the data. Similar measurements were made on a number of samples with different nickel thicknesses, and the results are summarized in Fig. 1(b). The sensitivity of the technique is apparent as Fig. 1(b) shows measurements of  $0.1 \mu_B$  per Ni atom in film thicknesses of 3 nm.

Ferromagnetic thin films are of particular interest to the hard disk industry, and consequently are a popular subject for measurement. The technique lends itself to any thin film sample that displays a non-zero mean magnetization, however, and has been successfully applied to subjects as diverse as vortex lattices in superconductors (e.g. Ref. [15]), percolating spin glasses (e.g. Ref. [16]) and magnetic 'dead' layers at interfaces [17].

3.1.2. Polarized reflectometry with analysis

Samples that have no mean magnetization, e.g. ferromagnetic layers that are antiferromagnetically coupled, or samples that have non-collinear magnetic structures require that the polarization of the analysed beam is also measured. The experimental configuration for specular reflectivity is also relatively straightforward to realize and adequate theory to analyse the data has been established [11]. Four polarization-dependent reflectivities are measured: two non-spin flip ( $\mathfrak{R}^{++}$  and  $\mathfrak{R}^{--}$ ); and two spin flip ( $\mathfrak{R}^{+-}$  and  $\mathfrak{R}^{-+}$ ).

The magnitudes of the polarization-dependent reflectivities depend upon the relative orientation of the polarization to the local magnetization axes of the sample and to the scattering vector. The most common geometry, however, is with the polarization in the plane of the sample and perpendicular to  $\mathbf{Q}$ . This geometry is generally chosen more for reasons of the physics of the problem than any concern for instrument configuration: many experiments require some field in the plane of the sample, and the neutron polarization will be collinear with any applied field. Manipulation of Eq. (4) reveals that the non-spin flip reflectivity is sensitive to the chemical structure of the sample, through the magnitude of  $\rho(r_{\perp})\bar{b}(r_{\perp})$ , and the components of the magnetization densities that are collinear with the neutron polarization. The spin flip reflectivity depends upon the components of the magnetization densities that are perpendicular to both the neutron polarization and the scattering vector,  $\mathbf{Q}$ .

An example of such a measurement is given in Fig. 2 [18]. This experiment aimed to measure the magnetization as a function of depth in a  $\text{Ni}_{80}\text{Fe}_{20} | \text{Fe}_{55}\text{Pt}_{45}$  bilayer. The system is a known ‘exchange-spring’ magnet, whereby a twist can be induced in the magnetic structure by applying a magnetic field to the sample. The four polarization dependent reflectivities

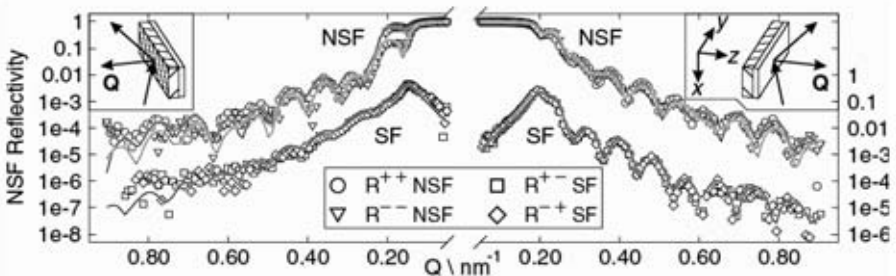


FIG. 2. The polarization dependent specular reflectivity from the front (right) and back (left) faces of a  $\text{Fe}_{55}\text{Pt}_{45}$  200 Å/ $\text{Ni}_{80}\text{Fe}_{20}$  500 Å bilayer in an applied field of 16 mT. (Figure reprinted with permission from Ref. [18]. Copyright 2002 by the American Physical Society.)

## APPLICATION OF POLARIZED NEUTRON REFLECTOMETRY

were measured from the front and back of the sample and are shown in the figure. The data show two distinct features which enabled the magnetic structure to be determined. The first is the presence of non-zero spin flip reflectivities, which is unambiguous evidence that the magnetic structure has components that are not collinear with the applied field. The second is a difference in the critical edge for the two non-spin flip reflectivities, clearly visible at  $Q \sim 0.2 \text{ nm}^{-1}$  in the data to the left of the figure, due to the change in sign of  $\cos\phi = \mathbf{b}_r \cdot \mathbf{P}_0$  in Eq. (4). The difference is less apparent in the right hand data, and allowed a distinction between the direction of the magnetization at the top and bottom of the film. The data were fitted at a number of fields and twisted magnetic structures, shown in Fig. 3, could be derived [18].

This form of measurement is now commonly used as a default for PNR, the logic being that one never knows whether some spin flip is present in the reflected beam. The data clearly give information about the mean magnetization direction as a function of depth, and this alone makes it an extremely valuable technique. The data can, however, be further analysed to give information on larger or smaller length scales than normally accessed by reflectometry. For example, specular PNR with polarization analysis can give information about the size and orientation of magnetic domains in the surface of the sample [19], or changes in the orientation of sublattice magnetic moments as a function of depth [20].

The data in Fig. 2 are clear evidence for a magnetic structure with a chiral component, however, it must be noted that the experimental configuration

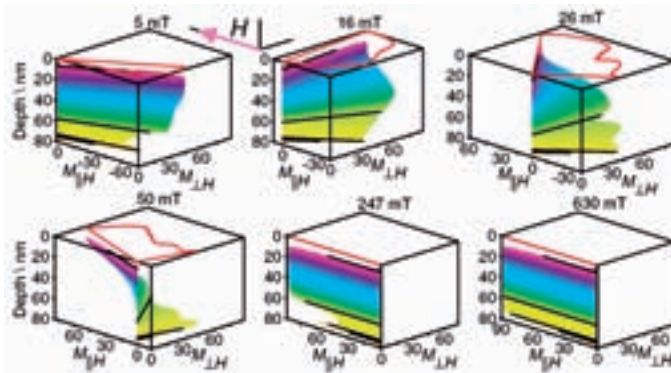


FIG. 3. The derived magnetic structures of the  $\text{Fe}_{55}\text{Pt}_{45} 200 \text{ \AA} / \text{Ni}_{80}\text{Fe}_{20} 500 \text{ \AA}$  bilayer used for the measurement in Fig. 2 as a function of applied field. The NiFe layer in colours purple to green, while the FePt layer is in yellow. The layers are separated by the heavy black lines. (Figures reprinted with permission from Ref. [18]. Copyright 2002 by the American Physical Society.)

chosen, with the neutron polarization perpendicular to the scattering vector, does not allow the handedness of the twist to be determined. Eq. (4) shows that the spin flip reflectivities have a dependence on the cross-product of the reflectivity structure operator,  $\mathbf{b}_r$ , which could lead to a difference between the two reflectivities  $\mathfrak{R}^-$  and  $\mathfrak{R}^+$  and would allow the chirality to be determined. This difference, however, will only be visible when the neutron polarization is *parallel* to the scattering vector. Such a measurement is not currently possible when a field must be applied in the plane of the sample, as was the case for the experiment [18], as the neutron polarization then becomes collinear with the applied field.

### 3.2. Off-specular scattering

Constraining glancing incident measurements to specular reflectivity limits an experiment to a determination of the mean scattering potential as a function of depth within the sample. Specular reflectivity can give no information about in-plane structures: for example, it cannot distinguish between an interface that is rough or an interface where two media have inter-diffused. This information comes from the measurement and analysis of the *off-specular* scattering, where the angle of incidence and the angle of reflection differ. The analysis of off-specular scattering is non-trivial, often involving integrals that cannot be solved analytically, and theoretical approaches to solve problems are still in development. This is in evidence with the continuing attempts to understand the theory of off-specular scattering of X rays — a field that is far in advance of the equivalent field for neutrons, particularly when the added complication of the neutron polarization is considered. Off-specular polarized neutron reflectometry promises much, however, as magnetic roughness, non-trivial magnetic structures, domain walls, and magnetic proximity effects can all be investigated. While still a new field, analysis methods have been suggested (see Refs [6, 10, 11, 13]) and interesting experiments are beginning to be published.

#### 3.2.1. A polarized incident beam with no analysis

While setting the polarization of the well collimated incident beam is relatively straightforward, it is difficult to reliably determine the polarization of what is generally the broad and diffuse off-specular scattering. However, information can be obtained and data modelled when only the polarization of the incident beam is known.

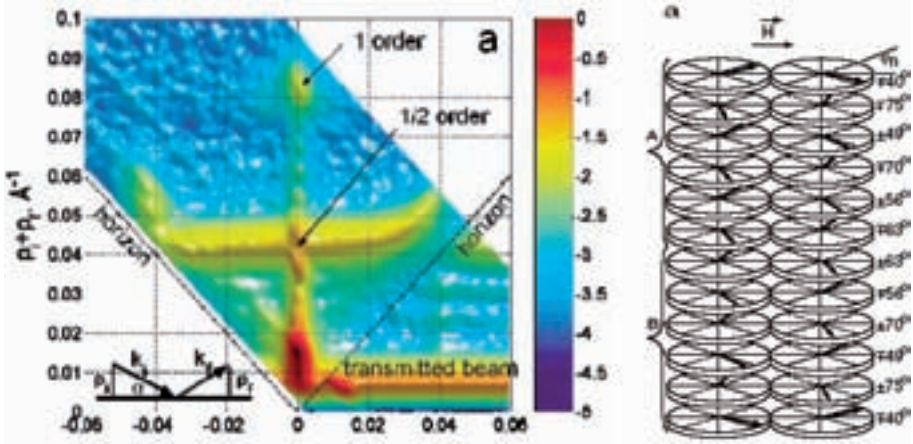


FIG. 4. (left) The measured scattering from a  $(\text{Fe } 67 \text{ \AA}/\text{Cr } 9 \text{ \AA})_{12}$  multilayer with a  $(-)$  incident polarization and no analyser. The horizontal axis is  $\mathbf{p}_i - \mathbf{p}_f$  and the vertical ridge at is  $\mathbf{p}_i - \mathbf{p}_f = 0$  is the specular reflection. The data were successfully modelled to find that the magnetic structure was split into two domains, each domain with a structure shown in (b) (right). (Figures reprinted with permission from Ref. [21]. Copyright 2002 by the American Physical Society.)

Figure 4(a) shows one such example from an experiment on a Fe/Cr superlattice [21]. The measurement was made with the incident polarization in the  $(-)$  direction and the data therefore contain the  $(--)$  and the  $(+-)$  scattering. Clearly visible is the first order multilayer Bragg peak, and a Bragg sheet at a position corresponding to twice the bilayer repeat distance. Such a feature immediately suggests that there is antiferromagnetic coupling between bilayers. Careful modelling, combined with a polarization analysis measurement of the specular reflection, showed that the sample was broken into magnetic domains and that the magnetic structure within a domain was one of the two rather complicated models shown in Fig. 4(b).

This type of measurement is particularly useful for investigations of in-plane ferromagnetic perturbations and structures. Correlations in the magnetic roughness can be measured and distinguished from magnetic domain structures [22, 23], along with effects of interdiffusion which can sometimes lead to a magnetic ‘dead’ layer. Modern lithographic techniques allow well defined patterned structures to be made, such as stripes and arrays of circular or rectangular islands. Ferromagnetic patterned structures are of particular interest in electronics, and have been successfully investigated using off-specular PNR with no analysis [24, 25]. No polarization analysis is required if

there is a clear separation between the directions of spin flip and non-spin flip scattering. This has been shown to be the case for spin-dependent reflectometry in a strong field, where Zeeman splitting leads to a divergence of the spin flipped and non-spin flipped neutrons [26].

### 3.2.2. Polarized scattering with analysis

Far more detailed information can, of course, be determined if the polarization of the off-specular scattering can also be determined. Domain size, orientation and wall thicknesses; complex magnetic structures, including helices, fans and spin density waves; the influence on the magnetic properties of roughness and interdiffusion at an interface; proximity effects when one magnetic structure is placed in contact with another, or with a superconductor: these are some examples of the physics that can be investigated with PNR, but require polarization analysis of the off-specular scattering.

While the technique offers huge potential, relatively few measurements have been published. This is due to the difficulties in measuring the polarization dependence of off-specular scattering, as suitable instrumentation is still being developed. The common technique of using polarizing supermirrors to analyse the scattered beam polarization suffers from being able to accept only a narrow angular range and having a polarization and transmission that depend on the incident angle. This makes them ideal for specular reflectivity, which is usually well defined in angle, but less efficient for diffuse off-specular scattering.

Nevertheless, useful measurements can be carried out with these devices. Recent efforts have quantified magnetic interfaces [27] and investigated the effects of refraction due to a change in the neutron spin state [28]. Supermirrors will also be extremely efficient when the off-specular scattering is well defined in angle, as is the case for the scattering from patterned samples that will give Bragg peaks. A recent experiment measured the spin dependence of the scattering from an array of Au/Co/Au dots, produced by lithography techniques [29]. Analysis of the data, shown in Fig. 5, allowed the magnetic interactions between the dots to be investigated as a function of the applied field.

Recent developments in neutron instrumentation have resulted in  $^3\text{He}$  gas being used as neutron polarizing filters on neutron reflectometers [12, 30]. The  $^3\text{He}$  nucleus has a very high neutron absorption cross-section which depends on the spin of the nucleus. If the spins on all the  $^3\text{He}$  nuclei can be preferentially oriented, one spin state of a neutron beam would be preferentially absorbed and the beam would be polarized [31]. Such a filter has enormous potential for neutron scattering, as the polarization of the beam is

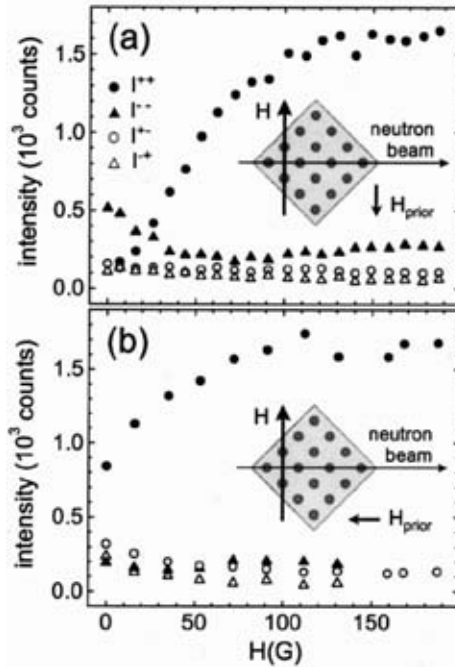


FIG. 5. Measurement of the polarization dependent intensities from an off-specular Bragg peak which results from  $4\mu\text{m}$  dots in a square lattice of  $10\mu\text{m}$  side length. Each dot was a Au  $75\text{ \AA}$ /Co  $200\text{ \AA}$ /Au  $75\text{ \AA}$  trilayer. (Reprinted with permission from Ref. [29]. Copyright 2001, American Institute of Physics.)

completely decoupled from the optics of the beam, meaning that an instrument can be better optimized for a measurement. Importantly for reflectometry, the gas can be contained in a cell of arbitrary shape and size with windows that produce minimal small angle scattering, meaning that the polarization dependence of broad and diffuse off-specular scattering can be measured.

A recently published study of the exchange bias system Co/CoO used the  $^3\text{He}$  filter to measure the spin dependent off-specular scattering [32], and the data are shown in Fig. 6. The specular reflectivity, where the incident angle equals the scattered angle, is clearly visible for each spin state. There are also clear neutron spin-dependent features that are present for constant incident angles in the spin flip scattering. These features were interpreted as due to scattering from domain walls. The features are visible at values of the incident angle that vary with the neutron spin states, and this was explained by the Zeeman effect, where the neutron may lose energy depending on the relative orientation of its spin to the applied magnetic field [32, 26].

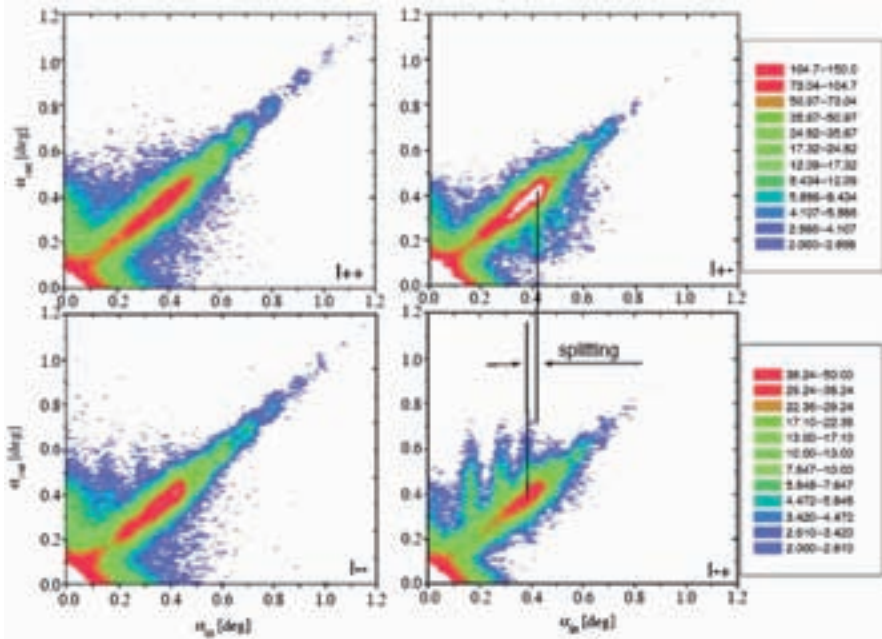


FIG. 6. The specular and off-specular polarization dependent scattering from a CoO 25 Å/Co 200 Å bilayer. The specular reflection appears as the diagonal line where  $\alpha_{in} = \alpha_{out}$ . The off-specular scattering shows some fringes at fixed values of  $\alpha_{in}$ . The difference between the values of  $\alpha_{in}$  was attributed to a change in the refractive index of the material when the neutron spin state was flipped (after Ref. [32]).

Further developments in instrumentation and in the theory used to analyse the data will result in off-specular scattering with polarization analysis becoming a highly demanded and important tool for thin film, surface and interface magnetism and superconductivity.

#### 4. CONCLUSIONS AND FUTURE PROSPECTS

The computer industry continues to force the miniaturization of electronic components and computer memory bits, along with increased sensitivity on magnetic reading heads, leading to the development of ‘spintronics’ where the electron’s spin is used as an integral part of a computer circuit. There are high hopes for spintronics, as it is believed that this may ultimately lead to quantum computing. Detailed knowledge, both empirical

and theoretical, of the behaviour of magnetism on the nanometre scale is required for the technology to work and PNR has the unique ability to measure magnetic correlations over these length scales. Consequently, the user base for PNR will increase substantially, particularly as questions over the interpretation of the data are answered.

The technique can answer many other, more fundamental questions. An aspect of magnetism that is frequently overlooked is the interaction between nuclear moments. The neutron scattering potential is sensitive to the nuclear moment, as is evident in Eq. (2). Normally, the nuclear moments are randomly oriented, thus the scattering from the nuclear moments is incoherent. If, however, the nuclear moments are ordered, neutron scattering can and has been applied to probe the structure [33]. Polarized neutron reflectometry may be used for future studies of nuclear magnetism in thin films.

To date, the polarized neutron reflectometry techniques have been limited by the fact that only certain orientations of the neutron polarization relative to the sample and the scattering vector can be realized experimentally. As previously mentioned, the polarization direction is limited to one axis, and this is generally in the plane of the surface of the sample. The techniques would benefit enormously if the scattering could be measured for an arbitrary initial and final neutron polarization, therefore, measuring a polarization rotation tensor for the sample. Such a measurement would enable a complete and unambiguous measurement of  $\mathbf{b}_r$ , therefore giving a complete solution for the magnetic structure of the sample. Effectively, this technique bypasses the age-old 'phase problem' for scattering experiments, whereby it is not possible to immediately determine a structure from a scattering pattern because only the amplitude of the scattered wave is measured and all phase information is lost. This technique has been successfully applied to diffraction, being called spherical neutron polarimetry [34], and has been used to solve many difficult magnetic structures [35].

Spherical neutron polarimetry is currently a zero-field technique; however, it is not possible to make such a measurement on ferromagnets, or on a sample in an applied field. This certainly limits its potential for use in PNR for, as shown in the examples, the majority of PNR measurements are on ferromagnets and/or require an applied field. Technical and experimental developments are underway, including using the Larmor precession of a neutron in a magnetic field to determine an arbitrary polarization direction at the sample [36, 37], which *might* make it possible to use spherical polarimetry in a field, although they still face many challenges to work with ferromagnets. If and when the hurdles can be overcome, spherical neutron polarimetry for reflectometry will be a mighty experimental tool indeed.

In conclusion, polarized neutron reflectometry is still a relatively new technique with enormous potential. There are many instruments in the world capable of the techniques, and there is a solid and expanding user base. The current understanding of the theory, particularly for off-specular scattering, is incomplete, however enough is known to make unambiguous conclusions from the data in many experiments. Similarly, PNR instrumentation is still in development. As new instrumentation becomes available, more complete experiments will be possible, enabling the most difficult and complex magnetic structures and interactions to be determined in thin films and multilayers.

### ACKNOWLEDGEMENTS

The author would like to thank K. Andersen, R. Cubitt and G. Fragneto of the Institut Laue-Langevin for their critical reading of the manuscript and their helpful comments.

### REFERENCES

- [1] FITZSIMMONS, M.R., et al., Neutron scattering studies of nanomagnetism and artificially structured materials, *J. Magn. Magn. Mater.* **271** (2004) 103.
- [2] ZABEL, H., THEIS-BRÖHL, K., Polarized neutron scattering studies of magnetic heterostructures, *J. Phys.: Condens. Matter* **15** (2003) S505.
- [3] FELCHER, G.P., et al., Polarized neutron reflectometry: Recent developments and perspectives, *Physica B* **297** (2001) 87.
- [4] ANKNER, J.F., ZABEL, H., Applications of neutron reflectivity to nanoscience: Thin films and interfaces, *MRS Bull.* **28** (2003) 918.
- [5] BLUNDELL, S.J., BLAND, J.A.C., Polarized neutron reflection as a probe of magnetic films and multilayers, *Phys. Rev. B* **46** (1992) 3391.
- [6] TOPERVERG, B.P., Specular reflection and off-specular scattering of polarized neutrons, *Physica B* **297** (2001) 160.
- [7] HICKS, T.J., Experiments with neutron polarization analysis, *Adv. Phys.* **46** (1996) 243.
- [8] BLUME, M., Polarization effects in the magnetic elastic scattering of slow neutrons, *Phys. Rev.* **130** (1963) 1670.
- [9] MALEEV, S.V., et al., The scattering of slow neutrons by complex magnetic structures, *Sov. Phys. Solid State* **4** (1963) 2533.
- [10] TOPERVERG, B.P., et al., Towards 3D polarization analysis in neutron reflectivity, *Physica B* **297** (2001) 169.

## APPLICATION OF POLARIZED NEUTRON REFLECTOMETRY

- [11] RÜHM, A., Supermatrix approach to polarized neutron reflectivity from arbitrary spin structures, *Phys. Rev. B* **60** (1999) 16073.
- [12] NICKEL, B., et al., Spin-resolved off-specular neutron scattering maps from magnetic multilayers using a polarized  $^3\text{He}$  gas spin filter, *Rev. Sci. Instrum.* **72** (2001) 163.
- [13] SINHA, S.K., et al., X-ray and neutron scattering from rough surfaces, *Phys. Rev. B* **38** (1988) 2297.
- [14] HOPE, S., et al., Thickness dependence of the total magnetic moment per atom in the Cu/Ni/Cu/Si(001) system, *Phys. Rev. B* **55** (1997) 11422.
- [15] HAN, S.-W., Orientation of vortices in a superconducting thin film: Quantitative comparison of spin-polarized neutron reflectivity and magnetization, *Phys. Rev. B* **62** (2000) 9784.
- [16] SWERTS, J., Polarized neutron reflectivity on dilute magnetic alloys, *Europhys. Lett.* **68** (2004) 282.
- [17] ANKNER, J.F., et al., Magnetic dead layer in Fe/Si multilayer: Profile refinement of polarized neutron reflectivity data, *J. Appl. Phys.* **73** (1993) 6436.
- [18] O'DONOVAN, K.V., Pinpointing chiral structures with front-back polarized neutron reflectometry, *Phys. Rev. Lett.* **88** (2002) 67201.
- [19] RADU, F., et al. Interfacial domain formation during magnetization reversal in exchange-biased CoO/Co bilayers, *Phys. Rev. B* **67** (2003) 134409.
- [20] TE VELTHUIS, S.G.E., et al., Spin flip transition in a finite antiferromagnetic superlattice: Evolution of the magnetic structure, *Phys. Rev. Lett.* **89** (2002) 12703.
- [21] LAUTER-PASYUK, V., Transverse and lateral structure of the spin-flop phase in Fe/Cr antiferromagnetic superlattices, *Phys. Rev. Lett.* **89** (2002) 16703.
- [22] VAN DE KRUIJS, R.W.E., et al., Probing magnetic structures by neutron reflectometry: Off-specular scattering from interfaces and domains in FeCoV/TiZr multilayers, *Physica B* **297** (2001) 180.
- [23] SYROMYATNIKOV, V.G., et al., Off-specular polarised neutron scattering from rough interfaces in Co/Ti and Fe/Al multilayered systems, *Physica B* **267–268** (1999) 190.
- [24] THEIS-BRÖHL, K., Magnetization reversal of periodic arrays of magnetic elements, *Physica B* **345** (2004) 161.
- [25] LEE, W.-T., et al., Measuring lateral magnetic structures in thin films using time-of-flight polarized neutron reflectometry, *Physica B* **335** (2003) 77.
- [26] FELCHER, G.P., et al., Zeeman splitting of surface scattered neutrons, *Nature* **377** (1995) 409.
- [27] VAN DE KRUIJS, R.W.E., et al., Polarization analysis of off-specular neutron scattering from domains and rough interfaces in a FeCoV/RiZr multilayer, *Appl. Phys. A* **74** (2002) S1550.
- [28] KRIST, T., Non-specular reflectivity of spin flipped neutrons, *Physica B* **267–268** (1999) 194.
- [29] TEMST, K., Application of off-specular polarized neutron reflectometry to measurements on an array of mesoscopic ferromagnetic disks, *Appl. Phys. Lett.* **79** (2001) 991.

- [30] CHEN, W.C., et al., Polarized  $^3\text{He}$  analyzers for neutron reflectometry, *Physica B* **335** (2003) 196.
- [31] SURKAU, R., et al., Realization of a broad band neutron spin filter with compressed, polarized  $^3\text{He}$  gas, *Nucl. Instrum. Methods Phys. Res., Sect. A* **384** (1997) 444.
- [32] RADU, F., Spin-resolved neutron scattering from magnetic domain walls using the polarized  $^3\text{He}$  gas spin filter, *Physica B* **335** (2003) 63.
- [33] STEINER, M., et al., Neutron diffraction determination of the nuclear spin ordering in Cu and Ag at nano- and subnano-K temperatures, *J. Appl. Phys.* **79** (1996) 5078.
- [34] TASSET, F., et al., Spherical neutron polarimetry with Cryopad-II, *Physica B* **267–268** (1999) 69.
- [35] BROWN, P.J., Polarised neutrons and complex antiferromagnets: An overview, *Physica B* **297** (2001) 198.
- [36] SCHWEIKA, W., Time-of-flight and vector polarization for diffuse neutron scattering, *Physica B* **335** (2003) 157.
- [37] MAJOR, J., et al., Combining of neutron spin echo and reflectivity: A new technique for probing surface and interface order, *Physica B* **336** (2003) 8.

# ***n*/X MATERIALS SCIENCE REFLECTOMETER AT FRM-II IN GARCHING**

A. RÜHM, U. WILDGRUBER, J. FRANKE, J. MAJOR, H. DOSCH  
Max-Planck-Institut für Metallforschung,  
Stuttgart, Germany

## **Abstract**

The Max-Planck-Institut für Metallforschung in Stuttgart has conceived and constructed a combined neutron/X ray reflectometer for materials science (MatSci-R) at the new FRM-II research reactor in Garching. The instrument can be operated in both vertical and horizontal geometry and is therefore also suitable for reflectometry and grazing incidence scattering studies on free liquid surfaces. The reflectometer can be used for polarized neutron reflectometry and off-specular scattering to investigate magnetic materials, e.g. magnetic multilayers. It is also planned to implement a novel spin-echo resolved grazing incidence scattering (SERGIS) technique for high resolution off-specular scattering experiments without collimation. As a further novel feature, the MatSci-R instrument will routinely be equipped with an add-on X ray reflectometer which allows in situ neutron/X ray contrast reflectometry studies.

## **1. FOCUSED NEUTRON RESEARCH INITIATIVE OF THE MAX PLANCK SOCIETY AT FRM-II**

The Max Planck Society has launched a research initiative (“Materials Science at the New Neutron Source FRM-II”) at the new FRM-II research reactor in Garching, near Munich, integrating several Max Planck institutes. As part of this research initiative, a novel reflectometer for materials science (MatSci-R) and a novel triple axis spectrometer (NRSE-TAS) have been built. The two instruments are currently in the commissioning phase. This paper reports on the technical realization of the MatSci-R reflectometer [1] and gives an overview over its scientific potential.

## **2. FEATURES OF MatSci-R**

MatSci-R offers the following special features:

- The incoming neutron beam can be tilted towards the floor, allowing the study of free liquid surfaces.
- It will be possible to conduct SERGIS (spin-echo resolved grazing incidence scattering [2]) and NSE (neutron spin echo [3]) experiments in reflection geometry. In experiments where the available neutron intensity is crucial, the SERGIS technique with inclined magnetic field borders will offer a considerable intensity enhancement, so new experiments become feasible which would otherwise be impossible due to lack of signal. In the conventional NSE geometry, i.e. with parallel field borders, the inelastic scattering processes and thus the dynamics of solid and liquid interfaces can be studied.
- An add-on X ray reflectometer will enable neutron/X ray contrast methods. This will allow to obtain additional information about the structure and physics of samples. As an example, the atomic structure of a magnetic multilayer system can be characterized with high precision with X rays, while neutrons allow unravelling the magnetic structure of the multilayer. The most interesting application of simultaneous n/X measurements lies in new in situ investigations of irreversible processes such as interdiffusion phenomena in complex multilayered structures, e.g. magnetic multilayers.

### 3. TECHNICAL REALIZATION AND CHARACTERISTICS

Figure 1 shows the design of MatSci-R with the optional SERGIS setup (see Section 4) and the optional add-on X ray reflectometer (see Section 5) installed. Not shown in Fig. 1 is the  $^3\text{He}$  spin filter which will be available for wide angle spin analysis, e.g. in polarized neutron reflectometry and off-specular magnetic scattering experiments [4]. A setup used for this purpose at EVA (ILL, Grenoble) is displayed in Fig. 2. It can be mounted in front of the detector tower on the left instead of or in addition to the SERGIS equipment.

In its default configuration, the MatSci-R instrument is designed as a liquid reflectometer. This means that the reflection plane is vertical and free liquid surfaces can also be studied by tilting the beam impinging on the surface towards the floor. The beam tilt is achieved by a mechanical coupling between the sample tower and the monochromator stage, which is displayed in Fig. 3 and also partly visible within the shielding in Fig. 1. The monochromator is made of 11 motorized highly oriented pyrolytic graphite (HOPG) crystals which can focus the beam horizontally onto the sample or detector position to increase the monochromatic intensity for the experiment. In the vertical direction the beam is collimated by custom slits made of boron rich plastic

blades to achieve the required  $q$  resolution perpendicular to the sample surface. The currently installed HOPG monochromator crystals have a ‘mosaicity’ of about  $0.4^\circ$  and select a narrow (2%) wavelength band out of the ‘white’ beam, providing useful neutron intensities in the wavelength range 2–6 Å (cold source).

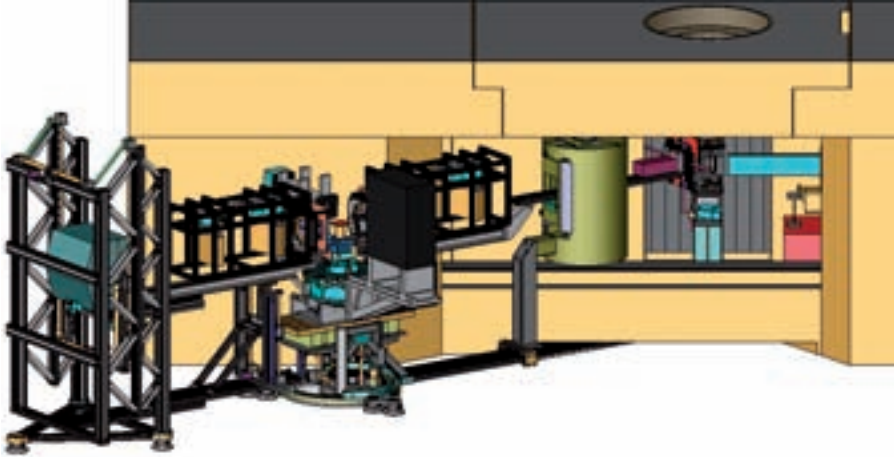


FIG. 1. Design view of MatSci-R at neutron guide NLI at the new FRM-II research reactor. The movable shielding wall is removed in the figure to allow a view of the tiltable focusing monochromator.



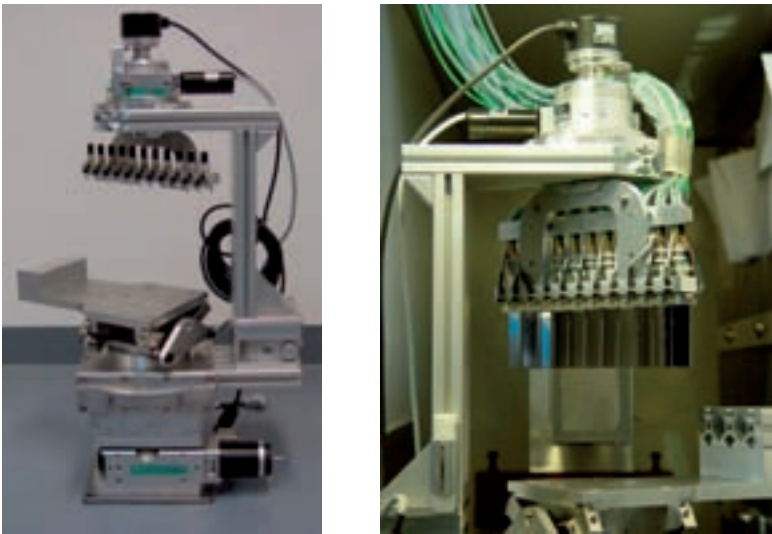
FIG. 2. Coils for polarized neutron reflectometry and off-specular magnetic scattering with wide angle  $^3\text{He}$  spin analysis as it was used in an experiment at EVA (ILL, Grenoble) [4]. The  $^3\text{He}$  bottle itself is not shown in the picture.

Figure 4 shows a close-up of the sample table. The Huber stack visible between the two custom slit systems can be used with small sample environments. Larger sample environments can be placed on the big Huber goniometer underneath. The sample table can then support heavy sample environments of up to 400 kg.

The two dimensional neutron detector, a  $^3\text{He}$  wire chamber supplied by ESRF (Grenoble), is located in the blue shielding box on the left in Fig. 1. It can be moved vertically to adjust the investigated reflection angle. In addition to the conventional reflectometry mode, the detector tower can be rotated horizontally around the sample table on air pads to enable grazing incidence scattering experiments. Likewise, the sample tower can be rotated around the monochromator position so that different wavelengths can be utilized with the same monochromator.

From first neutron flux measurements in the ‘white’ beam (see Fig. 5) we expect a monochromatic intensity of  $3 \times 10^6$  neutrons $\cdot\text{cm}^{-2}\cdot\text{s}^{-1}$  at the sample position. This intensity is comparable to the intensity available at the reflectometers ADAM and EVA at ILL.

Further instrument parameters are summarized in Table 1. More information about MatSci-R and other instruments at FRM-II can be found on-line (<http://www.frm2.tum.de/instruments/index.shtm>).



*FIG. 3. The monochromator stage, shown without crystals in the left image, can hold 11 crystal stacks to focus the beam horizontally using 11 stepper motors. The right image shows a close-up of the stage with 11 single HOPG crystals mounted.*

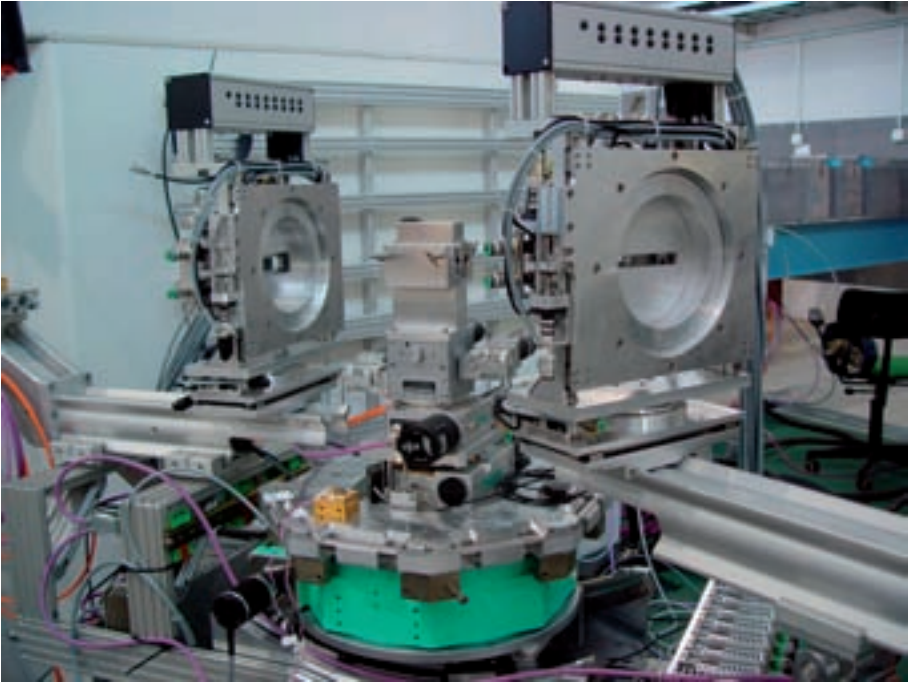


FIG. 4. Close-up of the MatSci-R sample table between two custom slit systems. The box mounted on the sample table contains two alignment lasers.

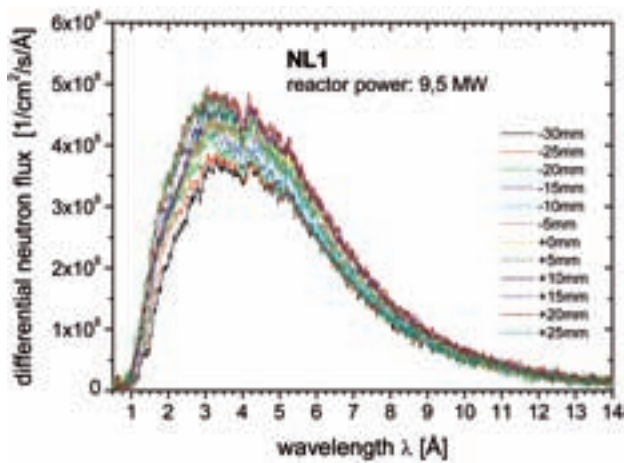


FIG. 5. Wavelength spectrum of the cold source at the NL1 monochromator position, measured at different horizontal positions within the beam cross-section. These measurements were conducted at a reactor power of 9.5 MW, the nominal reactor power for routine operation is 20 MW.

TABLE 1. MatSci-R INSTRUMENT PARAMETERS (FOR LIQUID MODE)

Neutron wavelength range	2–6 Å
Neutron guide cross-section	6 cm (horiz.) × 12 cm (vert.)
Beam cross-section accepted by the monochromator	6 cm (horiz.) × 1 cm (vert.)
Monochromator	11 × 3 HOPG crystals, horizontally focusing (mosaicity 0.32–0.65°)
Energy resolution	2%
Max. incidence angle	5°
Max. exit angle	20°
Max. out-of-plane momentum transfer (specular)	0.55 Å <sup>-1</sup>
Max. total momentum transfer (within reflection plane)	1.35 Å <sup>-1</sup>
Max. in-plane momentum transfer (grazing angle diffraction)	> 5.4 Å <sup>-1</sup>
Total neutron flux at monochromator	4 × 10 <sup>9</sup> neutrons·cm <sup>-2</sup> ·s <sup>-1</sup>
Peak neutron flux at monochromator	4 × 10 <sup>8</sup> neutrons·cm <sup>-2</sup> ·s <sup>-1</sup> Å <sup>-1</sup> (at 4 Å)
Monochromatic neutron flux for reflectometry at sample	3 × 10 <sup>6</sup> neutrons·cm <sup>-2</sup> ·s <sup>-1</sup> (estimated)

#### 4. THE SERGIS OPTION

In 1972, Mezei has suggested the neutron spin echo (NSE) technique [3] as a means to encode the energy transfer of a sample onto a neutron in the neutron spin. In 1978, Pynn extended this idea by suggesting the use of inclined magnetic field borders for momentum transfer encoding. A schematic view of such an experiment is shown in Fig. 6. This idea of using inclined magnetic field borders was first realized in bulk scattering experiments in 1978 [5] and has recently also been applied to surface scattering experiments (spin-echo resolved grazing incidence scattering, SERGIS) [2]. The SERGIS technique is a promising novel option for reflectometers, especially for intensity critical experiments since it obtains high  $q$  resolution without collimating the beam and thus without reducing the available neutron intensity. MatSci-R is one of the first which is committed to make extensive use of SERGIS for routine sample characterization (off-specular scattering). We are currently developing an

NRSE-SERGIS (neutron resonance spin-echo SERGIS) setup at EVA, ILL, which will be implemented at MatSci-R, FRM-II, in 2005. (In an NRSE-SERGIS setup the extended magnetic field regions are replaced by pairs of resonance coils [6]. As a further alternative, the resonance coils can be replaced by thin ferromagnetic sheets [7].)

The SERGIS technique exploits the neutron spin to obtain high  $q$  resolution in one direction without collimation of the incident beam. The neutron spin precesses in two magnetic field regions before and after the sample (see Fig. 6). The precession angles in the two field regions are different if the sample changes the propagation direction of the neutron during the scattering process. The total precession angle of the neutron spin at the detector position is given by

$$\Delta\Phi = \Phi_2 - \Phi_1 \cong (\varphi_2 - \varphi_1) \cdot \frac{\gamma_n}{v_n} \cdot BL \cot \eta_0$$

where  $\varphi_{1,2}$  are the inclination angles of the incident and scattered neutron momentum with respect to the forward direction,  $v_n$  is the gyromagnetic ratio of the neutron,  $v_n$  the neutron velocity,  $B$  the magnetic field,  $L$  the length of the magnetic field region, and  $\eta_0$  the inclination angle of the magnetic field borders. The total polarization of the scattered neutron beam integrated over the  $y$ -direction (see Fig. 6) is proportional to the (real space) pair correlation function  $g(\delta^{SE})$  of the sample in this direction. The independent parameter  $\delta^{SE}$ ,

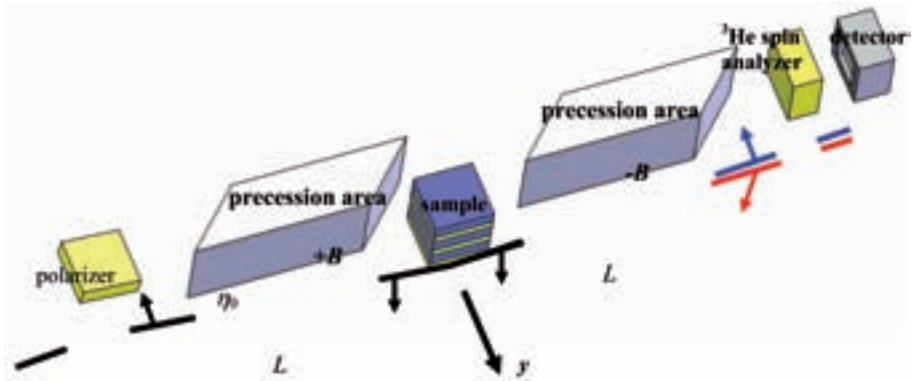


FIG. 6. Basic scheme of a SERGIS experiment. The specularly reflected neutron beam (blue) for symmetry reasons has the same spin state as the incident beam. The in-plane off-specularly scattered neutron beam (red) has travelled different path lengths in the two magnetic field regions, rendering its spin state different from the one of the incident beam.

which determines the length-scale probed in the experiment, is called spin-echo length. It is given by

$$\delta^{SE} = \frac{m_n \gamma_n}{\pi h} \lambda^2 \cdot LB \cot \eta_0$$

where  $m_n$  denotes the neutron mass,  $h$  is Planck's constant, and  $\lambda$  the neutron wavelength. The length scale probed in the experiment can thus be conveniently adjusted through the magnetic field  $B$  and/or the inclination angle  $\eta_0$ .

The result of an NRSE–SERGIS test experiment at FLEX, HMI, is shown in Fig. 7. Long wavelength periodicities of 2800 Å could be measured easily, which means that a very high  $q$  resolution could be achieved without collimation of the beam in the  $y$  direction, i.e with the full intensity of the primary beam at all values of  $\delta^{SE}$  (as reflected in the constant error bars). The  $q$  resolution is given by  $\Delta q = (N^{1/2} \delta^{SE})^{-1}$ , where  $N$  is the total number of precessions in the magnetic field region. A similar NRSE–SERGIS system as used in this experiment will be available at MatSci-R in 2005.

One has to note that the SERGIS technique in its basic version only works for elastic scattering on non-magnetic samples, since an inelastic scattering process or a magnetic field in the sample would alter the spin state of the neutron at the detector position and thus seriously complicate the data analysis.

## 5. IN SITU NEUTRON/X RAY CONTRAST OPTION

As a special novel feature, MatSci-R also provides a so far unique combination of a neutron reflectometer with an add-on X ray reflectometer,

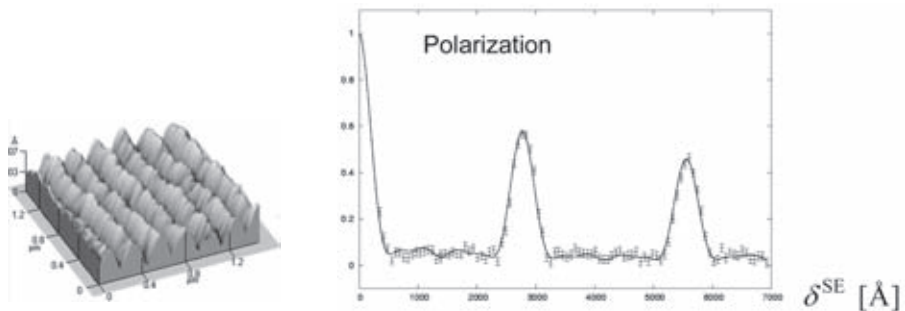


FIG. 7. Left: Optical grating investigated with NRSE–SERGIS at FLEX, HMI. Right: Experimental NRSE–SERGIS scan obtained in this experiment.

which allows routine in situ neutron/X ray contrast studies. Experiments using both probes can be conducted independently of each other at the same time, which can save measurement time compared to a sequential characterization and, more interestingly, also enables combined in situ studies of (e.g. irreversible) kinetic processes such as sample growth or chemical reactions.

When combining neutron with X ray reflectometry/scattering, the advantages of both probes can be utilized. X rays from a sealed tube source are available continuously and provide a high intensity compared to that of the neutron source. They can be used to routinely characterize the structural details of samples with high accuracy, while the magnetic or dynamic properties of the samples can simultaneously be measured with neutrons. As an example, at MatSci-R we plan to study the structure and the magnetism of buried interfaces of magnetic multilayers (GMR materials) with both X rays and neutrons.

For technical reasons the two beams at MatSci-R are crossed at a 90° angle. Therefore, more than one combined *n/X* measurement may be necessary in the case of anisotropic surfaces (e.g. vicinal crystal surfaces or optical gratings) to fully characterize the sample with both probes. The custom made X ray source (EFG, Berlin, Germany) is mounted on one side of the sample table, an X ray detector is mounted on the opposite side. The add-on X ray reflectometer will become available for experiments in 2005.

### **6. STATUS AND SCHEDULE**

At present, the installation of the MatSci-R instrument is almost completed. We are currently commissioning the neutron area detector (ESRF, Grenoble) and are preparing to align the focusing HOPG monochromator in the beam. The add-on X ray source is expected to be delivered in March 2005. The X ray detector system will be commissioned afterwards. Also in progress is the programming of the Labview based instrument control software. Next steps towards regular experiments are the installation of additional shielding, sample environments, spin filters and spin echo equipment. Regular user operation is expected to start in fall 2005.

### **7. FIELDS OF APPLICATION**

The MatSci-R instrument will allow studies of the structure, dynamics and magnetic properties of solid and liquid surfaces, interfaces, thin films and multilayers. The special focus lies on the characterization of complex

nanostructured materials, soft matter surfaces, thin films and membranes, complex magnetic liquids [8], and spin mapping on magnetic multilayers with non-collinear spin structures, to mention a few. We will routinely conduct in situ neutron/X ray contrast studies, especially of irreversible dynamic processes on interfaces. Spin echo equipment will be utilized to study the dynamics of interfaces (NSE energy mode) and to obtain high resolution scattering data (NSE momentum mode). In the following we will briefly mention two possible applications of the instrument: (a) polarized neutron reflectometry on magnetic multilayers; and (b) neutron/X ray contrast studies on soft matter films.

### 7.1. Magnetic multilayers, polarized neutron reflectometry and the supermatrix formalism

The characterization of the structure and magnetism of magnetic multilayers with polarized neutron reflectometry requires a detailed spin dependent analysis of the specular reflectivity and the off-specular scattering of the sample. In this context, the growing complexity of modern magnetic materials demands for revised experimental techniques and theoretical concepts. In an experiment on an FeCr multilayer at the EVA reflectometer at ILL (Grenoble), we have employed a one dimensional position sensitive detector (PSD) in combination with a polarized  $^3\text{He}$  gas analyser for a wide angle analysis of the spin state of the reflected neutrons [4]. For data analysis we have developed a supermatrix formalism [4, 9] that can be utilized for model calculations of polarized neutron reflectometry and off-specular scattering data [10].

Figure 8 (left) displays the non-collinear structure that can arise from a frustration of the magnetization in adjacent Fe layers in an Fe–Cr multilayer [11–13]. In addition to the magnetic roughness, a real multilayer sample also contains domains of a finite lateral extension (as shown schematically in Fig. 8 (right)). Both the domain morphology and the internal magnetic structure in an average domain can be revealed in a polarized neutron reflectometry experiment. In the following, we ignore the domain structure and focus on the magnetic roughness within a typical domain.

Figure 9 shows the scattering geometry of the polarized neutron reflectometry experiment, indicating also the magnetizations in the Fe layers and the neutron beam polarization direction in the weak external guide field of 560 G. For experiments with neutron spin analysis, a  $^3\text{He}$  spin analyser is placed between the sample and the one dimensional position sensitive detector.

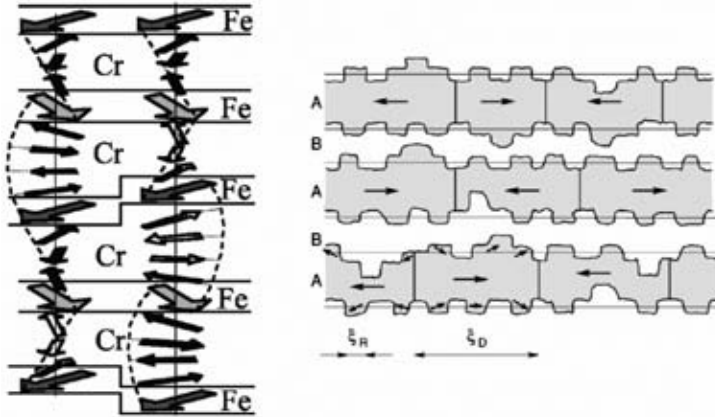


FIG. 8. Left: Non-collinear coupling of the magnetization in the Fe layers of an Fe-Cr multilayer. Right: Magnetic domain structure and magnetic roughness in a real sample (A: Fe layers, B: Cr layers,  $\xi_R$ : roughness in-plane correlation length,  $\xi_D$ : magnetic domain size).

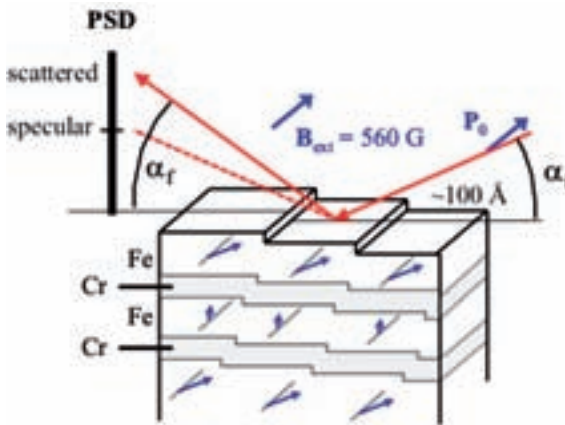


FIG. 9. Scattering geometry in the polarized neutron reflectometry experiment on EVA (ILL, Grenoble).

Figure 10 shows the result of an unpolarized measurement, in which exit angle profiles ( $\alpha_f$  spectra) were recorded with the PSD for a series of incidence angles ( $\alpha_i$ ). The two diffuse streaks originate from the roughness of the interfaces in the magnetic multilayer. The upper one reflects the chemical and ferromagnetic periodicity in the sample, whereas the lower one, located at half

the momentum transfer in reciprocal space, reflects the antiferromagnetic superstructure in the Fe layers.

Employing polarized neutrons and polarization analysis of the scattered neutrons yields additional information about the scattering signals displayed in Fig. 10. Figure 11 (left) shows the same data as in Fig. 10, but now the magnetic origin of the scattering signals is resolved: The half-order superstructure streak is actually purely spin-flip in nature. At first hand, this is understandable as the antiferromagnetic component of the Fe layer magnetizations rotates the incident neutron spin (see the experimental geometry in Fig. 9). However, as the reflection of the neutrons from a magnetic multilayer is a very complex process, involving spin precessions around the various layer magnetizations throughout the multilayer, the calculation of the polarization of the scattered neutrons is actually more involved. The supermatrix formalism we applied for data analysis, however, takes care correctly of all the spin precessions in the various layers. The result of the model calculations is shown on the right hand side in Fig. 11. The qualitative agreement is quite good, and the hypothesized magnetic structure of the multilayer (see Fig. 8) can therefore be regarded as confirmed. To achieve a detailed quantitative agreement between experiment and model calculation, however, further experiments will need to be conducted on reference samples with tailored properties and with a lower  $^3\text{He}$  pressure in the spin analyser to enhance the experimental data quality.

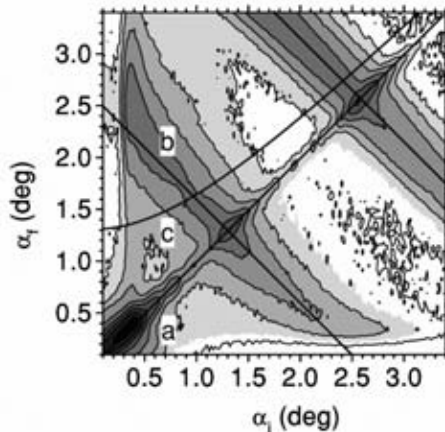


FIG. 10. Off-specular scattering signal obtained with a PSD with unpolarized neutrons. The lines indicate three typical one dimensional scans: (a) specular scan; (b) diffuse  $q_{\parallel}$  scan; and (c) diffuse  $q_{\perp}$  scan.

## 7.2. Neutron/X ray contrast studies on soft matter films

The physical properties of polymers are determined by both their static structure and morphology and their dynamics on short and long timescales, ranging from picoseconds to seconds. This opens a field where neutron and X ray analysis techniques can be successfully combined to obtain a more complete picture of the physics in the sample. At MatSci-R, we intend to characterize the static structure and order in thin polymer films, e.g. in situ during the dewetting processes, using conventional time resolved neutron and X ray scattering, as well as to investigate the fast Rouse dynamics at the surface using NSE in reflection geometry. This novel mode of NSE in reflection geometry, which allows one to focus on the surface and thin film dynamics in the experiment, was recently employed in a combined NSE and XPCS (X ray photon correlation spectroscopy) study on smectic membranes [14]. This study provides a good example of the complementary time and momentum transfer ranges of NSE and XPCS. Relaxation times between 0.07 and 8  $\mu\text{s}$  were measured with XPCS and NSE as a function of in-plane momentum transfer  $q^\perp$  in the range  $3 \times 10^{-4} \text{ nm}^{-1}$  to  $0.3 \text{ nm}^{-1}$ . The overview plot of the resulting relaxation times as a function of in-plane momentum transfer  $q^\perp$  in Fig. 3 of Ref. [14] highlights the complementary  $q$ - and relaxation time ranges that the

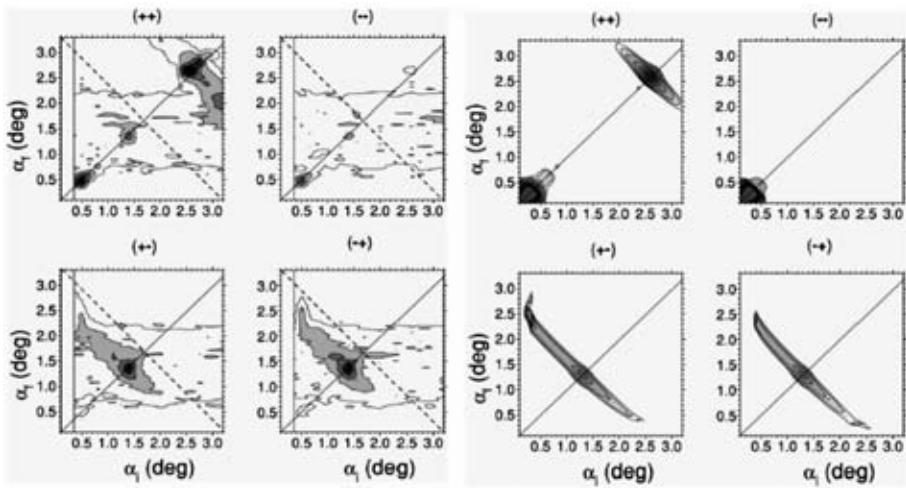


FIG. 11. Off-specular scattering signal obtained with a PSD with polarized neutrons. Left: Experimental data, separated into non-spin-flip ( $++$ ,  $--$ ) and spin-flip ( $+-$ ,  $-+$ ) signals. Right: Model calculation based on the supermatrix formalism.

two experimental techniques provide. From the combined data, the elastic properties of the membranes can be determined.

## ACKNOWLEDGEMENTS

This work was supported by focused neutron research funding of the Max Planck Society.

## REFERENCES

- [1] [http://www.mf.mpg.de/en/abteilungen/dosch/frmII/frmIIintro\\_en.shtml](http://www.mf.mpg.de/en/abteilungen/dosch/frmII/frmIIintro_en.shtml)
- [2] FELCHER, G.P., et al., in *Advances in Neutron Scattering Instrumentation* (Proc. SPIE), (ANDERSON, I.S., GUÉRARD, B., Eds), Vol. **4785**, SPIE Optical Engineering Press, Bellingham, WA (2002) 164; MAJOR, J., et al., Combining of neutron spin echo and reflectivity: A new technique for probing surface and interface order, *Physica B* **336** 8 (2003).
- [3] MEZEI, F., Neutron spin-echo – New concept in polarized thermal–neutron techniques, *Z. Phys.* **255** (1972) 146; *Neutron Spin Echo* (MEZEI, F., Ed.), Springer, Heidelberg (1980); *Neutron Spin Echo Spectroscopy* (MEZEI, F., PAPPAS, C., GUTBERLET, T., Eds), Springer, Heidelberg (2003).
- [4] NICKEL, B., Spin-resolved off-specular neutron scattering maps from magnetic multilayers using a polarized  $^3\text{He}$  gas spin filter, *Rev. Sci. Instrum.* **72** (2001) 163.
- [5] MEZEI, F., in *Neutron Inelastic Scattering 1977* (Proc. Symp. Vienna, 1977), IAEA, Vienna (1978) 125.
- [6] GOLUB, R., GÄHLER, R., A neutron resonance spin echo spectrometer for quasi-elastic and inelastic scattering, *Phys. Lett. A* **123** (1987) 43.
- [7] FITZSIMMONS, M.R., FRITZSCHE, H., GIERLINGS, M., MAJOR, J., PYNN, R., Measuring scattering angles with neutron spin echo, *Nucl. Instrum. Methods Phys. Res. A* **529** (2004) 10; PYNN, R., Optimization of neutron scattering instrumentation using neutron spin echo: Application to the discrimination of diffuse scattering in neutron reflectivity experiments, *Rev. Sci. Instrum.* **73** (2002) 2948.
- [8] VOROBIEV, A., MAJOR, J., DOSCH, H., GORDEEV, G.D., ORLOVA, Magnetic field dependent ordering in ferrofluids at  $\text{SiO}_2$  interfaces, *Phys. Rev. Lett.* **93** (2004) 267203.
- [9] RÜHM, A., TOPERVERG, B.P., DOSCH, H., Supermatrix approach to polarized neutron reflectivity from arbitrary spin structures, *Phys. Rev. B* **60** (1999) 16073.
- [10] Supermatrix analysis software download, [http://www.mf.mpg.de/en/abteilungen/dosch/software/mfintro\\_en.shtml](http://www.mf.mpg.de/en/abteilungen/dosch/software/mfintro_en.shtml)

- [11] PIERCE, D.T., UNGURIS, J., CELOTTA, R.J., STILES, M.D., Effect of roughness, frustration, and antiferromagnetic order on magnetic coupling of Fe/Cr multilayers, *J. Magn. Magn. Mater.* **200** (1999) 290.
- [12] SCHREYER, A., et al., Magnetic structure of Cr in exchange coupled Fe/Cr(001) superlattices, *Phys. Rev. Lett.* **79** (1997) 4914; SCHREYER, A., Non-collinear and collinear magnetic structures in exchange coupled Fe/Cr(001) superlattices, *Phys. Rev. B* **52** (1995) 16066.
- [13] SLONCZEWSKI, J.C., Overview of interlayer exchange theory, *J. Magn. Magn. Mater.* **150** (1995) 13.
- [14] SIKHARULIDZE, I., FARAGO, B., DOLBANYA, I.P., MADSEN, A., DE JEU, W.H., Surface and Bulk Elasticity Determined Fluctuation Regimes in Smectic Membranes, *Phys. Rev. Lett.* **91** (2003) 165504.



# NEUTRON SPECULAR REFLECTOMETRY

## *Some aspects of theory*

H. LEEB

Atominstytut of the Austrian Universities,  
Vienna University of Technology,  
Vienna, Austria

### **Abstract**

The quantum mechanical description, as well as the analysis of neutron specular reflection data in terms of nuclear and magnetic scattering length density profiles, are reviewed. Particular emphasis is given to the so-called phase problem, which hampers the unambiguous reconstruction of profiles. Recent proposals to determine the full reflection coefficient (modulus and phase), specifically those based on polarization measurements, are revisited.

## 1. INTRODUCTION

Reflectometry with neutrons and X rays provide a non-destructive way to investigate the structure of surfaces [1–5]. Specular reflection measurements, in particular, are simple and have become a standard tool in surface science and materials science. Of particular interest is the use of polarized neutrons in reflectometry because they can provide important information on the magnetic field profile and/or the spin structure of the sample. This option of modern neutron reflectometer set-ups is increasingly applied to study thin magnetic films and superlattices [6–8].

The basic quantity measured in reflection experiments is the reflectivity  $r(q)$ , which is the ratio of the reflected to the incoming intensity at a given momentum  $q$ . Knowing the depth profile of the sample it is straightforward to evaluate the specular reflectivity  $r(q)$  within one dimensional quantum mechanics. The inverse problem, i.e. an unambiguous and model independent reconstruction of the depth profile from specular reflection data, is less trivial and in addition it is plagued by the so-called phase problem. This problem, widely discussed in structure analysis (e.g. see Refs [9–11]), refers to the fact that the measured reflectivities  $r(q)=|R(q)|^2$  provide only the modulus of the reflection coefficient, while the full knowledge (modulus and phase) of the complex reflection coefficient  $R(q)$  is required for a unique reconstruction of the profile.

In the last decade, considerable effort has been devoted to the phase problem in neutron specular reflection and several schemes for its solution have been proposed. Essentially, there are three groups of schemes: (i) the reference layer methods, where one makes use of the interference between the reflections of a known reference layer and the unknown surface profile [12–17]; (ii) the Lloyd’s mirage technique [18]; and (iii) the dwell time method [19]. Among these the reference layer methods are most promising because they require minor modifications of the usual set-up. However, none of them has become a standard tool. To our knowledge only the method of Ref. [12] has been implemented for a specific case by Majkrzak et al. [20], who also proposed and tested experimentally the related surround method [21].

In this contribution, we review some theoretical aspects of neutron specular reflection and the corresponding procedures for analysis. In Section 2, we briefly revisit the description of the reflection process within one dimensional quantum mechanics and give the essential relations of the corresponding inverse scattering problem together with some examples. In Section 3, we focus on the phase problem and the various proposals for neutron specular reflection. Here, we restrict ourselves to the most promising reference layer methods which make use of spin polarized neutron reflectometry for the phase determination. Finally, in Section 4 some concluding remarks are given.

## 2. BASIC THEORY

The reflection of a neutron off a surface has to be described as a scattering process within quantum mechanics. Here, we restrict ourselves to neutron specular reflection at a plane surface, where the sample is of stratified structure with layers aligned with the surface. In the energy range relevant for neutron reflectometry ( $E < 200 \mu\text{eV}$ ), the interaction between the neutron and the sample is given by a mean potential composed of a nuclear and a magnetic part,

$$V = V_{nucl} + V_{magn} = 4\pi\rho a - \frac{m}{\hbar^2} g_s \mu_N \vec{\sigma} \cdot \vec{B} \quad (1)$$

where  $\mu_N = 3.15245166 \cdot 10^{-8} \text{ eV T}^{-1}$  is the nuclear magneton,  $\frac{g_s}{2} = 2 \times (-1.9130428)$  is the gyromagnetic spin factor of the neutron,  $\vec{B}$  is the magnetic field strength, and  $\vec{\sigma}$  is the vector formed by the Pauli matrices. The first term describes the nuclear interaction which is given by the product of the nuclear density  $\rho$  and the coherent scattering

## NEUTRON SPECULAR REFLECTOMETRY

length  $a$ . This so-called nuclear scattering length density is usually spin independent. The magnetic interaction is spin dependent due to the occurrence of the Pauli matrices  $\vec{\sigma}$  and therefore the observed reflection depends on the polarization  $\vec{P}_0$  of the incident beam.

In the following we assume that the surface of the sample is aligned with the  $(y, z)$  plane, and the beam propagates in the sample in  $x$  direction (see Fig. 1).

Because of the layered structure the potential depends only on  $x$ , i.e.  $V(x)$ , and is often denoted as depth profile. In addition we assume that the reflecting surface is at  $x = 0$  and  $V(x)$  vanishes for  $x < 0$ .

Specular reflection is essentially a one dimensional problem and requires the solution of the one dimensional Schrödinger equation,

$$\left\{ \frac{d^2}{dx^2} + q^2 - V(x) \right\} \psi(q, x) = 0 \quad (2)$$

where  $q = (2\pi/\lambda)\cos\vartheta$  is the component of the wave number perpendicular to the surface. Here,  $\lambda$  is the neutron wave length and  $\vartheta$  is the angle of incidence of the neutron beam. This one dimensional problem is solved for an incident wave from the left employing the boundary conditions

$$f_+(q, x) = \begin{cases} [e^{iqx} + R(q)e^{-iqx}] / T(q) & \text{for } x < 0 \\ e^{iqx} & \text{for } x \rightarrow +\infty \end{cases} \quad (3)$$

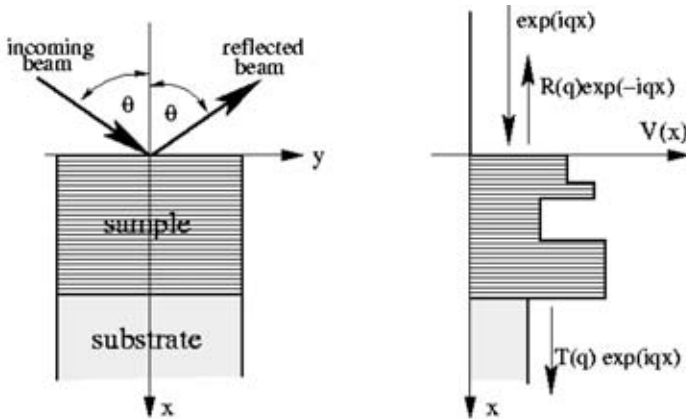


FIG. 1. Schematic set-up of a reflectometer experiment and the corresponding potential.

Thus, one obtains the Jost solution  $f_+(q, x)$ . Analogously, one can determine the corresponding Jost solution  $f_-(q, x)$  for incidence from the right

$$f_-(q, x) = \begin{cases} e^{-iqx} & \text{for } x \rightarrow -\infty \\ [e^{iqx} + \bar{R}(q)e^{iqx}] / \bar{T}(q) & \text{for } x > 0 \end{cases} \quad (4)$$

Here,  $\bar{q} = \sqrt{q^2 - V_s}$  is the wave number in the substrate and  $T(q)$  and  $R(q)$  are the transmission and reflection coefficient for incidence from the left, respectively. The quantities  $\bar{T}(q)$  and  $\bar{R}(q)$  are the transmission and reflection coefficient for incidence from the right. Taking into account the spin of the neutron the solutions  $\psi(q, x)$  and  $f_{\pm}(q, x)$  are two dimensional vectors and  $V(x)$ ,  $R(q)$ ,  $T(q)$ ,  $\bar{R}(q)$  and  $\bar{T}(q)$  are  $2 \times 2$  matrices.

For a scattering length density profile composed of a sequence of layers (each layer with a specific but constant potential  $V_i(x)$ ), the reflection and transmission coefficients can be determined via the transfer matrix formalism [22]. In its simplest form the transfer matrix  $\mathbf{M}_i$  provides the relationship of the wave function and its derivative at the interfaces at  $x_{i-1}$  and  $x_i$  of the  $i$ th layer,

$$\begin{pmatrix} \psi(q, x_{i-1}) \\ \psi'(q, x_{i-1}) \end{pmatrix} = \mathbf{M}_i \begin{pmatrix} \psi(q, x_i) \\ \psi'(q, x_i) \end{pmatrix} = \begin{pmatrix} \cos q_i d_i & \frac{1}{q_i} \sin q_i d_i \\ -q_i \sin q_i d_i & \cos q_i d_i \end{pmatrix} \begin{pmatrix} \psi(q, x_i) \\ \psi'(q, x_i) \end{pmatrix} \quad (5)$$

where  $d_i$  is the thickness of the  $i$ th layer and  $q_i = \sqrt{q^2 - V_i}$  is the wave number in the  $i$ th layer. For a sample composed of  $N$  layers with the reflecting surface at  $x_N$  and the interface with the substrate at  $x_0$ , the reflection and transmission coefficients can be obtained from the equation

$$\begin{aligned} & \begin{pmatrix} T(q) \\ iq_0 T(q) \end{pmatrix} e^{iq_0 x_0} \\ &= \mathbf{M}_1 \mathbf{M}_2 \cdots \mathbf{M}_N \begin{pmatrix} e^{iq_{N+1} x_N} + R(q) e^{-iq_{N+1} x_N} \\ iq_{N+1} e^{iq_{N+1} x_N} - iq_{N+1} R(q) e^{-iq_{N+1} x_N} \end{pmatrix} \end{aligned} \quad (6)$$

Here,  $q_0$  is the wave number in the substrate, while  $q_{N+1}$  is the wave number in the medium in front of the sample. The formalism becomes particularly simple for a sample of thickness  $L$  with the reflecting surface at  $x_N = 0$ . The coefficients of  $\mathbf{M}_i$  are real valued and  $\det \mathbf{M}_i = 1$  (cf. Eq. (5)), but  $\mathbf{M}_i$  is not

unitary. For a more general derivation of the transfer matrix formalism, see Ref. [12].

In practical applications of neutron reflectometry we are interested in the reconstruction of the scattering length depth profile from the reflection data. This is a paradigm for a quantal inverse scattering problem in one dimension. Usually, one takes recourse to a simulation, i.e., one defines a realistic model depth profile, whose open parameters are adjusted via a fit to the measured reflectivities  $r(q) = |R(q)|^2$ . In order to obtain a model independent reconstruction of the depth profile, a solution of the corresponding inverse scattering problem should be performed. In the literature of X ray and electron scattering this is often called the direct method [23], by which is meant that the reconstruction of the profile is sought directly and not indirectly by simulation.

The general mathematical formalism for solving the one dimensional inverse scattering problem was developed long ago [24–26]. The method is based on the Marchenko integral equation

$$K(x, y) + B(x + y) + \lambda \int_{-x}^{+x} dz B(z + y) K(x, z) = 0 \text{ with } x > y \tag{7}$$

where the reflection properties of the system enter via the kernel

$$B(x) = \begin{cases} \frac{1}{2\pi} \int_{-\infty}^{+\infty} dq e^{-iqx} R(q) & \text{for } x > 0 \\ 0 & \text{for } x < 0 \end{cases} \tag{8}$$

Here, the strength parameter  $\lambda$  has been introduced with regard to the discussion of the Neumann series; for the inversion procedure we must use  $\lambda = 1$ . The depth profile is then given by

$$V(x) = \begin{cases} 2 \frac{dK(x, x)}{dx} & \text{for } x > 0 \\ 0 & \text{for } x < 0 \end{cases} \tag{9}$$

In general the solution of the integral equation (7) is numerically more involved than simulation techniques. Therefore, the latter have been extensively applied for analyses of reflection data, while the solution of the Marchenko equation has been numerically implemented only a decade ago [27]. A typical example for a reconstruction of a depth profile via the solution of the Marchenko equation is displayed in Fig. 2. Further examples are given in

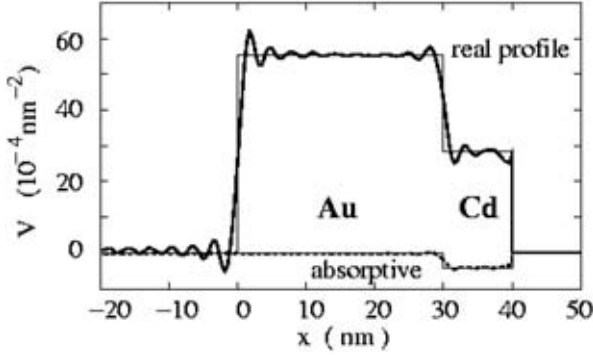


FIG. 2. Reconstruction of the depth profile of a gold-cadmium layer from the reflection coefficients in the momentum range  $-1 \leq q \leq nm^{-1}$ . The reconstructed profiles are shown by thick solid and dashed lines, respectively. For reference the original profile is shown by thin solid lines. The example is taken from Ref. [16].

Ref. [27], which clearly demonstrate the quality of reconstruction which can be achieved via the solution of the integral equation (7).

The quality of reconstruction depends strongly on the range of  $q$  values for which  $R(q)$  is known. Let us denote with  $q_{\max}$  the upper boundary of this range; then we expect oscillatory defects in the reconstruction with the period  $\pi/q_{\max}$ . This cutoff  $q_{\max}$  defines also the finite resolution which is best seen in the reconstruction of discontinuities in the profile (see, for example, Fig. 5(c)).

Reconstructions via solution of the Marchenko equation require the knowledge of the complex reflection coefficient  $R(q)$  for positive and negative values of  $q$ . For real potentials  $V(x)$  the reflection coefficient at  $q < 0$  is simply given by [8]

$$R(-q) = R^*(q) \quad (10)$$

For complex potentials  $V(x)$  the comparison of the Wronskians of the Jost solutions, Eqs (3) and (4), lead to the relationship (see Ref. [27])

$$R(-q) = \frac{\bar{R}(q)}{R(q)\bar{R}(q) - T(q)\bar{T}(q)} \quad (11)$$

Hence, the knowledge of all coefficients  $R(q)$ ,  $\bar{R}(q)$ ,  $T(q)$  and  $\bar{T}(q)$  for  $q > 0$  is required for the determination of  $R(q)$  at  $q < 0$ . In addition, the right and the left transmission coefficient satisfy the relationship (see Ref. [27])

$$\bar{T}(q) = \frac{q_0}{q_{N+1}} T(q) \tag{12}$$

In principle, the Marchenko equation is derived with the assumption of a real potential  $V(x)$ . However, the integral equation works satisfactorily also for potentials with small imaginary parts as shown in Fig. 2 (see examples in Refs [16] and [27]).

In general, solving the Marchenko equation is numerically involved. Therefore, one might prefer a perturbative approximation based on a finite Neumann series which is given by the first  $M + 1$  terms of the expansion of the solution  $K(x,y)$  of Eq. (7) in the parameter  $\lambda$ :

$$K_{Neu}^{(M)}(x, y) = \sum_{n=0}^M \lambda^n K_n(x, y) \tag{13}$$

with

$$K_n(x, y) = - \int_{-x}^{+x} dz K_{n-1}(x, z) B(z + y) \quad \text{and} \quad K_0(x, y) = -B(x + y) \tag{14}$$

The convergence of the Neumann series is only given under the condition

$$\|B\|_x^2 = \int_{-x}^{+x} dy \int_{-x}^{+x} dz |B(y + z)|^2 < 1 \tag{15}$$

The numerics based on the Neumann series are significantly faster, but at the expense of the quality of reconstruction. In Fig. 3 the example of the reconstruction of a step potential with Neumann series of different order is given.

The example clearly shows that a Born approximation ( $M = 0$ ) can reproduce the profile only in the surface region. With increasing depth higher order terms of the Neumann series become important.

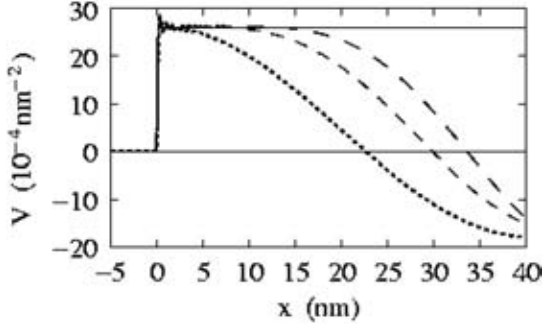


FIG. 3. Reconstruction of a step potential with  $V_s = 26 \times 10^{-4} \text{ nm}^{-2}$ . The solutions of the Marchenko equation corresponding to the Neumann series with  $M = 0$  (dotted line) and  $M = 1$  and  $2$  (dashed lines, from left to right) are shown.

### 3. THE PHASE PROBLEM

#### 3.1. The importance of the phase

The phase problem refers to the fact that standard experiments in reflectometry determine only the reflectivity  $r(q)=|R(q)|^2$  for positive  $q$  values; usually the phase of  $R(q)$  remains undetermined. The importance of the phase for the reconstruction of the profile is easily seen by the simple example of a two layer structure. Let us consider the reflection given by the potentials

$$\begin{aligned}
 V_a(x) &= \begin{cases} h_1 & \text{for } -a \leq x \leq 0 \\ h_2 & \text{for } 0 \leq x \leq a \\ 0 & \text{for } x < -a \text{ and } x > a \end{cases} \\
 \text{and } V_b(x) &= \begin{cases} h_2 & \text{for } -a \leq x \leq 0 \\ h_1 & \text{for } 0 \leq x \leq a \\ 0 & \text{for } x < -a \text{ and } x > a \end{cases}
 \end{aligned} \tag{16}$$

where the two layers are interchanged. The calculation of the corresponding reflection coefficients  $R_a(q)$  and  $R_b(q)$  is straightforward and leads to lengthy expressions which should not be given here. Instead we give the relation between the two reflection coefficients

$$R_b(q) = -R_a^*(q) \exp[2i(q_1 + q_2 - 2q)a] \tag{17}$$

where  $q_1$  and  $q_2$  are the wave numbers in the layers with the potential strength  $h_1$  and  $h_2$ , respectively. From Eq. (17) it is obvious that the interchange of the two layers leads to different reflection coefficients, but the reflectivity is the same for both profiles. Hence, the reflectivity alone does not allow one to distinguish between the two profiles.

A more general consideration of this ambiguity makes use of the analyticity of the reflection coefficient  $R(q)$ . In the absence of bound states the reflection coefficient can be written in the form (see, for example, Refs [28, 29]):

$$R(q) = \prod_{n=1}^N \left( \frac{q - a_n}{q - a_n^*} \frac{q + a_n^*}{q + a_n} \right) R^{(H)}(q) \quad (18)$$

where, for a one sided potential,  $V(x) = 0$  for  $x < 0$ , the zeroes  $a_n$  lie in the upper half-plane,  $\text{Im}a_n > 0$ . The Hilbert reflection coefficient

$$R^{(H)}(q) = \sqrt{r_+(q)} \exp[i\phi_H(q)] \quad (19)$$

is completely determined by the reflectivities

$$\phi_H(q) = -\pi - \frac{q}{\pi} \mathcal{P} \int_{-\infty}^{+\infty} dq' \frac{\ln r(q')}{q'(q' - q)} \quad (20)$$

where  $\mathcal{P} \int$  denotes the principal value of the integral. The phase problem thus reduces to the problem of the unknown complex zeroes  $a_n$  in the upper half of the  $q$  plane. It is possible to calculate in closed form the effect on the profile of any number of zeros included in the reflection coefficient [19]. It is important to remark that the inclusion of a single pair of zeroes may result in a considerable difference in the profile  $V(x)$ . Hence, the Hilbert reflection coefficient alone cannot provide a glimpse on the true profile.

### 3.2. Experimental determination of the reflection phase via reference layers

Over the last decade, several so-called local methods of phase determination have been proposed, some for unpolarized neutrons, some for polarized ones with external or internal magnetic fields. By a *local* method we mean that one recovers the phase of  $R_S(q)$  from measurements at the same  $q$  value, while the Hilbert phase Eq. (20) represents a *global* method because it requires measurements at all  $q$  values to determine  $R_S(q)$ . Here, we restrict ourselves to reference layer methods which make use of the properties of spin-polarized

neutrons in magnetic fields. For a more complete list of proposals for phase determination and corresponding references see Ref. [30].

The reference layer methods are based on the interference of the known reflection of the reference layer with that of the unknown sample. Thus one can extract the reflection phase of the latter. The concept was first suggested in Refs [18, 31] and experimentally implemented by Majkrzak et al. [20]. The concept is best demonstrated by the example of a reference layer mounted on top of the sample (Fig. 4).

The effect of the reference layer of thickness  $d$  and interaction  $V_R$  is best evaluated within the transfer matrix formalism of Eq. (5), which leads to the relationship

$$\begin{pmatrix} (1 + \widetilde{R}_S)A \\ iq(1 - \widetilde{R}_S)A \end{pmatrix} = \begin{pmatrix} \cos Qd & \frac{1}{Q} \sin Qd \\ -Q \sin Qd & \cos Qd \end{pmatrix} \begin{pmatrix} (1 - R) \\ iq(1 - R) \end{pmatrix} \quad (21)$$

Here,  $A$  is an unknown constant,  $Q = \sqrt{q^2 - V_R}$  is the wave number in the reference layer, and  $\widetilde{R}_S$  and  $R$  are the reflection coefficients of the sample (reflecting surface at  $x = 0$ ) and of the total arrangement, respectively. From Eq. (21) it is straightforward to eliminate the unknown  $A$  and after some algebra one obtains a relation of the form

$$|\widetilde{R}_S - z_0|^2 = c^2 \quad (22)$$

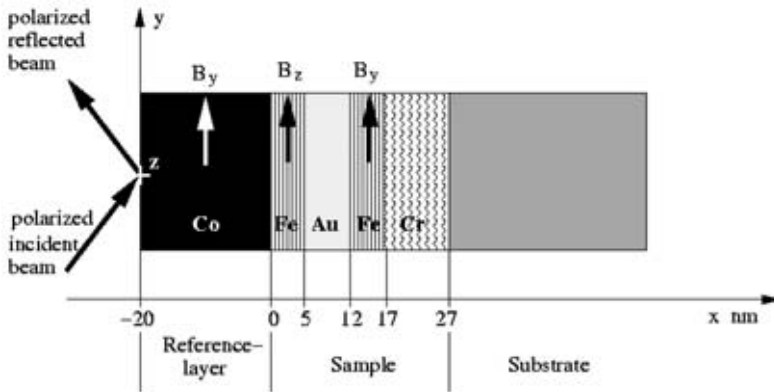


FIG. 4. Typical arrangement for the application of the reference layer method.

where  $z_0$  and  $c$  depend only on  $|R(q)|^2$  and the parameters of the reference layer. Thus the determination of the reflectivity of the total arrangement determines for  $R_S$  a circle in the complex plane with radius  $c$  and center  $z_0$ . In order to extract  $R_S$  uniquely, reflectivity measurements of three different arrangements of sample and reference layer are required [12, 13, 17]. The final value of  $R_S$  is then obtained as the intersection point of three circles. In the region below the critical momentum, however, the above-mentioned circles coincide and do not provide a unique intersection point. Recently, Aktosun and Sacks [17] considered this problem in the total reflection regime and derived a procedure for non-decaying potentials. In addition they derived a method for which only two reflectivity measurements are sufficient for a unique determination of  $R_S$  [17].

The reference layer method becomes particularly simple if one uses a magnetic reference layer and a polarized neutron beam. Due to the spin dependent interaction of the neutron, the reflectivity of the total arrangement depends on the polarization of the incident beam. Hence, one has to perform at a fixed  $q$  value one reflectivity measurement without reference layer and two of the total arrangement, one with spin-up and one with spin-down polarization of the neutron beam [12, 13, 32]. A detailed derivation of the formalism, also including extended magnetic fields, is given in Ref. [32]. The surround method proposed by Majkrzak et al. [22] is a variation of these concepts, where the ‘backing’ or ‘fronting’ of the sample has the function of the reference layer.

### 3.3. Methods based on polarization measurements

Polarized neutrons are an ideal probe for the study of the spin and magnetic structure of films and surfaces. Hence, the availability of reflectometers with polarization option has been continuously increasing in recent years. In this subsection we consider the use of polarized neutrons for phase determination of non-magnetic samples. The retrieval of depth profiles of magnetic samples is discussed in Section 3.4.

In spin polarized neutron reflectometry the reflection coefficient  $R(q)$  becomes a  $2 \times 2$  matrix in spin space,

$$R = \begin{pmatrix} R_{++} & R_{+-} \\ R_{-+} & R_{--} \end{pmatrix} \quad (23)$$

The diagonal elements  $R_{\pm\pm}$  describe the reflection without change of the spin state,  $R_{\pm\mp}$  while give the spin flip amplitude. The polarization  $\rho^0$  of the incident neutron beam yields the density matrix

$$\rho^0 = \frac{1}{2} \left( \mathbf{1} + \overline{P^0} \cdot \overline{\sigma} \right) \quad (24)$$

where  $\overline{\sigma}$  is the vector formed by the standard Pauli matrices

$$\overline{\sigma} = \begin{pmatrix} \hat{z} & \hat{x} - i\hat{y} \\ \hat{x} + i\hat{y} & -\hat{z} \end{pmatrix} \quad (25)$$

The reflected beam is described by the density matrix

$$\rho = \frac{1}{\text{Trace}(R\rho^0R^\dagger)} R\rho^0R^\dagger \quad (26)$$

The polarization of the reflected beam is then given by

$$\overline{P} = \text{Trace}(\rho\overline{\sigma}) \quad (27)$$

In the following we consider a method for phase determination based on measurements of the polarization of the reflected beam [14]. The method requires the arrangement of Fig. 4, i.e. a magnetic reference layer on top of a non-magnetic sample. Within the reference layer the magnetic field  $\overline{B}(x)$  is directed in the  $z$  direction, which is assumed to be the quantization axis. In addition, we assume that  $\overline{B}(x)$  vanishes outside the reference layer. Using Eqs (23)–(27), the evaluation of the components of  $\overline{P}$  yields

$$P_+ = P_x + iP_y = 4 \frac{R_{++}^* R_{--} P_+^0}{r_{++} (1 + P_z^0) + r_{--} (1 - P_z^0)}$$

and  $P_z = 2 \frac{r_{++} (1 + P_z^0) - r_{--} (1 - P_z^0)}{r_{++} (1 + P_z^0) + r_{--} (1 - P_z^0)} \quad (28)$

where  $r_{\pm\pm} = R_{\pm\pm} R_{\pm\pm}^*$  are the reflectivities in the two spin states. The appearance of the product  $R_{\pm\pm}^* R_{\mp\mp}$  in  $P_+$  arises from the interference of the two spin components of the wave functions and allows the determination of the phase if the polarization of the incident beam is not aligned with  $\overline{B}$ . With Eq. (28) the quantity  $s = R_{++}/R_{--}$  can be expressed in terms of the measurable polarization components

$$s = \frac{R_{++}}{R_{--}} = \frac{P_+^0}{P_+} \frac{1+P_z}{1+P_z^0} \quad (29)$$

The reflection coefficients of the arrangement of Fig. 4 can be expressed in terms of the unknown reflection coefficient of the sample and the known reflection properties of the reference layer,

$$R_{\pm\pm} = \frac{\eta^\pm \tilde{R}_S + R_R^\pm}{1 - R_R^\pm \tilde{R}_S} \quad (30)$$

where

$$\eta^\pm = T_R^\pm \overline{T_R^\pm} - R_R^\pm \overline{R_R^\pm} \quad (31)$$

Here  $R_R^\pm$  and  $T_R^\pm$  are the reflection and transmission coefficients of the reference layer for left incidence. Those for right incidence are denoted by  $\overline{R_R^\pm}$  and  $\overline{T_R^\pm}$ . Substituting Eq. (30) into Eq. (29) yields a quadratic equation for  $\tilde{R}_S$ ,

$$\alpha \tilde{R}_S^2 - \beta \tilde{R}_S - \gamma = 0 \quad (32)$$

with

$$\alpha = \eta^+ \overline{R_R^-} - s \eta^- \overline{R_R^+}, \quad \beta = \left( \eta^+ - R_R^+ \overline{R_R^-} \right) - s \left( \eta^- - R_R^- \overline{R_R^+} \right)$$

and  $\gamma = R_R^+ - s R_R^-$  (33)

There are two roots of the quadratic equation (32). The physical solution can be selected by continuity requiring the phase  $\phi$  to tend towards the limit  $\phi = -\pi$  at  $q = 0$ . At energies above the total reflection regime the physical solution is obtained by the requirement that  $r_s = |R_s|^2 \leq 1$ . In Fig. 5 we show the example of a reconstruction of the profile of Fig. 4 applying the method to simulated data. In the first step one reconstructs the reflection coefficient  $R_S$  of the sample for positive  $q < 1 \text{ nm}^{-1}$ . In the second step the extracted  $R_S$  values up to  $q < 1 \text{ nm}^{-1}$  have been used to reconstruct the depth profile via solution of the Marchenko equation.

The example demonstrates the feasibility of the retrieval of the phase information as well as the reconstruction of non-magnetic depth profiles via one polarization measurement using an arrangement with a magnetic reference layer. The need of a full three dimensional polarization analysis of the reflected

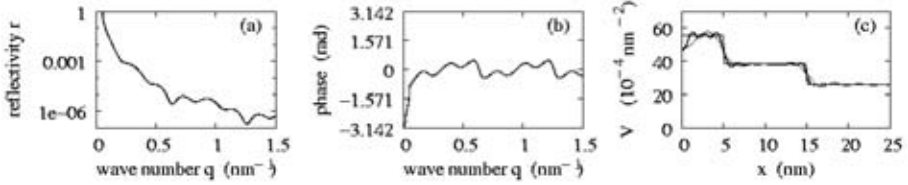


FIG. 5. Example of a reconstruction of the depth profile from simulated polarization data via the reference layer method discussed in the text. (a) Reconstructed reflectivity  $r = |R_S|^2$ ; (b) reconstructed phase of  $R_S$ ; (c) evaluation of the depth profile from the retrieved polarization data via solution of the Marchenko equation. Polarization data up to  $q_{\max} = 2\text{nm}^{-1}$  (solid line) and  $1\text{nm}^{-1}$  (dashed line) have been used.

beam limits the applicability of the method at present because available set-ups allow only for the preparation and analysis of the polarization in one direction, e.g. the  $y$  direction. Recently, we have investigated the possibility of phase retrieval based on such an incomplete polarization measurement [33]. We found out that for a non-magnetic sample we obtain a fourfold ambiguity. Two solutions are unphysical ( $|R_S|^2 \geq 1$ ) and can be eliminated immediately. From the remaining two solutions only one shows the behaviour  $\phi \rightarrow -\pi$  for  $q \rightarrow 0$  which is the physical one. In addition, some knowledge about the structure of the sample allows to identify the physical solution because the profiles associated with the two remaining solutions differ quite significantly.

The methods of phase determination discussed so far make use of a reference layer mounted on top of the sample. There might be some difficulties in the preparation of such an arrangement, e.g. for liquid samples. Therefore, we have recently developed a method [16], where the reference layer is mounted directly on the substrate and the sample on top of it. The reflection coefficients of the total arrangement is again given by Eq. (30), but with  $R_R$  and  $R_S$  interchanged. Introducing again the measurable quantity  $s$  via Eq. (29), one can derive the relationship

$$\overline{R_S}(-q) = -\frac{R_S(q)}{\eta_S(q)} = \frac{(R_R^+ - sR_R^-) - \overline{R_S}(q)R_R^+R_R^-(1-s)}{(1-s) - \overline{R_S}(q)(R_R^- - sR_R^+)} \quad (34)$$

where  $\eta_S(q) = T_S \overline{T_S} - R_S \overline{R_S}$  corresponds to Eq. (31) for the sample and therefore it does not depend on the polarization component  $\pm$ . For a full determination of  $\overline{R_S}(q)$  at least two sets of measurements with different reference layers are required. This leads to two different relations of the form of Eq. (34) which can be cast into a quadratic equation for  $\overline{R_S}(q)$ . The physical solution

$\overline{R}_S(q)$  can again be selected either by continuity  $\phi \rightarrow 0$  for  $q \rightarrow 0$  or by the condition  $|\overline{R}_S|^2 \leq 1$ . The latter may fail at some  $q$  values, and must be accompanied by continuity in certain momentum regions. The selection by continuity implies measurements of  $s$  over the whole range of positive  $q$  values. The solution  $\overline{R}_S(q)$  at negative  $q$  values is given via Eq. (34) and therefore the method also allows to extract the full reflection coefficient in the presence of absorption. The extracted reflection coefficient  $\overline{R}_S(q)$  for  $-\infty < q < +\infty$  can be used in the inverse scattering formalism, Eqs (7)–(9), in order to evaluate the scattering length depth profile. The profile of Fig. 1 has been evaluated from  $R_S(q)$  values retrieved from simulated polarization measurements for  $-1.0 \leq q \leq 1.0 \text{ nm}^{-1}$  using this method. The depth profile is well reproduced even in the imaginary part. From this one may conjecture that the Marchenko equation works sufficiently well also for small absorptive potentials although it has been rigorously derived only for Hermitean interactions [24].

### 3.4. Phase determination of magnetic samples

Spin polarized specular reflection has become an important tool to study the properties of thin magnetic films and superlattices [8]. In present spin polarized neutron specular reflection experiments [6, 8], only the moduli of the elements of the reflection matrix, Eq. (23), are actually determined. Hence, the nuclear and magnetic depth profile can be extracted from these data only in a model dependent way because for an unambiguous retrieval of the profile the full knowledge (moduli and phases) of all matrix elements of  $R_s$  is required. It is obvious that dealing with the full spin dependence of  $R_s$  the extraction of the phases will be more involved and requires a two step procedure [15, 34]. In order to sketch this procedure we cast the reflection matrix  $R$  into the form

$$R = R_{++} G = R_{++} \begin{pmatrix} 1 & G_{+-} \\ G_{-+} & G_{--} \end{pmatrix} = R_{++} \begin{pmatrix} 1 & R_{+-}/R_{++} \\ R_{-+}/R_{++} & R_{--}/R_{++} \end{pmatrix} \quad (35)$$

The first step consists of polarization measurements of the reflected beam for differently polarized incident beams. Similar to the procedure for non-magnetic samples, we define the quantity

$$s_{P^0} = \left( \frac{P_+}{1 + P_z} \right)_{P^0} \quad (36)$$

where the lower index  $\overline{P^0}$  denotes the polarization of the incident beam. This quantity can be completely determined via the measurement of the polarization of the incident beam. The quantity can also be expressed by the matrix elements of  $G$

$$s_{\overline{P^0}} = \frac{G_{-+}(1+P_z^0) + G_{--}G_{+-}^*(1-P_z^0) + G_{--}P_+^0 + G_{-+}G_{+-}^*P_-^0}{(1+P_z^0) + G_{+-}G_{+-}^*(1-P_z^0) + G_{+-}P_+^0 + G_{+-}^*P_-^0} \quad (37)$$

There are six real unknowns, i.e. the real and imaginary parts of  $G_{+-}$ ,  $G_{-+}$  and  $G_{--}$ , which should be determined by a set of three–six measurements with differently polarized incident beams. In the case of fully polarized beams, a set of three measurements suffices for a full determination of the matrix  $G$ . Hence, the matrix  $G$  can be fully determined via polarization measurements and we have reduced the problem of phase determination to one unknown phase, i.e. that of  $R_{++} = |R_{++}| \exp(i\phi_{++})$ .

The determination of  $R_{++}^s$  represents the second step of the procedure and requires a set of polarization measurements of the first step for arrangements with and without reference layer. Using the matrix generalization of Eq. (30),

$$R = R_R + T_R R_S \left[ 1 - \overline{R_R} R_S \right]^{-1} T_R \quad (38)$$

one obtains after some algebraics a quadratic equation for  $R_{++}^s$ . For the details of the evaluation of  $R_{++}^s$  see Ref. [15].

In Fig. 6 we show an example of a reconstruction of nuclear and magnetic depth profiles from simulated polarization data. The original profiles displayed with thin solid lines are well reproduced within the resolution of the data given by the momentum range  $0 \leq q \leq 1 \text{ nm}^{-1}$ .

#### 4. SUMMARY AND PERSPECTIVES

Neutron specular reflection is well understood within quantum mechanics and widely applied in condensed matter physics, materials science, biology, etc. Quantitative calculations of the reflection and transmission coefficients for a given profile are straightforward. We give a brief sketch of the quantum mechanical formulation and some details of the widely used transfer matrix formalism. The analysis of specular reflection data is usually performed within a model adjusting the open parameters to fit the measured reflectivities. However, there exists also a closed form relationship for the determination of

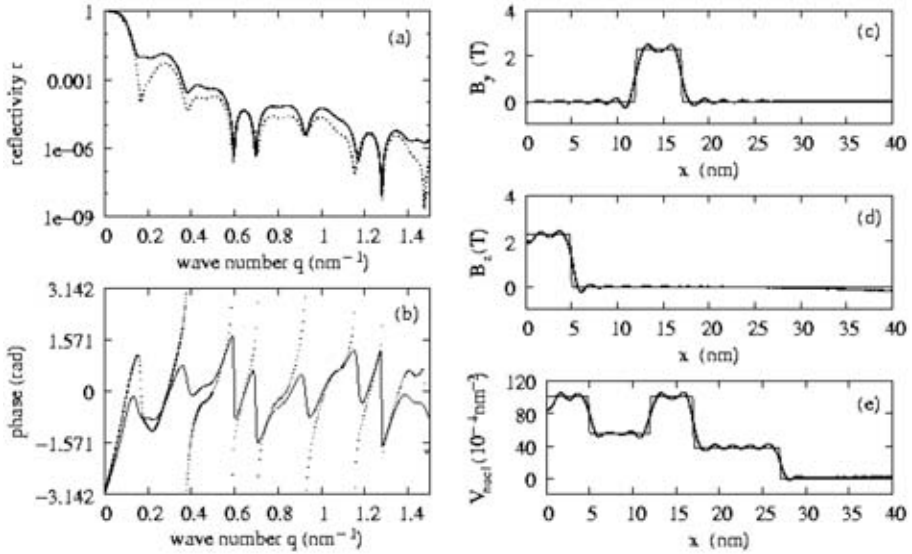


FIG. 6. Example of a reconstruction of the depth profile of Fig. 4 from simulated polarization data via the reference layer method for magnetic samples discussed in the text: (a) reconstructed reflectivities  $r_{11}$ (solid line) and  $r_{22}$ (dotted line); (b) reconstructed phase  $\phi_{11}^s$ (solid line) and  $\phi_{22}^s$ (dotted line). Depth profiles obtained via solution of the Marchenko equation using the reconstructed  $R_S$  values are shown in (c)–(e).

the profiles from the reflection coefficient. The basic formulas of this inverse scattering technique based on the Marchenko equation are outlined.

The unambiguous analysis of specular reflection data is usually hampered by the so-called phase problem. This problem refers to the fact that one measures intensities of the reflected waves, but not their phases. Recently, several schemes for the determination of the phase of the reflection coefficient have been proposed. Here, we review reference layer methods with particular emphasis on proposals based on polarization measurements. These methods are very promising and require only minor changes of standard reflectometer set-ups. The main difficulty arises with thick samples because  $R_S$  exhibits strong oscillations with varying  $q$  which must be resolved in a measurement. In principle, the phase problem in neutron specular reflection is solved even in the presence of magnetic fields and absorption. However, none of these proposals has become a standard procedure in neutron specular reflection so far.

Future neutron reflectometer set-ups at new facilities will certainly include a full polarization option in order to tackle the challenging questions of thin magnetic films and superlattices, which have a high potential for novel technologies. In these developments, and especially in the competition with X

ray sources, the demand for uniqueness and therefore for phase determination will be of great importance in neutron reflectometry.

### ACKNOWLEDGEMENTS

The collaboration with R. Lipperheide, J. Kasper and M. Weber on various aspects of neutron reflectometry is gratefully acknowledged. The work has been supported in part by INTAS contract 03-51-6426.

### REFERENCES

- [1] FELCHER, G., RUSSEL, T.P. (Eds), Workshop on methods of analysis and interpretation of neutron reflectivity data, *Physica B* **173** (1991) 1.
- [2] PENFOLD, J., Instrumentation for neutron reflectivity, *Physica B* **173** (1991) 139.
- [3] PENFOLD, J., THOMAS, R.K., The application of the specular reflection of neutrons to the study of surfaces and interfaces, *J. Phys. Condens. Matter* **2** (1990) 1369.
- [4] MAJKRZAK, C.F., "Thin film neutron optical devices: Mirrors, supermirrors, multilayer monochromators, polarizers and beam guides", (Proc. SPIE 0983 (1988).
- [5] XIAO-LIN ZHOU, SOW-HSIN CHEN, Theoretical foundation of X-ray and neutron reflectometry, *Phys. Rep.* **257** (1995) 223.
- [6] SCHREYER, A., et al., Oscillatory exchange coupling in Co/Cu(111) superlattices, *Phys. Rev. B* **47** (1993) 15324.
- [7] ZABEL, H., Spin polarized neutron reflectivity of magnetic films and superlattices, *Physica B* **198** (1994) 156.
- [8] SCHREYER, A., et al., Non-collinear and collinear magnetic structures in exchange coupled Fe/Cr(001) superlattices, *Phys. Rev. B* **52** (1995) 16066.
- [9] HAUPTMANN, H.A., The phase problem of X-ray crystallography, *Rep. Prog. Phys.* **54** (1991) 1427.
- [10] COWLEY, J.M., *Diffraction Physics*, North-Holland, Amsterdam (1975).
- [11] BUERGER, M.J., *Crystal Structure Analysis*, Wiley, New York (1967).
- [12] MAJKRZAK, C.F., BERK, N.F., Exact determination of the phase in neutron reflectometry, *Phys. Rev. B* **52** (1995) 10827.
- [13] DE HAAN, V.O., VAN WELL, A.A., ADENWALLA, S., FELCHER, G.P., Retrieval of phase information in neutron reflectometry, *Phys. Rev. B* **52** (1995) 10831.
- [14] LEEB, H., KASPER, J., LIPPERHEIDE, R., Determination of the phase in neutron reflectometry by polarization measurements, *Phys. Lett. A* **239** (1998) 147.

## NEUTRON SPECULAR REFLECTOMETRY

- [15] KASPER, J., LEEB, H., LIPPERHEIDE, R., Phase determination in spin-polarized neutron specular reflection, *Phys. Rev. Lett.* **80** (1998) 2614.
- [16] LEEB, H., GRÖTZ, H., KASPER, J., LIPPERHEIDE, R., Complete determination of the reflection coefficient in neutron specular reflection by absorptive nonmagnetic media, *Phys. Rev. B* **63** (2000) 45414.
- [17] AKTOSUN, T., SACKS, P., Inversion of reflectivity data for nondecaying potentials, *SIAM (Soc. Ind. Appl. Math.) J. Appl. Math.* **60** (2000) 1340; Phase recovery with nondecaying potentials, *Inverse Problems* **16** (2000) 821.
- [18] GUDKOV, V.P., OPAT, G.I., KLEIN, A.G., Neutron reflection interferometry: Physical principles of surface analysis with phase information, *J. Phys. Condens. Matter* **5** (1993) 9013.
- [19] FIEDELDEY, H., LIPPERHEIDE, R., LEEB, H., SOFIANOS, S.A., A proposal for the determination of the phases in specular neutron reflection, *Phys. Lett. A* **170** (1992) 347.
- [20] MAJKRZAK, C.F., Phase determination and inversion in specular neutron reflectometry, *Physica B* **248** (1998) 338.
- [21] MAJKRZAK, C.F., BERK, N.F., SILIN, V., MEUSE, C.W., Experimental demonstration of phase determination in neutron reflectometry by variation of the surrounding media, *Physica B* **283** (2000) 248.
- [22] MAJKRZAK, C.F., BERK, N.F., Exact determination of the phase in neutron reflectometry by variation of the surrounding media, *Phys. Rev. B* **58**, 15416 (1998).
- [23] PENDRY, J.B., HEINZ, K., OED, W., Direct methods in surface crystallography, *Phys. Rev. Lett.* **61** (1988) 2953.
- [24] KAY, I., The inverse scattering problem when the reflection coefficient is a rational function, *Commun. Pure Appl. Math.* **13** (1960) 371.
- [25] Agranovich, Z.S., Marchenko, V.A., *The Inverse Problem of Scattering Theory*, Gordon and Breach, New York (1963).
- [26] CHADAN, K., SABATIER, P.C., *Inverse Problems in Quantum Scattering Theory*, 2nd edn, Springer, Berlin (1989).
- [27] LIPPERHEIDE, R., REISS, G., LEEB, H., FIEDELDEY, H., SOFIANOS, S.A., Solution of the inverse scattering problem in specular reflection, *Phys. Rev. B* **51**, 11032 (1995).
- [28] KLIBANOV, M., SACKS, P.E., Phaseless inverse scattering and the phase problem in optics, *J. Math. Phys.* **33** (1992) 3813.
- [29] REISS, G., LIPPERHEIDE, R., Inversion and the phase problem in specular reflection, *Phys. Rev. B* **53** (1969) 8157.
- [30] LIPPERHEIDE, R., WEBER, M., LEEB, H., Phase determination in neutron reflection, *Physica B* **283** (2000) 242.
- [31] SIVIA, D.S., HAMILTON, W.A., SMITH, G.S., RIEKER, T.P., PYNN, R., A novel experimental procedure for removing ambiguity from the interpretation of neutron and X-ray reflectivity measurements: "Speckle holography", *J. Appl. Phys.* **70** (1991) 732.

- [32] LEEB, H., LIPPERHEIDE, R., REISS, G., Unique analysis of neutron specular reflection measurements, *J. Phys. Soc. Jpn.* **65**, Suppl. A (1996) 138.
- [33] LEEB, H., JERICHA, E., KASPER, J., PIGNI, M.T., RASKINYTE, I., Unique reconstruction of depth profiles in neutron specular reflectometry: Practical aspects, *Physica B* **356** (2005) 41.
- [34] LEEB, H., WEBER, M., KASPER, J., LIPPERHEIDE, R., Unique analysis of specular reflection data, *Physica B* **276–278** (2000) 75.

## LIST OF PARTICIPANTS

- Basu, S. Solid State Physics Division,  
Bhabha Atomic Research Centre,  
Trombay, Mumbai 400085, India  
Email: sbasu@apsara.barc.ernet.in
- Cubitt, R. Institut Laue-Langevin,  
6 Rue Jules Horowitz,  
B.P. 156, 38042 Grenoble Cedex 9, France  
Email: cubitt@ill.fr
- Leeb, H. Atominstitut of the Austrian Universities,  
Vienna University of Technology, Vienna, Austria  
Email: leeb@kph.tuwien.ac.at
- Mergia, K. National Centre for Scientific Research  
“Demokritos”,  
Patriarhou Grigoriou Street,  
P.O. Box 60228,  
Aghia Paraskevi attikis 15310, Greece  
Email: kmergia@ipta.demokritos.gr
- Messoloras, S. National Centre for Scientific Research  
“Demokritos”,  
Patriarhou Grigoriou Street,  
P.O. Box 60228,  
Aghia Paraskevi attikis 15310, Greece  
Email: spyros@demokritos.gr
- Nelson, A. Bragg Institute, Building 58,  
Australian Nuclear Science and Technology  
Organisation,  
P.M.B. 1,  
Menai, NSW 2234, Australia  
Email anz@ansto.gov.au
- Noël, J.J. Department of Chemistry,  
University of Western Ontario,  
London, Ontario, N6A 5B7 Canada  
Email: jjnoel@uwo.ca

## LIST OF PARTICIPANTS

- Penfold, J. ISIS, Rutherford Appleton Laboratories,  
Chilton, Didcot,  
Oxfordshire, OX1 1OQX United Kingdom  
Email: J.Penfold@rl.ac.uk
- Rennie, A.R. NFL, Studsvik,  
Uppsala Universitet,  
61182 Nykoping, Sweden  
Email: Adrian.Rennie@studsvik.uu.se
- Rühm, A. MPI für Metallforschung,  
ZWE FRM-II,  
Lichtenbergstrasse 1,  
85747 Garching bei München, Germany  
Email: ruehm@mf.mpg.de
- Satija, S. Center for Neutron Research,  
National Institute for Standards and Technology,  
100 Bureau Drive, Stop 8562,  
Gaithersburg, MD 20899-8562,  
United States of America  
Email: sushil.satija@nist.gov
- Tun, Z. Neutron Program for Materials Sciences,  
Chalk River Laboratories,  
Chalk River, Ontario, KOJ 1PO Canada  
Email: zin.tun@nrc.gc.ca

Neutron reflectometry can be used to solve problems in science and technology ranging from materials science, polymers and soft matter, thin film magnetism, chemistry and biology. It is currently used to address issues in such areas as energy, nanotechnology, environment and medicine. This publication will be useful for scientists planning to develop a neutron reflectometer, for users at research reactors and external stakeholders. It will also be useful in disseminating knowledge and information to the material scientists, biologists and chemists working towards characterizing and developing new materials.

INTERNATIONAL ATOMIC ENERGY AGENCY  
VIENNA

ISBN 92-0-103906-9

ISSN 0074-1884